RADIATION SHIELDING DESIGN, VERIFICATION AND DOSE DISTRIBUTION CALCULATIONS FOR INDUSTRIAL AND INSECT IRRADIATION FACILITIES

Thomas Elphus Sibiya

A research report submitted to the Faculty of Science, University of the Witwatersrand, Johannesburg, in partial fulfillment of the requirements for the degree of **Master of Science**.

School of Physics

Johannesburg, 2010

Declaration

I declare that this research report is my own, unaided work. It is being submitted for the partial fulfillment of the requirement for the Degree of Master of Science in the University of the Witwatersrand, Johannesburg. It has not been submitted before for any degree or examination in any other University.

Signature: 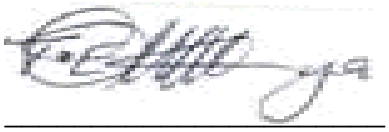 Date: 05 March 2010

Abstract

This study focused on analysis of the new radiation shield design, verification and dose distribution calculations for three irradiation facilities: The analysis of the new radiation design concrete shield for the Citrusdal facility, and shield verification calculations (radiological safety assessment) for the already constructed Stellenbosch and HEPRO irradiation facilities. Additionally, as a subordinate objective, the study reports on dose distributions in the irradiated insect containers of the Citrusdal irradiation facility, and sample product boxes of the HEPRO irradiation facility.

In 2006 a private company, Citrus Research International (CRI), began the engineering design of a new insect sterilization facility in Citrusdal in the Western Cape region of South Africa, which was then constructed from ordinary concrete density (**3** ¸ 2.35 g/cm**$**) in the year 2007. This facility employs a very successful ionising radiation based method, the Sterile Insect Technique (SIT), for drastically reducing or controlling insect population, which poses a serious pest problem in the Citrusdal agricultural area. The SIT uses the radionuclide ^{60}Co as the source of ionising radiation. The design-base activity of the ^{60}Co source for the Citrusdal facility was 740 TBq (20 kCi). Therefore, the new radiation shield design was done for this source strength. Analysis of the shield design has been carried-out using the integrated point-kernel (QAD-CGGP and the MathCAD worksheet) and confirmed with a Monte Carlo (MCNPX) radiation transport computer codes. This was done by considering the concrete shielding walls, the roof as well as the entrance/exit labyrinth at critical points for radiological protection purposes. However, only MCNPX was used to ascertain whether the labyrinth entrance/exit was radiologically safe because the point-kernel uses a semi-analytical, approximate methodology that is not able to account for radiation streaming through labyrinth. Satisfactory agreement was found between the three computational methods.

Stellenbosch irradiation facility is being operated by the Agricultural Research Council as insect sterilization facility at Nietvoorbij, that is situated approximately 70 km from Cape Town. This facility uses a radiation based Sterile Insect technique; using ^{60}Co as the source of ionising radiation. The facility is designed chiefly for sterilization of fruit flies which presents a major problem in the agricultural area in South Africa. The facility was designed for a 5 kCi (0.185 PBq) ^{60}Co source, but is now operated with a 10 kCi (0.37 PBq) ^{60}Co source (reference source strength in the year 1999). The source activity was 3.32 kCi (0.12 PBq) in October 2007, i.e., shield verification calculations was performed for this activity. This was carried out using QAD-CGGP and verified with MCNPX radiation transport computer codes, and where possible, validated with measurements. Dose rates were measured with a calibrated gamma-ray monitor, GRAETZ X5C. The spatial distribution of dose rates around the shielding concrete walls, on top of the roof and in various positions along the maze were considered. The dose rates at the closest distance (at 10 cm) from the exterior of the concrete shielding walls were slightly higher. However, good agreement was found between measured and simulated (calculated) values.

HEPRO is a commercial irradiation facility situated in Ferrule Avenue, Montagu Gardens, Milnerton, City of Cape Town, Western Cape, South Africa. The HEPRO facility is mainly used for food irradiation and sterilization of medical instruments. This

facility was originally designed to operate with a maximum ^{60}Co source strength of 1 MCi (37 PBq). However, to increase the product throughput rate, the source strength had to be increased to a nominal 1.5 MCi (55.5 PBq) in 2005/6. Nevertheless a radiological safety assessment was performed for a source strength of 2 MCi (2 , 37 PBq œ 74 PBq) ^{60}Co, because any radiation safety system such as radiation shielding must have a “safety factor”. Again the point-kernel method was used for radiological safety assessment and verified with MCNPX radiation transport computer code. Observation of critical spots and where possible the spatial distribution of dose rates were measured using a calibrated gamma-ray monitor, GRAETZ X5C, to provide additional confirmation of results. The spatial distribution of dose rates around the shielding concrete along the walls, roof, cable penetration inside the hut on roof, inside irradiation vault, above water pool, hotspot on wall, pneumatic pipe penetrations, sliding plug-door, and ducts of the hoist-cable situated on the roof of the locked hut were considered. The comparison of dose rate values obtained using the aforementioned methods showed a slight deviation such that they were considered satisfactory.

The use of Monte Carlo computational tools such as MCNPX in support of the prediction/assessment of the absorbed dose distributions in the irradiated product of the irradiation facilities can prove to be economically effective, representing savings in the utilization of dose meters, among other benefits. The absorbed dose distributions within the insect containers were calculated with the model developed in MCNPX for one hour of exposure. The modelling was carried out for a ^{60}Co source with a nominal activity of 16.8 kCi, i.e., 622 TBq. The calculated values were compared to an average value from the preliminary experimental (sterility test) measurements. The sterility test for the insects, False Codling Moths, was done during the onset of the SIT programme at Citrusdal irradiation facility. The variability of the dose distribution inside the insect canisters were within acceptable dose values for adequate sterilising False Codling Moths.

A systematic computational calculation methods was used to model/simulate the sample product undergoing irradiation in a ^{60}Co source for HEPRO industrial irradiator facility. This was carried-out using the Monte Carlo code—MCNPX. The calculation was done for a source-rack containing 4 , 25 œ 100 ^{60}Co pins, having a total activity of about 1 MCi (37 PBq). Four boxes were stacked around about 50 cm away from the source centerline. Each square box of sample product was rotated by 90° around the horizontal axis (perpendicular to the source rack), i.e., three times so that each of the four side of the box faced the source rack once during an irradiation session. A specific Fortran-90 code uses an algorithm to calculate the absorbed dose distribution for equal-time irradiation was therefore applied. The Fortran-90 code uses the dose values calculated by MCNPX and sums them in a suitable way in order to reproduce the mentioned rotations. The calculations revealed highest absorbed dose at the edges of the box, and even slightly higher at the four corners. The lowest absorbed dose was noticed at the centre of the sample product.

Dedication

This work is dedicated to my lovely family for believing that I have the potential to make a difference in the academic world.

This work is a true reflection of one's failure not to be defined by somebody's success, and as well success not to be defined by somebody's failure. There is nothing noble about being superior to some other people. True nobility lies in being superior to your previous state in life-time. In addition, a person who never made a mistake never tried anything new. Thus education should never be regarded as a duty but as the enviable opportunity to learn to know the liberating influence of beauty in the realm of the spirit for one's own personal joy and to the profit of the community to which your later work belongs. Albert Einstein could not have put it better.

Acknowledgements

The steadfast financial support and understanding of the South African Nuclear Human Asset Research Programme (SANHARP) throughout the several months required for the completion of my research work, have been an essential contribution from the outset. For this I will always be grateful. I am deeply appreciative to the following SANHARP management: Mr Gcobane Quvile, Mrs Zikhona Lose, Ms Zethu Maseko, and Ms Angeline Mdhluli. They took care of all the logistics, and I thank them for their efforts. They became more than colleagues. Therefore be counted as friends.

I am deeply grateful to Mr Johann Van Rooyen and Prof Tom Nam for mentoring, advising me both in my academic and my personal life. I thank them for giving me the wonderful opportunity to work with them throughout my MSc study. Their guidance, support, patience and encouragement have made the completion of this project possible.

I would like to thank the University of the Witwatersrand, particularly the School of Physics for allowing me to be based at Necsa—the South African Nuclear Energy Corporation during the period of my research work. In particular, I would like to express my sincere thanks to Prof John Carter for his endless support and advise.

My deeply appreciation to the Radiation and Reactor Theory (RRT) section at Necsa for their support and assistance in all aspects of my work. iThemba LABS—Gauteng[1], and iThemba LABS—Cape Town are thanked for their welcoming support during my academic visit. I would like to express my thanks to Mrs Hantie Labuschagne, the support staff and the entire team of scientists in the RRT section, for their constant help during the period of my research.

I wish to acknowledge the useful help I received from the management staff of the INFRUITEC—Stellenbosch, Citrusdal, and HEPRO irradiation facilities. Their time and useful information have also led the work to the right direction.

My work would not have been as enjoyable, were it not for my lovely family and friends. To all, I express sincere thanks.

[1] Formerly Schonland Research Institute for Nuclear Sciences.

Table of contents

List of figures

List of tables

Abbreviations

CCC.....Computer Code Collection (of the RSICC)

CS.....Compton scattering

DAF.....Dose Attenuation Factor

GP..... Geometric Progression

IAEA..... International Atomic Energy Agency

ICRP.....International Commission on Radiological Protection

LHS..... Left hand side

MCNP..... Monte Carlo N-Particle Transport Code

MCNPX.....Monte Carlo All-Particle Transport Code

QAD-CGGP.....A point-kernel photon transport code using the Geometric Progression (GP) buildup factor formalism, and Combinatorial Geometry (CG)

PEA..... Photo-electric absorption

PP..... Pair production

RCC.....Right Circular Cylinder

RHS..... Right hand side

RPP.....Rectangular Parallelepiped

RSICC..... Radiation Safety Information Computational Center (at Oak Ridge National Laboratories, United State of America)

SA.....South Africa

SIT.....Sterile Insect Technique

SPH..... Sphere

Units

Practically all radiation transport codes use the centimetre-gram-second (CGS) system of units. The two radiation transport codes used in this work—MCNPX and QAD-CGGP—both use the units cm for length and gram for mass. To avoid confusion, this work therefore employs the CGS system and expresses the dimensions of radiation shields in the unit cm, particle fluence rate in $cm^{\bullet 2}.s^{\bullet 1}$ and mass-density in the unit $g.cm^{\bullet 3}$. The engineering standard of reporting building and component dimensions in the unit mm is therefore not followed in the present work.

Chapter 1
Introduction

1.1 Necessity to shield ionising radiation

The protection of human-kind and the environment against ionising radiation have been a great concern since the discovery of X-rays by Wilhelm Conrad Röntgen in 1895 and the discovery of radioactivity by Antoine-Henri Becquerel in 1896. Ionising radiation is a health hazard. High doses can cause acute radiation syndrome, i.e., "radiation sickness." Lower doses cannot cause acute symptom, but carry a risk of radiation-related cancer and heritable ill health. A large body of radio-epidemiological studies on Japanese nuclear bomb survivors, e.g., has shown that the incidence of cancers increase with radiation dose (cf. e.g. www.rerf.or.jp as well as IAEA safety series 115, 1996; ICRP publication 103, 2007; Wrixon, 2008).

It is possible to attenuate the intensity of ionising radiation to acceptable levels, by using appropriate radiation shielding. Many textbooks on the subject of radiation shielding have been published, a more recent example of which is ***Radiation Shielding*** by Shultis and Faw (1996).

An international advisory body on radiological protection, the International Commission on Radiological Protection (ICRP) has laid down dose limits (see Appendix A.1), as well as the imperative that radiation protection (RP) must be optimised (ICRP publication 103, 2007), i.e., radiation doses must be kept ALARA—As Low As Reasonably Achievable.

1.2 Radiation safety system

Many decades of theoretical analyses and practical experience have led to the conclusion that a radiation protection programme must be based on the following threefold set of principles: (1) engineered radiation safety systems, (2) management controls and (3) fostering a "safety culture" in an organisation. The more intense and dangerous the sources of ionising radiation are, the higher the reliance on engineered radiation safety systems must be.

The two pillars of engineered radiation safety systems are: (1) a radiation containment system to shield the radiation so that fluence rates and dose rates in regions occupied by people and radiosensitive equipment are below levels regarded as adequately safe, and (2) an access control system to control access to radiation areas, e.g., prevent human entry into radiologically dangerous areas.

1.3 The three irradiation facilities under analysis

1.3.1 The Citrusdal insect sterilization facility

In 2006, a private company, *Citrus Research International (CRI)* began the engineering design of a new insect sterilization irradiation facility in Citrusdal in the Western Cape, South Africa (SA). This facility is constructed from ordinary concrete density (**3** ¸ 2.35 g/cm**$**) and equipped with a ^{60}Co source partly funded by the International Atomic Energy Agency (IAEA). The intended source strength of the ^{60}Co source is, nominally, 20 kCi, i.e., 740 TBq. In practice, of course, a source will always be delivered with an activity that is not exactly equal to the above nominal source strength, and this activity will also diminish with time.

1.3.2 The Stellenbosch insect sterilization facility

The Agricultural Research Council (ARC) operates an insect sterilization facility at Nietvoorbij, Stellenbosch, about 70 km from Cape Town, SA. This facility received once-off funding from the IAEA, and uses ionising photons from a ^{60}Co source as the source of ionising radiation (Barnes, personal communication, 2006), to sterilize the pest insects.

According to engineering drawings and staff members employed for several decades, the facility is constructed from "high density" concrete. However, the actual elemental composition and the mass-density **3** of the concrete is unknown. It was therefore assumed that the elemental composition of the concrete was that of magnetite concrete. The only free variable that now remained was the mass-density **3** of the concrete. Several dose-rate calculations with selected concrete mass-densities were carried out and compared with dose-rate measurements. This led to an estimated density of 2.63 g/cm**$**, assuming that the elemental composition of the concrete is that of steel-magnetite concrete, as listed in textbooks such as Shultis and Faw (1996). The facility was originally designed for a 5 kCi (0.185 PBq) ^{60}Co source, but has been partly upgraded in the 1990s for operation with a 10 kCi (0.37 PBq) ^{60}Co source.

1.3.3 The HEPRO irradiation facility

"HEPRO" is an initialism for **H**igh **E**nergy **PRO**cessing; the design company behind HEPRO is PicoWave Technology. HEPRO is a commercial irradiation facility situated in Ferrule Avenue, Montagu Gardens, Milnerton, City of Cape Town, Western Cape, S A. The facility uses a **'!**Co gamma-ray source rack, as the source of ionising radiation.

The **'!**Co source used at HEPRO is in the form of a rectangular source rack, composed of three sub-racks mounted on top of each other, each about 48 cm in height, with equal sides of 75 cm, composed of **$, a% , #&b œ** 300 **'!**Co pencils clad in stainless steel. For the purpose of the MCNPX modelling of the source, this has been slightly simplified to a

single source rack, 150 cm high, with equal sides of 75 cm, composed of % , #& œ 100 '!Co pencils.

The HEPRO facility is mainly used for food irradiation and the sterilization of medical instruments. This facility was originally designed to operate with a maximum '!Co source strength of 1 MCi (37 PBq). However, to increase the product throughput rate, the source strength had to be increased to a nominal 1.5 MCi (55.5 PBq) in 2005/6. This report presents a shield verification for a source strength of 2 MCi (2 , 37 PBq œ 74 PBq) ^{60}Co, because any radiation safety system such as radiation shielding must have a "safety factor".

Entwistle and Adrian (1986) prepared a Safety Assessment Report (SAR) on the HEPRO facility. In their 1986 report, they referred to shield design calculations for HEPRO, carried out by De Beer (1986), then of the Atomic Energy Commission (AEC) of South Africa[2]. This shielding study by De Beer (1986) was apparently never published as a formal report, but was in the form of handwritten notes, which were lost. It is therefore important that an in-depth radiation safety assessment report for the HEPRO facility be performed and published.

More detailed descriptions of these three irradiator facilities supplemented by several photographs are presented in Chapter 3.

1.4 Literature review for shield design at irradiation facilities

Several studies have been done on the shielding of ionising photons from radiation sources. Sarangapani *et al.* (2006) used Monte Carlo radiation transport code, MCNP, to calculate radiation streaming through penetrations in the shield around a nuclear reactor. Calculated photon spectra were compared with experimental measurements using a HPGe detector at a number of positions outside the duct. Photon dose rates were measured with a dose rate meter as well as with thermoluminescent dosimeters (TLDs). Good agreement was found between calculated and measured spectra and dose rates. Based on these results, the authors recommended that a safety factor of 2 be used in shield design calculations carried out with the code MCNP.

Raisali *et al.* (2006) presented an analysis of neutron and photon streaming along the multi-bend concrete walled labyrinth/maze of an accelerator-based radionuclide production vault, using the code MCNP/4C. Calculated and experimental results agreed to within 20%. Concrete thicknesses ranged from 100 - 200 cm. Cell importance biasing, which in turn invokes particle splitting and Russian roulette variance reduction algorithm, were used to effect variance reduction.

Oliveira *et al.* (2000) calculated radiation dose rates in a gamma-irradiation facility using the code MCNP/4B2. The source was a rack of 160 pins containing high activity '!Co

[2] Today: Necsa — the South African Nuclear Energy Corporation.

sources. The irradiator had ordinary concrete shielding walls of thicknesses ranging between 180 and 200 cm. Good agreement was found between calculated and experimentally determined dose rates—results differed by no more than 12%. Cell importance biasing (particle splitting and Russian roulette variance reduction algorithm) was employed as variance reduction technique. Point tallies were used, at several positions inside the irradiator chamber and the labyrinth; at every point, the dose rate as well as the photon energy spectrum were determined.

Oliveira and Salgado (2001) determined isodose distributions and dose uniformity for the same above mentioned gamma-irradiation facility using MCNP/4B2. The authors concluded that MCNP is an important tool for performing prospective dose mapping inside products to be irradiated.

Oliveira *et al.* (2002) performed Monte Carlo studies of gamma-irradiation geometry using the code MCNP/4B2. Eight different source rack configurations were simulated to ascertain dose per source activity as well as dose uniformity.

Tsai *et al.* (2005) evaluated the dose rate distribution inside a ^{60}Co gamma-irradiation facility that employs a single-rod source of reference activity 1.07 PBq. Dose-rate distributions were determined using QAD-CGGP, and collaborated with radiochromic dye films and an ion chamber. The scattered ionising photons from the walls of the irradiator cell were also evaluated by using MCNP. The authors estimated the contribution to the dose rate from the scattered gamma-rays at distance of 25 cm from the guide tube axis to be approximate 25%.

Conclusions from literature review

Based on this survey of available literature on irradiator shield design and dose-rate distributions inside vaults as well as in irradiated products, it may be concluded that much general work has been performed on shielding using MCNP and QAD-CGGP at several irradiation facilities. The use of the codes QAD-CGGP and MCNPX for shield design, dose rate mapping and dose mapping, are well established and are accepted methodologies used by radiation protection regulators as well as organisations operating irradiator facilities. It may also be inferred from the limited survey that a comparison of the outcome of the two independed codes in shield design and verification has yet to emerge. This study is aimed at providing such comparison when used to evaluate and verify the shielding, and dose rate values around three irradiation facilities.

1.5 Goals of the present work

Because of operational needs, the work was divided into two phases. The first phase was to design concrete shielding walls, the roof as well as the entrance/exit labyrinth for the new insect irradiation facility located at Citrusdal, using the Monte Carlo radiation transport code MCNPX and the point-kernel integration code QAD-CGGP. These calculations were urgently required for an actual construction project (Hofmeyr, personal communication, 2006). The second phase was to perform shield verification calculations

for the already constructed HEPRO and Stellenbosch irradiation facilities. The source and shielding walls were modelled with the radiation transport codes MCNPX version 2.5.0 (RSICC CCC-730, 2005) as well as QAD-CGGP version of QAD-P5A (RSICC CCC-493, 1989). Calculations were verified by comparison with measured dose rates outside the accessible shielding walls and the roof of the existing irradiator facilities.

Where possible, dose rates outside shielding walls were calculated using 3 independent methodologies:

- MCNPX calculations, i.e., Monte Carlo calculations that employ rigorous radiation transport methods.
- Calculations with the point-kernel code, QAD-CGGP.
- Calculations with a MathCAD worksheet developed by Van Rooyen (personal communication, 2006), using a point-kernel method for point sources surrounded by a single-material shield in spherical-symmetrical geometry.

Calculated dose rates obtained by these three completely independent methods were used as QA (Quality Assurance) check on, and verification of, the accuracy and limitations of the models. The main goal of this study.

A secondary aim was to calculate dose distributions in the irradiated food and insect containers using MCNPX. This is because the code QAD-CGGP is not useful for accurate dose-distribution calculations in irradiated products. It uses an analytical, approximate method, and does not perform rigorous radiation transport calculations. Whilst MCNPX can be used for dose rate calculations at various positions inside the entrance/exit labyrinths at the Citrusdal and Stellenbosch facilities, the QAD-CGGP code cannot model radiation streaming through such structures; QAD-CGGP can only perform “ray-tracing” calculations using a simple analytic approximation known as the point-kernel method.

1.6 Outline

This work is presented in eight chapters and five appendices.

- Chapter 2 outlines some theoretical considerations of important to the theory of shielding against ionising radiation, specifically ionising photons. This chapter describes the nature of ionising photons and its behaviour when interacting with a shielding material.
- The irradiation facilities and their source characteristics are presented in Chapter 3.
- Chapter 4 presents the point-kernel integration code, QAD-CGGP version of QAD-P5A (RSICC CCC-493, 1989), the MathCAD worksheet (Van Rooyen, personal communication, 2006) and the Monte Carlo radiation transport computer code, MCNPX 2.5.0 (RSICC CCC-730, 2005).
- The results of the dose rate calculations and measurements (where applicable) for the Citrusdal irradiator facility are presented in Chapter 5; the results for the

Stellenbosch irradiator facility are presented in Chapter 6, whereas the results for the HEPRO irradiator are presented in Chapter 7.

- Finally, a summary and outlook, including remarks on the use of point-kernel and Monte Carlo methods is presented in Chapter 8.
- Appendix A presents the criteria for evaluating radiation shielding effectiveness, as well as an overview of dose limits and dose constraints.
- Appendix B presents the contributions made to the industry as a results of this study. In addition, the observation and recommendation for the HEPRO irradiation facility is also presented.
- The sample input files for the Citrusdal insect sterilization irradiator facility, for the codes QAD-CGGP and MCNPX, are given in Appendix C. This and the subsequent appendices gives the input files for the spherical (SPH) and rectangular parallelepiped (RPP) geometry that were used for calculations and a line-by-line explanation of the input data sets.
- Appendix D presents the QAD-CGGP and MCNPX sample input files for the Stellenbosch insect sterilization facility.
- The QAD-CGGP and MCNPX sample input files for the HEPRO irradiation facility are given in Appendix E.

Chapter 2
Theoretical rumination

2.1 Introduction

Although beneficial use of ionising photons cover such various fields such as sterilization of medical products, irradiation of food, insect sterilization, polymer polymerization, and radiotherapy, such photons, i.e., X-rays and gamma-rays, do pose a potential hazard to radiation workers, members of the public, (which includes non-radiation workers), and the environment. There is therefore a need to achieve a high degree of safety and reliability in order to beneficially use these sources. As pointed out in §1.1 and §1.2, an appropriately designed shield can attenuate the intensity of ionising photons, so that during normal operation radiation exposure of radiation workers as well as members of the public will be low enough to ensure/prevent the dose limits recommended by the ICRP as well as dose constraint in force at a facility are not exceeded.

To analyse a proposed shield design and simulate radiation transport in a shield with the aim of calculating dose rates, using radiation transport computer codes (discussed in Chapter 4), an understanding of the nature of the radiation source(s) is imperative. In this chapter the interactions and biological hazard of ionising photons, is presented. The nature of the ionising photons emitted by a ^{60}Co source that is of pertinent of this study is presented separate in Chapter 3.

Energy-dependence of the biological harmfulness of ionising photons

The energy dependence of the effective dose response function, $Å_{\#ÐIÑ}$, for four different types of ionising radiation, is shown in Figure 2.1 on page 8. This graph was obtained from Monte Carlo calculations of a broad, parallel beam of mono-energetic ionising radiation striking an anthropomorphic phantom from the front (Ferrari, *et al.*, 1996; Ferrari, *et al.*, 1997a, 1997b and 1997c). From Figure 2.1, it can be seen that the effective dose response function for photons, $Å_{\#ÐIÑ}$, increases practically monotonically with photon energy. It is also seen that, for the same fluence-rate, 9, and same incident energy, I, ionising photons are less harmful than other classes of radiation. From the first observation, it follows that the mere lowering of photon energy will contribute to photon shielding, because a given fluence of low energy photons will contribute a considerably lower effective dose than the same fluence of high-energy photons.

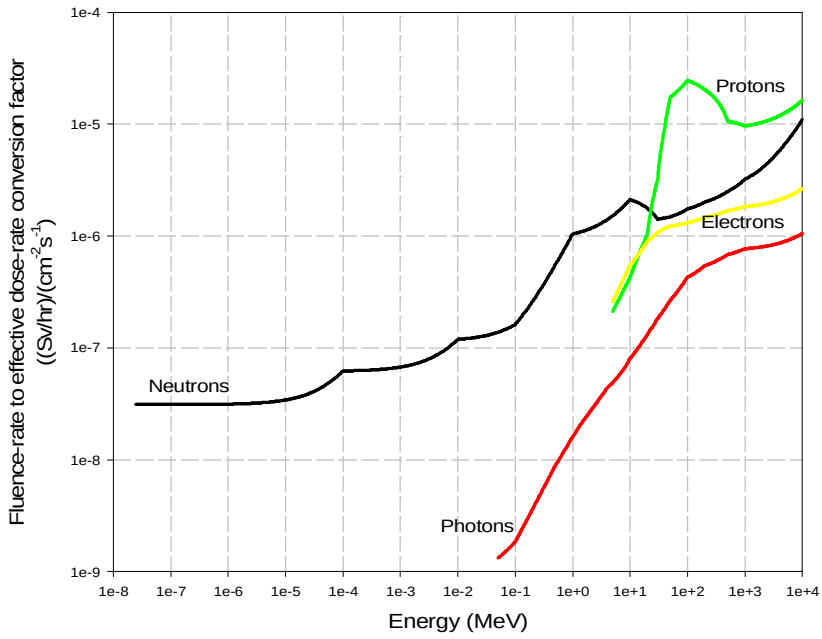

Figure 2.1: *The response functions for four types of ionising radiation for converting fluence-rate to effective dose rate.*

Of note in Figure 2.1 is a monotonic increase in biological hazard of ionising photons with incident photon energy.

2.2 Photon interaction mechanisms

Introduction

Photons are quanta of electromagnetic radiation; they are electrically neutral, have zero mass, and a velocity - ¸ $, "!) m/s# in a vacuum (Shultis and Faw, 1996; Turner, 1995; Cember, 1996). Since they are electrically neutral, they do not steadily lose energy as they penetrate matter, via Coulombic interactions with atomic electrons as do charged particles, such as alpha-particles and electrons. Instead, they travel a considerable distance before undergoing a more "*catastrophic*" interacting with an atom, leading to partial or complete transfer of their energy to electron energy. These secondary electrons produced by photon interactions, will subsequently impart their energy to the medium. Ionising photons, then, are indirectly ionising radiation, because their energy is transferred to the medium by secondary electrons produced by photon interactions.

Penetration of ionising photons through matter is governed statistically by the linear interaction coefficient, ., which depend on the photon energy, the type of interaction, and the elemental composition and mass-density of the specific medium traversed (Shultis and Faw, 1996; Turner, 1995).

When ionising photons interact with the medium, they may be absorbed and disappear or possibly scattered, changing its original direction of travel, with varying loss of energy. Thomson scattering and Rayleigh scattering are two interaction mechanism by which

ionising photons interact with matter without considerable loss or transfer of energy (Turner, 1995: 170). Thomson scattering is an incoherent scattering mechanism, and refers to the interaction of a photon with an individual electron as distinguished from the coherent Rayleigh scattering interaction of a photon with all electrons of an atom (Shultis and Faw, 1996: 40; Turner, 1995: 170). During Thompson scattering, the atomic electron in the electromagnetic field of the incident photon vibrates with the same frequency as that of the incident photon, thereby giving rise to the emission of secondary electromagnetic radiation, i.e., photons of the same frequency ν. The collective effect of incoherent scattering, which is an elastic interaction mechanism, is the *redirection* of some incident photons with no transfer of energy to the medium. Thompson scattering is the low-energy limit of incoherent (Compton) scattering, as the incident photon energy approaches zero, and also the basis for computing Rayleigh scattering cross-sections for coherent interaction of ionising photons with atomic electrons (Shultis and Faw, 1996: 40; Turner, 1995: 170). In competition with the Thomson (incoherent) scattering of photons by individual electrons, is Rayleigh (coherent) scattering by the electrons of an atom collectively (Shultis and Faw, 1996: 42; Turner, 1995: 170; Knoll, 1999: 49). The scattering angle for coherent scattering is normally very small; and there is no significant loss of photon energy to the atom, which, nevertheless, does recoil enough to conserve momentum. It is seen in Figure 2.2 that coherent scattering cross sections may greatly exceed incoherent scattering cross sections, particular for low-energy photons and high atomic number materials. Nonetheless, because of the insignificant effect on photon energy and direction, and since the coherent scattering cross section is far less than the cross section for the photoelectric absorption, the contribution of Rayleigh scattering to photon attenuation is relatively insignificant. Thomson scattering is often ignored in the production of photon interaction data for transport codes (Shultis and Faw, 1996) because its impact on the transport of ionising photons is negligible.

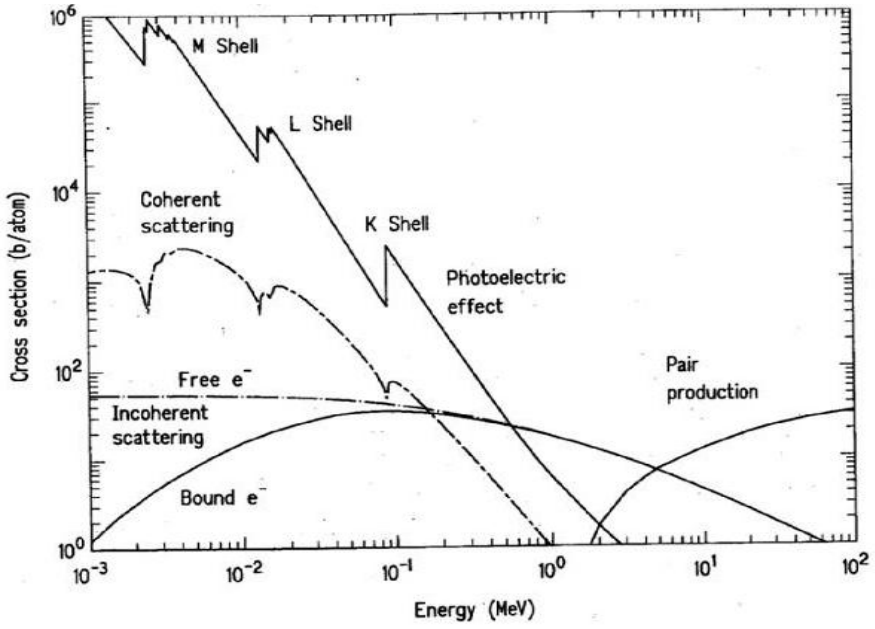

Figure 2.2: *Comparison of typical cross-sections for photoelectric absorption (PEA), Compton scattering (CS) and pair production (PP) for ionising photon interactions in lead (Shultis and Faw, 1996: 43).*

For *radiation protection* purposes, three mechanisms of energy deposition by ionising photons in matter dominate, namely, photoelectric absorption (PEA), Compton scattering (CS), and pair production (PP). Photons emitted by radionuclides practically always have energies less than circa 8 MeV (Shultis and Faw, 1996); and for this energy range, the cross-sections of photonuclear interactions, i.e., nuclear reactions produced by photons, are zero except for three isotopes, namely ^{2}H, ^{9}Be and ^{7}Li (Knoll, 1999; Cember, 1996).

Two of the above three dominant photon interaction mechanisms, photoelectric absorption and Compton scattering, both of which involve interactions only with orbital electrons of the medium, predominate in the case where the energy of the photons does not greatly exceed "þ!## MeV, the energy identical to the rest-mass of two electrons. The photoelectric absorption predominates at lower photon energies, and Compton scattering at intermediate energies. In the case of high-energy photons, pair production dominates, which is a direct conversion of electromagnetic energy into mass (Pratt, 2004).

All three the above interaction mechanisms (PEA, CS and PP) result in the emission of electrons from the medium. Very high energy photons, I# ¦ #7/-#ß may also be absorbed into the nuclei of the absorber atoms; they then initiate nuclear reactions (photonuclear reactions) that result in the emission, from the excited nuclei, of other radiations.

2.2.1 Photoelectric absorption

In photoelectric absorption, a photon interacts with an entire absorber-atom, resulting in the emission of an energetic photo-electron from one of its bound shells, normally from the tightly bound K-shell of the atom, i.e., shell with principal quantum number 8 equal to one. The difference between the photon energy, I# œ 2/, and the electron binding energy, I,, is distributed between the electron and the recoil atom; however, the photoelectron carries off the majority of the original photon energy as kinetic energy, X, because of the comparatively small electron mass (Shultis and Faw, 1996; Knoll, 1999). Thus, the mathematical relationship between X, I# and I, is

$$X \text{ œ } I_{\#} \bullet I_{,}. \tag{2.1}$$

Photoelectric absorption leaves an ionised absorber atom with a vacancy in one of its bound electron shells, which, is quickly filled through the capture of a free electron from the medium, or the rearrangement of electrons from other shells of the atom. This may lead to the emission of one or more characteristic X-ray photons; this process is termed the emission of *fluorescence* radiation. PEA is illustrated in Figure 2.3 on page 11.

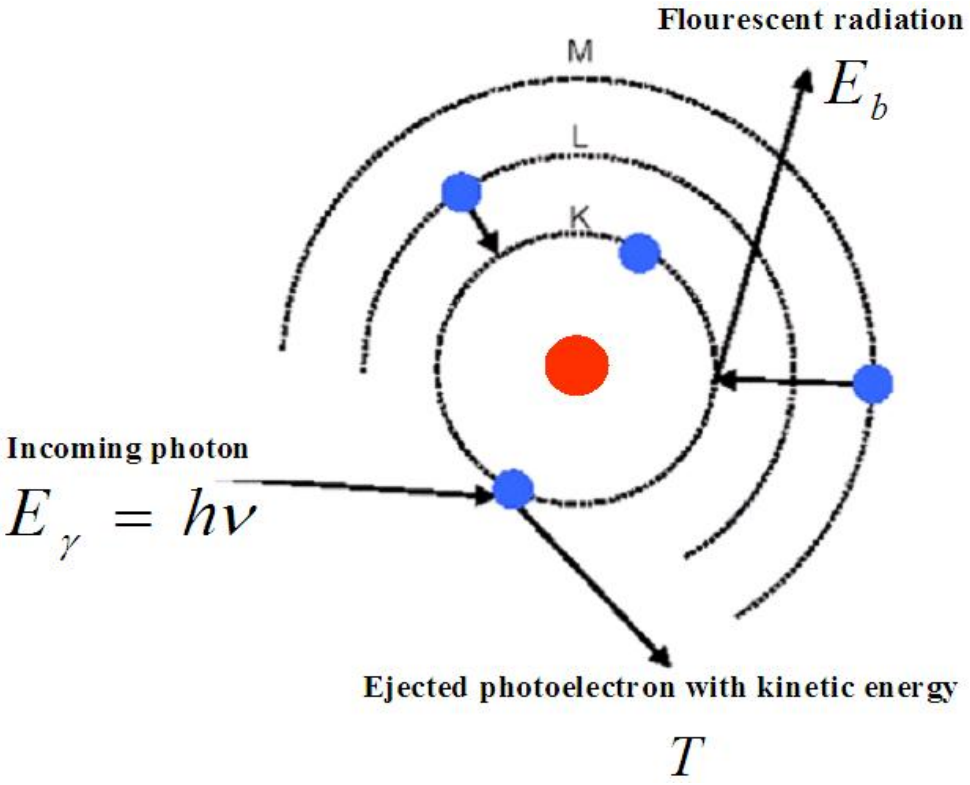

Figure 2.3: *Events in the photoelectric absorption process (Alphen, 1990: 59).*

It can be noted in Figure 2.3, the incoming photon is absorbed and the atom ejects a photoelectron. Then an outer orbital electron moves into the vacancy left by the departure of the ejected electron. The most probable event is that the electron is emitted from the K-shell (principal quantum number **8 œ** 1), and that this vacancy is filled by an electron from the L-shell (**8 œ** 2) or M-shell (**8 œ** 3). The transition of the electron from a higher energy state to an available lower energy state, is followed by the fluorescent emission of a characteristic X-ray.

The photoelectric absorption mechanism is the predominant mode of interaction for photons of relatively low energies, and this process is also more likely for absorber material of high atomic number **^**. There is no single analytic expression that is valid for the probability (cross-section $\mathbf{5}_{\mathrm{PEA}}$) of photoelectric absorption per atom over all ranges of photon energies, **l # œ 2/**, and atomic numbers **^**; nevertheless, a reasonable approximation is

$$\mathbf{5}_{\mathrm{PEA}}\mathbf{a^{\wedge}ß\ l b\ ° \frac{^{8}}{a\,l_{\#}b^{7}}}, \qquad (2\text{Þ}2)$$

where the empirically determined best-fit exponent **8** varies between 4 and 5, **7** between 3 and 4 over the photon energy region of interest. For qualitative purposes, approximate integer exponents can be assumed, so that Eq. (2.2) becomes

$$\mathbf{5}_{\mathrm{PEA}}\mathbf{a^{\wedge}ß\ l b\ ° \frac{^{\%}}{a\,l_{\#}b^{\$}}}. \qquad (2\text{Þ}3)$$

The strong dependence of the photoelectric absorption cross-section on the atomic

number Z of the absorber, explains why PEA is dominant over quite a large energy range, for high atomic number materials such as lead (Pb), tungsten (W) and depleted uranium (DU), and why these materials are such excellent shielding materials against ionising photons. For low-Z absorber materials, PEA is relatively unimportant over a wide photon energy range. The high exponential power to which the variable $h\nu/E$ is raised, indicates that the contribution of photoelectric absorption to the attenuation of photons, diminishes sharply with increasing photon energy. Generally, σ_{PEA} becomes negligibly low, compared to the cross-section for Compton scattering, above $h\nu \approx 1$ MeV.

Linear interaction coefficient for photo-electric absorption

An approximate mathematical expression for the linear interaction coefficient μ for PEA can be derived, because $\mu = N\sigma$ where N is the nuclide number density and σ is the cross-section. It is easily shown from first principles that

$$N = \frac{N_A \rho}{A_r}. \tag{2.4}$$

for a simple medium, where N_A is the number of Avogadro, ρ is the mass-density of the medium, and A_r is the relative molar mass of the atom in the single-element medium. However, $A_r \approx E$, and, furthermore, $E \approx 2Z$ for a typical element. Therefore

$$N \approx \frac{N_A \rho}{2Z} \propto \frac{\rho}{Z}, \tag{2.5}$$

so that the following proportionality will hold quite well,

$$\begin{aligned} \mu_{PEA} &\propto \left(\frac{Z^4}{(h\nu)^3}\right)\left(\frac{N_A \rho}{2Z}\right) \\ &\propto \frac{\rho Z^3}{(h\nu)^3}, \end{aligned} \tag{2.6}$$

so that, at a given photon energy,

$$\mu_{PEA} \propto \rho Z^3. \tag{2.7}$$

Eq. (2.7) will be used later to reach an important conclusion about material choices for optimal shields against ionising photons.

2.2.2 Compton scattering

In the Compton scattering process, the incident photon collides with a free electron, assumed to be initially at rest in the absorbing material. It is normally the predominant interaction mechanism for ionising photons emitted by most radionuclides, i.e., in the photon energy $h\nu$ range of [0.1; 2 MeV] sources. The incoming photon is deflected through an angle θ with respect to its original direction; it transfers part of its energy to the recoiling electron. Since all angles of scattering are physically possible, the energy

transferred to the electron can vary from zero to a large fraction of the incident photon energy. This mechanism is illustrated in Figure 2.4, which depicts an elastic collision between a photon and a free electron.

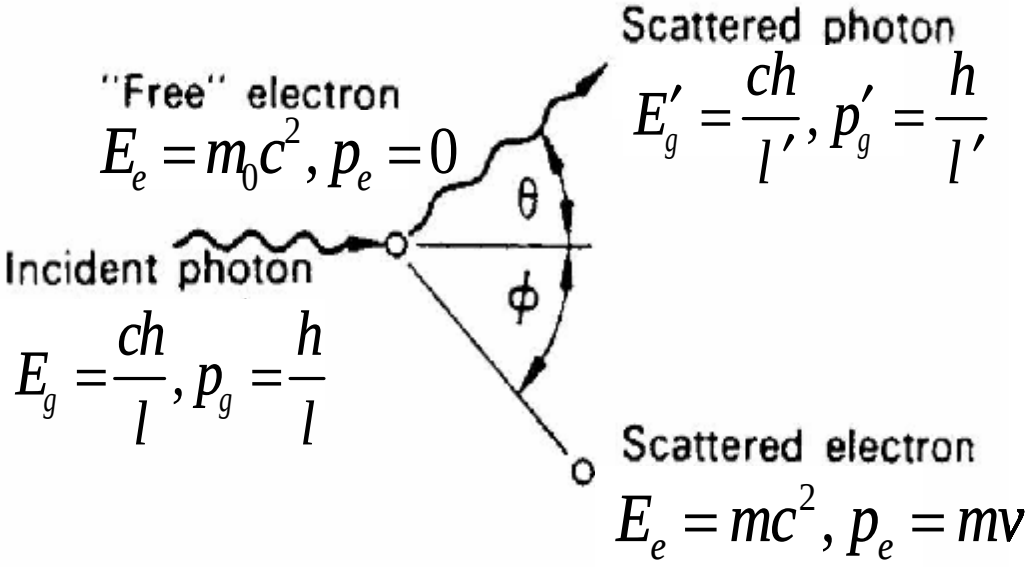

Figure 2.4: *Events in the Compton scattering process (Cember, 1996:142).*

Of note in Figure 2.4, is the Compton scattering of photon with energy **l#**, momentum **2Î-**, from an electron, assumed to be initial free and at rest with total energy **l/**. The photon is scattered through an angle **)**, and has a reduced energy of **l#W œ 2/"a œ -2Î-"b** and momentum **: œ 2Î-"**, and the electron recoils at angle **9** with total energy **l/ œ 7-#** and momentum **7@**. The mathematical relationship between energy transfer and the scattering angle for any given interaction can easily be derived by considering simultaneous expressions for the conservation of energy and linear momentum. Many textbooks provide a summary of the derivation, such as Cember (1996), Turner (1995) and Krane (1987). These textbooks list the formulas,

$$l'_\# = \frac{l_\#}{1 + (l_\#/7_/-^\#)(1 - \cos)} \quad (2.8)$$

and

$$l_/ = l_\# - \frac{1 - \cos)}{7_/-^\#/l_\# + 1 - \cos)} \quad (2.9)$$

where the product **7/-#** is the rest mass energy of the electron, **7/-# œ !ÞâÄÄ** MeV; the rest of the variables have the same meanings as explained above.

Compton scattering is important in radiation shields, because a high-energy photon loses a greater fraction of its energy when it is scattered than a low-energy photon does. Compton scattering is a very efficient photon energy lowering mechanism for large

photon scattering angles—in particular for) ¸ 180° (complete backscattering). However, Compton scattering becomes dynamically strongly forward biased at higher incident photon energies. The net result is that Compton scattering contributes most to the energy degradation of intermediate energy photons.

Linear interaction coefficient for Compton scattering, . GW

A useful proportionality for the linear interaction coefficient for Compton scattering, $.\,_{CS}$ (unit: cm^{-1}) for an element with mass density **3**, can be derived as follows, by using the defining expression . œ R5. Compton scattering involves incoherent scattering from an essentially "free" electron, so that 5_{CS} will be essentially independent of the medium (excluding the possible effect of local electron-density variations inside an atom). From Eq. (2.4) it is known that R º $\frac{R_E 3}{\wedge}$ for atomic number density, so that the electron number density $R_/ º \hat{} \frac{R_E 3 \wedge}{\wedge} ‰ º 3ß$ so that $.\,_{CS}$ will be given by the following proportionality,

$$.\,_{CS} º 3. \tag{2.10}$$

Eq. (2.10) will be used later to reach an important conclusion about optimal material choices for shields against ionising photons.

2.2.3 Pair production

The third of the three principal interaction process by which ionising photons are attenuated by matter, is pair production (PP), which can be represented as

$$\# Ò /^{€} € /^{•}.$$

When the energy $I_\#$ of the incident photon is at least twice or that of the electron rest-mass energy, $a7/-^{\#}b$, i.e., $I_\# \quad \#a7/-^{\#}bß$ i.e., in excess of "Þ!## MeV, the conversion of the photon into an electron-positron pair in the field of an atomic nucleus becomes energetically possible, hence the term pair production. The photon cross-section for this interaction process remain quite low until $I_\#$ approaches several MeV, and as a result, pair production is the dominant interaction mechanism for high-energy photons. Figure 2.5 on page 15 shows events in the pair production processes. The incident photon of energy 2/ approaches a nucleus, and an electron-positron pair is produced, $/^{€}$ and $/^{•}$. The positron-electron pair is generally projected in the forward direction, relative to the direction of the photon. The degree of forward projection increases with increasing photon energy.

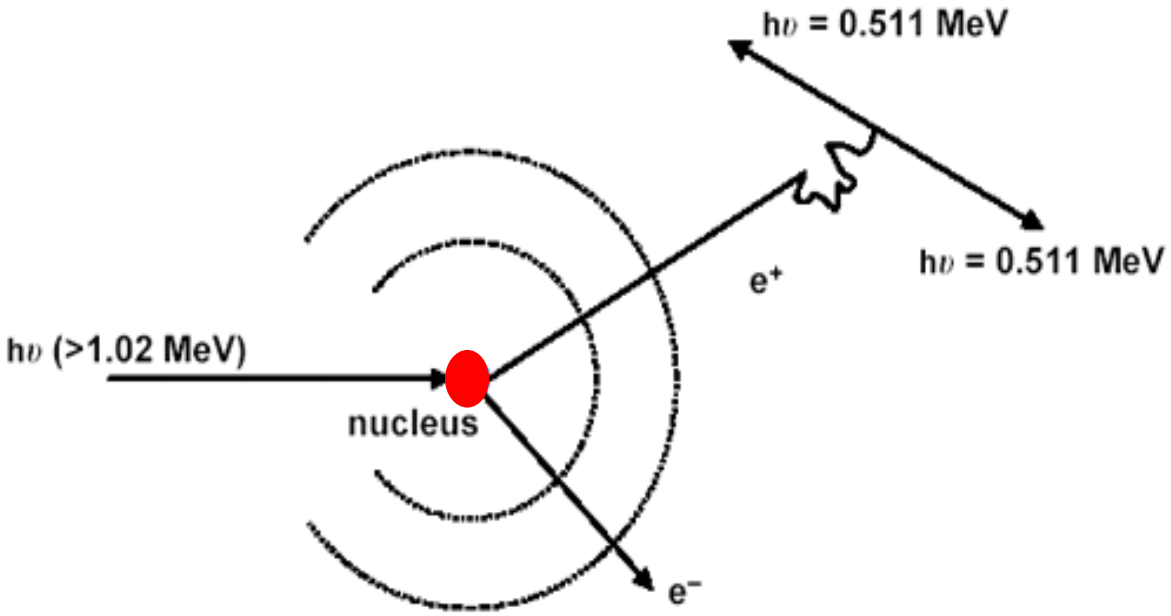

Figure 2.5: *Events in the pair production process (Alphen, 1990: 71).*

Pair production may also occur in the field of an atomic electron, but the cross-section for this is significantly lower than the cross-section for this happening in the electrical field of an atomic nucleus. Furthermore, the photon threshold energy, $I_{\#\_PP\_th}$ depends on the mass Q of the recoil particle, whose coulomb field allows the pair production process to occur. In the field of a nucleus,

$$I_{\#\_PP\_th} \approx 2m_e c^2 \left(1 + \frac{m_e}{Q}\right)$$

where m_e is the mass of an electron (Leroy and Rancoita, 2004: 158; Marmier and Sheldon, 1969: 123). For this reason, when the pair production occurs in the vicinity of a nucleus, the threshold energy is $I_{\#\_PP\_th} = 2m_o c^2$, because $m_e \ll Q$, while in the proximity of an electron, $I_{\#\_PP\_th} = 4m_o c^2$, because $\frac{m_e}{Q} = 1$. When pair production occurs in the proximity of an atomic nucleus, in the electrical field of a nucleus, the massive nucleus recoils with negligible energy. Then essentially all the photon energy, $I_\# \approx I$, is converted into $2m_o c^2$ of mass, plus the kinetic energies K_{e^+} and K_{e^-} of the positron and electron pair (Turner, 1995: 183; Krane, 1987: 201),

$$I_\# \approx 2m_o c^2 + K_{e^+} + K_{e^-}. \qquad (2.11)$$

In this case, the excess energy is continuously distributed between the electron-positron pair, a negligible amount going to the recoiling nucleus. However, the kinetic energy of the electron or the positron can vary from zero to a maximum of $I_\# - 2m_o c^2$. After production of a pair, the positron and electron are projected in a forward direction, relative to the direction of the incident photon, and lose their kinetic energy by excitation, ionisation, *bremsstrahlung* production (continuous-spectrum X-rays), as with any other high energy electron (charged particles). The energies of the *bremsstrahlung* photons produced in this way are far lower than that of the incident photon. When the positron, has lost most of its energy, it recombines with its anti-particle, namely a

negatively charged electron (negatron), and form positronium. Positronium is the bound system, analogous to the hydrogen atom, formed by an electron positron pair orbiting about their mutual center of mass. Positronium exists for about 10^{-7} seconds before the electron and positron annihilate. Both leptons disappear, and two *annihilation photons,* each of which has an energy equal to the rest-mass of an electron, 0.511 MeV, are produced:

$$e^- + e^+ \rightarrow 2\gamma (0.511 \text{ MeV}).$$

The two annihilation photons move in opposite directions, at an angle of approximately 180°.

Cross-section for pair production

The cross-section for pair production dominates both photoelectric absorption and Compton scattering in the high energy region. As a result, it is the dominant photon attenuation mechanism for photons with energy $h\nu > 5$ MeV for media with $Z > 25$. It is evident that pair production can easily lower photon energies by an order of magnitude (e.g., from 5 MeV to 0.511 MeV). This final energy (0.511 MeV) falls right in the energy region where the photoelectric absorption dominates photon attenuation, especially in higher-Z materials. In this fashion, pair production can serve as the first event in the chain of interactions that will eventually degrade photon energy to a value below the threshold for ionisation. When photons reach such a low energy, they are highly absorbable and have also practically lost most of their ionising nature and biological hazard potential.

Above the threshold energy for pair production, the cross-section for pair production, $\sigma_{pp}(h\nu, Z)$, is a function of the incident energy $h\nu$ and the atomic number Z of the attenuating medium. If the incident energy $h\nu$ is kept constant, it is found that (Marmier and Sheldon, 1969),

$$\sigma_{pp}(Z) \propto Z^2. \qquad (2.12)$$

If the variable Z is kept constant, it is found that $\sigma_{pp}(h\nu)$ is zero below the threshold energy, then rises monotonically with $h\nu$, tending to a plateau (Figures 2.7, 2.8 and 2.9).

Incident energy ($h\nu$) and atomic number (Z) regions where the three principal photon attenuation mechanisms dominate, are depicted in Figure 2.6 on page 18.

Linear interaction coefficient for pair-production

An expression for the linear interaction coefficient for pair production can also be easily derived, τ_{pp}, for an element with mass density ρ and atomic number Z. Because

$\mu = \rho R_5$, where $R = R_0 \frac{3}{A}$, it follows from the expression for μ_{PP} that,

$$\mu_{PP} = \left(\frac{3}{A}\right) Z^2 = 3A. \qquad (2\text{-}13)$$

This expression will be used later to reach an important conclusion about material choices for optimal shields against ionising photons.

Dependence of the linear interaction coefficient μ for the three dominant attenuation mechanisms for ionising photons, on Z and I

As explained, ionising photons interact and lose energy by three main reaction mechanisms: (1) photo-electric absorption, (2) Compton scattering and (3) pair production. These 3 principal interactions of ionising photons and their linear interaction coefficients are summarised in Table 2.1, using equations (2.7), (2.10) and (2.13).

Table 2.1: *The three principal interaction mechanisms of ionising photons, and their linear interaction coefficients.*

Interaction	**Linear interaction coefficient**
Photo-electric absorption (PEA)	$\mu_{PEA} = 3Z^3$
Compton scattering (CS)	$\mu_{CS} = 3$
Pair production (PP)	$\mu_{PP} = 3Z$

It follows clearly from Table 2.1 that there exists a simple recipe for maximising the efficiency of a photon shield: ***Maximise the atomic number Z and maximise the density ρ of the shielding material.***

In the high photon-energy region, where pair production is dominant, both ρ and Z should be maximised with equal weight to maximise shield efficiency. In the low-energy region, where photo-electric absorption of photons is dominant, it pays significantly more to maximise Z than to maximise ρ. In the intermediate photon energy region, where Compton scattering dominates, the atomic number Z has very little effect on shield efficiency, and the parameter that should be maximised to maximise shield efficiency, is the mass-density ρ of the shield. The overall "recipe" for optimal shield design against ionising photons, is to maximise both the atomic number Z and mass-density ρ of the shielding material. Some of the best shields against ionising photons will therefore be tungsten (W; $\rho = 18.9$ g.cm^{-3}; $Z = 74$), lead (Pb; $\rho = 11.3$ g.cm^{-3}; $Z = 82$) and depleted uranium (DU; $\rho = 18.9$ g.cm^{-3}; $Z = 92$).

Incident energy and atomic number regions where the different photon interaction mechanisms dominate

Figure 2.6 shows that Compton scattering is the dominant mechanism for the lowering of photon energy for incident photons in the approximate energy ranges,

$$I_{\#}^{\,w} - \begin{cases} \text{Ú} \grave{0}0.1\ \text{MeV}; 10\ \text{MeV}\acute{0} & \text{for } \wedge\ \ddot{Y}\ \#!\ \text{Þ} \\ \text{Ý} \grave{0}0.2\ \text{MeV}; 8\ \text{MeV}\acute{0} & \text{for } \#!\ \bullet\ \wedge\ \ddot{Y}\ \%! \\ \hat{\text{U}} \text{ý} \grave{0}0.3\ \text{MeV}; 6\ \text{MeV}\acute{0} & \text{for } \%!\ \bullet\ \wedge\ \ddot{Y}\ '!\ \text{ß} \\ \text{Ù} \grave{0}0.5\ \text{MeV}; 5\ \text{MeV}\acute{0} & \text{for } \wedge\ \check{z}\ '!\ \grave{a} \end{cases}$$

Also shown in Figure 2.6, are lines illustrating the values of Z and $I_{\#} = 2$@ for which the two neighbouring cross-sections are equal; the regions where each type of interaction is dominant, are also shown.

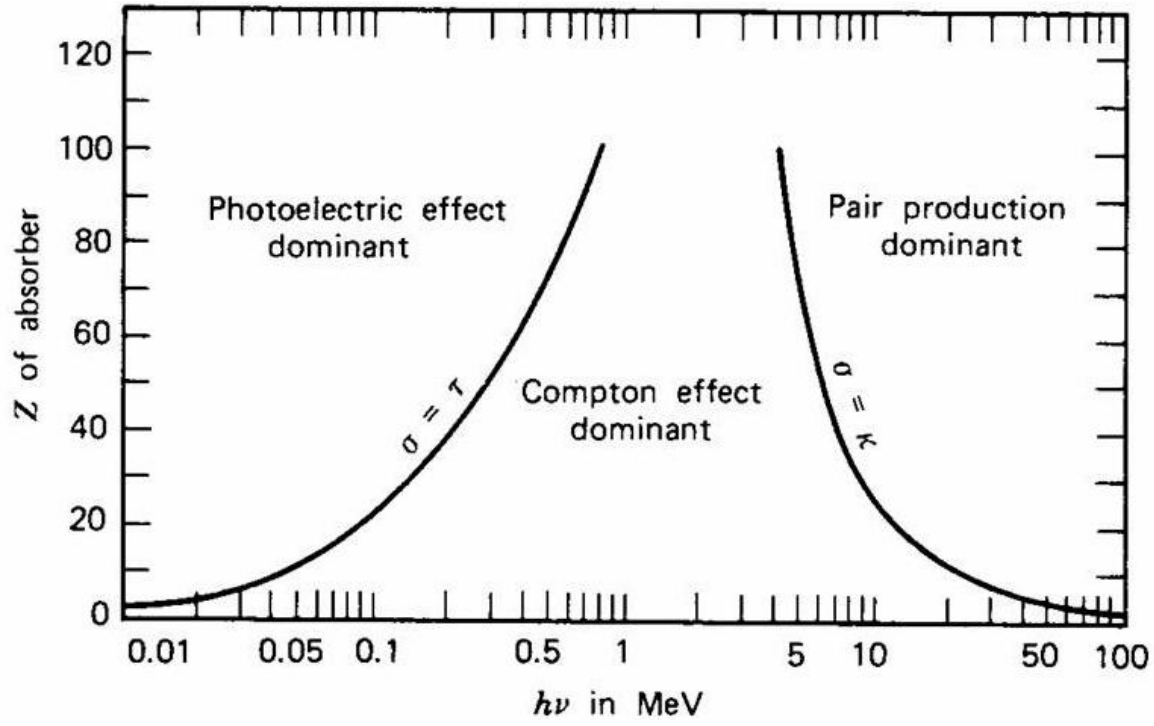

Figure 2.6: *The relative importance of the three major types of interaction mechanisms of ionising photons (Knoll, 1999:52).*

As explicated, the photon cross-section for pair-production process remain quite low until $I_{\#}$ approaches several MeV, and as a result, pair production is the dominant interaction mechanism for high-energy photons. This cross-section for pair production, $\mathbf{5}_{PP}$, is illustrated in Figures 2.7, 2.8 and 2.9 (page 19 to 21) for the elements hydrogen (Z = "), lead (Z = 82) and iron (Z = 26).

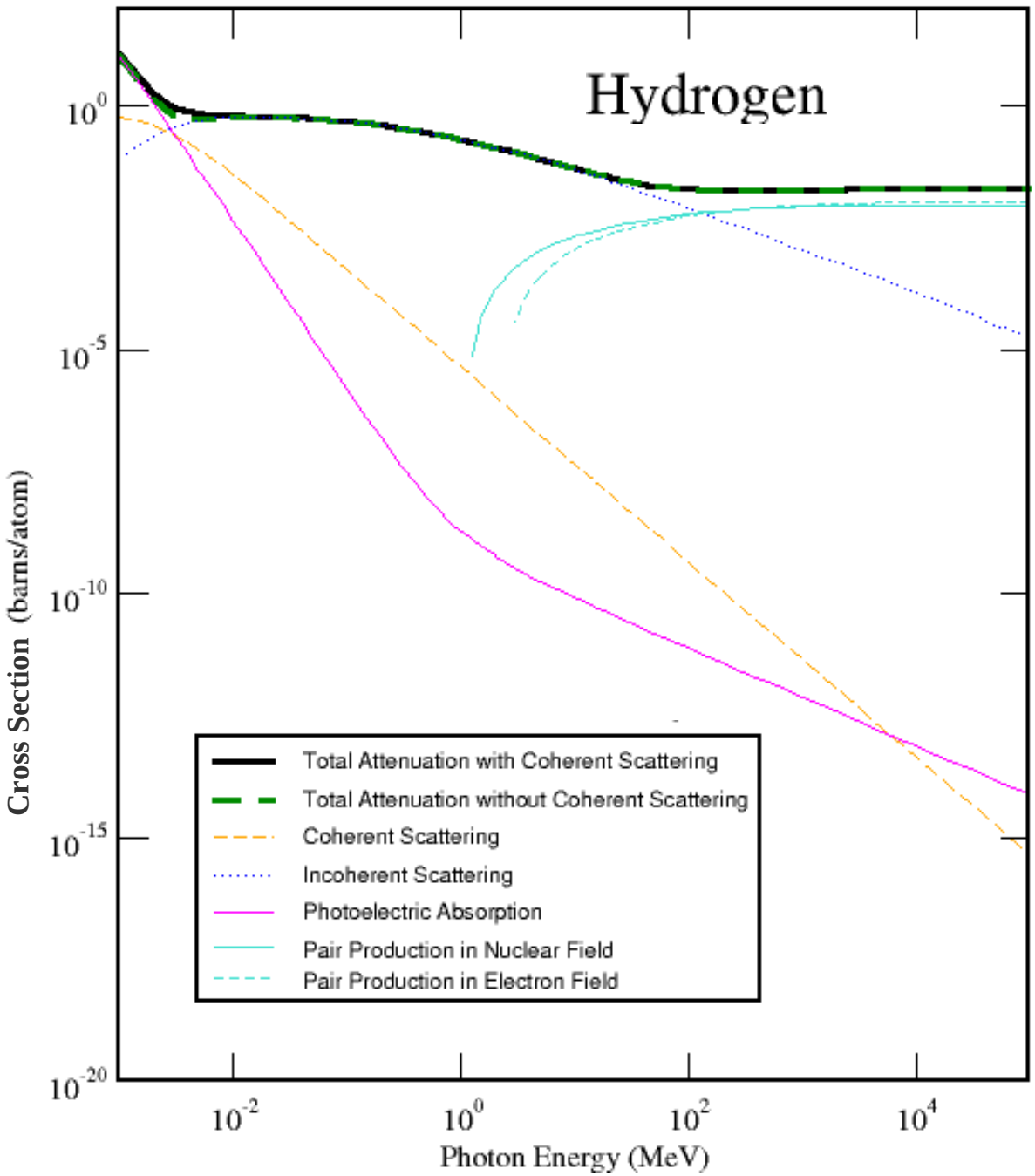

Figure 2.7: *Pair production cross-sections for photon interactions in hydrogen (H) (NIST, 1998).*

It is notable in Figures 2.7 that photoelectric absorption only dominate for $\lambda \approx 3 \exp(-3)$ MeV. CS dominate for $3 \exp(-3) \approx \lambda \approx 100$ MeV. PP only dominate for $\lambda \gg 100$ MeV.

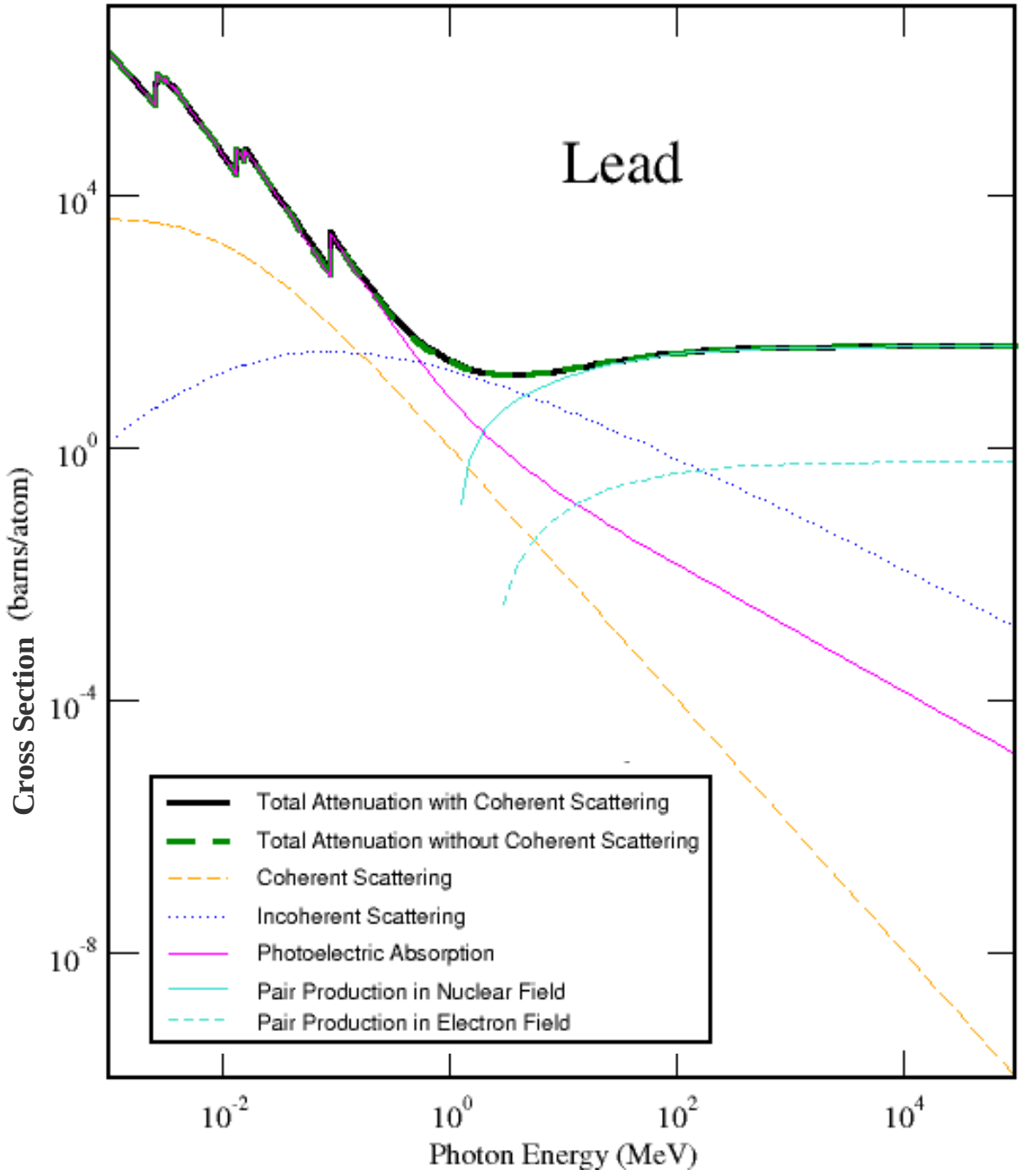

Figure 2.8: *Pair production cross-sections for photon interactions in lead (Pb) (NIST, 1998).*

Of note in Figure 2.8, PEA only dominate for $\mathbf{l}_{\#}\ \mathbf{p}$ 1 MeV. CS dominate for 1 $\mathbf{p}\ \mathbf{l}_{\#}$ $\mathbf{p}$ 2 MeV. PP only dominate for $\mathbf{l}_{\#}\ \mathbf{q}$ 2 MeV.

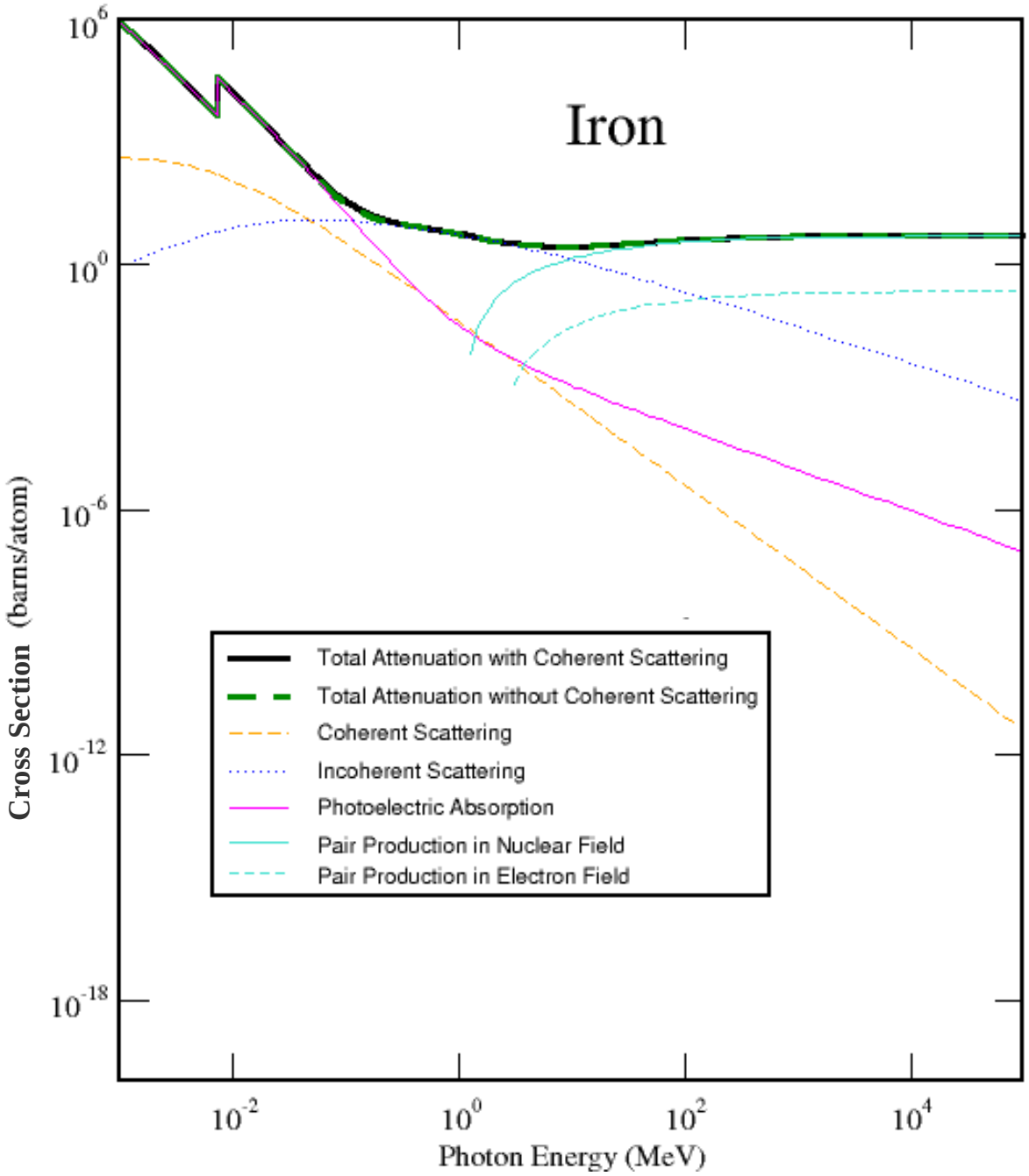

Figure 2.9: *Pair production cross-sections for photon interactions in iron (Fe) (NIST, 1998).*

It is evident in Figure 2.9 that PEA only dominate for $l_{\#} p$ 1 exp(•1) MeV. CS dominate for 1 exp(•1) $p\ l_{\#}\ p$ 10 MeV. PP only dominate for $l_{\#}\ q$ 10 MeV.

2.2.4 Photonuclear reactions

In photonuclear reactions, the absorber nucleus captures an ionising photon and emits a nucleon produced in a nuclear reaction; in most instances, a neutron is emitted. The photon energy $l_{\#}$ must exceed a threshold value, which depends on the absorbing nucleus, to make photonuclear reactions, i.e., photon-induced nuclear reactions, possible.

Threshold energies for photonuclear reactions are well above the energies of the photons emitted by ^{60}Co, ^{137}Cs, and most other radionuclides. The cross-section for photonuclear reactions are also orders of magnitude smaller than the combined probabilities for the photoelectric absorption (§2.2.1), Compton scattering (§2.2.2), and pair production (§2.2.3). However, unlike these three mechanisms, photonuclear reactions can produce neutrons, which pose special *radiation protection* problems, and can produce neutron absorption reactions in matter and so induce residual radioactivity. Furthermore, residual nuclei following photonuclear reactions are often radioactive themselves.

Two isotopes have particularly low energy thresholds for a#ß8b nuclear reactions: ^{9}Be at 1.667 MeV and ^{2}H at 2.225 MeV (Shultis and Faw, 1996: 84). Beryllium is not found in food, but ^{2}H is present as a small fraction of hydrogen, at a natural abundance of about 0.015%. Therefore all food will contain some ^{2}H. For this reason, the maximum photon energy that may be used in food irradiation, must be below 2.225 MeV, and preferably also below 1.667 MeV, in the unlikely event that some beryllium is present in the irradiation chamber. As a result, it is not permitted to employ photon sources emitting ionising photons with energies above about 1.6 MeV in food irradiators. The use of higher energy ionising photons will produce neutrons and residual radioactivity in food, which is totally unacceptable, of course. The maximum photon energy emitted by ^{60}Co is 1.332 MeV, which is safely below the threshold energy for Ð#ß8Ñ and other types of photonuclear interactions.

2.3 Behaviour of photons in an absorber

As pointed out in §2.2, ionising photon penetration in matter is governed statistically by the probability per unit distance travelled that a photon interacts by one physical mechanism or another. This likelihood is called the linear interaction coefficient, ., or macroscopic cross section, and has the dimensions of inverse length (cm•"). This macroscopic cross section is of great importance in matters concerning *radiation shielding;* it is, however, dependent on the shielding material (Bashter, 1997). The density of a material does not have a unique value but depends on the physical state of the material, for instance, in the case of concrete, its moisture content. The linear interaction coefficient for ionising photons of a given energy in a given material comprises the individual contributions from the significant physical mechanisms explained in §2.2.1 to §2.2.3 and is given as

$$\cdot_{\text{total}} = \cdot_{\text{PEA}} + \cdot_{\text{CS}} + \cdot_{\text{PP}}.$$

where $\cdot_{\text{PEA}}$, $\cdot_{\text{cs}}$, and $\cdot_{\text{PP}}$ represents, respectively, the linear interaction coefficients for photoelectric absorption, Compton scattering and pair production. Use of the linear interaction coefficient is limited by the fact that it varies with the density of the absorber, even though the absorber material is the same. As a result, the attenuation properties of ionising photons are practically always listed, in compilations or databases, as the *mass attenuation coefficient,* which is defined as (Knoll, 1999: 54)

$$\text{Mass attenuation coefficient } \left(\frac{\mu}{\rho}\right)_{\text{total}} = \frac{1}{\rho}\left(\tau_{\text{PEA}} + \sigma_{\text{CS}} + \kappa_{\text{PP}}\right). \qquad (2.14)$$

where ρ represents the mass-density of the medium. For the given photon energy, the mass attenuation coefficient does not change with the mass-density of a given absorber; for instance, it is the same for water whether present in liquid form (high density) or vapour form (low density).

The mass attenuation coefficient of a mixture, or compound, of elements can be computed; hence, Eq. (2.14) becomes

$$\left(\frac{\mu}{\rho}\right)_{\text{compound}} = \sum_{i} A_i \left(\frac{\mu}{\rho}\right)_i .$$

where the A_i factors represent the mass-fraction of element i in the compound or mixture. Figure 2.10 illustrates the mass attenuation coefficients for a number of materials for photons with energies from 0.01 MeV to 10 MeV. The graphs reflects the physical mechanisms discussed in §2.2. At low photon energies the binding of the electrons must be taken into account, and photoelectric absorption is the main interaction. High atomic number Z materials provide remarkable attenuation and absorption of low-energy ionising photons, which decrease quickly with increasing photon energy. When the photon energy is several hundred keV or more, the binding of the atomic electrons becomes relatively less important and the predominant interaction is Compton scattering. Compton scattering continues to be dominant essential above the 1.02 MeV pair production threshold until the latter process takes over as the main interaction. Attenuation by means of pair production is normally enhanced by a large nuclear charge of the absorber, i.e., pair production.

Since all chemical elements, except hydrogen, contain about the same number of electrons per unit mass, there is relatively little difference between the values of the mass attenuation coefficients for the different materials — see Figure 2.10 on page 24.

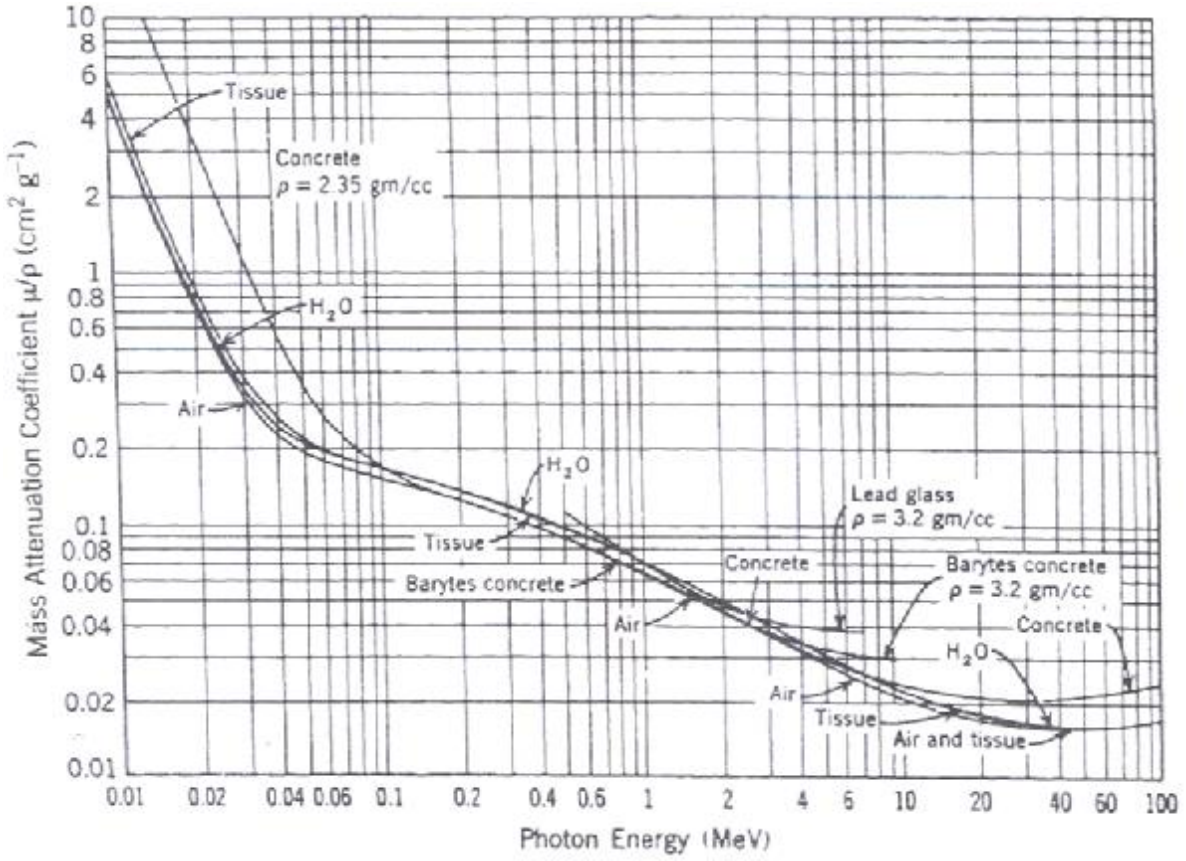

Figure 2.10: *Mass attenuation coefficients for different materials (Turner, 1995:188).*

Cross-section data compilations used by practically all radiation transport codes, contain photon cross-sections as mass attenuation coefficients, in unit (cm^2 g). The user specifies material densities in the input data set, which are then used by the code to calculate the linear interaction coefficients . for the transport calculation.

2.4 Absorption and transfer of photon energy

The energy absorbed by the absorber, and the energy transferred to the absorber are related to the linear interaction coefficients. As discussed in §2.2, the attenuation is a result of three principal interactions types; not all energy of the incoming photons that interact in the material is necessarily absorbed. This section will discuss each of the principal energy loss mechanisms in turn, examine both the energy transfer coefficients and the energy absorption coefficients.

In the photoelectric absorption, absorption of a photon with energy, , by an atom of the absorber produces a secondary electron with initial kinetic energy given in Eq. (2.1). Following the ejection of the photoelectron, the inner shell vacancy in the atom of the absorber is instantly filled by an electron from an upper level. This and succession electronic transitions are accompanied by the simultaneous emission of photon or Auger

electrons[3]. The fraction of the incident intensity transferred to electrons, that is, the photoelectron and Auger electrons, can be expressed as $\mu \cdot \delta/\rho$, where δ (delta) is the average energy emitted as fluorescence radiation following photoelectric absorption in the material. In accordance with the mass attenuation coefficient defined in Eq. (2.14), describing the fraction of photons that interact by photoelectric absorption per $g\,cm^{-2}$ of matter traversed, the mass energy transfer coefficient can then be expressed as

$$\frac{\tau_{tr\_PEA}}{\rho} = \frac{\tau_{PEA}}{\rho}\left(\mu - \frac{\delta}{h\nu}\right) \tag{2.15}$$

This gives the fraction of the intensity that is transferred to the electrons per $g\,cm^{-2}$. Although the Auger electrons and even the photoelectrons are likely to be completely stopped in the absorber; to the extent that the photoelectron and Auger electrons subsequently emit photons as bremsstrahlung, the energy transfer coefficient does not satisfactory explain energy *absorption* in the absorber (Turner, 1995). This point will be explained after defining the mass energy transfer for pair production and Compton scattering.

For Compton scattering of monoenergetic photons (Figure 2.4), the mass energy transfer coefficient is defined as,

$$\frac{\tau_{tr\_CS}}{\rho} = \left(\frac{\tau_{CS}}{\rho}\right)\left(\frac{E_{avg}}{h\nu}\right). \tag{2.16}$$

The factor $E_{avg}/h\nu$ gives the average fraction of the incident photon energy that is converted into the kinetic energy of the Compton electrons. As for the photoelectric absorption, the energy transfer coefficient [Eq. (2.16)] take no consideration of succession bremsstrahlung by the Compton electrons.

A photon of energy defined in Eq. (2.11) produces an electron positron pair with a total initial kinetic energy, defined after Eq. (2.11). Accordingly, the mass transfer coefficient for pair production is related to the mass attenuation coefficient, defined in Eq. (2.14), as:

---

[3] Auger electron emission is an atomic process (and not a nuclear process) whereby an electron is ejected from an atom. A preceding process leaves the atom with a vacant state in its electron configuration. Usually, an electron with a higher energy state will drop into the vacant state and the energy difference will be emitted as an X-ray. The energy of the X-ray will be the energy difference between the two levels

$$h\nu_{Xray} = h_2 - h_1.$$

Occasionally, instead of producing an X-ray, the energy is transferred to an outer electron, causing it to be ejected from the atom. The emitted Auger electron has an energy

$$h\nu_{Auger} = (h_2 - h_1) - h,$$

where h, is the binding energy of the emitted electron. Auger emission is favoured for low-Z materials where electron binding energies are small. Auger electrons have low kinetic energies.

$$\frac{\rho_{tr\_PP}}{\rho} = \frac{\rho_{PP}}{\rho}(E_\gamma - 2m_e c^2) \qquad (2.17)$$

This mathematical relationship applies to pair production in the field of an atomic nucleus; the small contribution from triplet production is neglected (§2.2.3). So, the total mass energy transfer coefficient (μ_{tr_total}/ρ) for photons of energy E_γ in a given material is obtained by combining the last three equations,

$$\frac{\rho_{tr\_total}}{\rho} = \frac{E_\gamma}{\rho}(\mu_{tr\_PEA} + \mu_{tr\_CS} + \mu_{tr\_PP}). \qquad (2.18)$$

This coefficient $\frac{\rho_{tr\_total}}{\rho}$ determines the total initial kinetic energy of all electrons generated by the photons, both directly as in photoelectric absorption, Compton scattering, pair production, and indirectly as Auger electrons. Except for possible subsequent bremsstrahlung generated by these electrons, the energy absorbed in the instant proximity of the interaction site would be the same as energy transferred there.

Let K be the average fraction of the initial kinetic energy transferred to electrons that is subsequently emitted as bremsstrahlung, then the mass energy absorption coefficient can be defined as,

$$\frac{\rho_{en}}{\rho} = \frac{\rho_{tr\_total}}{\rho}(1 - K). \qquad (2.19)$$

Generally, the factor K is largest for materials having high atomic number Z and for photons of high energy. Figure 2.11 on page 27 illustrates the mass energy absorption coefficients for the materials considered in §2.3.

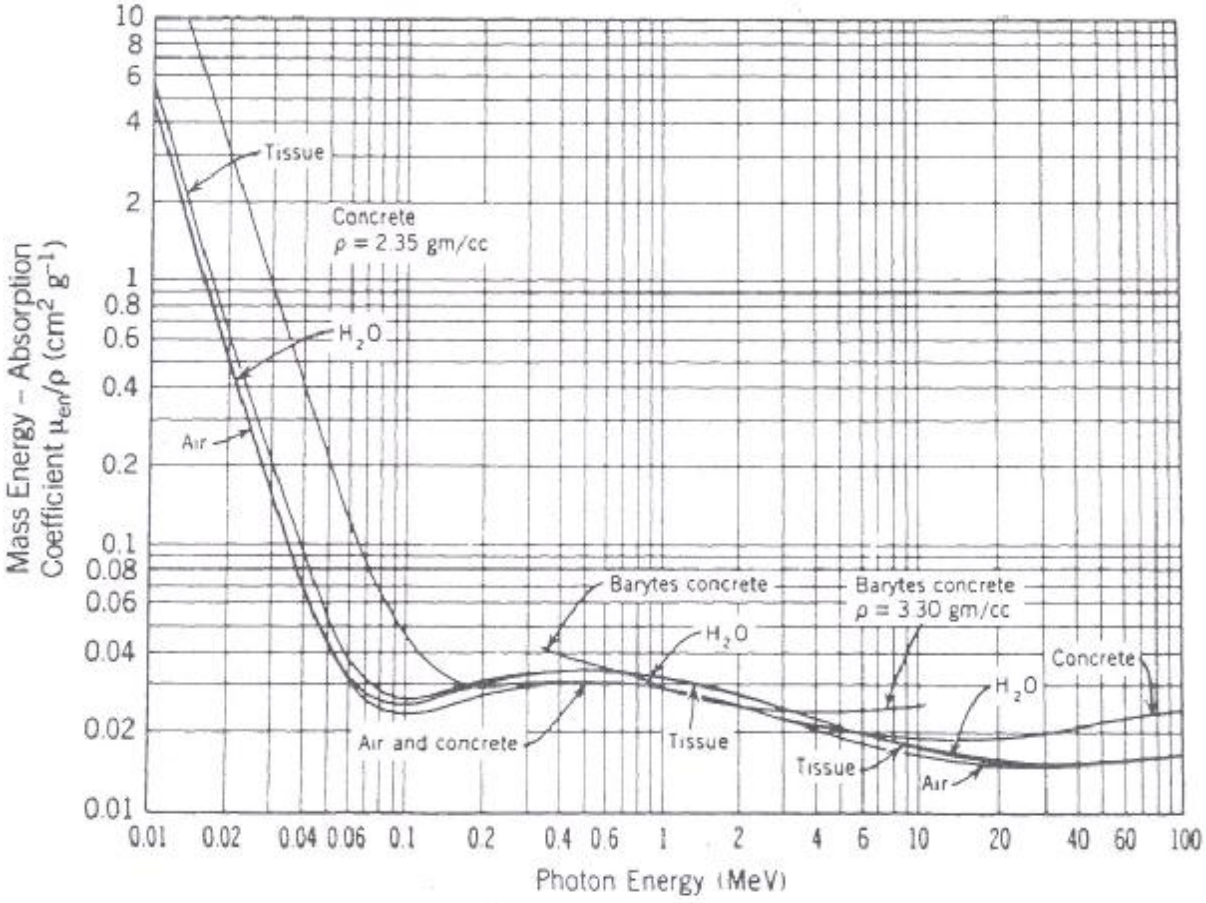

Figure 2.11: *Mass energy-absorption coefficients for different materials (Turner, 1995:194).*

Differences in the various coefficients are illustrated by the data shown for water and Pb in Table 2.2, page 28. It is clear that bremsstrahlung is relatively insignificant in water for photon energies less than ¸ 10 MeV, that is, .$_{tr}$Î3 is not much larger than .$_{en}$Î3. In lead, on the other hand, bremsstrahlung accounts for a significant difference in the mass energy transfer and mass energy absorption coefficients at much lower energies; as expected from a high atomic number ^ material.

Table 2.2: *Mass attenuation, mass energy transfer, and mass energy absorption coefficient ($cm^{\#}g^{-1}$) for photons in water and lead (Turner, 1995:195).*

Photon Energy (MeV)	Water			Lead		
	μ/ρ	μ_{tr}/ρ	μ_{en}/ρ	μ/ρ	μ_{tr}/ρ	μ_{en}/ρ
0.01	5.33	4.95	4.95	131.	126.	126.
0.10	0.171	0.0255	0.0255	5.55	2.16	2.16
1.0	0.0708	0.0311	0.0310	0.0710	0.0389	0.0379
10.0	0.0222	0.0163	0.0157	0.0497	0.0418	0.0325
100.0	0.0173	0.0167	0.0122	0.0931	0.0918	0.0323

Tenth-value thicknesses

For the effective shielding of ionising photons, the atomic number ^ and density 3 of an element should be as high as possible as can be seen from Table 2.1. Accordingly, lead (atomic number ^ œ 82; density 3 œ 11.3 g.cm•^{3}) is a particularly effective shield against ionising photons. Depleted uranium (atomic number ^ œ 92; density 3 œ 18.9 g.cm•^{3}) would be even more effective. Tungsten (^ œ 74, density 3 œ 18.9 g.cm•^{3}) is also generally a somewhat better shielding material against ionising photons than lead (Pb), on account of its high mass-density.

A convenient concept to use as an approximate measure of shielding effectiveness against ionising photons, is the ***tenth-value thickness.*** This is the thickness of material that will reduce the dose rate to fraction $\frac{1}{10}$ of its original value. The tenth-value thicknesses for important radionuclides that emit ionising photons, and some common materials, are listed in Table 2.3 on page 29 .

Table 2.3: *The tenth value thickness for combinations of important shielding materials, and important radionuclides that emit ionising photons.*

Material	**Tenth value thickness** (cm)				
	^{60}**Co**	^{137}**Cs**	^{22}**Na**	^{24}**Na**	^{65}**Zn**
Lead (Pb)	4.5	2.3	3.4	5.7	3.9
Iron (Fe)	8.2	7.1	7.9	11.1	8.7
Aluminium (Al)	24	24	26	34	28
Concrete	27	25	28	38	30
Water (H_2O)	59	58	62	81	65

2.5 Conclusions and application

From Table 2.1 on page 17 it is seen that the simple recipe for maximising the ability of a given thickness of shielding material to attenuate photons, is to maximise the atomic number **^** and the mass-density **3**. In principle, therefore, materials such as lead and tungsten will be the best photon shields. However, for an industrial irradiation facility, the cost of the shield must be minimised, while shield thickness is of no concern. Therefore, rather than using 20 cm tungsten, e.g., concrete walls with thicknesses of e.g., 150 cm to 200 cm thickness, are used—this makes much more economic sense.

2.6 Biological shielding and maximum tolerable dose rates

A “biological shield” is a shield that has to shield ionising radiation so well that the dose rate outside it is safe enough for prolonged human occupation. When a biological shield is designed, a material composition, material placement and material thickness prescription must be given that will ensure that the dose rate outside the shield is acceptably low.

How low is “acceptably low”? This question must be answered with reference to (1) dose limits and (2) the average natural background dose rate at the surface of planet earth. Under the assumption that the person outside the biological shield is not a radiation worker, so that the dose limit of 1 mSv per annum applies, and that the person works there for 8 hours per shift, 240 shifts per year, the maximum tolerable dose rate, will be $\frac{1000\ \mu Sv}{240\ ,\ 8\ hours}$ **œ** 0.52 µSv/h. The average annual background dose rate, coming from sources outside the human body, on the surface of planet earth is composed of 0.5 mSv from terrestrial radiation, plus 0.4 mSv from cosmic radiation, giving a total of about 0.9 mSv per year, i.e., a dose rate of 0.11 µSv/h. From these two derived dose rates, derived from

the dose limit as well as from natural background dose rates, the following guidelines may be formulate, using a little sound judgment:

- If human occupancy close to the outside surface of the biological shield around a radiation source will be below 1 hour per shift, and/or restricted to radiation workers, then transmitted dose rates must be below about 1 µSv/h.
- If human occupancy close to the outside surface of the biological shield around a radiation source will be above 1 hour per shift, and if persons who are not registered radiation workers will have to work there, transmitted dose rates must be below about 0.1 µSv/h.

Chapter 3
Irradiation facilities

3.1 Introduction

Most industrial and insect sterilization irradiators utilize either ^{60}Co or ^{137}Cs as the source of radiation. These radionuclides are chosen because of the relatively high energy of their gamma rays and fairly long half-life (5.27 years for ^{60}Co and 30.1 years for ^{137}Cs). ^{60}Co is almost solely used as the gamma radiation source for industrial use nowadays because of the production method being easier and its non-solubility in water. For safe use the radiation source must be enclosed with well-designed bulk shielding (also referred to as the biological shield) of adequate thickness. This is needed to maintain dose rates outside the irradiation chamber at acceptably low values, i.e., at levels that will ensure that personnel and the public will never be exposed beyond the legal predefined dose limits (Appendix A.1). These shields are *passive* (stationary) radiation containment systems, which form the foundation of the engineered radiation safety system of irradiators. For example, concrete is the material of choice for the biological shielding walls of practically all irradiation facilities. Irradiation chambers may also have thick shielding doors ("plug doors") which are *active* (motorised, mobile) facets of radiation containment systems. This chapter describes the key features of the three irradiation facilities under study, as well as the characteristics of the ^{60}Co ionising photon source employed in these facilities.

3.2 The sterile insect technique

The sterile insect technique (SIT) is a biological method that has proven to be an effective method for the area-wide control or eradication of pest insects species such as mosquitoes. It is a species-specific and environmentally non-polluting technique. The technique is based on insect genetics for population control or eradication, and it can be applied only to pest species that reproduce by sexual means. This distinguishes the SIT from the use of chemical and physical agents such as alkylating agents, antimetabolites, that poses hazards to both workers in mass-rearing factories, and to the non-targeted species. The SIT is effective only if the sexually sterile males are aggressive enough and successfully compete with wild males in searching for and mating with indigenous females resulting in no viable offspring. The method should be used only when a thorough knowledge has been acquired of the biology, ecology and behaviour of the targeted pest species.

The SIT may be considered as a form of *"birth control"* for pest insect populations. The technique involves the colonisation and mass rearing of the targeted pest species by the sterilization of the male species by exposing the insects to a specific dose of gamma radiation emitted from such radionuclides as ^{60}Co (§3.8) or ^{137}Cs and then sustained systematic releases of the sterile males among the indigenous population. Over time, the

fertile population and reproductive capacity are progressively reduced until fertile matings do not occur and the population is eliminated. Most researchers have concluded that sterilized females do not play an essential role in controlling or eradicating the pest as it may be detrimental to the control/eradication efforts (Robinson, *et al.*, 1999). In spite being sterile, they may attempt to aviposit, or obtain a blood meal, and so cause the type of damage that the control/eradication program is intended to overcome. Highly successful, area-wide SIT programs have been conducted against the New World screwworm, in the USA, Mexico and Central America and also in Libya, where the SIT was used in the successful control of a serious outbreak. Other targets of area-wide, SIT programs include the Mediterranean fruit fly (medfly), in various parts of Latin America and the codling moth, in Canada, and tsetse flies, in Nigeria and Zanzibar.

3.3 Food and polymer irradiation

Irradiation can be used to destroy pathogens and parasites in food products and packaging materials such as polyethylene film. Over the years irradiation has been shown to extend the shelf life of fresh fruits and vegetables, to control sprouting of fresh vegetables (garlic, onion, potatoes, carrots), to accelerate the maturing of cheese, to function as a replacement for post-harvest fumigants (methyl bromide, ethylene dibromide, and ethylene oxide) used in grain products, and to extend the shelf life of fresh meat products.

During irradiation, the food pallets are exposed to the ionising energy source to be discussed in §3.8 and the food absorbs the required dose of radiation. The absorbed dose is controlled by the intensity of the radiation source and the time of exposure of food to the source. No harmful by products are produced when food is irradiated at the low doses prescribed for fruits and vegetables. Irradiation kills foodborne pathogens by destroying the DNA of the bacteria. The exposure times and energy levels of radiation sources approved for food are inadequate to induce radioactivity in the food products.

When a polymer is exposed to the source (§3.8) emitting ionising radiation, its electronic chemical bonds are broken and new bonds are formed between adjacent polymer molecules. For example, polyethylene film is often used as a packaging material that can be shrink-wrapped around the product. To increase the strength of such polythylene wrap, gamma irradiation of the plastic greatly increase its strength. The stabilization process—which occurs during, immediately after, or even days, weeks, or months after irradiation—often results in physical and chemical cross-linking or chain scission. Resultant physical changes can include embrittlement, discoloration, odor generation, stiffening, softening, enhancement or reduction of chemical resistance, and an increase or decrease in melt temperature.

3.4 The Citrusdal insect sterilization facility

Organisation and mission

During 2007, a private company, Citrus Research International constructed a new, commercial insect sterilization irradiation facility in Citrusdal in the South Western Cape region of South Africa (Hofmeyr, personal communication, 2006). This facility employs a very successful ionising radiation based method for drastically reducing pest insect population. The SIT discussed in §3.2, uses the radionuclide ^{60}Co as the source of ionising radiation. The Citrusdal facility is designed for the sterilization of insects, notably False Codling Moth, which poses a serious pest problem in the Citrusdal agricultural area in South Africa. The insects are irradiated to a dose of ionising radiation sufficient to sterilize them, and are subsequently mass released (see Figure 3.1 on page 34) into the environment to reduce its local population.

Cobalt-60 source

The design-base activity of the ^{60}Co source for the Citrusdal facility was 740 TBq (20 kCi), i.e., the shield design was done for this activity. The actual activity of the source will initially be close to the design-base activity of 740 TBq, and will, of course, diminish with time, as a result of continuous radioactive transitions. The ^{60}Co source was acquired with once-off funding and logistical assistance from the IAEA, based in Vienna, Austria.

The source 15 cm long cylindrical pin and of 1.5 cm in radius is mounted inside a longer, thin-walled stainless steel cladding tube. Its surface area is 155.5 cm$^{\#}$ (**E œ #1<# € #1<2**). The source is raised to a height of about 70 cm above floor level during irradiation and when not in use, it is lowered into a shielding pot which mainly employs lead (Pb) as shielding material. When the ^{60}Co source is lowered into this lead pot, it is in its shielded position. With the source in this safe position, personnel are allowed access to the irradiation vault.

Insect release over farmland

Figure 3.1 on page 34 shows the technique common used to release sterilized insects over farmlands, using a gyrocopter. The insects stream from the black pipe underneath the pilot.

Figure 3.1: *A Gyrocopter releasing false codling moths sterilized with the SIT.*

Turntable

In order to perform irradiation of insects, the source rod is hoisted out of its shielded position underneath the turntable. The active part of the source rod is raised to a position just above a circular primary turntable fitted with eight smaller secondary turntables — see Figure 3.2. The main turntable slowly turns while irradiation is in progress, to ensure uniform dose distribution within the insects-containers (insects-canisters).

Figure 3.2: Left hand side: *The main turntable with 8 mini-turntables.*
Right hand side: *Electrical motor driving the turntable.*

Worth mentioning on the left hand side in Figure 3.2, is the lead shroud at ceiling level, which cuts down on radiation streaming through the roof penetration. Also note the large shielding container underneath the turntable. This steel structure is filled with lead and the ^{60}Co source is lowered into this lead shield after irradiation, in order to make human entry into the vault radiologically safe.

The cylindrical containers filled with insects, are placed on top of the mini-turntables, which turn at a higher rotational speed than the main turntable during irradiation. Figure 3.3 presents an orderly piled of six stacked cylindrical containers that are used to fill in insects 60% (2.1 cm) of available 3.5 cm inside-depth for irradiation. The height of each container is 4.2 cm with the diameter of 20 cm and its height of free space inside is 3.5 cm. Each has a wall thickness of 0.5 cm. These containers are made from Polyvinyl Chloride (PVC); are stacked on a polystyrene spacer (20 cm wide , 70 cm high) on each mini-turntable during irradiation.

Figure 3.3: *An orderly pile of six cylindrical containers used for insects irradiation.*

The polystyrene forms an integral part of the system such that an optimum (or central target) dose within the irradiated volume of insects is achieved. This is because insect that receive too low a dose are not sufficiently sterile, and those that receive too high a dose will be non-competitive, reducing the effectiveness of the SIT programme.

During all phases of irradiation and transport, the insects are kept at a temperature of approximately 4°C in order to ensure both survival and sterility. For this purpose, cold air is continually pumped into the irradiation chamber via a cold-air duct mounted on the underside of the concrete roof.

Concrete biological shield

A biological shield of ordinary concrete (**3** = 2.35 g/cm$) was constructed to standard engineering requirements for massive concrete constructions, taking into consideration the loadbearing characteristics of the site. Figure 3.4 presents a schematic top-view[4] of the irradiation chamber, showing the source and the surrounding concrete shielding structure. Figure 3.4 indicates wall thicknesses, the source location inside the vault, test-source (TS) location and the designation of each wall, for the purpose of the calculation. The horizontal (**B**-**C**) position of the source is not exact. This shielding design was decided upon following scoping calculations with the code QAD-CGGP, backed up with

[4]**Note:** in this Chapter, all the drawings of the irradiation facilities are not to scale.

quality assurance validation calculations with a MathCad implementation of the point-kernel method (Van Rooyen, personal communication, 2006). The dimensions given in Figure 3.4 are the result of investigative calculations. Detailed model calculations were performed to verify that this design is radiologically safe, that is, the input of the code includes a complete description of the source geometry, stainless steel and the concrete walls. MCNPX was used to ascertain whether the labyrinth entrance/exit was radiological safe, and dose rates along the line from the source point P▪ directly opposite the exposed source. For the purpose of comparing the results, dose rate values at the point P▪ were calculated with the MathCAD worksheet, QAD-CGGP and MCNPX computer codes. This was performed for three identical spherical (SPH[5]) concrete shields around a point source of ^{60}Co at the centre (elucidated in Chapter 5, 6 and 7).

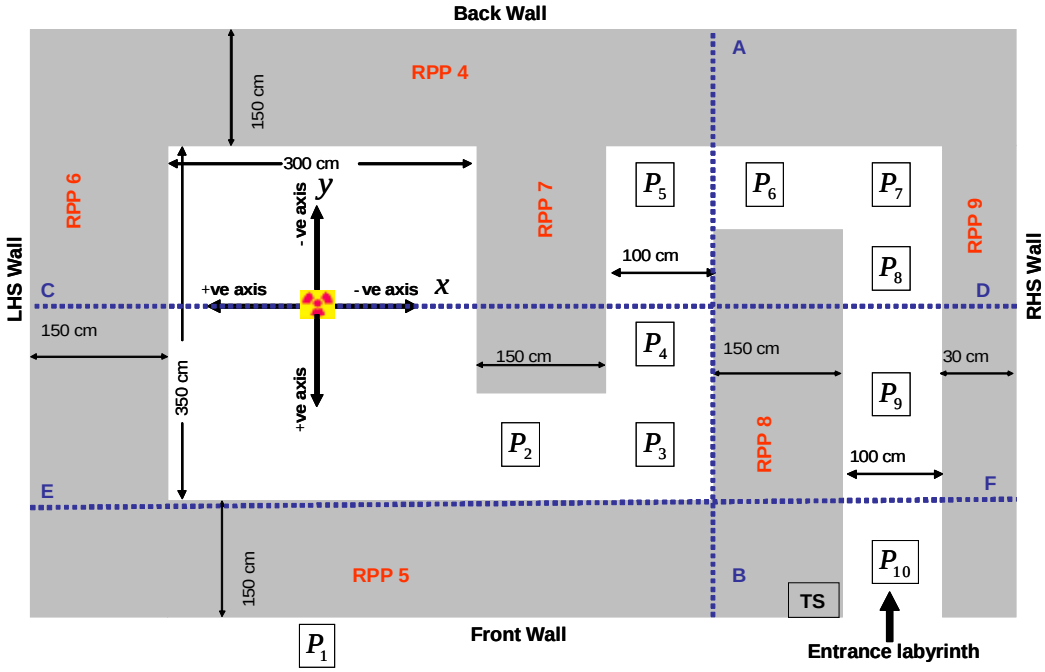

Figure 3.4: *Top-view of the irradiator chamber at Citrus Research International insect irradiator (Citrusdal), illustrating the concrete shielding around the source.*

Of note in Figure 3.4, the different walls have distinctive names, viz., RPP5, RPP6, etc. All walls are 150 cm thick, except the rightmost (RPP9) wall, which is 30 cm thick. The roof is in two sections: roof section RPP10 is to the left of line AB, and has a vertical thickness of 120 cm; roof section RPP11 is to the right of line AB, and has a vertical thickness of 60 cm. P▪ is 10 cm outside the exterior of the front (RPP5) wall, i.e., on the plane (!ß335) and at height 70 cm above the floor level. P_2, P_3,...., P_{10} points along the multi-bend maze are 190, 340, 440, 540, 640, 740, 840, 940 and 1040 cm, respectively, from ^{60}Co source. The **B** and **C** axes are shown; the **D** axis protrudes vertically upwards from the page.

Since insect irradiation is performed at a room temperature of ¸ 4°C, a powerful air conditioning system has been installed. A 20 cm diameter pipe delivering the cold air or

[5]**Note:** for the purpose of verifying the results, calculation of dose rate values using a concrete shield with symmetrically spherical geometry (SPH) was employed for all the three facilities.

coolant into the irradiation chamber, runs along the walls of the labyrinth passage, in a channel mounted near the underside of the roof. There is no undue radiation streaming through this pipe because it follows the exact contour of the labyrinth.

Required radiation safety features

The Citrusdal insect irradiator is constructed in accordance with IAEA standards, as set forth in IAEA safety series 107 and 115 (1992 and 1996) as well as the IAEA course material on “Radiation Protection and Safety at Industrial Irradiation Facilities” (IAEA safety series 107, 1992). This instructional material is available from the IAEA on CDs, and includes full detail on required safety standards for irradiator facilities.

Radiation safety interlock system

In this section, the electronic safety interlock system which operates in relation to the source position, is discussed.

The operation of the vault door is electronically interlocked to the source position. This is designed to prevent the source from being lifted from its shielded position while the door is open. To lift the source from its shielded position the door has to be closed, locked, and the door key is inserted and turned in the control panel in the control room, it is only possible to raise the source if all interlock conditions are in place and all safety systems function correctly. In the unlikely event of some reason the interlock malfunction are non-conformance of the procedure occurs, the source is immediately lowered to its shielded position. Figures 3.5 and 3.6 on page 38 illustrates the main switchboard and strobe light, which, are integrated into the interlock system for enhancing safe operation of the plant.

Figure 3.5: *The main switchboard illustrating the main switch, warning lights for the rotating turntable, as well as "active source" and "fault" warnings for the entire control system.*

Figure 3.6: *The mechanical source interlock system and strobe light-system.*

Notable in Figure 3.6, is the red warning strobe light that flashes while the source is raised "up" to the irradiation position. A green light means that the ^{60}Co source is in its safe, shielded position inside the lead "pot" or "pig" underneath the turntable.

Installed radiation detectors

A radiation detector is installed as area radiation monitor (ARM) in the maze passage (i.e., the labyrinth), just outside the irradiation chamber. There is a video camera inside

vault, bolted on the underside of the roof concrete slab. An LCD panel, closed-circuit television monitor mounted on the front wall is used to displays the state of the source inside the irradiator chamber, as seen by the video camera. This system is shown in Figure 3.7.

Figure 3.7: *Television and area detector monitor which displays the status of the source inside the irradiator chamber and the radiation monitor used to display the dose rate at the detector position.*

Handheld radiation detectors

Two handheld radiation detectors with self-scaling digital readouts are available. The use of such a detector during vault entries is a standard operating procedures (SOP). This provides defence in depth: multiple, independent, readouts safety system.

Test-source

Quality assurance standards for radiation monitoring require regular checking of accuracy of instrumentation, since it is unsafe to assume that a radiation detector will function faultlessly between annual calibrations. A low-activity check-source, mounted in a small cavity, behind a small, hinged shielding door, just behind the entrance door to the labyrinth, i.e., at position TS in Figure 3.4, is used for instrument checking. Every week, each radiation monitor must be "check-source tested" by holding it at a predetermined distance from the check-source and observing whether the expected dose rate reading is indeed obtained, and results are logged. ^{137}Cs is the radionuclide used as check-source because it has a long half-life. All aforementioned electronic devises play a paramount and integrated role in ensuring a high degree of reliability in the safe operation of the irradiation facility.

3.5 The Stellenbosch insect sterilization facility

The Agricultural Research Council operates an insect sterilization facility at Nietvoorbij, Stellenbosch, that is situated approximately 70 km from Cape Town. This facility also uses the radiation-based Sterile Insect technique discussed in §3.2.

This facility received a once-off funding from the IAEA, and uses ^{60}Co as the source of ionising radiation (Barnes, personal communication, 2006). The facility is designed chiefly for the sterilization of fruit flies which pose a major problem in this agricultural area in South Africa. The facility was designed for a 5 kCi (0.185 PBq) ^{60}Co source, but is now operated with a 10 kCi (0.37 PBq) ^{60}Co source (reference source strength in the year 1999). The active source is a 2.5 cm long cylindrical pin with a 1.05 cm radius, which is mounted inside a longer thin-walled stainless steel rod. The source area is 23.4 cm$^{\#}$. When not in use the source is stored in an underfloor shielded position. The source activity was 3.32 kCi (0.12 PBq) in October 2007—the dose rate measurements were carried-out on this month.

Turntable

The source is raised out from underfloor shielded position to perform irradiation, i.e., the active part of the source rod is lifted to a position just above a circular main turntable with eight smaller secondary turntables (Figure 3.8), that slowly turn while irradiation is in progress to ensure an even dose distribution inside insect-containers. Figure 3.8 shows the main turntable with the cylindrical containers filled with insects on top of the secondary turntables. These containers turn at a higher angular velocity during irradiation than the main-turntable.

Figure 3.8: *A circular main turntable with the cylindrical containers filled with insects on top of the mini-turntables.*

Concrete biological shield

Figure 3.9 on page 41 illustrates a top-view of the irradiator cell, showing the source position and the enclosing concrete structure density **3** of approximately 2.63 g/cm$^{\$}$.

Also shown in Figure 3.9, is the respective wall thicknesses and radiation source position inside the vault.

The radiological safety assessment was carried out using the computer code QAD-CGGP. This was confirmed with quality assurance validation calculations using MCNPX as well as dose rate measurements. MCNPX was used to ascertain whether the labyrinth entrance/exit was radiologically safe, and dose rates along the line from the source point P▪ directly perpendicular to the exposed source. Again, dose rates at the point P▪ calculated with QAD-CGGP and MCNPX, are compared.

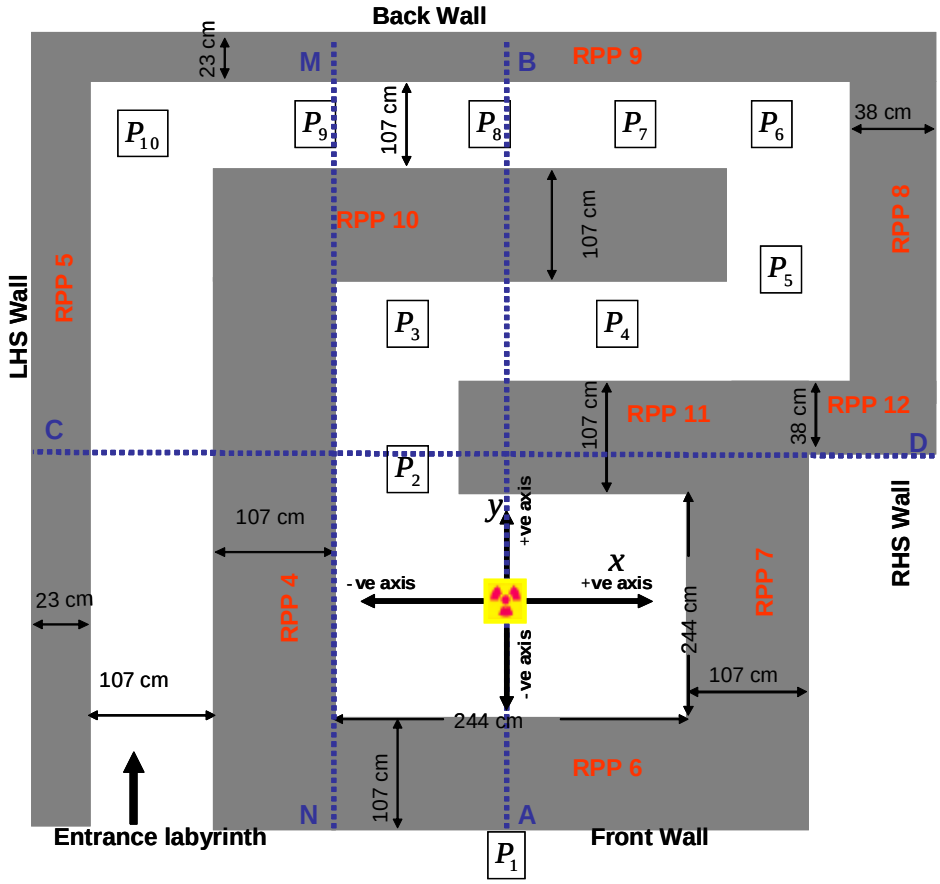

Figure 3.9: *Top-view of Infruitec irradiation chamber at Nietvoorbij—Stellenbosch, showing the concrete shielding around the source.*

It is apparent in Figure 3.9 that most walls are 107 cm thick, except the right (RPP8 and RPP12) walls towards the back, leftmost (RPP5) and the rear (RPP9) wall. Both the leftmost and the rear wall are 23 cm thick. The right wall towards the back is 38 cm. The roof is in two sections: roof section RPP13 is to the front of line CD; roof section RPP14 is to the back of line CD. Both the RPP13 and RPP14 roof sections are 91 cm thick. The point P▪ is 40 cm above the floor, and 10 cm outside the outer surface of concrete wall RPP6. The points P_2, P_3,...., P_{10} along the labyrinth are 129, 282, 436, 589, 746, 900, 1050, 1200 and 1350 cm, sequentially, from ^{60}Co source position. The **B** and **C** axes are shown; the **D** axis protrudes vertically upwards from the page.

3.6 The HEPRO irradiation facility

Introduction

HEPRO is an initialism for **H**igh **E**nergy **PRO**cessing; is a commercial irradiation facility in Ferrule Avenue, Montagu Gardens, Milnerton, City of Cape Town, Western Cape, South Africa. The design company behind HEPRO is PicoWave Technology. The facility is primary designed for irradiation of food (to destroy pathogens, i.e., disease causing microorganisms and parasites in food products) and polymer irradiation (to improve their properties, e.g., improve mechanical properties, decrease flammability and improve resistance to abrasion).

Radiation source

The facility uses ^{60}Co as the source of ionising radiation. The ^{60}Co sources used at HEPRO are of Canadian origin. They are doubly insulated in type C-188 stainless steel pencils. Each pencil is 45.2 cm long and about 1.1 cm in diameter. AECL type C-188 clad pencils have been used in gamma irradiators with water-filled storage pools since 1964, without problems such as failure of cladding integrity. In 1985, there were 12 500 type C-188 pencils in service. Routine wiping of source pencils and monitoring of water purification resin beds and filters of the water treatment plants have shown no evidence of any pencil failures in the above period. The integrity of the C-188 pencils have also been confirmed by metallurgical examinations of C-188 pencils returned after years of service. The main reason for the high integrity of the pencils despite the intense ionising photon fluence rate, is that ionising photons with energies below ~7 MeV do not interact with nuclei[6], but only with electrons, and this does not affect the mechanical properties of the metal.

Regular radiometric analyses of resin used to de-ionise the pool water (page 44), serve as "leak testing" of the sealed ^{60}Co sources.

The height of the rectangular source rack housing is 150 cm, and its side lengths are 75 cm. The source rack contains 12 modules, stacked 3 high to a side. Each module contains 25 source pencils positioned on 2.5 cm centres, giving a total of 12 , 25 œ 300 pencils.

A metal grid source-guard protects the source in the exposed ("up") position by shrouding it.

The source rack is lifted from the bottom of the pool (its shielded position) to the "up" position by a mechanical hoist, mounted in a locked hut on the roof of the irradiation chamber. Control of source movement is electro-pneumatical. A stainless steel cable passes through a narrow hole in the roof, and attaches at the centre of the source rack.

[6]Exceptions: ^{9}Be, ^{7}Li and ^{2}H.

Concrete biological shield

A concrete biological shield is constructed to standard engineering requirements for massive concrete constructions, taking into account the loadbearing characteristics of the site. A drawing of the concrete shielding is shown in Figure 3.10, which, illustrates the top-view of concrete shielding around the ^{60}Co source and the dimensions.

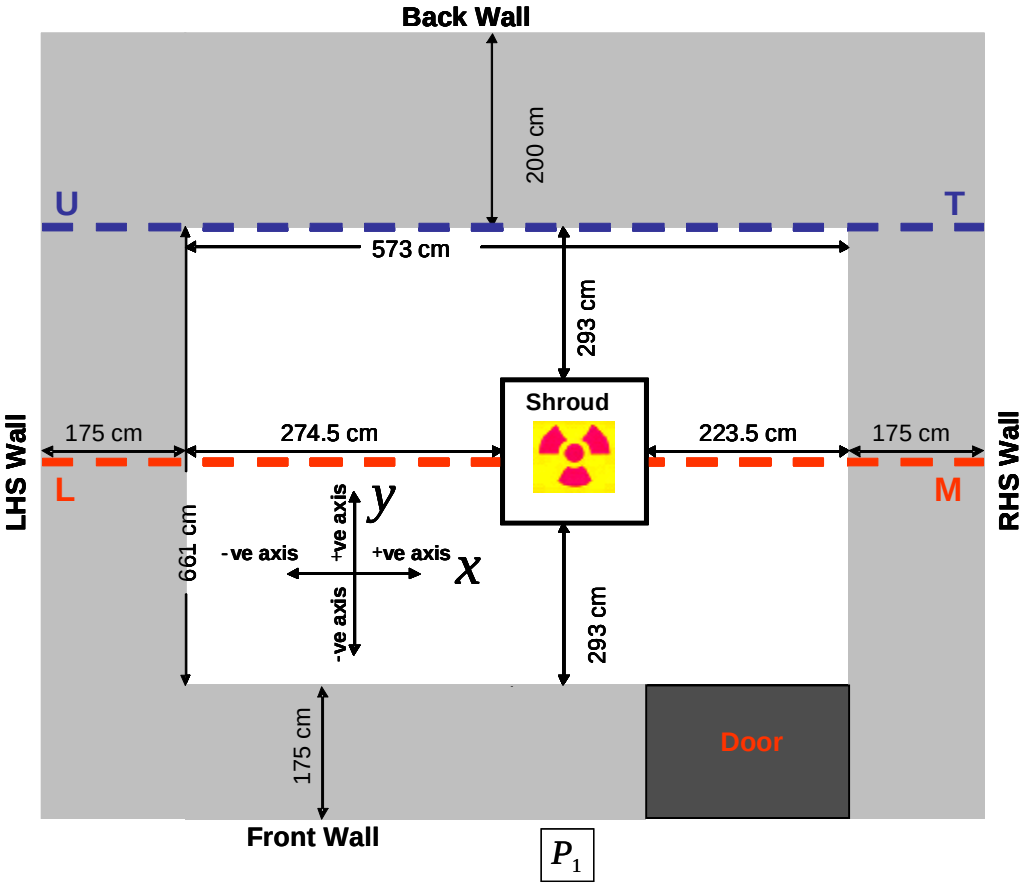

Figure 3.10: *Top-view of concrete shielding walls around ^{60}Co source of 2 MCi (74 PBq) activity.*

The walls to the front, left and right shown in Figure 3.10 are 175 cm thick, as is the roof. The wall at the back is 200 cm thick, because it is significantly closer to the site boundary than the other walls. The facility layout nomenclature indicated in Figure 3.10 of the irradiation cell will be used to refer to specific walls, so that reference will be made to the **"front wall,"** the **"back wall,"** the **"RHS wall"** and the **"LHS wall".** The point P▪ is 100 cm above the floor, and 10 cm outside the outer surface of the front concrete wall. Dose rates at the point P▪ calculated with the MathCAD worksheet, QAD-CGGP and MCNPX, are compared. The **B** and **C** axes are shown—**D** axis protrudes vertically upwards from the page.

Figure 3.11 on page 44 shows the blue sliding plug-door. The sliding plug-door (at the bottom right of Figure 3.10) is hydraulically operated and moves on rails. Door movement is electronically interlocked with the source position — the door can only be opened if the source is at the very bottom of the pool. The top and closing faces of the

door are stepped, and the bottom of the door is well below floor level to reduce radiation penetration ("shine"). A drawbridge, carrying a section of the trolley transport rail, is located near the inner face of the door, and is interlocked to the door movement. The door movement is an integral part of the overall interlocked safety system.

Figure 3.11: *The sliding plug-door leading to the irradiation vault (coloured blue).*

Water pool

Between exposures, the source is lowered into a water pool (Figures 3.12, 3.13 and 3.14). Figure 3.12 presents the side view of the source rack in the water pool.

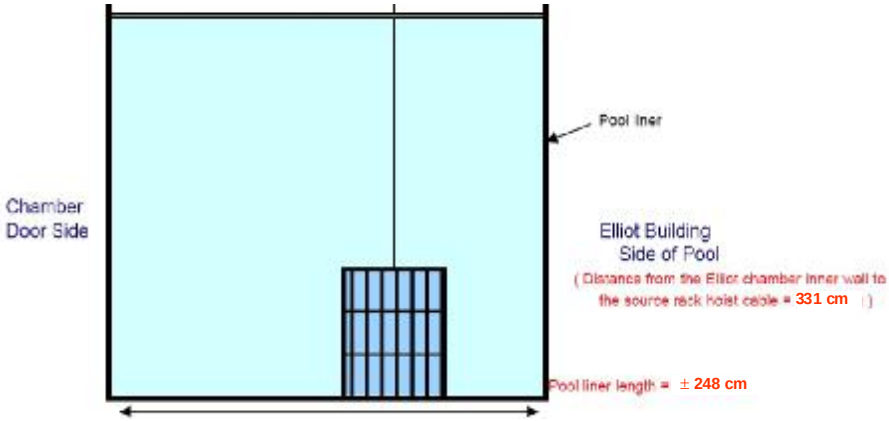

Figure 3.12: *Side view of the source rack in the water pool (drawing not to scale).*

At the lowered position of the source, the top of the ^{60}Co pins is covered by about 426 cm of water. A pneumatic hoisting device, driven from within a locked hut on top of the 175 cm thick concrete roof, raises and lowers the source rack. Guide cables guide the source rack in its movement. The hoisting cable moves through a small hole in the roof.

The top view of the source rack in the water pool is shown in Figure 3.13.

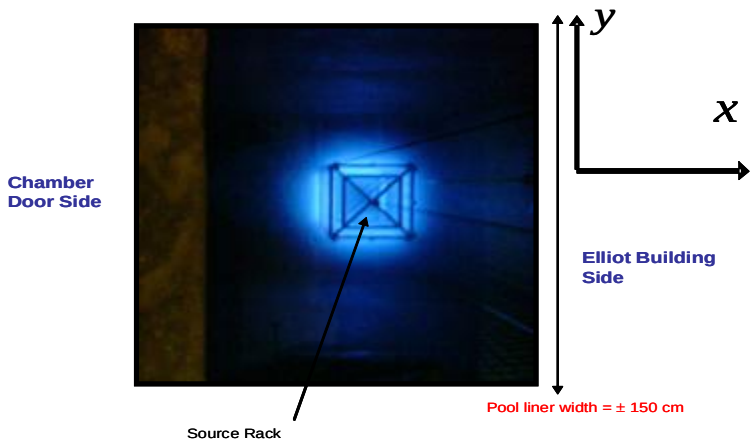

Figure 3.13: *Top view of the source rack in the water pool.*

The pool is 248 cm long, 150 cm wide and about 610 cm deep. The ^{60}Co source rack is stored at the bottom of the pool; source replenishment also takes place at the bottom of the pool. The blue "halo" around the source rack shown in Figure 3.13, is Cherenkov radiation, i.e., photons produced where the speed of the electrons emitted by ^{60}Co exceeds the phase-speed of photons in a material medium.

The front-view from the chamber door side of the source rack inside the HEPRO water pool is shown in Figure 3.14. The height of the source rack is 150 cm.

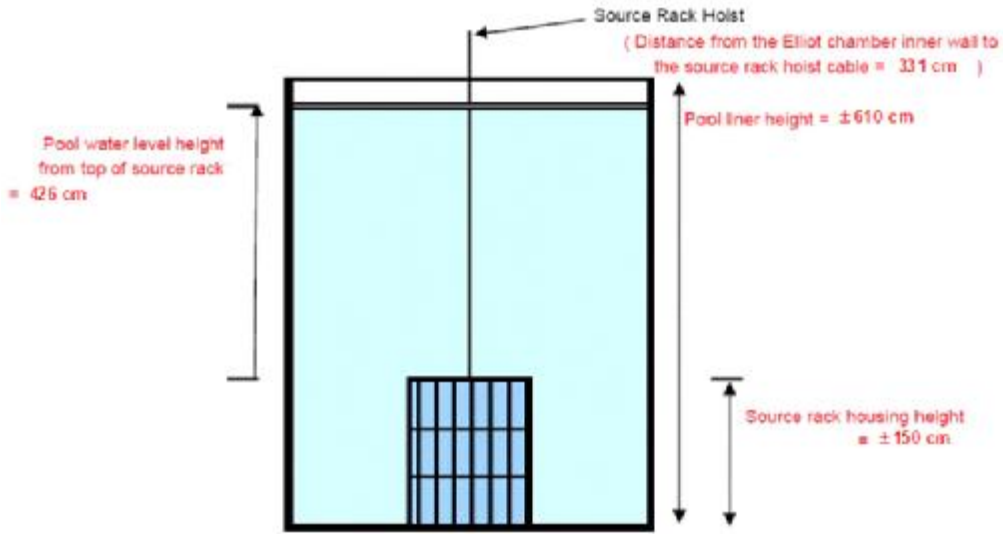

Figure 3.14: *Front-view of the source rack inside the HEPRO water pool (drawing not to scale).*

The walls of the pool are 40 cm thick reinforced concrete. The pool has a stainless steel type 304L (SS-304L) liner of 0.45 cm thickness. The water level is normally maintained 34 cm below the top of the pool liner. The present maximum source strength exceeds 0.5

MCi (18.5 PBq) and therefore a pool water chiller is installed to maintain pool water temperature within limits, and prevent excessive evaporation of the pool water.

Plant operation — overview

Inside the concrete irradiation chamber, goods to be irradiated are loaded onto each of 4 turntables. After the vault is formally cleared and locked, the source is raised out of the water pool. Figure 3.15 shows some loaded goods inside the irradiation chamber. Goods are stacked on pallets of a standard size, and then irradiated. A timer mechanism governs the duration of exposure. The turntables are rotated so that each of the 4 faces of the product is irradiated, in order to achieve as uniform a dose distribution as possible. After irradiation, the source is lowered into the pool.

Figure 3.15: *Goods ready to be irradiated inside the concrete irradiation chamber.*

3.7 Safety features at HEPRO

(i) Interlock system

The operation of the vault door is electronically interlocked with source movement. The ^{60}Co source can only be raised from its safe position at the bottom of the pool if all systems function correctly. Malfunction will cause the source rack to be immediately lowered to the bottom of the pool.

(ii) Installed radiation detectors

Three fixed radiation detectors are used.

Detector 1: The first radiation detector is placed inside the front wall of the biological shield, with a 100 cm concrete plug between the detector and the inside of the cell. The detector is aligned to face the centre of the exposed source rack. The detector is a

LUDLUM model 133-7 GM tube with a range of 0 – 3000 mSv/h. This detector's readout indicates whether the source rack is exposed or not.

Detector 2: The second detector is used as an area alarm and is fitted at the interface of the sliding plug door and the door frame. It is a LUDLUM model 133–6 GM tube with a range of 0 – 200 mSv/h. Should the dose rate be unsafe when the sliding plug door is opened, this detector will alarm, resulting in the source rack being lowered to the bottom of the water pool.

Detector 3: The third detector is fitted between the two cylinders of the ion exchange resin columns used to purify the pool water. It is a LUDLUM model 133–2, with range 0 – 2 mSv/h. This detector will alarm if the ^{60}Co cladding fails, and the radionuclide be dispersed in the pool water.

Alarm levels were set for each detector. When alarm levels are exceeded, the safety interlock system will ensure the immediate and fast lowering of the source rack into the storage pool.

(iii) Handheld radiation detectors

Handheld radiation detectors are available for interpretation (or measurement).

(iv) Additional safety measures

Four additional features prevent unauthorised raising of the source rack:

(1) The access door to the roof is locked;

(2) The roof hut door is locked;

(3) The pneumatic switch control box is locked, and

(4) The manual operation keys on the pneumatic switches have been sawn off.

3.8 The cobalt-60 gamma radiation source

Each of the three irradiator facilities in question uses the radionuclide ^{60}Co as source of ionising photons. Therefore an in-depth look at this radionuclide and its emissions is presented in this section.

The radionuclide ^{60}Co is the most commonly used source of gamma radiation for radiation technology, both for industrial (§3.4, §3.5 and §3.6) and medical purposes. Cobalt-60 is a radioactive isotope of cobalt, with a half life of 5.27 years. It disintegrates into a stable nickel-60 isotope (^{60}Ni) principally emitting one negative beta particle, of a maximum energy **!þ$"$** MeV. Figure 3.16 on page 48 shows the decay scheme of the

radionuclide ^{60}Co. Shown as well in Figure 3.16, is the emitted energies during decay which pose radiological hazard, and the stable daughter nuclide, ^{60}Ni.

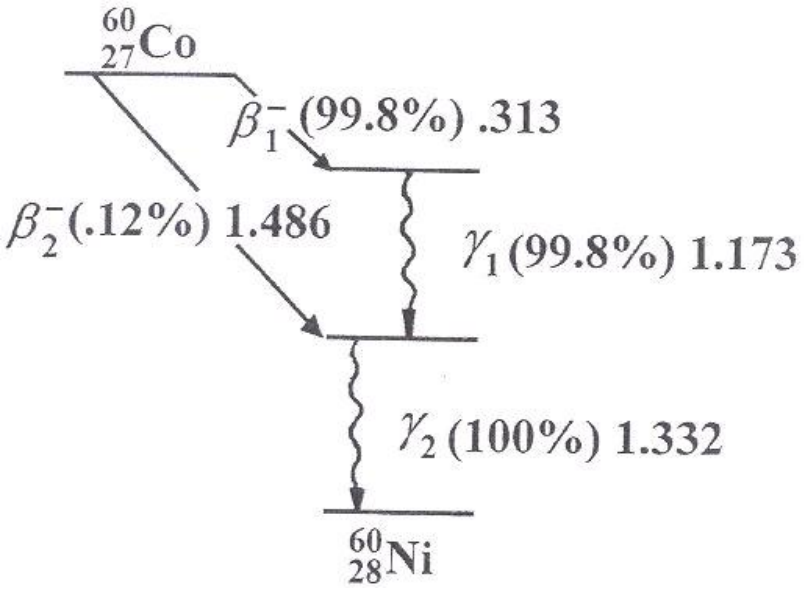

Figure 3.16: *The decay scheme of the radionuclide Cobalt-60.*

Nickel-60 thus produced is in an excited state, and it instantly emits two photons of energy **"þ"(** and **"þ$$** MeV in succession to reach its stable state. Both photons are utilised in radiation processing in irradiators and both pose radiation hazard to personnel if the dose rates are not minimised to acceptable levels by shielding. Table 3.1 summarises the radiologically important primary ionising photons emitted by the radionuclide ^{60}Co. The radionuclide ^{60}Co is used at previously mentioned facilities (§3.4, §3.5 and §3.6).

Table 3.1: *Ionising photon emissions of radionuclide ^{60}Co (ICRP publication 38, 1983).*

Photon energy (MeV)	**Yield** (fraction)
1.173	0.999
1.332	1

Figure 3.17 on page 49 shows the photon emission characteristics of ^{60}Co.

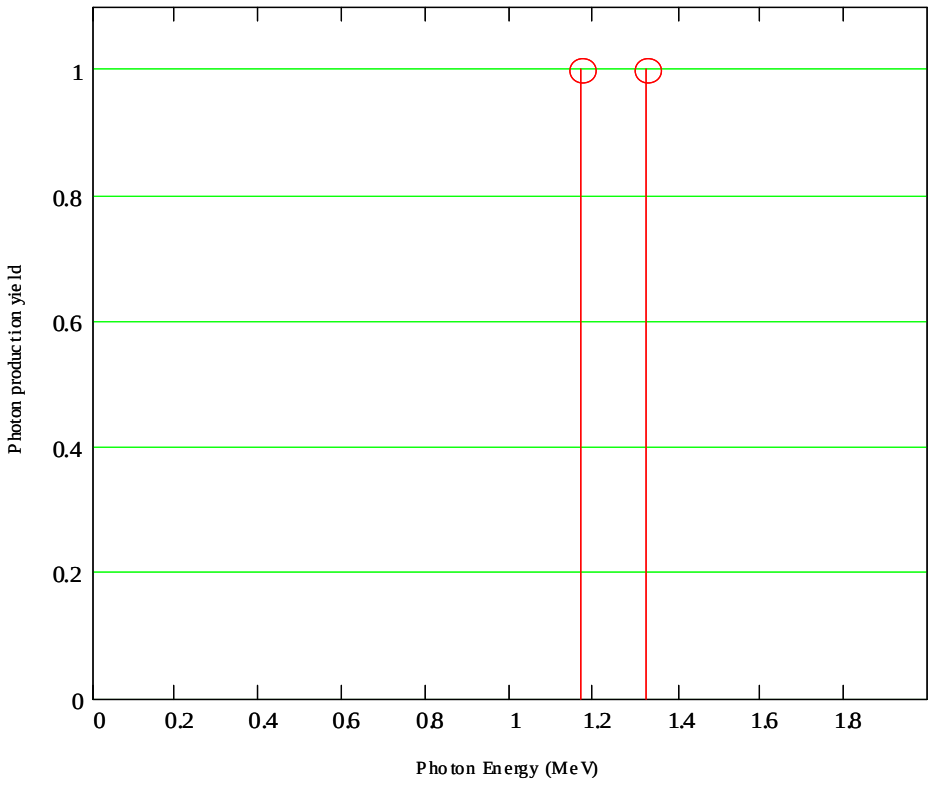

Figure 3.17: *Primary ionising photons emitted by the radionuclide ^{60}Co.*

Other types of ionising radiation emitted by ^{60}Co are not radiologically important, because their penetrating abilities are very low, namely the negative beta particles (β^-) and Auger electrons (e^-).

Chapter 4
Computational techniques

4.1 Introduction

In this chapter the computational methods used to model the three ^{60}Co irradiation facilities (presented in §3.4, §3.5 and §3.6) will be discussed. The actual results and discussion are presented in Chapters 5, 6 and 7.

4.2 The point-kernel code QAD-CGGP

The code QAD-CGGP, a point kernel code system for neutron and photon shielding calculations, using the Geometric Progression (GP) buildup factor formalism (RSICC CCC-493, 1989), was used to perform dose rate calculations for the facilities. It is an approximate method that enables fast calculations and satisfactory accuracy for photon shielding problems. The point-kernel integration method represents a drastic simplification of radiation transport. It is used with great success for a wide variety of photon shielding problems. In essence, this method amounts to initially neglecting the inscattering integral of the Boltzmann transport equation (BTE). This means that scattering is not considered, and that the medium is viewed as purely absorbing in nature. A solution for the simplified problem is obtained and then multiplied by a *buildup factor* which corrects for the initial neglect of the contribution of scattered radiation to the response at the point of interest. The term "buildup" refers to the buildup of scattered radiation in the material region between the source and detector positions.

It is not correct to leave out the contribution of scattered radiation to the dose rate behind a radiation shield. However, to take it into account in a rigorous manner, is quite difficult. To do it properly, one must use Monte Carlo codes or three dimensional deterministic codes, both of which are not easy to use and can also take many days to simulate the radiation transport problem to the desired accuracy, especially if the shield is thick.

Consider a point source of ionising photons with source strength W, and a single shield layer with thickness x. In the point-kernel approximation, all scattering of radiation is initially ignored, and then corrected for by multiplication with a buildup factor. The effective dose rate H_{eff} at a point r on the personnel side of the shield, contributed by uncollided radiation, will be given by

$$H_{\text{eff}} \propto \frac{W \cdot \exp(-\mu x)}{4\pi r^2}. \qquad (4\text{-}1)$$

The $\left(\frac{1}{4\pi r^2}\right)$ term represents the "geometrical attenuation," i.e., the lowering of dose rate that is purely the result of the distance between the point source and the "detector" or

"receiver" position. The symbol **W** denotes the source strength, i.e., activity times the emission yield. The symbol **Å** denotes the fluence-to-dose conversion factor for the type and energy of the radiation — obtained from e.g., ICRP publication 60 (1990). The **e**exp**a** • **.>bf** term represents the attenuation of the radiation in the shield of thickness **>**. The symbol **.** denotes the linear interaction coefficient — the product of the "microscopic cross-section" **5** multiplied by the nuclide number density **R** and summed over the **3** chemical elements present in the shield,

$$. \text{ œ } \sum_{3} 5_3 R_3 .$$

For the point-kernel method, QAD-CGGP, the volume of the source is divided into many small sub-volumes. Each of these is now approximated as a little point-source, with all the radio-activity in every small subvolume assumed to be concentrated at its midpoint. Eq. (4.1) is used to determine the contribution of this small sub-volume of the source, to the "uncollided dose rate" at the detector point — the distance **<** is now the distance between the sub-volume "point source" and the detector or receiver position. However, the result is multiplied by a buildup factor to correct for the initial neglect of scattering. Formulas for buildup factors have been calculated for a wide variety of materials, using Monte Carlo calculations to calculate the true dose rates. (At present, the most advanced buildup factor formalism is the Geometric Progression formalism, which is used in QAD-CGGP). This process is repeated for all the sub-parts of the source. All the sub-answers are eventually summed to obtain the total dose rate at the detector point.

The point-kernel methodology is implemented in the code QAD-CGGP version of QAD-P5A (RSICC code CCC-493, 1989). A simple implementation of the point kernel method, for point sources, was coded in a MathCAD[7] worksheet (Van Rooyen, personal communication, 2006). This MathCAD worksheet was used as an independent check on the results obtained with QAD-CGGP — such an independent check is vital for quality assurance of results.

There are several ways to handle buildup factors, i.e., the correction for the contribution of scattered ionising photons to the dose rate. The Geometrical Progression (GP) method is used in QAD-CGGP and also in the MathCAD worksheet that is used to cross-check the results calculated with QAD-CGGP. The GP method for handling buildup is at present one of the more accurate methods of modelling "dose buildup". Better point-kernel codes than QAD-CGGP, such as Microshield and Mercurad (marketed by CANBERRA) are available, but these are not public-domain codes, and may be quite costly.

[7]**Note:** it is often a standard practice with an advanced code to first perform a simplefied calculation, which can with reasonable ease be checked independently, before proceeding to the more complex cases.

4.3 The Monte Carlo code MCNPX

To further increase the confidence and reliability of the calculated dose rates with the point-kernel integration code, the Monte Carlo N-Particle eXtended, MCNPX version 2.5.0 (RSICC CCC-730, 2005), was also used. Only MCNPX was used to evaluate the dose rates along the labyrinths because the point-kernel integration code, QAD-CGGP version of QAD-P5A, is unable to calculate any form of radiation streaming along the labyrinths.

MCNPX is a Monte Carlo radiation transport code for modelling the interaction of radiation with matter. This method is based in the probability distribution function for developing the random sampling of each event and performing the evolution of the particular phenomena being studied by means of convenient statistical techniques. The capabilities of this code involve the correct simulation of the physical problem and the geometrical configuration.

MCNPX is capable of tracking 34 particle types, including four light ions, at nearly all energies. It is coded in Fortran-90 (Chapman, 1998) and is fully three-dimensional. It utilizes the latest nuclear cross-section libraries and uses physical models for particle types and energies where tabular data are not available.

MCNPX can model 3-dimensional objects is space in exact or near-exact geometry. In addition to the three-dimensional combinatorial geometry syntax, the code also offers the ability to define general sources, a complete set of tally options, a broad scope of variance reduction techniques and an extensive collection of cross-section data. The code normally uses point-wise (i.e., continuous) cross-section data, but can also use multigroup cross-section data. The cross-section data supplied with the code covers the photon energy range from 1 keV to 100 GeV, and the electron energy range from 1 keV to 1 GeV. Most cross-section data libraries shipped with the code covers the neutron energy range from $10^{\bullet 11}$ to 20 MeV, but some neutron cross-section libraries extend up to 150 MeV. When MCNPX is used to model neutron transport at energies where cross-section tabulations are not supplied, the code switches over from using tabular cross-section data, to using nuclear models. This is called the cross-over from “table physics” to “model physics”. Using nuclear models in radiation transport instead of the actual evaluated cross-section data, is, of course, not as accurate as using the cross-section data.

The upper energy limit to cross-section tables and the switchover from evaluated tabular cross-section data to “model physics” is not relevant to the problem under analysis in this work, because only photons are transported and photon energies will not exceed 1.333 MeV.

Chapter 5
Results and discussion: Citrusdal insect sterilization facility

5.1 Dose rate evaluation

The insect sterilization vault at the Citrusdal irradiator facility, was modelled in QAD-CGGP, a point-kernel integration code, to determine the satisfactory of the various shield thicknesses. Obtained results were verified with a MathCAD worksheet and the Monte Carlo radiation transport code, MCNPX. This chapter mainly presents the Citrusdal results and discusses how the shield thicknesses shown in Figure 3.4 on page 36 were conclusively decided. Figure 3.4 will be used in referencing the specific walls.

5.2 Modelling with the code QAD-CGGP

The Citrusdal facility was modelled in great detail, including the exact geometry of the source, the vault walls and the roof, as shown in Figure 3.4 on page 36. The geometry was modelled using the combinatorial geometry (CG) coding required by QAD-CGGP. The ^{60}Co source was modelled as a homogeneous right circular cylinder (RCC) rod encapsulated in stainless steel. The walls were modelled as RPPs for the condition that the active part of the source rod was raised to an irradiation position of 70 cm above the floor level inside the vault of 220 cm height. The QAD-CGGP sample input data set is as shown in Appendix C.1.

Radiation transport codes calculate fluence-rates, Φ, which are then converted to dose rates via multiplication with a fluence to response conversion function, $R(E)$, evaluated at suitably photon energies, E. The fluence-to-dose conversion factors were calculated employing the ANS (1991) response function for effective dose, using a MathCAD worksheet as illustrated in Table 5.1. Point-kernel method in QAD-CGGP only uses these two fluence-to-dose conversion factors, as a result of the analytic simplification of radiation transport in this code.

Table 5.1: *Fluence to response conversion factors for the ionising photons emitted by a ^{60}Co source.*

Photon energy (MeV)	**Emission yield**	**Fluence-rate to dose-rate conversion factor** $\left[\frac{Sv}{cm^2 s}\right]$
1.17	1.00	1.09 E-12
1.33	1	1.23 E-12

The composition of concrete used was standard of NBS type 04 (ordinary concrete), with composition given in Table 5.2 (Shultis and Faw, 1996).

Table 5.2: *Elemental composition of NBS type 04 ordinary concrete (Shultis and Faw, 1996).*

Element	**Atomic number** ^	**Partial mass density** a g/cm•3 b
H	1	0.013
O	8	1.165
Na	11	0.040
Mg	12	0.010
Al	13	0.108
Si	14	0.740
S	16	0.003
K	19	0.045
Ca	20	0.196
Fe	26	0.030
Total		**2.35**

5.2.1 QAD-CGGP results

The detection limit for a typical commercial dose rate meter is about 0.3 µSvÎh; the natural background dose rate from penetrating, external ionising radiation is about 0.11 µSvÎh. As a result, calculated dose rates are graphical illustrated in proper perspective by including a green reference line at 0.11 µSvÎh representing the average natural ambient dose rate. Dose rates below this line are beneath the natural background levels, and therefore insignificant.

The dose rates were evaluated at a distance of 10 cm from the outer surface of the walls and 50 cm above the horizontal level of both parts of the roof. All dose rates (with the source in exposed position) were determined for heights 100 cm above ground level. This height was selected because vital radiosensitive organs in a body of typical human being are between the height of 100 and 150 cm. The thoroughly selected positions for dose rate evaluation was mainly to calculate projected maximum annual doses to radiation workers. For members of the public, including non-radiation workers, the dose rates were calculated at distance 1000 cm from the outer surface of the walls.

Roof

Figure 5.1 illustrates how dose rates on top of the concrete roof vary with lateral movement along line CD and EF, on the **B** axis (see Figure 3.4 on page 36). Line CD lies on the plane **C œ** 0 cm, and line EF on the plane **C œ** 175 cm. The maximum dose rates is about 22.8 µSv/h, and drops to 17.7 µSv/h at **B œ !** cm because of the stainless steel rod shielding the source (^{60}Co source). As one moves laterally away from **B œ !** cm, the effective thickness of concrete traversed by the photons, increases, and dose rates therefore rapidly drop to lower values. These dose rates decreases to lower values below background levels and are therefore insignificant.

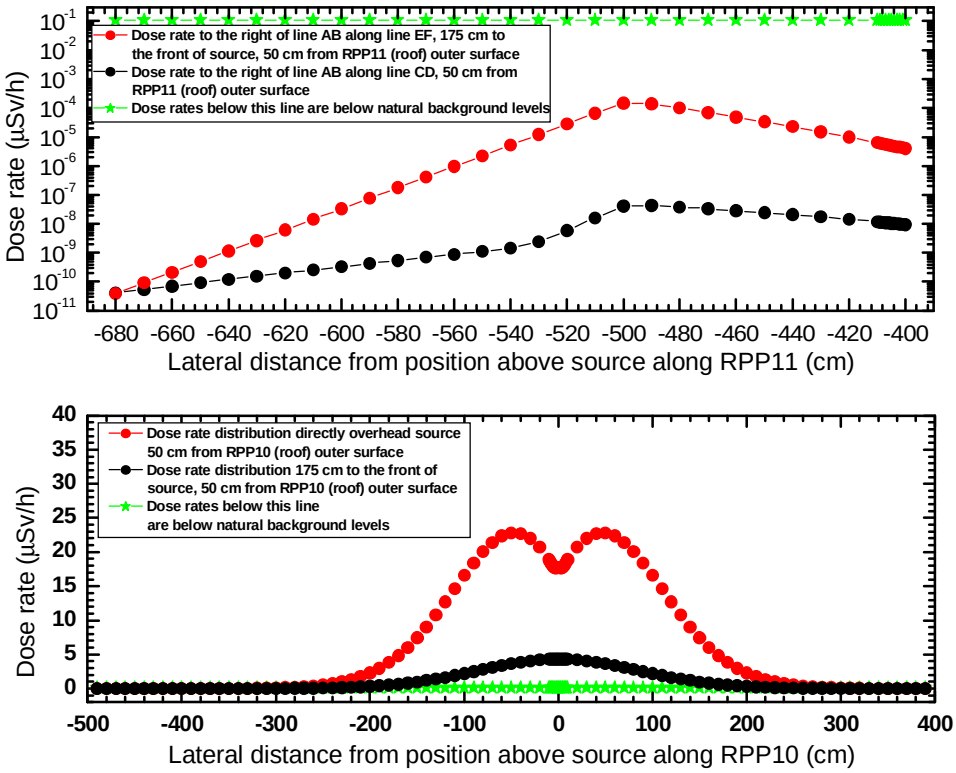

Figure 5.1: *Dose rates along the concrete roof (RPP10 and RPP11).*

It is notable in Figure 5.1 that the dose rates on the concrete roof vary from negligible values, to a peak value of about 22.8 µSv/h, directly overhead (RPP10—120 cm thick concrete roof) the exposed source and along the outside outer surface of the 60 cm thick concrete roof (RPP11) to the right of line AB (see Figure 3.4).

The intricate detail of dose rate distribution in Figure 5.1 is only apparent when plotted on a logarithmic scale. Figure 5.2 on page 56 shows the dose rates on the concrete roof, plotted on a logarithmic scale. The red line is for lateral movement along line CD, while the black line is for lateral movement along line EF (see Figure 3.4). Line CD runs along the plane y **œ** 0 cm and line EF along the plane y **œ** 175 cm. The point zero on the horizontal axis is at plane **B œ** 0 cm.

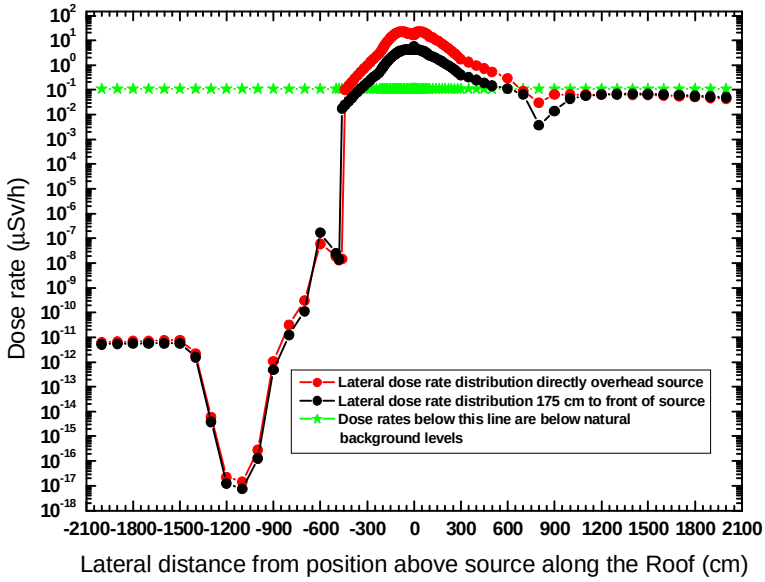

Figure 5.2: *Dose rates on the concrete roof, as seen with a logarithmic dose rate axis.*

The elaborate detail manifested in the dose rate distribution in Figure 5.2, is the result of the passage of the radiation through the three dimensional geometry of the concrete building—the rays traverse different thicknesses of concrete. The detailed fine structure in the low dose region, however, is irrelevant because dose rate values below the reference green line are below natural background levels, and are also not detectable with dose-rate meters.

Walls

Figure 5.3 presents calculated dose rates along the exterior axial direction of the back wall (RPP4) and front wall (RPP5). Dose rates varies from insignificant values to a maximum value of 1.4 µSv/h.

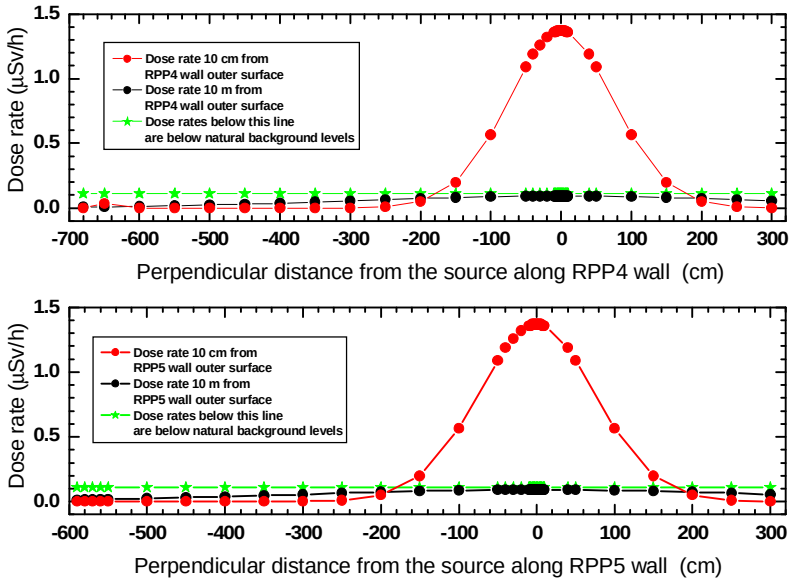

Figure 5.3: *Dose rates along the exterior axial direction of the back and front concrete wall.*

The dose rates at 100 cm height were calculated for distances of 10 cm as well as 10 m from the outer surface of the walls. At a close distance of 10 cm outside the outer surface of these walls, the highest dose rate is 1.4 µSv/h directly opposite the exposed source and at right angle to the source axis. At the 10 m distance, the dose rate drops to 0.091 µSv/h; a value below natural background level. The front wall (RPP5) has the same thickness and located at the same position from the source centreline as the back wall (RPP4), for this reason the dose rates are the same.

The dose rates obtained along the LHS (RPP6) wall as well as the rightmost wall (RPP9) are shown in Figure 5.4. The peak dose rate along the LHS wall is 1.59 µSv/h whereas dose rates along the rightmost wall remains below background level.

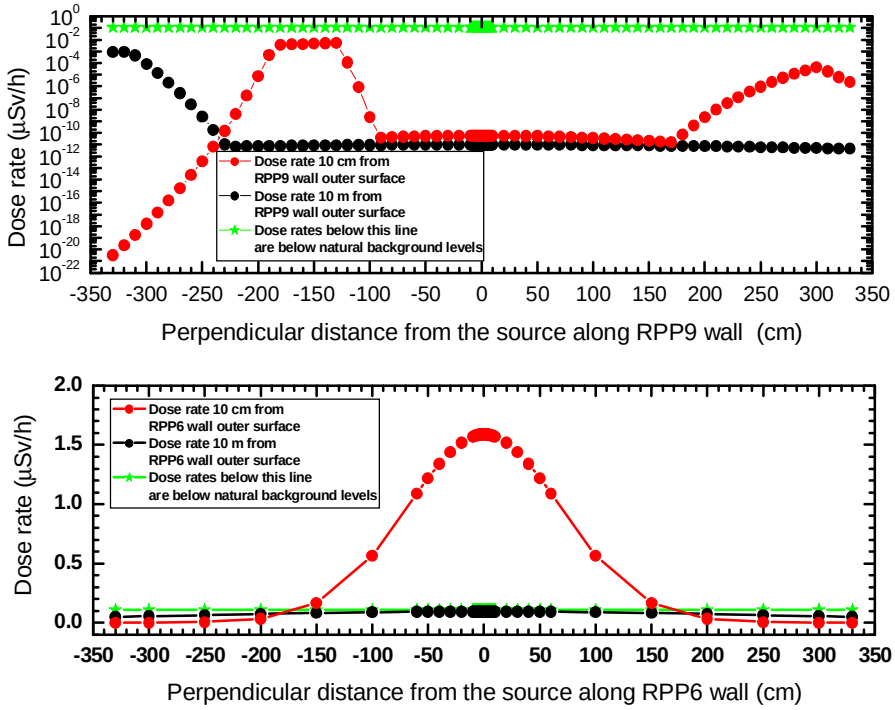

Figure 5.4: *Dose rates along the exterior of the LHS wall (RPP6) and the rightmost wall (RPP9).*

The dose rates along wall RPP6 changes from trivial values to a maximum value of 1.59 µSv/h directly opposite the exposed ^{60}Co source at 10 cm outside the outer surface of RPP6, at a height of 100 cm above the floor level. The dose rates along the rightmost wall, RPP9, are below the natural background level. These values are not unexpected as transmission is through a total concrete thickness of at least 330 cm. The peaks increase in Figure 5.4 are as a result of the change in wall thickness from 330 cm to 180 cm.

Spherical concrete shield geometry

In order to compare QAD-CGGP results using the MathCAD worksheet and MCNPX results, the dose rate values were calculated for three identical spherical concrete shields around a point source of ^{60}Co at the centre. This is because the MathCAD worksheet could not model the facilities for the exact physical concrete shield geometry, and as the MCNPX calculations produced no meaningful results for locations external to the

concrete shield. That is MCNPX yielded no meaningful results at a distance of 10 cm along the exterior axial direction of the walls. This is explained in §5.3 and §5.4. For this case, dose rate values and varying radial distances from the source centreline to points outside the outer surface of a 150 cm thick ordinary concrete shield were calculated using a shield with symmetrically spherical geometry (SPH—Sphere). The spherical concrete shield of 150 cm thick begins at radial distance of 175 cm up to 325 cm.

The dose rates obtained at radial distances and constant height above floor level, from the centreline of the source are shown in Figure 5.5. These dose rate values were calculated using the point-kernel integration code, QAD-CGGP.

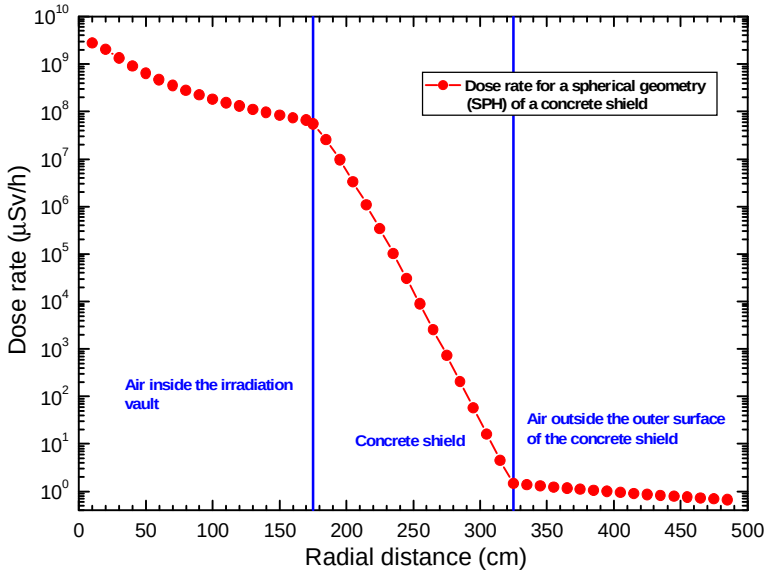

Figure 5.5: *Dose rates at various radial distances through a concrete shield of spherical geometry.*

Of note are extremely high dose rates at about 10 to 175 cm radial distances, and the sharp decrease as the radiation transverse the concrete shield. At 10 cm (point P") outside the outer surface of the shield, the dose rate is 1.4 µSv/h. This is the same value obtained when using RPPs geometric bodies.

5.3 Modelling with the MathCAD worksheet

Spherical concrete shield geometry

To ensure quality of the calculated dose rates with QAD-CGGP, a MathCAD worksheet that implements the point-kernel method with geometric progression and the build-up factors was used. However, the MathCAD worksheet has limitation in modelling the facilities. That is, the MathCAD worksheet could only model point sources, a single layer of a single shielding material of only ordinary concrete of density 2.35 g.cm$^{\bullet 3}$, and with all layers surrounded by vacuum on all sides. For this reason, the calculations was

carried-out for only the spherical-symmetrical concrete shield (spherically geometry—SPH) around a point source of ^{60}Co at the centre.

5.3.1 MathCAD worksheet results

The dose rates against changing radial distances from the point source centreline for an ordinary concrete shield of 150 cm thick and the dependence of the dose attenuation factor on shield thickness, are shown in Figure 5.6. The red line illustrates what the dose rates would be without a shield. The black line shows the effectiveness of the concrete shield, and the blue indicates the dependence of the dose attenuation factor on shield thickness. The source is located at the origin (**< œ** 0 cm) and the concrete shield start at radial distance of 175 and ends at 325 cm.

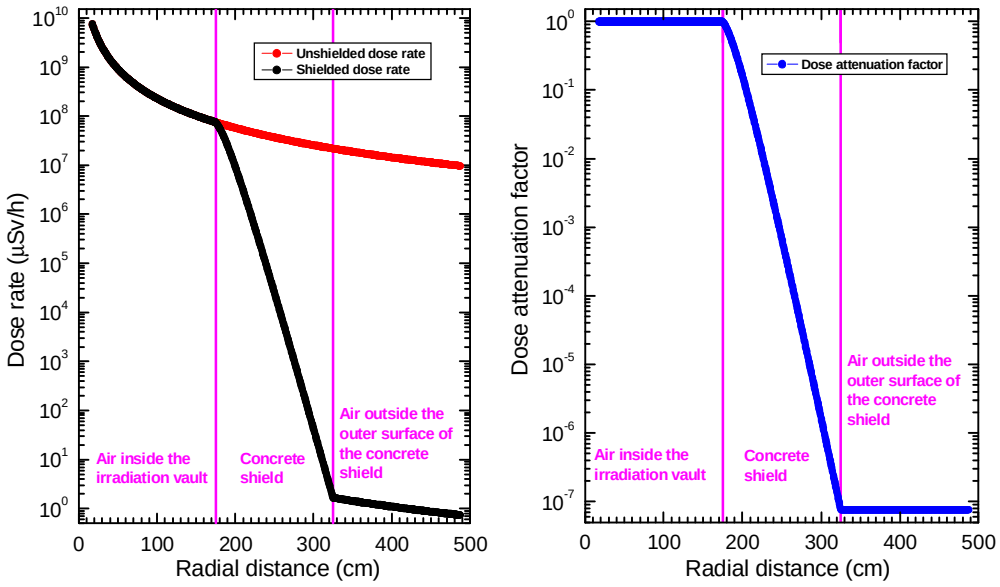

Figure 5.6: *Dose rates and the variation of dose attenuation factor with radial distance for a concrete shield of spherical geometry, obtained using MathCAD worksheet.*

At 10 cm outside the outer surface of the shield, the dose rate is 1.6 µSv/h. Of note in Figure 5.6, is dose attenuation factor of 7.6 **,** 10**•)** at 325 cm; implying that the dose rate with the shielding in position, is 7.6 **,** 10**•)** times lower than it would have been without the concrete shielding material. The implication is that thin ordinary shields material would be inadequate for the 20 kCi (0.74 PBq) ^{60}Co source; for example, a thickness of 25 cm (i.e., at a radial distance of 200 cm in Figure 5.6) will provide a DAF of 1.52 **,** 10**•"**, whereas a 150 cm thickness (radial distance of 325 cm) of an ordinary concrete will provide a DAF of 7.6 **,** 10**•)**.

5.4 Modelling with the code MCNPX

The Citrusdal insect sterilization facility was also modelled in MCNPX to verify the results obtained using point-kernel methods (§5.2 and §5.3). Comprehensive modelling of the facility, i.e., source geometry, walls and roof were identical to the model developed as input data set for QAD-CGGP (Appendices C.2 to C.4). A top and side view geometry of the facility modelled with the radiation transport computer code, MCNPX, is shown in Figure 5.7. Shown in green is the concrete source shielding. The top and side cylindrical stainless steel encapsulated ^{60}Co rod is shown in red. The blue colour represents air medium inside and outside the irradiation chamber. Top view **B** and **C** axis are shown, the **D** axis protrudes vertically upwards from the page; side view **D** and **B** axis are also shown, y axis thrust outwards from the page. The thickness of the walls are exactly as indicated in Figure 3.4 on page 36.

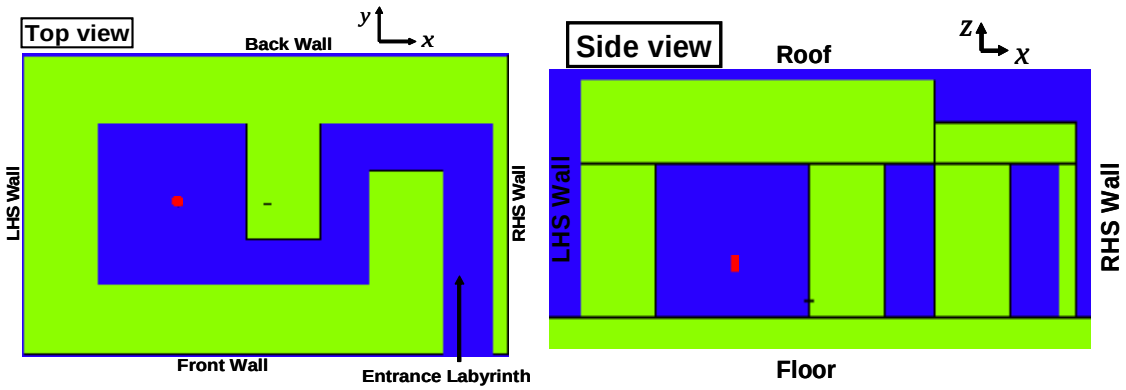

Figure 5.7: *Top and side view of the irradiation vault of the Citrusdal insect sterilization facility, modelled using MCNPX.*

Except for dose rates at selected positions along the labyrinth, the MCNPX calculations yielded no results for dose rates external to the physical concrete shield geometry shown in Figure 5.7. All the exterior axial dose rates were zeros for 7000 minutes of runs. This was because of the radiation streaming through a very thick concrete shield. Even with the computer run time increased by a thousand all dose rates results were zeros. Instead all dose rate values outside the concrete shield were calculated using symmetrically spherical geometry (SPH). To increase computational efficiency, a variance reduction (Russian roulette—geometry splitting) technique was used. This is because "*Russian roulette—geometry splitting*" works well for spherical-symmetrical geometry (RSICC CCC-730, 2005). The variance reduction method is based on controlling the population of the particles move to more important regions of the geometry. Different importances were assigned to cells, so as to keep the population of ionising photons nearly constant in every cell. The spherical-symmetrical geometry that was utilised with variance reduction technique is shown in Figure 5.8 on page 61.

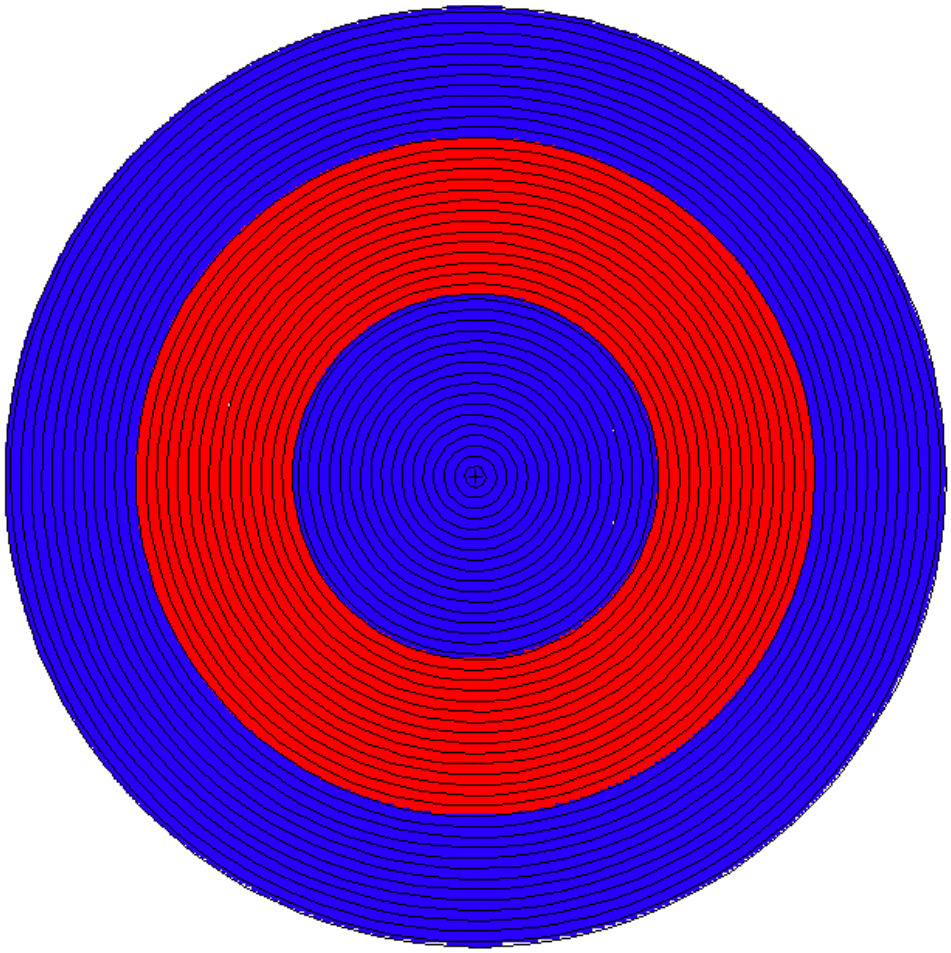

Figure 5.8: *A concrete shield of spherical geometry of the Citrusdal facility.*

Shown in blue colour is the air medium inside and outside the irradiation vault. The red colour depicts the concrete shield and solid lines (in black) indicates the variance reduction tool "Russian roulette—geometry splitting". The source was located at the centre with the shield position at 175 to 325 cm from the source centre.

5.4.1 MCNPX results

Spherical concrete shield geometry for external dose rate determinations

As pointed out, the dose rate calculations of the MCNPX runs were extremely slow, and generated no results for about 7000 minutes of runs. This was because of the deep penetration of radiation from the ^{60}Co source through a 150 cm thick concrete shield. A spherical geometry (shown in Figure 5.8) which was exactly identical to the one used in §5.2 and §5.3 was again employed with variance reduction tool to reduce the computer time required for obtaining results with acceptable statistical error of less than 10%. The run time in this case was 120 minutes.

Figure 5.9 on page 62 shows the dose rate along the radial direction that transverse a 150 cm thick spherical concrete shield. The dose rate values were calculated at radial

distances from the source centreline along the line through point P▪. As shown in Figure 3.4 on page 36, point P▪ is 10 cm outside the outer surface of the concrete shield and directly opposite the exposed source.

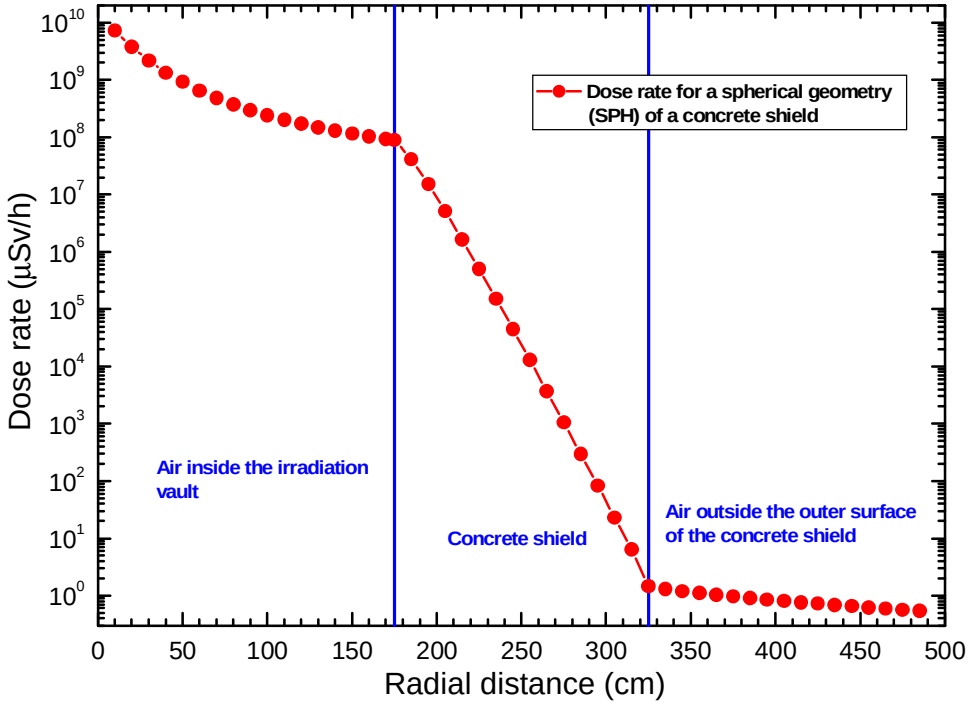

Figure 5.9: *The dose rate distribution along the radial direction of the 150 cm thick spherical concrete shield.*

The spatial dose rate distribution shows a sharp decrease as the radiation transverse the spherical concrete shield. The dose-rates were calculated from 10 to 485 cm from the source centreline. The dose rate is 1.3 µSv/h at point P▪

Dose rates at selected positions along labyrinth

The dose rates values along the multi-bend labyrinth were calculated using MCNPX radiation transport code. Only MCNPX was used because it is capable of evaluating dose rates streaming along labyrinth. The several selected positions in the labyrinth and the corresponding distances from the source centreline position are shown in Figure 3.4 on page 36. Figure 5.10 on page 63 presents the dose rates for several selected positions from the centre position of ^{60}Co source within the multi-bend labyrinth. The closest point P_2 is at 190 cm and the farthest point P▪ is at 1040 cm from the centre-position of the gamma emitting ^{60}Co source (refer to Figure 3.4 on page 36).

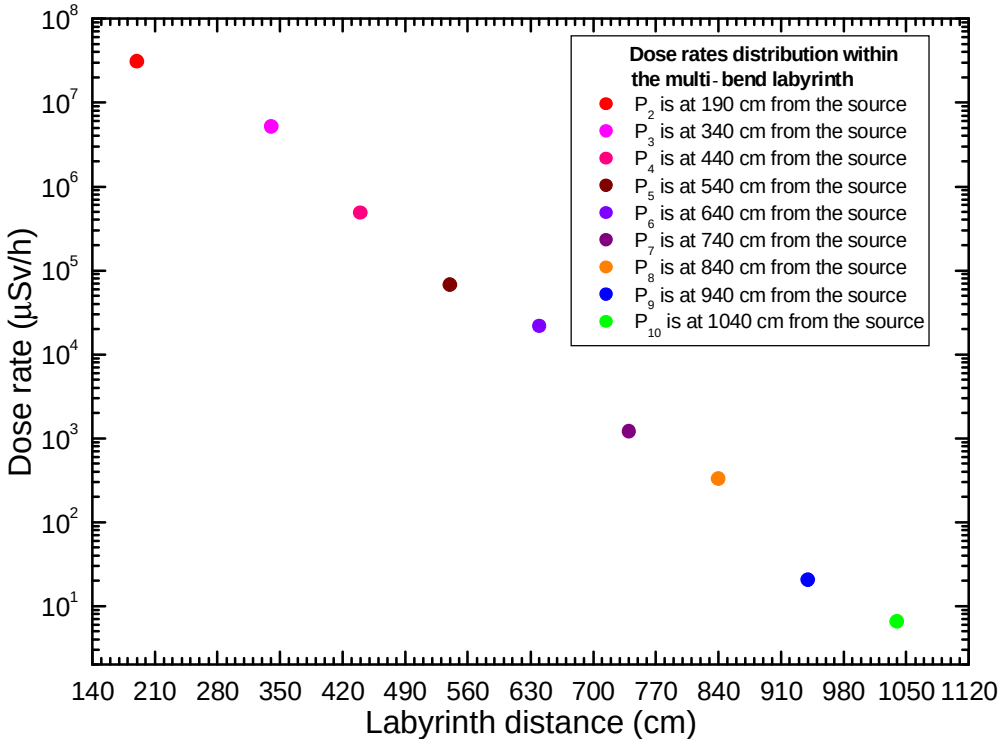

Figure 5.10: *Dose rate in several selected distances from the* centre-position of ^{60}Co source *within the multi-bend labyrinth.*

As can be noted, the dose rate is very high at the nearest position (P_2) to the source (of the order of 10^7µSv/h). As the distance increases farther away from the source along the labyrinth, the streaming radiation suffer multiple scattering and eventually the dose rates falls off very rapidly to the value of 6.54 µSv/h closer to the entrance/exit door position.

Spatial variation of dose rates within and outside shielded facility

Figure 5.11 on page 64 illustrates the spatial distribution of effective dose rates in µSv/h inside and outside the Citrusdal irradiation facility. Shown in red and orange indicates spatial regions of high relative dose rate, green intermediate dose rates and blue low relative dose rates. The colour-scale is automatically produced by MCNPX mesh tally plotting features, which does not generate a legend for the colours. For this reason, dose rate values in Figure 5.9 and 5.10 were used to indicate the variation of dose rates inside and outside the Citrusdal irradiation facility. The highest dose rate values are indicated in red colour (of the order of 10^9 µSv/h), whilst the lowest are elucidated in blue, i.e., in the order of 10^0 µSv/h.

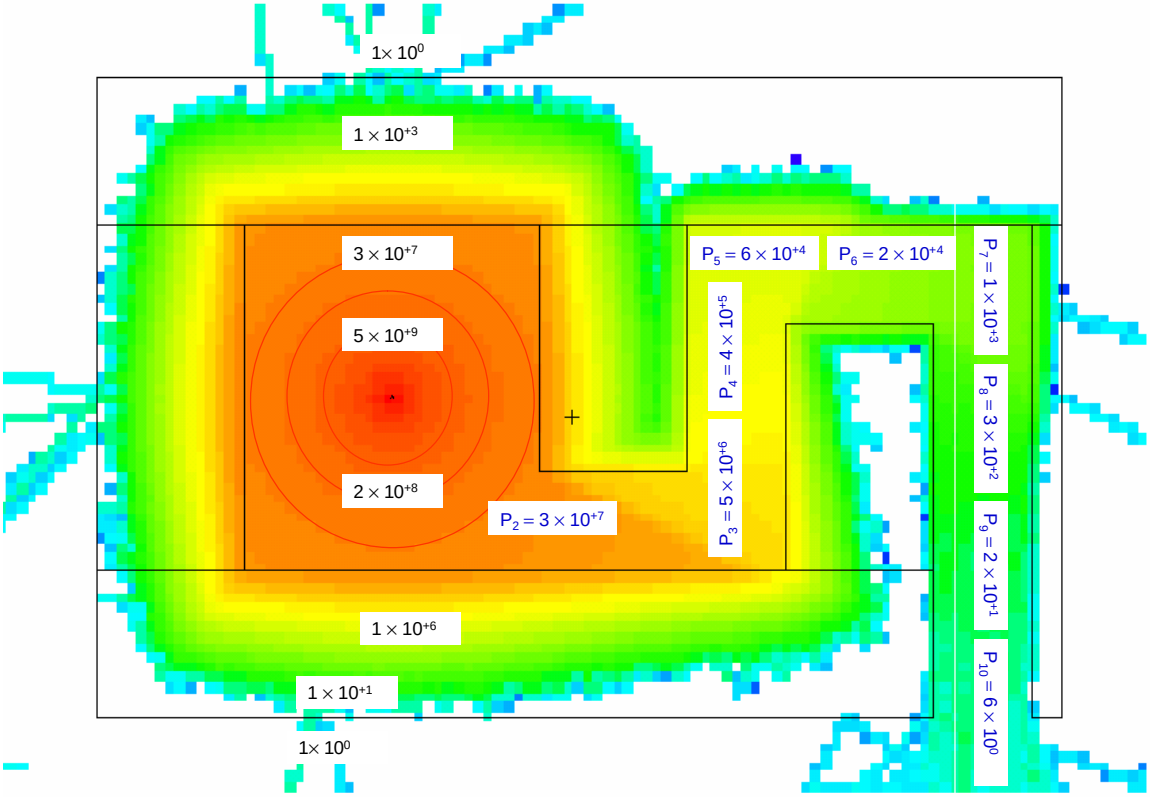

Figure 5.11: *Layout of the concrete shielding area as seen from the top, including the spatial distribution of dose rates in µSv/h (calculated using MCNPX).*

As noted in Figure 5.10, the dose rate values falls off very rapidly within the labyrinth as the distance increases farther away from the source and along the labyrinth towards the entrance/exit door position. Of note in Figure 5.11 is the effectiveness of the concrete shield around a 20 kCi (740 TBq) ^{60}Co source. The figures confirm that the concrete shield with the multi-bend labyrinth is of sufficient thickness for the source strength.

5.5 Comparison between dose distributions evaluated with QAD-CGGP, MathCAD and MCNPX

Spherical concrete shield geometry

In order to verify the dose-rate distributions calculated with the point-kernel integration code, the results obtained using a spherical geometry were compared with MCNPX predictions. Dose rates at the point P▪ are shown in Table 5.3, page 65. As explained, P▪ is at 10 cm outside the exterior of the front (RPP5) wall and at height 70 cm above the floor (refer to Figure 3.4 on page 36).

***Table 5.3** Comparison of dose-rate predictions at point P‟.*

Dose rate (μSv/h)		
MathCAD worksheet	QAD-CGGP	MCNPX
1.6	1.4	1.3

Figure 5.12 presents a comparison between the dose rates predictions.

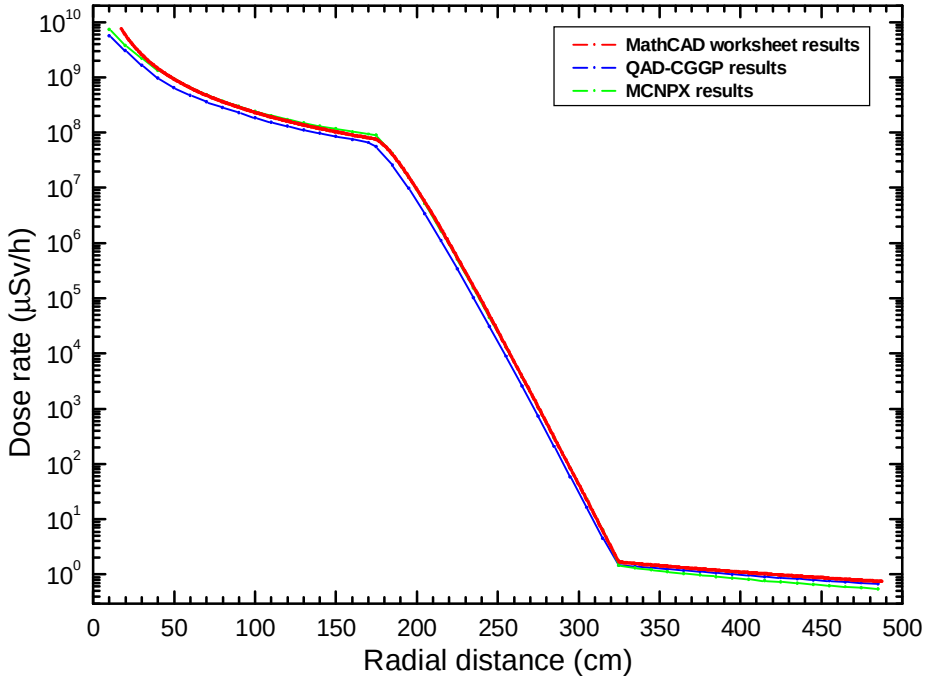

***Figure 5.12:** Comparison of dose-rate values for the spherical-symmetrically geometry case calculated with the MathCAD worksheet, QAD-CGGP and MCNPX.*

It can be noted in Figure 5.12, the dose rates calculated with QAD-CGGP computer code is the lowest from 10 to about 325 cm except outside the concrete shield. The variation in dose rate is mainly from the infinite medium buildup factor assumed in the QAD-CGGP calculation to account for the dose from scattered flux. As explained in Chapter 4, MCNPX uses far more computer time, but is able to model scattering and streaming because it simulates radiation transport rigorously whereas QAD-CGGP uses the point-kernel ray tracing technique for the computation of gamma dose rates.

For radiological protection purposes, the dose rate calculated with MathCAD worksheet is the highest at P‟ (the closest point to the concrete shield). This is as a result of the source being approximated as an isotropic point source and self shielding within the source volume was not considered. The MathCAD results differ by 13% from the QAD-CGGP results. For QAD-CGGP and MCNPX, the different is 7%. This relative deviation is because of the nature of the point-kernel integration over Monte Carlo method. Practically, there is no appreciable different between the results. Therefore, taking into consideration the semi-analytical approximation methodology of the point-kernel, these

results show good agreement. Such satisfactory agreement confirms that the QAD-CGGP results presented in §5.2.1 can therefore be accepted as reasonably accurate.

5.6 Projected annual doses

In this section the results predicted with the methods presented in Chapter 4 are discussed. The criteria for judging radiation shielding is presented in Appendix A.2.

For the worse case, the peak dose rates at 10 cm from the outside outer surface of the concrete shielding walls, directly opposite the source, and 50 cm above the outside outer surface of the roof concrete were used to calculate maximum realistic annual doses to radiation workers. The following assumptions pertaining to radiation workers were adopted:

- Maximum number of shifts per year being 360;
- Maximum daily stay time adjacent to the concrete wall, at peak dose rate position of 2 hours per shift;
- Maximum annual stay time on the roof of 24 hours per year;
- Maximum daily stay time adjacent to the maze, at the entrance door dose rate position of 2 hours per shift.

Table 5.4 summarises the evaluated dose rates based on the assumed annual occupancy times and projected maximum realistic annual doses to radiation workers.

Table 5.4: *Maximum effective dose rates, with assumed annual occupancy times for radiation workers.*

Maximum realistic doses to radiation workers			
Wall or closest position	Peak dose rate (µSv/h)	Realistic exposure time (h/yr)	Maximum realistic annual dose (mSv/yr)
RPP4	1.4	720	1
RPP5	1.4	720	1
RPP6	1.59	720	1.14
RPP9	0	720	0
RPP11 (Roof)	0	24	0
RPP10 (Roof)	22.8	24	0.54
Labyrinth*	6.54	720	4.70

* At the entrance/exit door position.

The maximum realistic annual dose shown in Table 5.4 are well below legal dose limits and also below the ICRP recommended dose limits (ICRP publication 103, 2007; Appendix A.1).

The peak dose rates at 1000 cm from the outside outer surface of the concrete shielding walls and 50 cm above the outer surface of the roof concrete were used to calculate the annual doses to members of the public. The figure of 1000 cm was adopted as the worse case scenario. The closest distance members of the public can approach the facility is far greater than 1000 cm. Assumptions pertaining to non-radiation workers were:

- Maximum number of shifts per year of 360;
- Maximum daily stay time adjacent to the concrete wall, at peak dose rate position being 2 hours per shift;
- Maximum annual stay time on the roof of 8 hours per year;
- Maximum annual stay time adjacent to the entrance door position of 8 hours per year.

Table 5.5 presents a summary of the dose rates, based on occupancy levels and the projected maximum realistic annual doses for members of the public. Included are staff not registered as radiation workers.

***Table 5.5** Maximum effective dose rates, assumed annual occupancy times, and maximum realistic doses, to members of the public.*

Maximum realistic doses to members of the public			
Wall or closest position	Peak dose rate (μSv/h)	Realistic exposure time (h/yr)	Maximum realistic annual dose (mSv/yr)
RPP4	0.091	720	0.065
RPP5	0.091	720	0.065
RPP6	0.095	720	0.068
RPP9	0	720	0
RPP11 (Roof)	0	8	0
RPP10 (Roof)	22.8	8	0.182
Labyrinth*	6.54	8	0.052

* At the entrance/exit door position.

The maximum realistic effective doses for non-radiation workers, shown in Table 5.5, are as well below legal dose limits and below the ICRP recommended annual dose limits of 1 mSv for non-radiation workers and below the generally recommended dose constraint value of 0.3 mSv/yr (ICRP publication 103, 2007; Appendix A.1), and as well

the average background dose value from natural occurring ionising radiation of approximate 2.5 mSv/year.

5.7 Dose distribution within the insect containers

Modelling with the code MCNPX

The dose distribution within the insect containers were modelled for one hour of exposure using MCNPX, and the computer run-time was 9900 minutes. The modelling was done for a ^{60}Co source with a nominal activity of 16.8 kCi, i.e., 622 TBq, (calculated 15 June, 2008). The active part of the source rod was raised to an irradiation position of 8.5 cm above the mini-turntables' level. A pile of six cylindrical PVC containers filled to 60% (2.1 cm) of the available space (3.5 cm) with insects, were stacked on a polystyrene spacer (20 cm , 7 cm) and placed on top of the mini-turntable with midpoints located 46 cm away from the source centreline. Each of the PVC containers had the same dimensions (refer to Figure 3.3 on page 35). A side-view geometry of the stacked PVC containers is shown in Figure 5.13. The **D** and **B** axes are as shown with the **C** axis thrust outwards from the page. The ^{60}Co source is mounted inside a longer, thin-walled stainless steel cladding tube. Orange colour depicts the air medium whereas yellow indicates the insects.

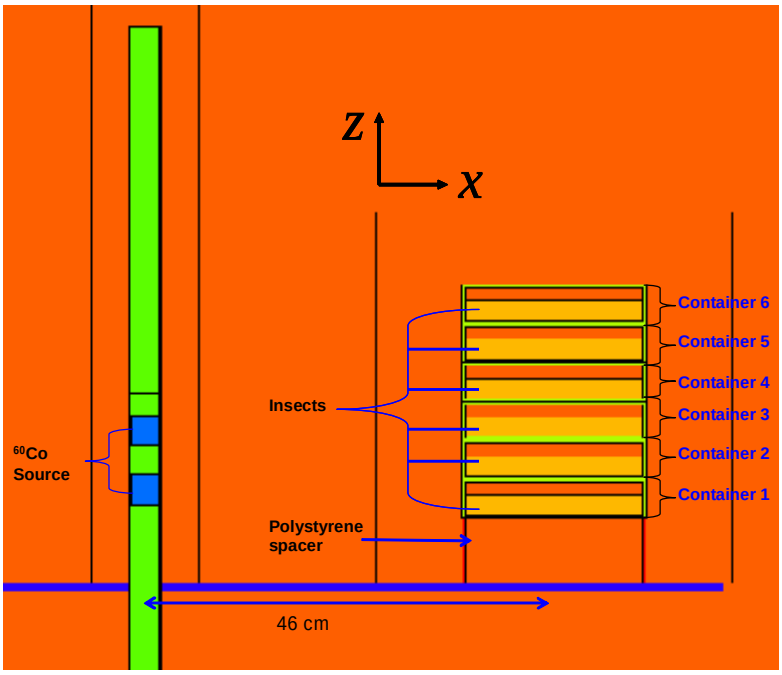

Figure 5.13: *A side-view geometry of six PVC containers filled to 60% of the available space with insects stacked on a polystyrene spacer, placed on top of the mini-turntable 46 cm away from the ^{60}Co source position.*

The first container on top of the polystyrene (herein referred as container 1) was located 7 cm above the mini-turntable level. Container 2 to the last one, container 6, were located at heights: 11.2, 15.4, 19.6, 23.8 and 28.0 cm above the mini-turntable level, respectively.

Results and discussion

The absorbed dose of radiation that is used to induce sterility is of critical importance to the SIT program. Insects that receive too low an absorbed dose retain too much fertility for programme purposes and, in some instances, could even compromise quarantine security. Too high an absorbed dose will result in insects that do not compete well against wild insects in the field. The absorbed dose needed to achieve a desired effect for any given SIT programme is determined through radiation research (sterility test), which involves determining the dose-effect relationship for the insects. The sterility test is done in consideration of programme requirements and effects of radiation dose on insect quality.

Figure 5.14 presents a sterility test (preliminary experimental work) for the insects, False Codling Moths, that was done during the onset of the SIT programme at Citrusdal irradiator facility (Hofmeyr, personal communication, 2006). The symbol T symbolise treated—irradiated insects, and U stand for untreated—not irradiated insects.

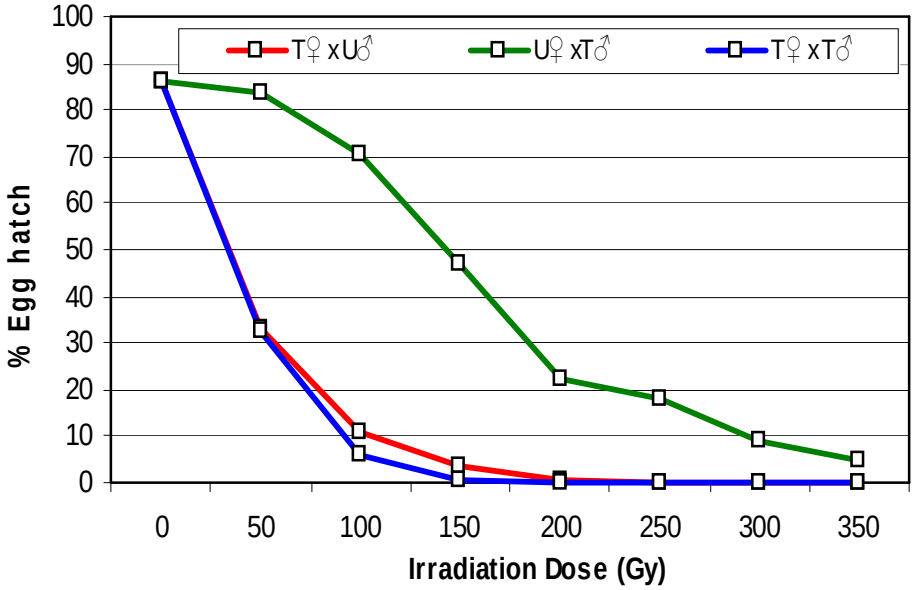

Figure 5.14: *An optimum (or average) dose necessary to sufficiently sterilize all False Codling Moths (insects) without treating large proportions with doses that are high enough to substantially reduce competitiveness.*

Figure 5.14 clearly reveals that the dose required to stop egg production in female (♀) False Codling Moths, is typically lower than the dose that is required to induce near-complete sterility in male insects (♂). Therefore in most practice, the minimum absorbed dose will be to some extent higher than the dose at which egg production stops. The irradiation (treatment) of both female (♀) and male (♂) insects resulted in establishment of a generic treatment dose of 150 Gy (minimum absorbed dose) for all False Codling Moths. In addition, because of the dose variability, the False Codling Moths actually receive a dose that is somewhat higher than that minimum. An average dose of 200 Gy is still acceptable and sufficient to provide quarantine security.

In an attempt to use MCNPX for dose calculations, rotation of the containers were also considered in order to enhance the dose uniformity. The containers were rotated by 180° around the horizontal axis (perpendicular to the source rod). A MathCAD worksheet was thereafter used for dose values calculated by MCNPX and summed them in an algorithmic way in order to reproduce the mentioned rotation.

Figure 5.15 shows an average dose distribution within the insect containers, i.e., container1 to 6, simulated with radiation transport computer code, MCNPX. Shown as well in Figure 5.15, is the dose distribution within container 2 for the angular rotation case. For this case the variation of doses in the radial direction were considered.

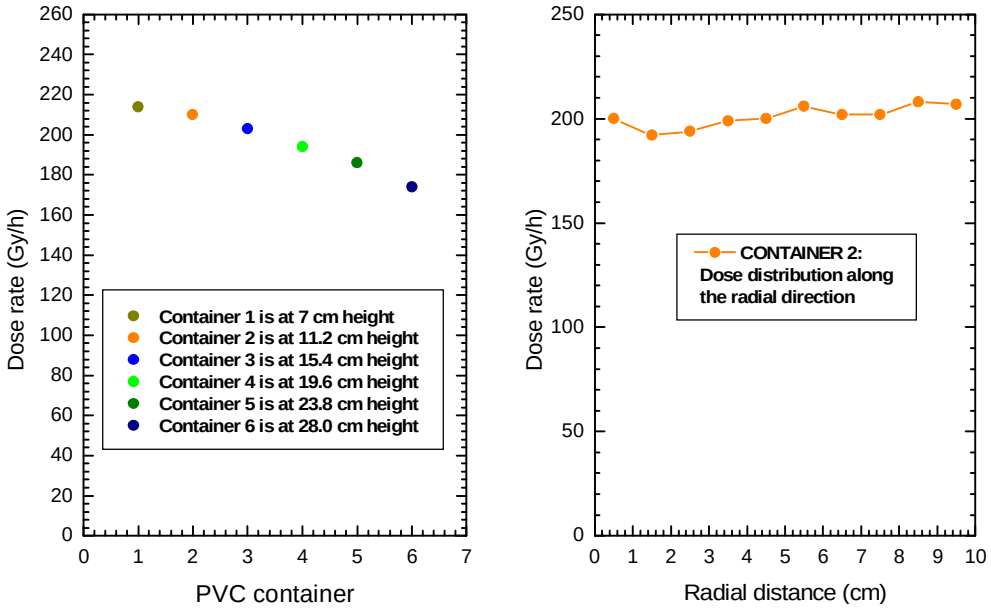

Figure 5.15: *Dose rate distribution within the insect canisters, and along the radial direction of container 2 for the angular rotational case.*

Of note in Figure 5.15 is the variation of dose rate with heights (container's positions) within the insect canisters indicating the dependence on the geometry of irradiation. Even with a computer runtime of 9900 minutes, the statistical uncertainty was above 20% for each of the volume elements (voxels) into which the insect volume was subdivided. The dose variability depicted in Figure 5.15 could be attributed to canister localisation relative to the source position. The dose, however, do not differ much from an average dose of 200 Gy which is still acceptable and sufficient for the SIT programme as shown in Figure 5.14. The highest dose distribution is 214 Gy in container 1 and the lowest is 174 Gy in container 6 for one hour irradiation. These dose distribution differ by 7 and 13%, respectively, from an average dose of 200 Gy.

The dose distribution along the radial direction in container 2 varies in a slightly random manner. For one hour irradiation the dose varies from 192 to 208 Gy. The dose of 208 Gy over estimate an average dose of 200 Gy by 4%. It is also notable that the dose values do not change significantly with the different radial distances. Therefore, the dose distribution inside six pile of insect containers are within acceptable range.

5.8 Summary

Irradiation chamber

This work partly focused on the shielding design for the Citrusdal insect irradiator facility. The distribution of dose rates from the ^{60}Co source through the concrete shielding material (walls and the roof) were considered. Most dose rates were way below the legal dose limits per year. The maximum dose rates were obtained on top of the roof where maintenance work are hardly ever performed. The maximum assumed exposure times in Tables 5.4 and 5.5 will probably never lead to undue expose of any radiation worker or member of the public beyond the legal dose limits.

The satisfactory agreement between the three calculational methods used confirms that the Citrusdal facility with the shield thicknesses specified in Figure 3.4 on page 36, appropriate radiation safety interlocks stated in §3.4, radiation safety management system as well as a carefully nurtured safety culture in the organisation in place, will operate safely.

Insects

The dose distribution within the insect containers were calculated using MCNPX. The variability of the dose rates inside the insect canisters were within acceptable dose values needed for sterilising False Codling Moths.

The conclusive agreement between the average dose value of 200 Gy and calculation (MCNPX predictions) results shows the MCNPX code to be a useful method for obtaining dose distribution profiles within product containers.

Chapter 6
Results and discussion: Stellenbosch insect sterilization facility

6.1 Dose rate evaluation

As in Chapter 5, the point-kernel integration and Monte Carlo codes were utilised to assess the radiological safety of the biological shielding at the Stellenbosch insect sterilization facility. The results were verified and validated with dose rate measurements at selected positions. The MathCAD worksheet was, however, not used because the concrete is of a higher density (**3** ¸ 2.63 g.cm$^{\bullet 3}$) than that of an ordinary concrete (**3** œ 2.35 g.cm$^{\bullet 3}$). The calculated dose rate profile around the concrete shielding at 10 and 1000 cm from the outside outer surface of the walls, and in the labyrinth including a comparison of the measurements with calculations, are presented in this chapter. The layout and dimensions of the facility, as displayed in Figure 3.9 on page 41, will be referred to for discussion of the results.

6.2 Modelling with the code QAD-CGGP

The spatial distribution of dose rates around the shielding concrete walls and on top of the roof were calculated using the point-kernel code, QAD-CGGP (as shown in the Appendix D.1). The source was modelled as a homogeneous RCC rod emitting isotropic gamma rays of 1.17 and 1.32 MeV. The rod was assumed to have the composition of stainless steel, and mass-density of 8 g.cm$^{\bullet 3}$. The walls and roofs thicknesses were modelled as RPP bodies and the active part of the source rod was raised from its shielded position to about 40 cm inside the vault of height 229 cm. The modelling was performed for concrete with estimated density value of 2.63 g.cm$^{\bullet 3}$.

The fluence-to-dose conversion factors for the ionising photons emitted by a ^{60}Co source is as illustrated in Chapter 5 (see Table 5.1).

6.2.1 QAD-CGGP results

Dose rates profile were calculated for positions 10 cm from outside the outer surface of the walls and 50 cm above the horizontal level of the roof, with the ^{60}Co source on the exposed position. All the dose rates were computed at 100 cm height. Evaluations were also performed at a distance of 1000 cm to determine the projected maximum annual doses to members of the public, which includes non-radiation workers.

Roof

Figure 6.1 shows the dose rate profiles on top of the concrete roof change with lateral movement along line AB and MN, on the **C** axis (refer to Figure 3.9 on page 41). Shown as well in Figure 6.1, is the elaborate detail of dose rate distribution with a logarithmic dose rate axis. Line AB lies on the plane **B** œ 0 cm, and line MN on the plane **B** œ • 122 cm. The red line is for lateral movement along line AB, while the black line is for lateral movement along line MN. The point zero on the axis is at plane **C** œ 0 cm.

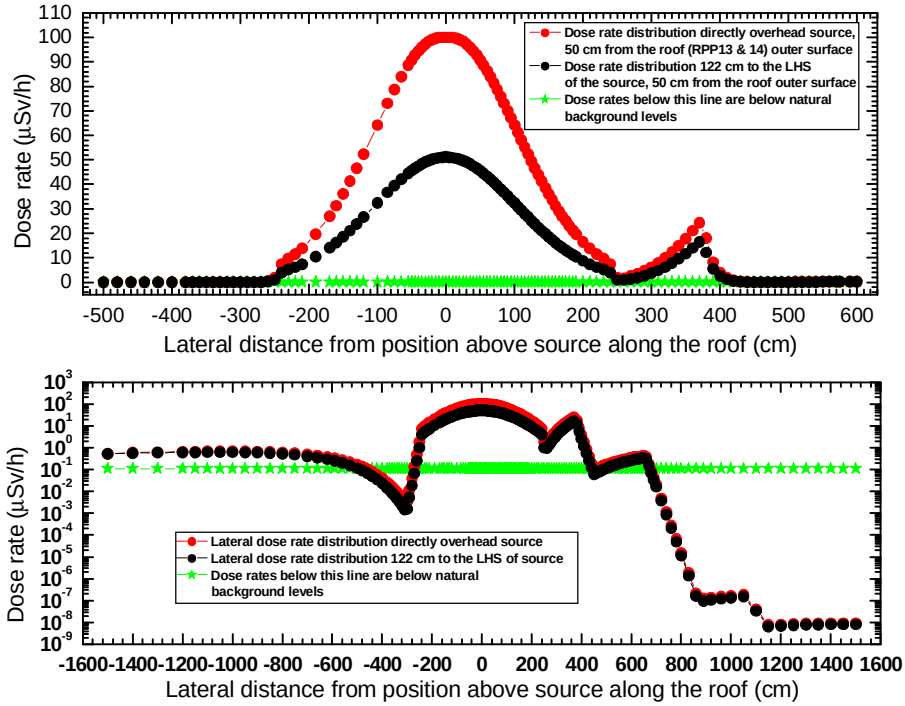

Figure 6.1: *Dose rate distributions on the 91 cm thick concrete roof.*

It is apparent in Figure 6.1 that the dose rate distributions on the concrete roof vary from negligible values, to a maximum value of 100 µSv/h, directly above (at plane **C** œ 0 cm) the exposed source. As the laterally position changes from **C** œ 0 cm, the effective thickness of the concrete traversed by the photons, increases resulting in the drop in dose rates to values below the background level. The intricate detail demonstrated in the dose rate profile is the result of the passage of the radiation through the three dimensional geometry of the concrete building—the radiation field traverse different thicknesses of concrete.

Walls

The axial distribution of dose rates calculated at a distance of 10 and 1000 cm from the outside outer surface of the leftmost (RPP5) and the back (RPP9) walls are shown in Figure 6.2, page 74. The dose rate changes from insignificant to a peak dose rate of 0.55 µSv/h at 10 cm from the exterior of RPP5 wall and 0.248 µSv/h from the outside outer surface of RPP9 wall.

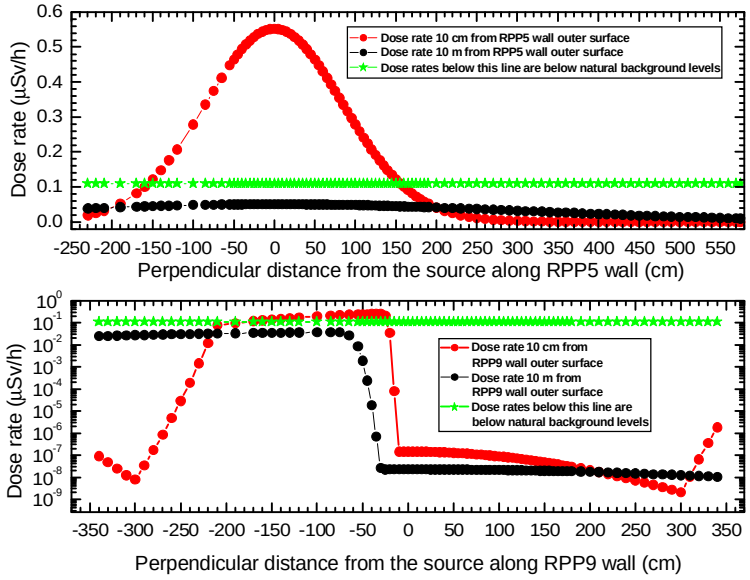

Figure 6.2: *Dose rate distributions along the exterior of the leftmost and back wall.*

It can be seen from Figure 3.9 on page 41, the radiation need to transverse a total of 130 and 237 cm thick concrete towards the negative **B** axis, and towards the positive **C** axis respectively. The efficacy of the shielding is highlighted from the calculated dose rate values.

The dose rates profile evaluated at 10 and 1000 cm from the exterior of the RHS (RPP7) and front (RPP6) wall are displayed in Figure 6.3. The front wall is at the same distance of 122 cm from the source centreline as RHS wall, therefore, the dose rate profiles for these walls are numerically equal.

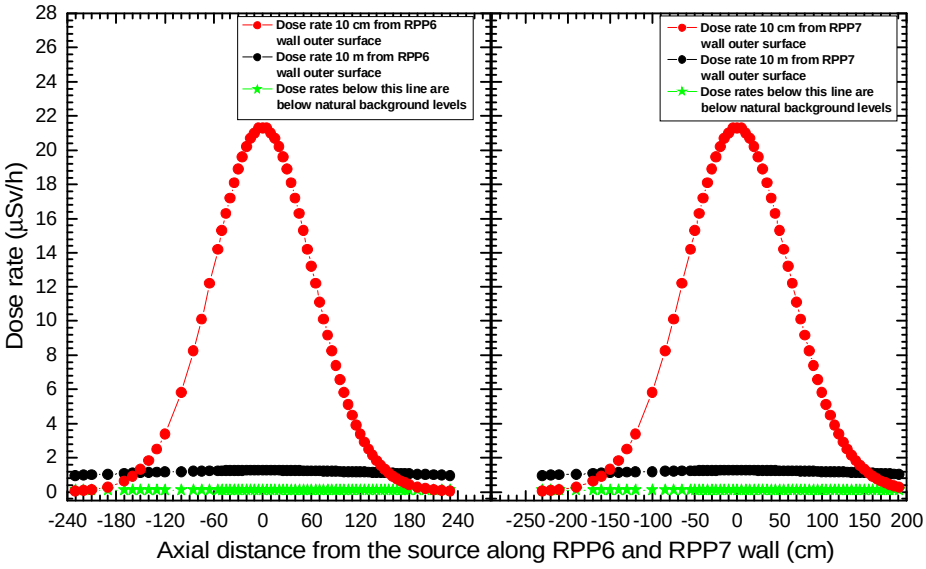

Figure 6.3: *Dose rates outside the outer surface of the RHS (RPP7) and front (RPP6) wall.*

The highest dose rate is 21.3 µSv/h at a distance of 10 cm from the outer surface of the walls, directly perpendicular the exposed ^{60}Co source. At the 1000 cm distance, the dose rate drops to a value of 1.26 µSv/h.

Figure 6.4 shows the spatial dose rate distribution along the LHS (RPP4) and the RHS *"towards the back"* (RPP8) wall (refer to Figure 3.9 on page 41). The axial dose rates along the RPP4 wall were only evaluated at a distance of 10 cm from the outside outer surface of the wall. This was because of the geometric location of RPP4 wall with respect to the source and RPP5 wall position. The spatial dose rates profile along RPP8 wall were calculated at a distance of 10 and 1000 cm from the exterior. These dose rates were computed at maintained height of 100 cm to the exposed source.

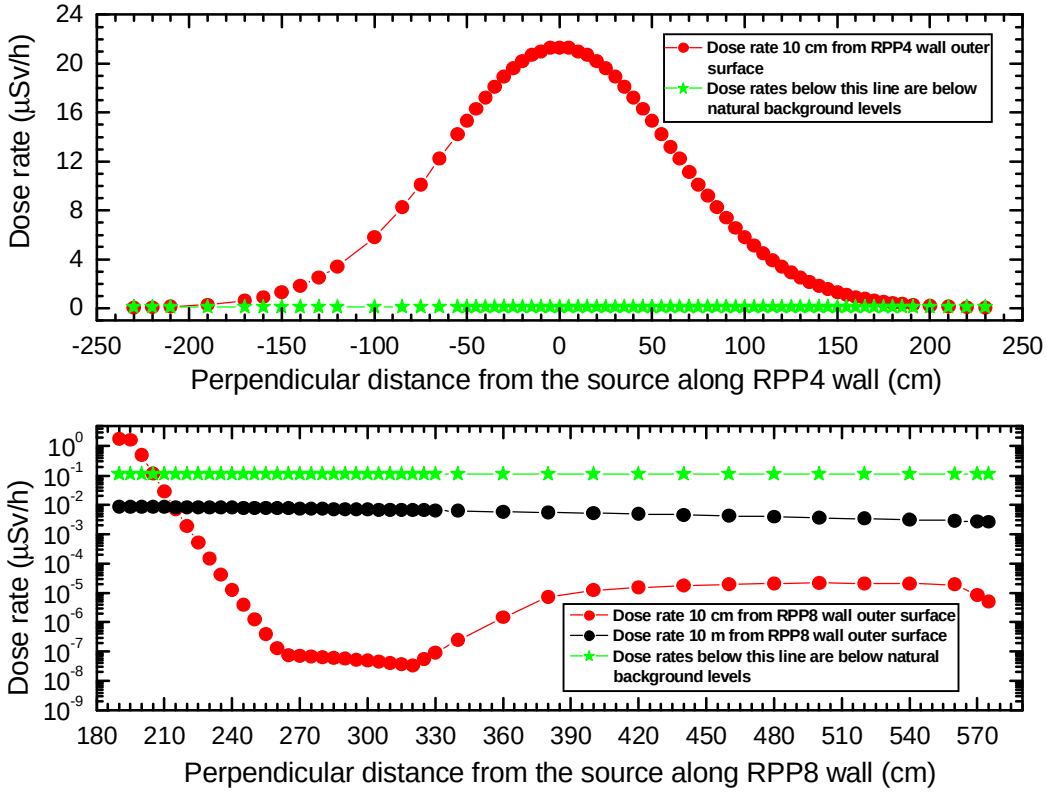

Figure 6.4: *The axial dose rate distributions along the outside outer surfaces of RPP4 and RPP8 walls.*

As expected, the peak dose rate of 21.3 µSv/h on the RRP4 wall correspond to the dose rates of RPP7 and RPP6, for the reason that the geometric dimensions with respect to the source location are the same. Of note in Figure 6.10 on page 80, at about 180 to about 210 cm along RPP8 wall, there is a noteworthy contribution of dose rate directly from RPP7 wall. As a result, the highest dose rate at 190 cm along RPP8 is 1.78 µSv/h. At 1000 cm, the calculated dose rates along RPP8 wall are below natural background levels, hence, insignificant.

Spherical concrete shield geometry

For comparison purpose, the dose rate values were calculated at several radial distances using a spherical-symmetrical (SPH) geometry of a concrete shield. The dose rates were

calculated at several radial positions, at sustained height above the floor from the source centreline. The results are shown in Figure 6.5. The 107 cm thick concrete shield starts at a radial distance of 122 cm and ends at 229 cm.

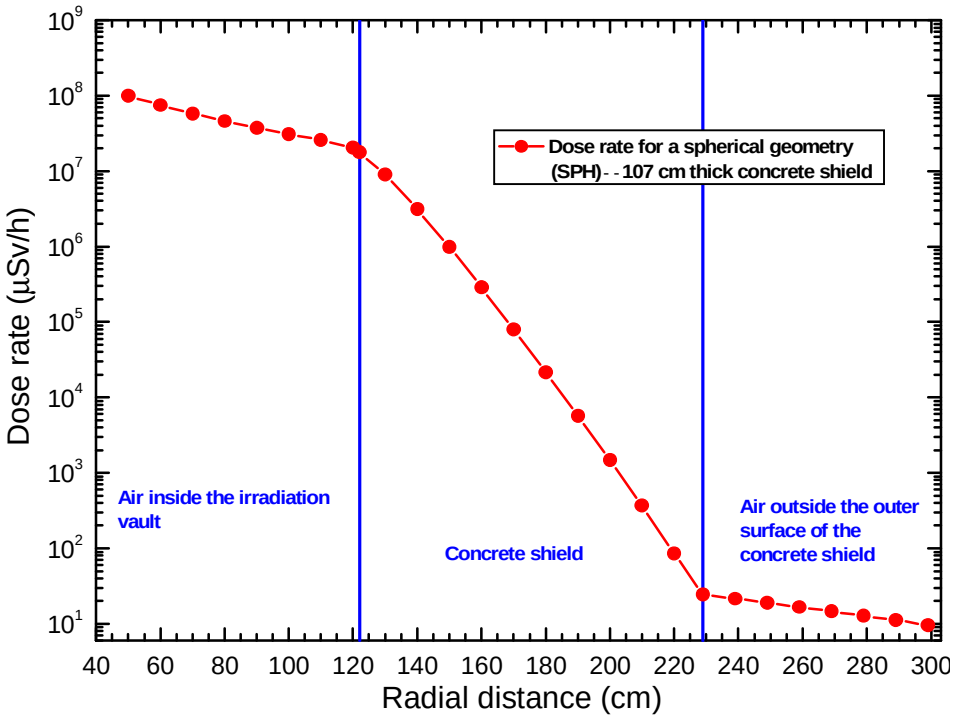

Figure 6.5: *Dose rates at various radial positions from the source centreline through a spherical geometry of a concrete shield, obtained using QAD-CGGP.*

It is apparent in Figure 6.5 that as the radiation stream across the concrete shield, the dose rates drops very sharply. At a radial distance of 10 cm from the outside outer surface of the concrete shield, the dose rate is 21.3 µSv/h. This value corresponds to the value obtained when using the RPP geometric bodies.

6.3 Modelling with the code MCNPX

The Stellenbosch insect sterilization facility was modelled using MCNPX (as shown in the Appendices D.2 to D.4), to confirm the results obtained using point-kernel method. This was done for the exact dimensions of the facility as indicated in Figure 3.9 on page 41. A top and side view geometry of the Stellenbosch facility modelled in MCNPX is presented in Figure 6.6, page 77. Displayed in red is the concrete shielding around the source; green represents the top and side view of the ^{60}Co source rod and in blue colour indicates the air medium inside and outside the irradiation chamber. The thicknesses of the walls are exactly as indicated in Figure 3.9. Top view **C** and **B** axis are shown with the **D** axis perpendicular to the page. Side view **D** and **B** axis are displayed with the **C** axis thrust upwards from the page.

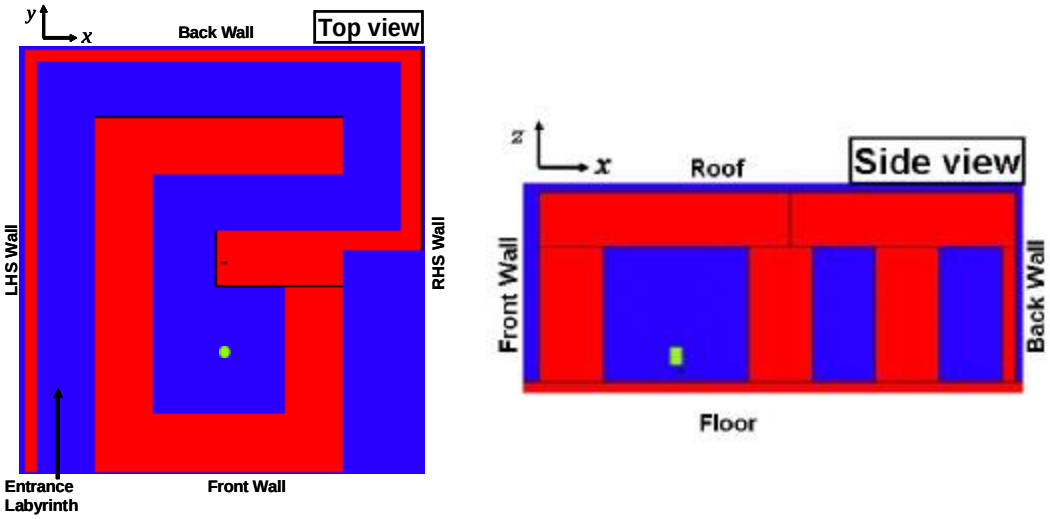

Figure 6.6: *Top and side view of the irradiation vault of the Stellenbosch Facility.*

Again as expected for the Stellenbosch facility, the radiation transport computer code, MCNPX, calculations produced no meaningful results for positions external to the concrete shield for the geometry presented in Figure 6.6. That is the statistical error was above 30% for 7500 minutes of computer run time. This may be due to the radiation having to pass through the 107 cm thick concrete shield and the assumed density of 2.63 $g.cm^{\bullet 3}$ used. Therefore, an ideal spherical (SPH) concrete shield geometry with variance reduction technique to improve computational efficiency was employed. As pointed-out in Chapter 5, Russian roulette—geometry splitting technique works well for spherical shield geometric body. Figure 6.7 represents the SPH geometry of the concrete shield. The red colour represents the concrete shield. The blue colour depicting the air medium inside and outside the irradiation vault, and solid line in black indicates the variance reduction (Russian roulette—geometry splitting) tool.

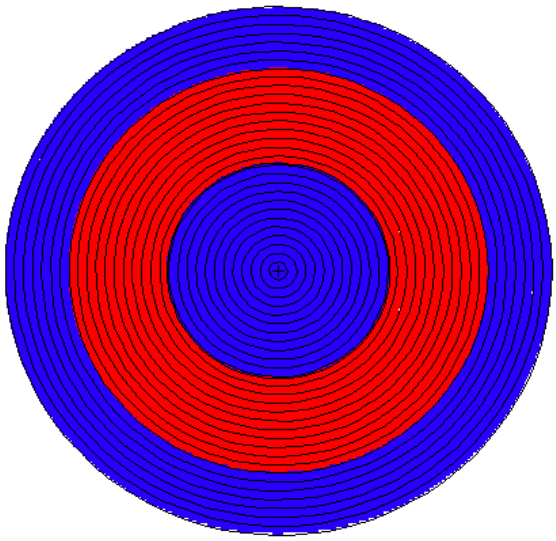

Figure 6.7: *A concrete shield of spherical geometry of the Stellenbosch facility.*

The variance reduction tool was used to evaluate the dose rate at different radial distances. The source was located at the centre. The concrete shield starts at 122 and ends at 229 cm from the source centre.

6.3.1 MCNPX results

Spherical concrete shield geometry for external dose rate determinations

The dose rate calculations of the MCNPX runs were extremely slow, and produced results with very high statistical error of more than 30% for 7500 minutes of run time. A spherical geometry shown in Figure 6.7 was used with variance reduction technique to reduce computer time required to produce satisfactory results. Figure 6.8 shows dose rate profiles that were evaluated at various radial distances from the source centreline. The dose rate values were evaluated at radial positions from the source centreline along the line through point P‟. Point P‟ is 10 cm outside the outer surface of the concrete shield wall and directly opposite the exposed source (refer to Figure 3.9 on page 41).

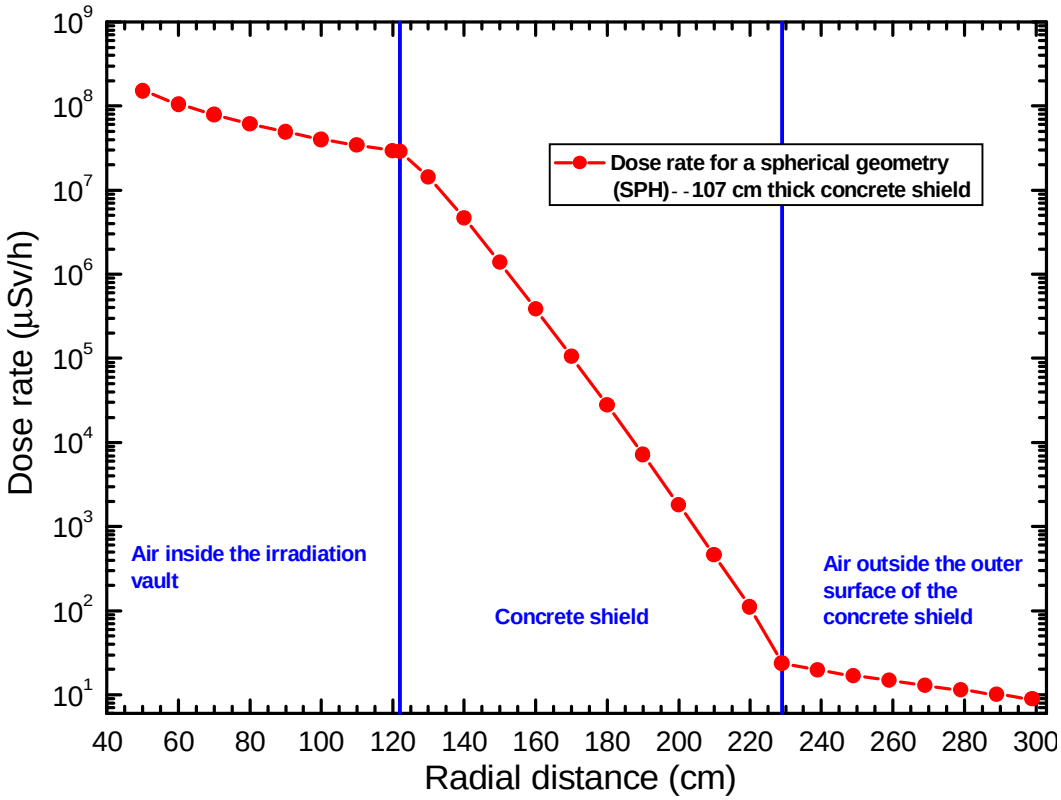

Figure 6.8: *The dose rate distributions along the radial direction on the 107 cm thick spherical concrete shield, calculated using MCNPX.*

As can be seen from Figure 6.8, the dose rate rapidly drops to a value of 19.6 µSv/h at point P_1 as the radiation stream across the spherical concrete shield.

Dose rates at selected positions along labyrinth

The dose rate distributions were calculated at various points along the labyrinth (maze) using radiation transport computer code, MCNPX. The various points along the maze and the corresponding distances from the source centreline are shown in Figure 3.9 on page 41. These points, because of their localisation relative to the ^{60}Co source position, are extreme cases adopted as the worse case scenario. As pointed out in Chapter 5 (§5.4.1), MCNPX was used because of its capability to evaluate dose rates streaming along the labyrinth. The results for dose rate distributions at several positions in the maze are shown in Figure 6.9.

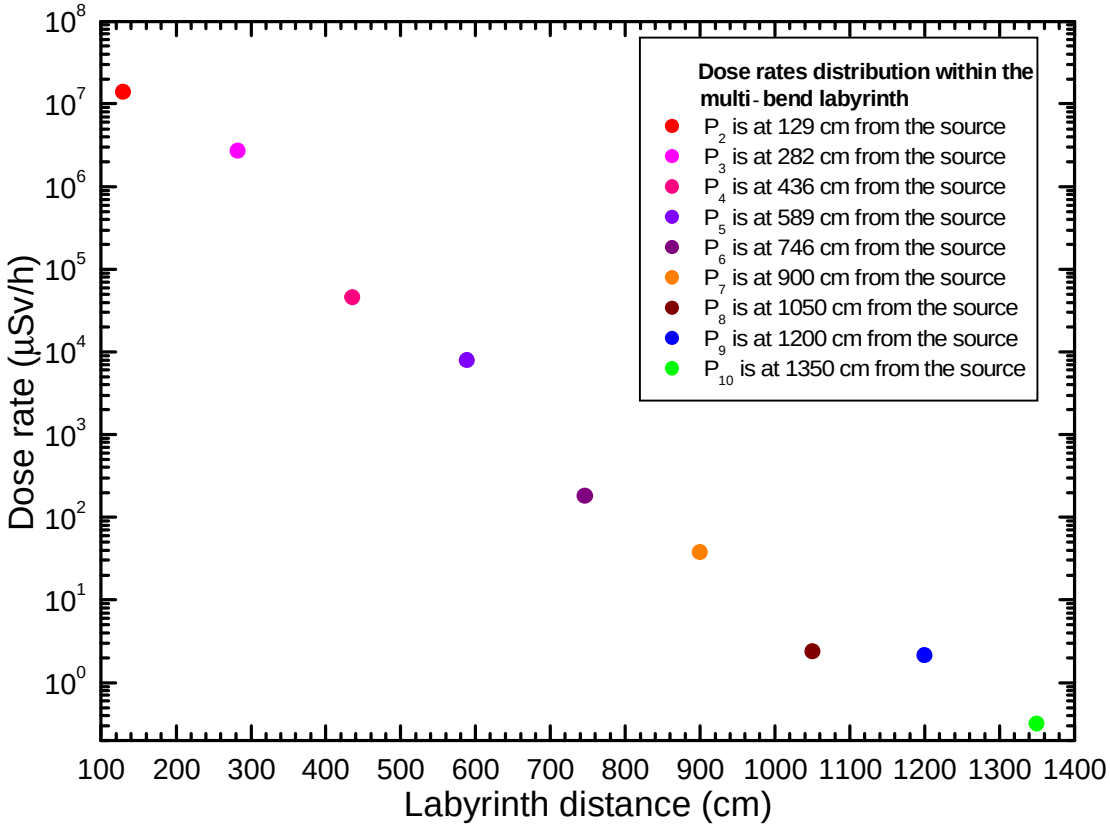

Figure 6.9: *Dose rates distribution at various positions along the multi-bend labyrinth.*

As the radiation streams in the direction of the entrance/exit position, multiple scattering within the long labyrinth walls occurs. The dose rate close to the entrance/exit at point P¡, was calculated to be 0.32 µSv/h (refer to Figure 3.9 on page 41).

Spatial variation of dose rates within and outside shielded facility

Figure 6.10 (page 80) again shows how dose rates changes as the radiation streams across the concrete shield, and along the labyrinth. These doses are given in terms of µSv/h. As in Figure 3.9 on page 41, Figure 6.10 depicts the top-view of the facility. As explained in Chapter 5 (§5.4.1), the colour-scale is automatically generated by MCNPX mesh tally plotting features, which does not generate a legend for the colours. As a result, dose rate values in Figure 6.8 and 6.9 were used to indicate the spatial distribution of

dose rates inside and outside the Stellenbosch insect sterilization facility. The variation of dose rate profiles as the radiation streams across the concrete shield are indicated in red, yellow, green and blue colour. The highest dose rates are shown in red whereas the lowest in blue. The highest doses are in the order of 10^8 µSv/h while the lowest in the order of 10^0.

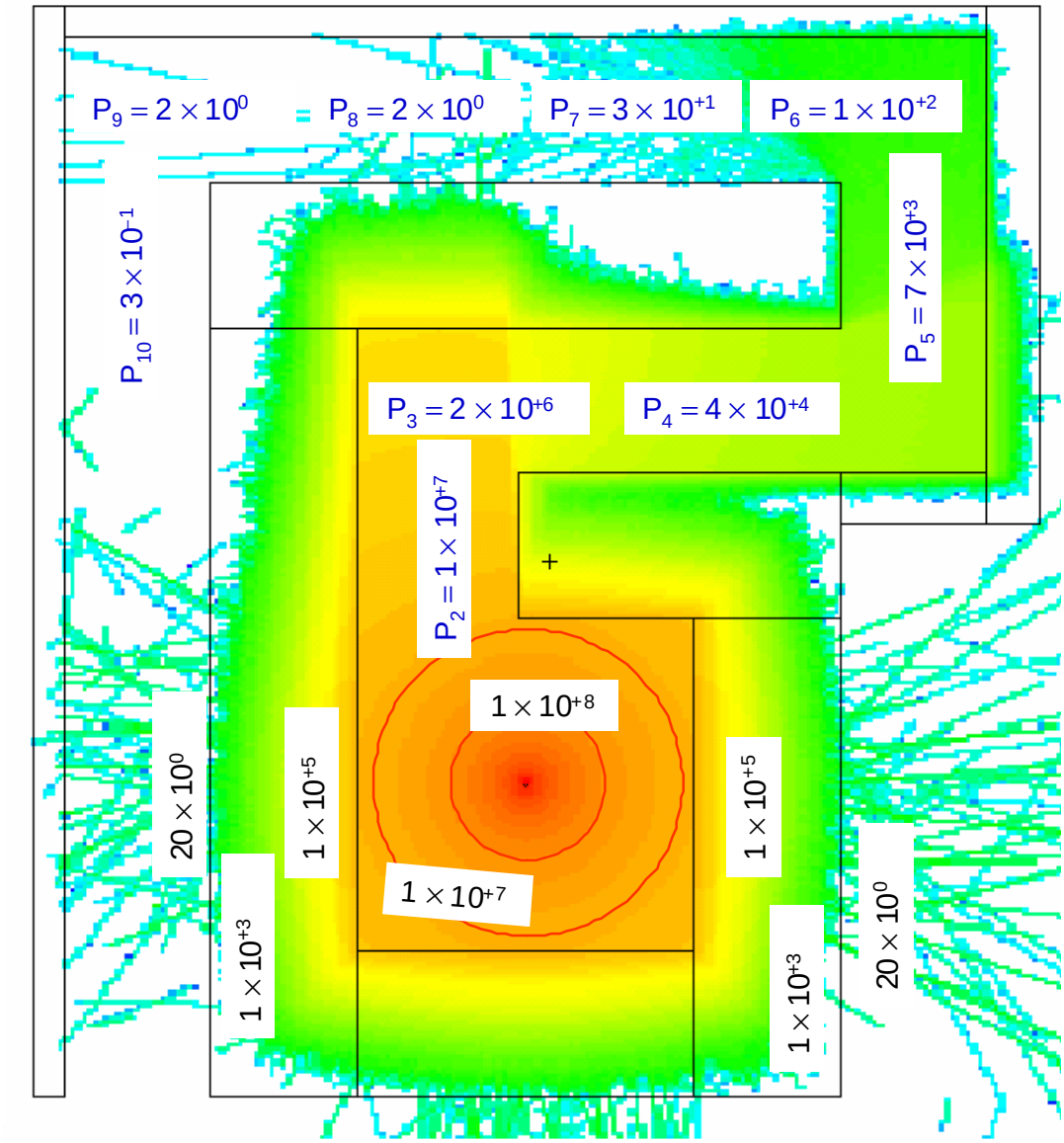

Figure 6.10: *Layout of the shielding area as seen from above, including the variation of dose rate profiles within and outside the shielding concrete of the Stellenbosch irradiator facility, obtained with the radiation transport computer code (MCNPX).*

It can be noted in Figure 6.10 that the radiation suffer multiple scattering as it streams within the labyrinth. The drop in dose rate outside the shielding concrete shows that the concrete is reasonably effective for shielding a ^{60}Co source of 10 kCi (0.37 PBq) activity.

6.4 Dose rate measurements

Introduction

The dose rates were measured at various distances along and 10 cm from the outside outer surface of the shielding concrete walls. The roof and front wall (RPP6—refer to Figure 3.9 on page 41) were, however, excluded because access to these areas for measurements to be taken were disallowed. In principle, the dose rates measured on wall RPP7 should be the same as for RPP6 (refer to Figure 6.3), because of their physical locations with respect to the ^{60}Co source position. A gamma ray monitor, GRAETZ X5C, calibrated in May 2007, was used for all dose-rates measurements.

Walls

Except for the RPP7 wall, The measured dose rates were below natural backgrounds (0.11 µSv/h). Figure 6.11 shows the dose rates 10 cm away from the outer surface and along RPP7 wall; with peak dose rate value peaking at 14.6 µSv/h.

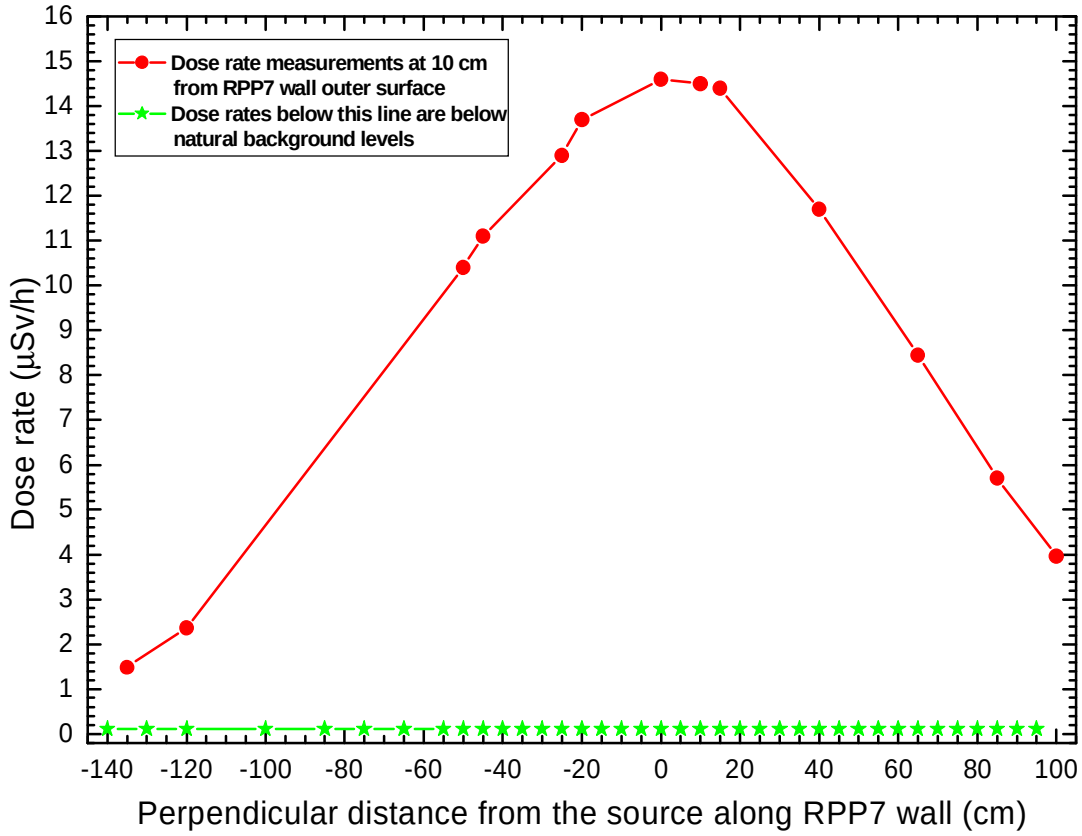

Figure 6.11: *Dose rates distribution along the outside outer surface of the RPP7 wall.*

It is apparent from Figure 6.11, that the measured dose rate values are significantly higher than the natural background levels. The minimum dose rate value is 1.49 µSv/h.

Dose-rate distribution along the maze

The dose rate profiles were, where possible, measured at six various points along the maze using gamma-ray monitor. The various points along the maze and corresponding distances from the source location are shown in Figure 3.9 on page 41. Figure 6.12 presents dose rate values measured at six different points along the maze.

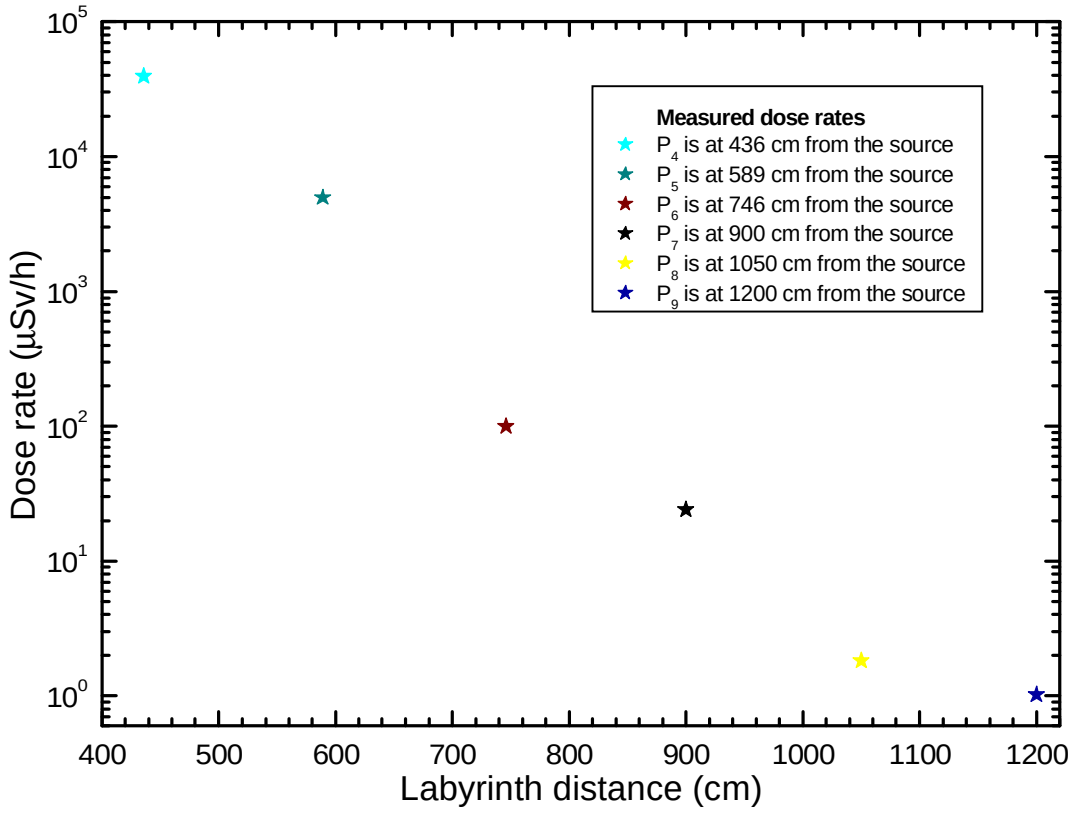

Figure 6.12: *Measured dose-rates at six different positions along the labyrinth.*

As can be seen, the dose rates falls off very rapidly as the position changes, with the values being lower as one moves farther away from the source location and along the maze. The measured dose rates at point P) and P_9, towards the entrance/exit, were 1.82 and 1.02 µSv/h, respectively. This indicates the level of dose rates to be practically insignificant towards the entrance/exit position.

6.5 Comparison of dose rate results

Spherical concrete shield geometry

Table 6.1 on page 83 gives dose rates at point P▪ obtained from measurements as well from MCNPX and QAD-CGGP computer codes simulation, point P▪ being 10 cm outside the outer surface of the front wall and directly opposite the exposed source (refer to Figure 3.9 on page 41).

Table 6.1 *Comparison of the dose rate predictions at point P▪.*

Dose rate (μSv/h)		
Measured	QAD-CGGP	MCNPX
14.6	21.3	19.6

The calculated dose rate values using the two mentioned methods for the spherical geometry case is graphically shown in Figure 6.13.

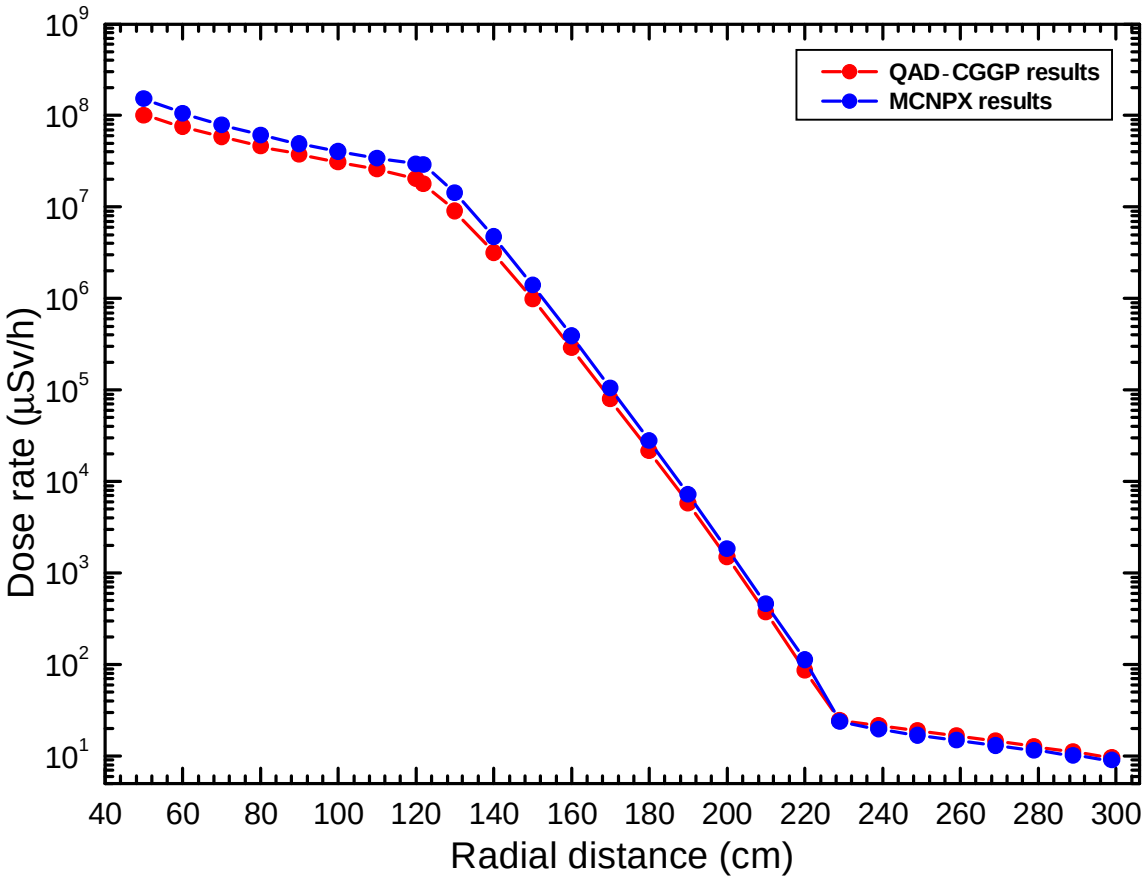

Figure 6.13: *Dose rates calculated with QAD-CGGP and MCNPX computer codes.*

Again (as seen in Chapter 5 §5.5), the dose rates calculated with the radiation transport computer code, MCNPX, are the highest from 50 to about 229 cm except outside the concrete shield. As pointed out in §5.5, the main reason of the discrepancy in dose rate has in the use of the infinite medium buildup factor in the QAD-CGGP calculation to account for the contribution from scattered flux. Furthermore the point-kernel uses a ray tracing technique to approximate the dose rates at several points of interest. The QAD-CGGP calculations for dose rate at point P▪ agree with the MCNPX within 8%. The QAD-CGGP relative fractional error is 31% when compared to the measured value. For MCNPX the error is 26%. These relative fractional percentage errors are the results of the slightly higher density used for the 107 cm thick concrete shielding material. This implies that in the case of a concrete shield with less density and thickness, radiation can easily stream across and leading to a smaller relative fractional error. For radiation

protection purposes, such discrepancy between the measured and calculated results are general considered satisfactory.

Wall

The dose-rate distribution estimated with QAD-CGGP and the measurements along the outside outer surface of the RHS (RPP7) wall are shown in Figure 6.14. Of note in Figure 6.14 is the calculated and the measured peak dose rate at **B œ !** cm on the **B** axis—dose rate at point P▪ (refer to Figure 3.9 on page 41).

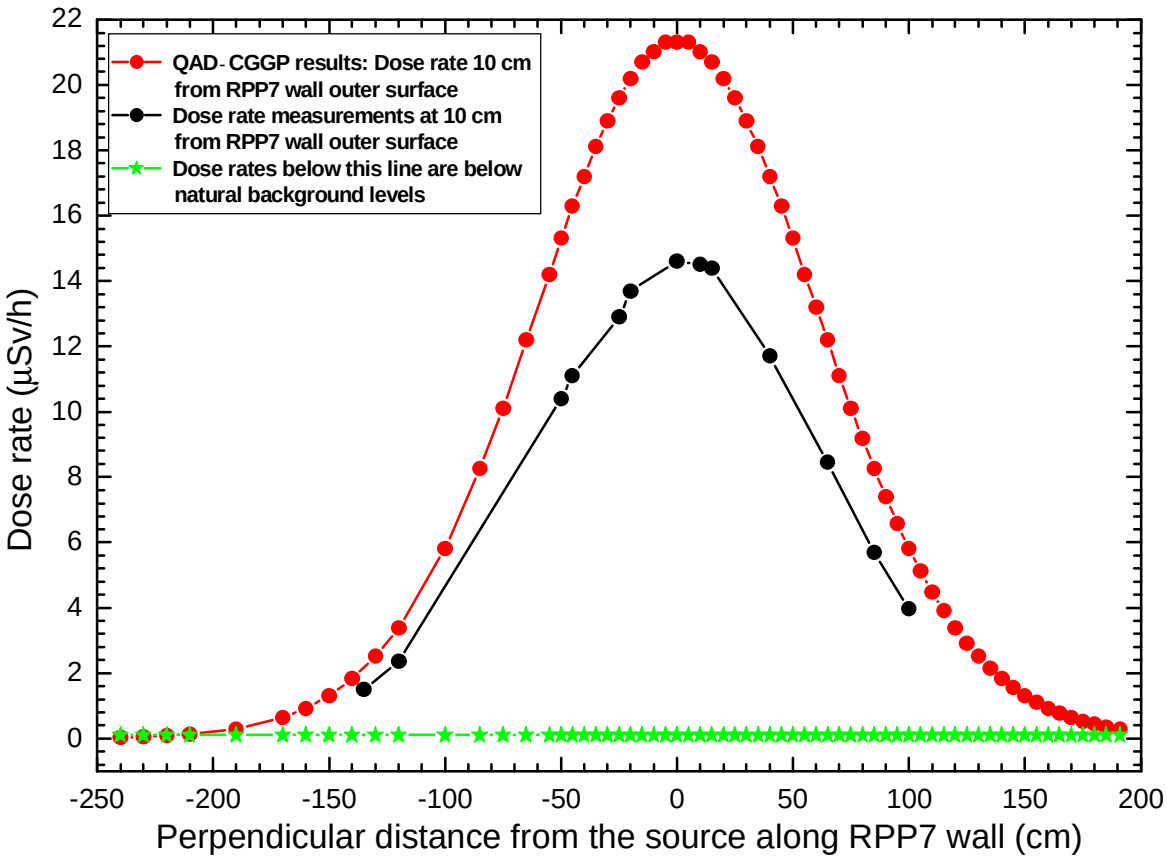

Figure 6.14: *Comparison of calculated and measured dose rates along the outside outer surface of the RHS (RPP7) wall.*

The calculated and the measured peak dose-rate are 21.3 and 14.6 µSv/h, respectively. Compared to a value from measurements, the point-kernel code over estimated the dose rate by about 31% at **B œ !** cm. However, the dose rates estimated with QAD-CGGP deviate slightly from measurements as one moves laterally away from **B œ !** cm.

Labyrinth

The comparison of calculated results with measured values at various positions along the maze is presented in Figure 6.15 on page 85. As expounded in §6.3.1 and 6.4, several positions along the multi-bend maze and the corresponding distances from the source centreline are shown in Figure 3.9 on page 41. The points, P_2, P_3 and P_4 are the closest

whereas P_8, P_9 and P_{10} are the farthest (towards the entrance/exit door position) from the ^{60}Co source position.

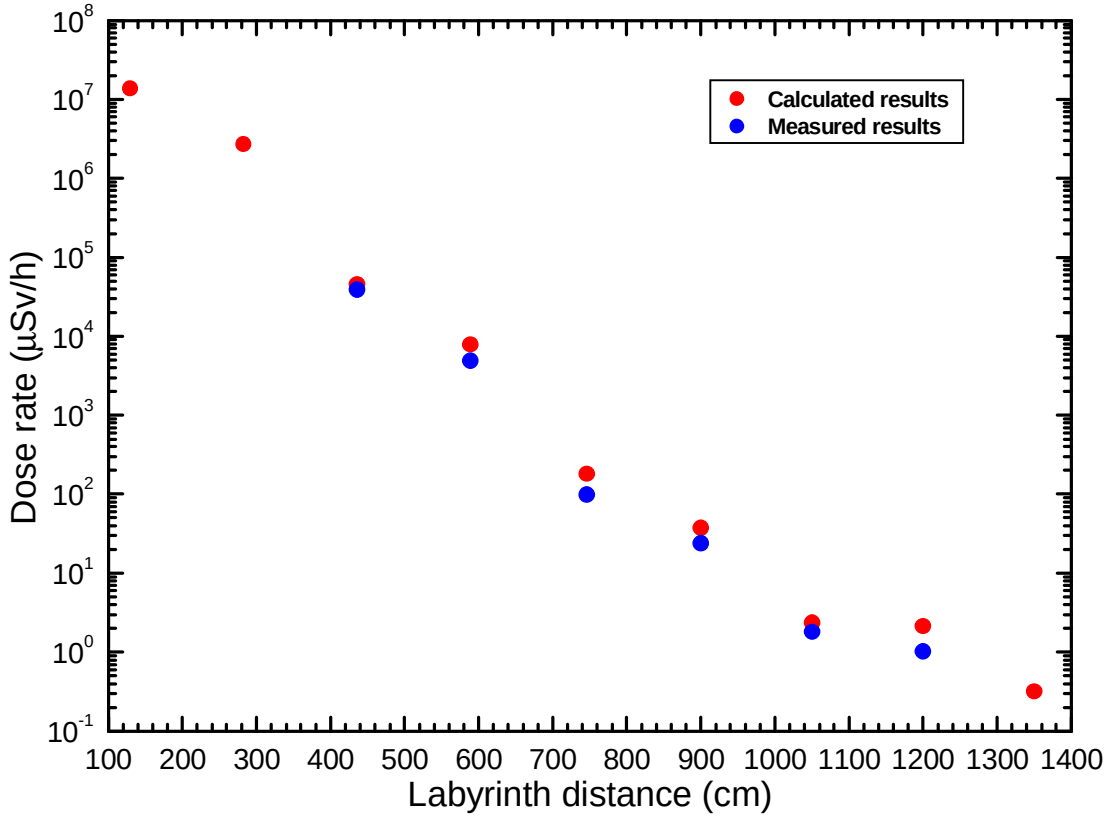

Figure 6.15: *Comparison of calculated and measured dose rates at selected positions from the centreline of ^{60}Co source within the multi-bend maze.*

The calculated results show a reasonable agreement with the measured values. For example, from point P% (at 436 cm) to the ^{60}Co source position, and P* (at 1200 cm farthest from the ^{60}Co source location) towards the entrance/exit door position within the labyrinth, the dose rates are 4.56 , 10^4 µSv/h, 2.14 µSv/h and 3.91 , 10^4 µSv/h, 1.02 µSv/h, respectively; representing a 14% to 52% discrepancies between the calculated and measured values.

The relatively close agreement between the computer generated dose rate values and the measured values provide support that the results presented in §6.2.1 can again be accepted as reasonably accurate.

6.6 Projected annual doses

This section discusses the results presented in the preceding sections. The criteria for judging radiation shielding is presented in Appendix A.2.

The irradiator building at the Stellenbosch insect irradiation facility is quite isolated from the personnel offices. For the worse case, the peak dose rates at 10 cm from the exterior of the concrete shielding walls, directly opposite the source, and 50 cm above the horizontal exterior surface of the roof concrete were used to calculate maximum realistic annual doses to radiation workers. Assumptions pertaining to radiation workers are:

- Maximum number of shifts per year of 360;
- Maximum daily stay time adjacent to the concrete wall, at peak dose rate position of 1 hours per shift;
- Maximum annual stay time on the roof of 8 hours per year;
- Maximum daily stay time adjacent to the maze, at the entrance/exit area dose rate position of 1 hours per shift.

Table 6.2 gives the projected maximum realistic annual doses to radiation workers at different locations and at the assumed annual occupancy times.

***Table 6.2** Maximum effective dose rates, annual occupancy times and maximum realistic doses to radiation workers.*

Maximum realistic doses to radiation workers			
Wall or closest position	Peak dose rate (µSv/h)	Realistic exposure time (h/yr)	Maximum realistic annual dose (mSv/yr)
RPP4	21.3	360	7.66
RPP5	0.55	360	0.19
RPP6	21.3	360	7.66
RPP9	0.248	360	0.09
RPP13 and 14 (Roof)	100	8	0.8
RPP8	1.78	360	0.64
RPP7*	21.3	360	7.66
RPP7**	14.6	360	5.25
Labyrinth*	2.14	360	0.77
Labyrinth**	1.02	360	0.37

*Calculated value.

**Measured value.

The maximum realistic annual dose shown in Table 6.2 are well below legal dose limits and also below the ICRP recommended dose limits (ICRP publication 103, 2007; Appendix A.1).

The peak dose rates at 1000 cm from the outside surface of the concrete shielding walls and 50 cm above the outer surface of the roof concrete were used to calculate the annual

doses to members of the public. The following assumptions pertaining to non-radiation workers were made:

- Maximum number of shifts per year of 360;
- Maximum daily stay time adjacent to the concrete wall, at peak dose rate of 1 hours per shift;
- Maximum annual stay time on the roof of 6 hours per year;
- Maximum annual stay time adjacent to the entrance/exit area position leading to the labyrinth of 6 hours per year.

Table 6.3 presents a summary of the dose rates, occupancy levels and the projected maximum realistic annual doses to members of the public, including staff not registered as radiation workers.

***Table 6.3** Maximum effective dose rates, assumed annual occupancy times, and maximum realistic doses to members of the public.*

Maximum realistic doses to members of the public			
Wall or closest position	Peak dose rate (µSv/h)	Realistic exposure time (h/yr)	Maximum realistic annual dose (mSv/yr)
RPP5	0.05	360	0.018
RPP6	1.26	360	0.453
RPP9	0.036	360	0.012
RPP13 and 14 (Roof)	100	6	0.6
RPP8	0.008	360	0.002
Labyrinth*	2.14	6	0.012
Labyrinth**	1.02	6	0.006
RPP7	1.26	360	0.453

*Calculated value.

**Measured value.

The maximum realistic effective dose for non-radiation workers, shown in Table 6.3, are well below legal dose limits and below the ICRP recommended annual dose limits of 1 mSv for non-radiation workers. Some of the values are however higher than the generally recommended dose constraint of 0.3 mSv/yr (ICRP publication 103, 2007; Appendix A.1). The fact that the dose constraint of 0.3 mSv/yr is not considered as a legal dose limit per year but voluntary limit, and the average background dose to ionising radiation is approximate 2.5 mSv/yr, the levels should nevertheless be taken into consideration.

6.7 Summary

The radiological safety assessment was carried out using MCNPX and QAD-CGGP computer code, and validated with measurements. The dose rates at the closest distance (10 cm) from the exterior of the concrete shielding walls were slightly higher. The QAD-CGGP relative fractional error were within 31% when compared to the measurement. The measurement and MCNPX calculation were within 26% in satisfactory agreement. For the labyrinth the discrepancies increases with the distance. The reasonable agreement between the calculations and measurements confirms that the Stellenbosch insect irradiator facility can with appropriate signposting on the RPP4 wall where there is cable penetration, and the adoption of good radiation safety practice in place, operate safety with the present shielding thickness in place.

Chapter 7
Results and discussion: HEPRO irradiation facility

7.1 Dose rate evaluation

Again (as in Chapter 5 and 6) the computational techniques discussed in §4.2 and §4.3 were used to model the HEPRO irradiation facility in order to verify the suitability of the present shield for a source strength indicated in §1.3.3. This Chapter is devoted to the HEPRO results and discusses them with respect to the present shield. Referencing will be made to Figure 3.10 on page 43 for elaboration.

7.2 Modelling with the code QAD-CGGP

The exact geometry (as shown in Figure 3.10 on page 43) of the chamber walls, including the roof was modelled in QAD-CGGP (Appendix E.1). However, as a result of the source geometry complexity, it was therefore modelled as a single square source rack, 150 cm high, with equal sides of 75 cm, composed of % , #& œ 100 '! Co pencils, having a total activity of 2 MCi, i.e., 74 PBq. The wall thicknesses (including the roof) was modelled as RPPs and the active part of the source rack was raised-out from the water pool (its shielded position) to an irradiation position of about 100 cm inside the vault of height 312 cm.

The fluence to response conversion factors for the ionising photons emitted by ^{60}Co source and the composition of the concrete used are shown in Chapter 5 (Tables 5.1 and 5.2). According to Entwistle and Adrian (1986), as well as De Beer (1986) report, concrete density was assumed to be 2.5 g.cm$^{\bullet 3}$. In the calculations presented in this Chapter, a density of 2.35 g.cm$^{\bullet 3}$ was assumed, because the material of the steel reinforcing rods are not homogeneously admixed into the concrete matrix, resulting in the presence of numerous shine paths. The ionising photon radiation is expected to see a concrete density of 2.35 g.cm$^{\bullet 3}$ through the traversed volume.

The water pool shielding surrounding the source when the source is not needed, enables safe personnel access to the irradiation vault (see Figures 3.12 to 3.14 on page 44 to 45). Accordingly, the correct geometry of the water pool with the source submerged was also modelled to establish the shielding effect of the water. The modelling details were similar except that the approximated composition of the source was taken to be that of water of density 1 g.cm$^{\bullet \$}$.

7.2.1 QAD-CGGP results

Dose rates profile were calculated at distances of 10 cm outside the outer surface of the walls and 50 cm above the horizontal level of the roof (with the exposed ^{60}Co source at 100 cm height) to determine projected maximum annual doses to radiation workers. For members of the public including non-radiation workers, dose rates were calculated at 1000 cm.

Roof

Figure 7.1 shows how dose rates on top of the 175 cm thick concrete roof vary with lateral movement along line LM and UT, on the **B** axis (refer to Figure 3.10 on page 43). Line LM lies on the plane **C œ !** cm whereas line UT lies on the plane **C œ** 293 cm. The red line is for lateral movement along LM, while the black line is for lateral movement along line UT. The point zero on the horizontal axis is directly overhead the fully exposed source.

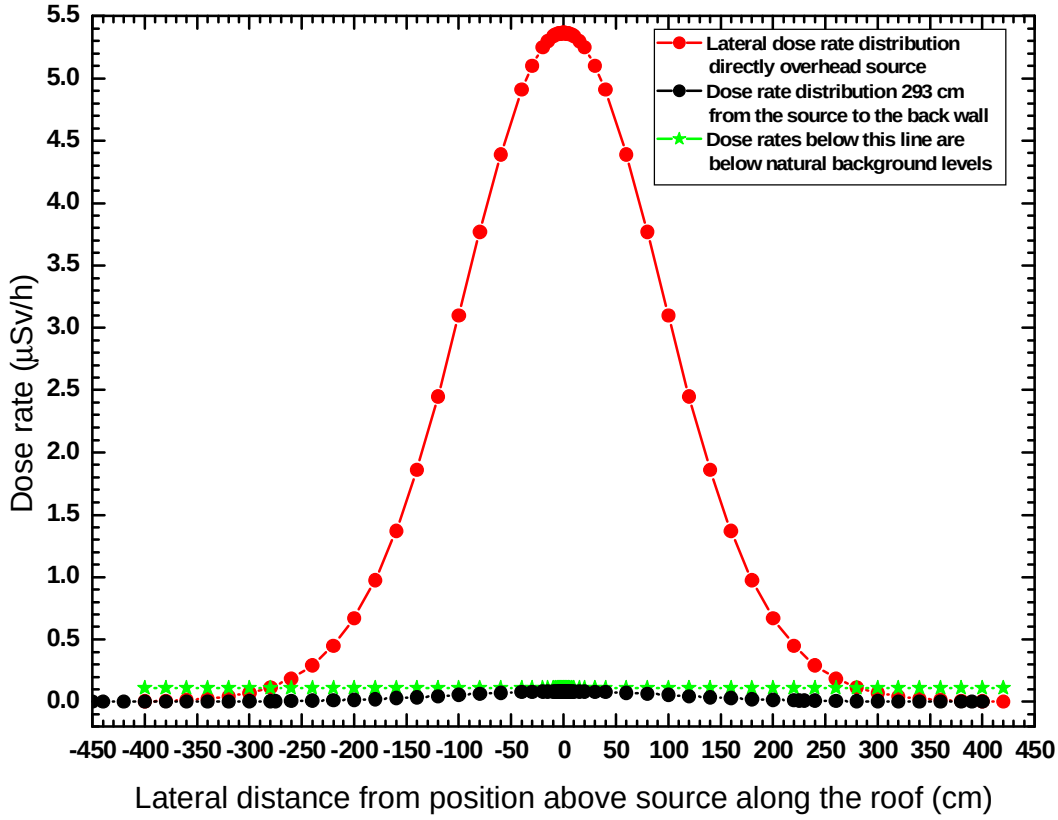

Figure 7.1: *Dose rate distributions on the 175 cm thick concrete roof.*

The maximum dose rate is about 5.37 µSv/h, directly overhead the exposed source. It is apparent that as one moves laterally away from the position directly overhead the exposed source, the effective thickness of concrete traversed by the photons, increases, resulting in a corresponding decrease in dose rates.

Walls

The axial distribution of dose rates calculated at a distance of 10 and 1000 cm (100 cm height above the floor level) from the outside outer surface of the LHS and RHS wall are shown in Figure 7.2.

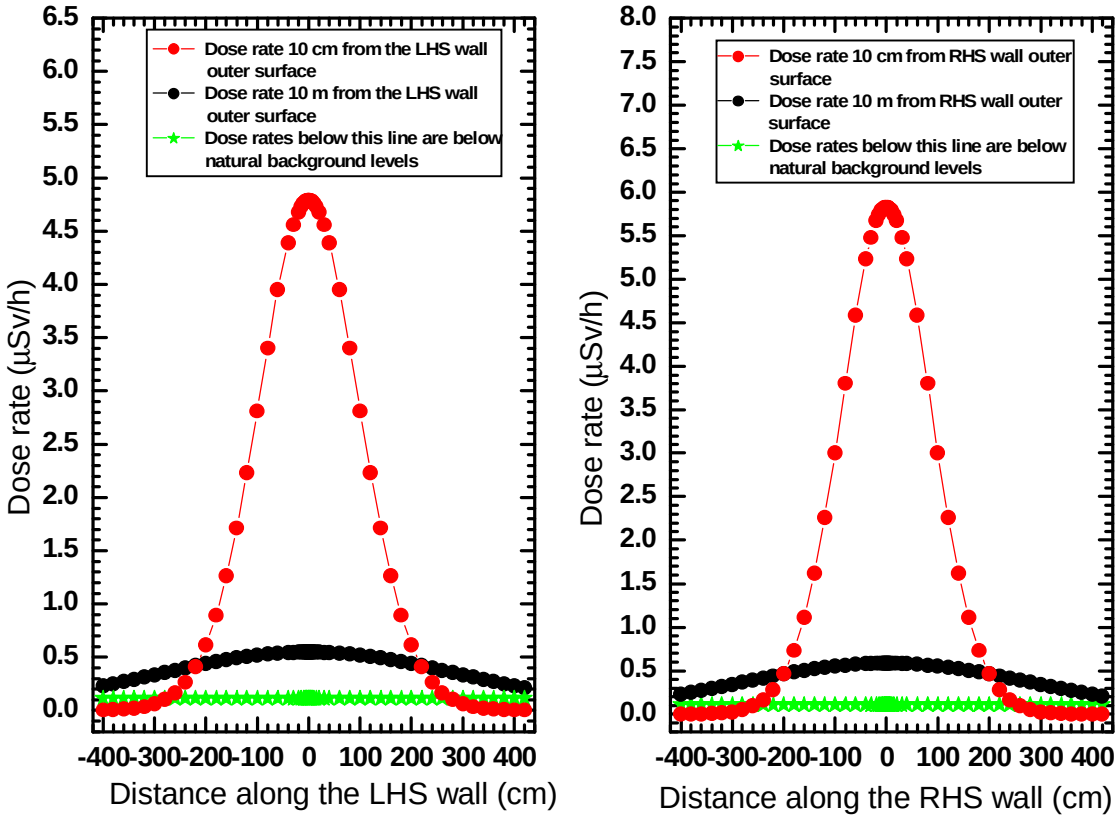

Figure 7.2: *Dose rate distributions along the outside outer surface of a 175 cm thick LHS and RHS wall.*

Of note, at a distance of 10 cm from the LHS wall, the calculated peak dose rate is 4.79 µSv/h directly opposite the exposed source, and at 1000 cm, the peak dose rate is 0.54 µSv/h. The peak dose rates is 5.87 µSv/h directly opposite the exposed source at a distance of 10 cm and 0.55 µSv/h at 1000 cm away from the RHS wall. The dose rates along the LHS wall are slightly lower than the ones along the RHS wall because the RHS wall is 51 cm closer to the source as compared to the LHS (refer to Figure 3.10 on page 43).

Figure 7.3 on page 92 shows the spatial dose-rates distribution along the front and the back wall. The dose rates were as well calculated at a distance of 10 and 1000 cm, and at 100 cm height above the floor level, from the outside outer surface of these walls.

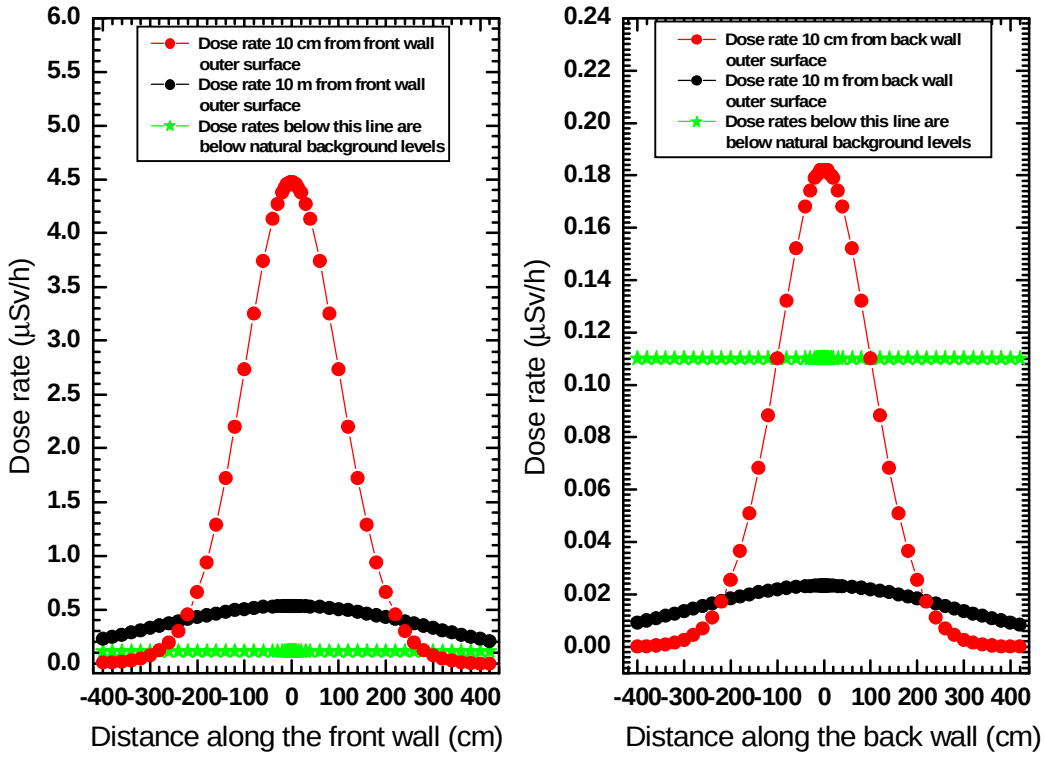

Figure 7.3: *Dose rates along the outside outer surfaces of the front and the back walls.*

At a distance of 10 cm from the front wall, the calculated peak dose rate is 4.47 µSv/h directly opposite the exposed source. At a distance of 1000 cm, the peak dose rate is 0.53 µSv/h. For the back wall, the calculated peak dose rate at a distance of 10 cm is 0.182 µSv/h directly opposite the exposed source and 0.023 µSv/h at a relative far distance of 1000 cm from the outer surface of the rear wall. Dose rates at 1000 cm are way below the natural background levels, as a results can be considered negligible. The dose rates distribution along the back wall are quite low compared to the dose rates values along the front wall. This is as a result of the differences in the thicknesses of these walls (refer to Figure 3.10 on page 43).

Spherical concrete shield geometry

In order to compare QAD-CGGP results with the MathCAD worksheet and MCNPX results, the dose rate values were also calculated for a concrete shield of spherical geometry. Figure 7.4 on page 93 shows the dose rates obtained at different radial positions (at maintained height above the floor from the source centreline), for a spherically geometric concrete shield. The 175 cm thick concrete shield start at a radial distance of 223.5 cm and ends at 398.5 cm. These dimensions were chosen because the closest RHS wall is 223.5 cm from the source centreline (refer to Figure 3.10 on page 43).

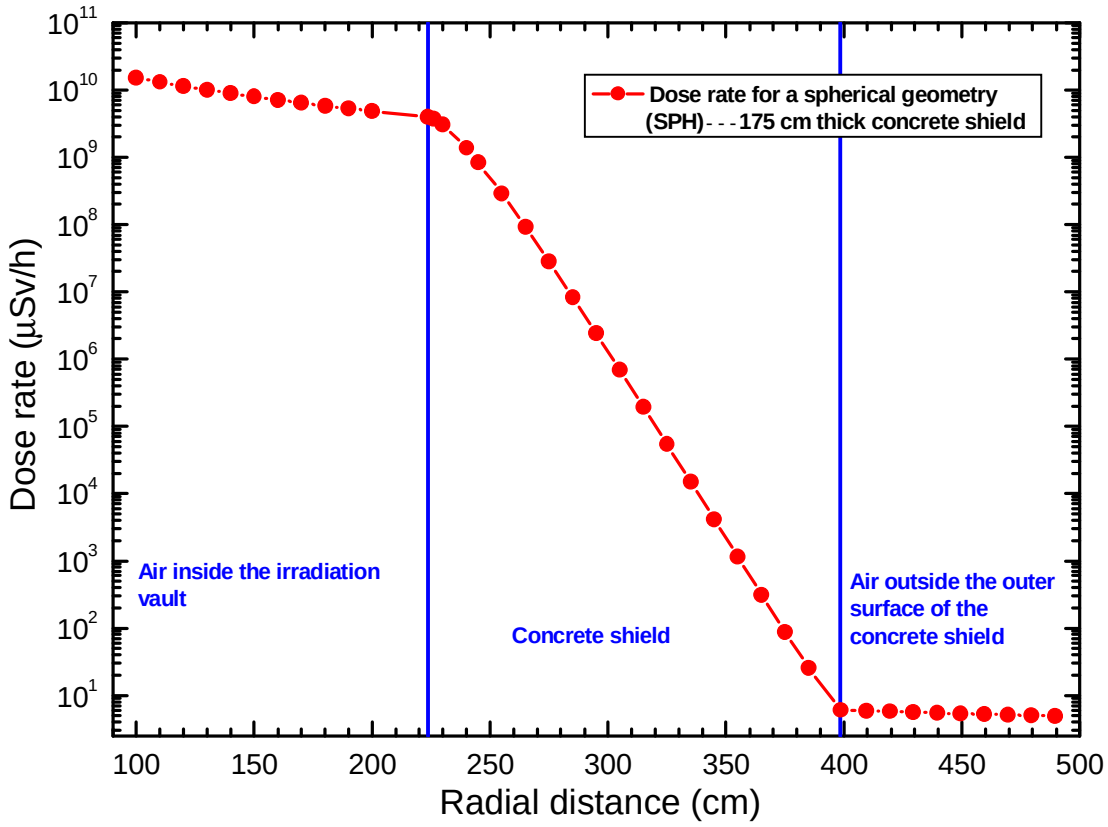

Figure 7.4: *Dose rates at different radial distances from the source centreline through a spherical geometry of a 175 cm thick concrete shield, calculated using QAD-CGGP.*

Of note from Figure 7.4 is the relatively sharp drop in the dose rates with the increase in concrete thickness. At 10 cm outside the outer surface of the concrete shield, the dose rate is again 5.87 µSv/h; the same value obtained when using RPPs geometric bodies.

Water pool

In order to verify the shielding effectiveness of the water pool, the dose rate profiles were calculated at different distances through water shield and across the pool centreline of 100 cm above the top of the platform covering the pool. Figure 7.5 on page 94 presents the dose rates at various axial distances through water shield and across the pool centreline 100 cm above the top of the platform covering the pool with the water level 34 cm from the top of the stainless steel pool liner.

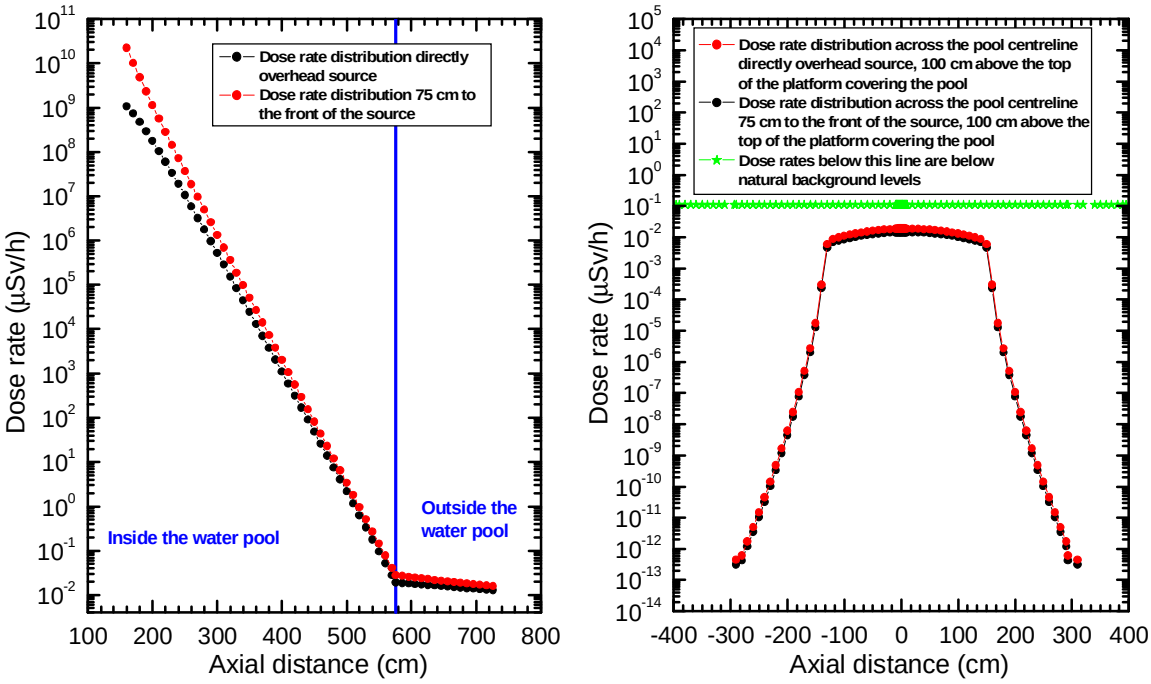

Figure 7.5: *Dose rates at various axial distances through water shield to about 160 cm above the pool surface and across the pool centreline 100 cm above the top of the platform covering the pool.*

Inside the submerged source rack, at 10 cm from the top of the source (shown as axial distance in Figure 7.5, **D œ** 160 cm), the average dose rates are as high as 10^{10} µSv/h. At an axial distance of 560 cm to the top of the pool surface, dose rates values are well below the natural background levels (0.11 µSv/h). Of note the water level is normally maintained at 576 cm from the bottom to the top of the pool; i.e., the top of the ^{60}Co source is covered by about 426 cm of water (refer to Figures 3.12 to 3.14 on page 44 to 45). The dose rates distribution across the pool centreline 100 cm above the top of the platform covering the pool are well below background level. As a results of the higher shielding effectiveness of concrete and soil as compared to that of water at lateral positions across the pool centreline, the dose rates drops off very sharply.

It is apparent in Figure 7.5 that the water pool performs an absolutely necessary shielding task. Although the probability that the pool water level will drop to a value below the safe values is very slightly, it was, however, necessary to examine the degree of safety should the water pool level drops to levels below the top of the pool liner. This is graphically shown in Figure 7.6 on page 95, where dose rates were calculated at a uniform height of 100 cm above the top of the platform covering the pool with water (top edge of the stainless steel pool liner) with respect to lowering the water pool level.

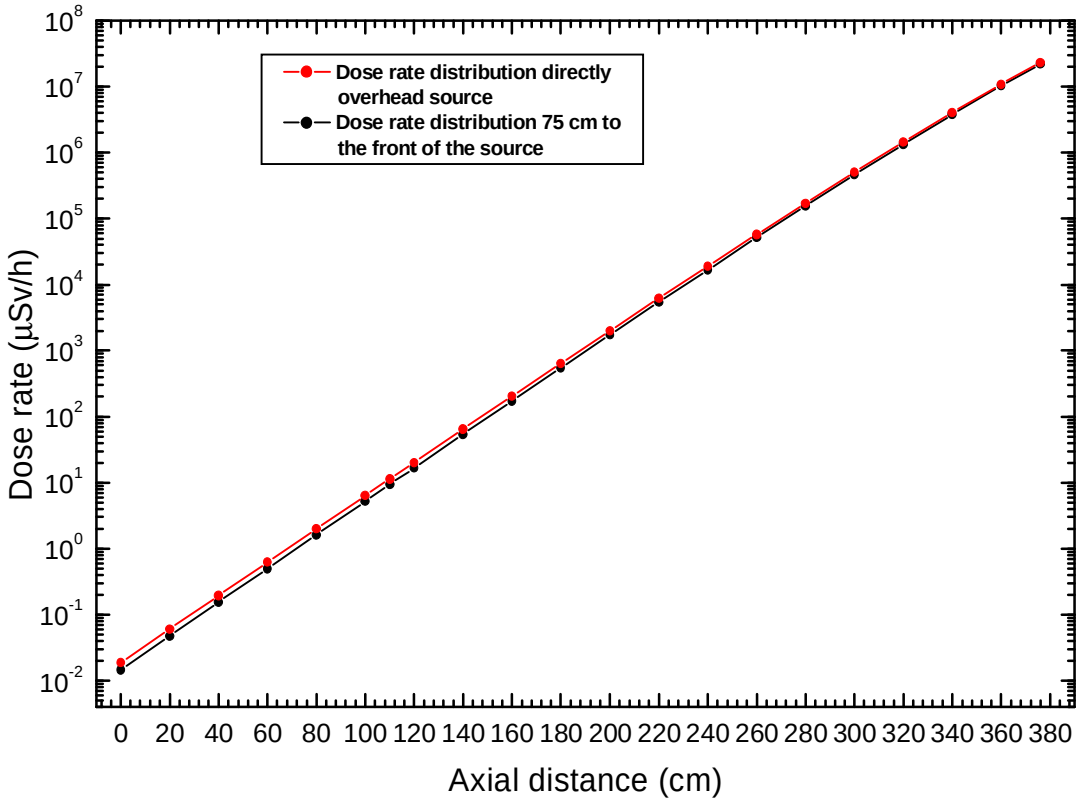

Figure 7.6: *Dose rates 100 cm above the top edge of the stainless steel pool liner, with respect to lowering the pool water level.*

At 466 cm (shown in Figure 7.6 as axial distance of 110 cm) water thickness, the dose rates are as high as 11.4 µSv/h above the source and 9.4 µSv/h at 75 cm to the front of the source. Bearing in mind that the occupancy inside the irradiation vault is short, such dose rates can be endured without unduly expose of personnel. This indicates sufficiency in safety margin can be provided by adopting a top gap of 110 cm between the top of the water level and the top of the stainless steel pool liner.

An automated water level sensing and water make-up system will react to undue drops in pool water level, and make-up for water losses. In an event of such catastrophic drop in water level the safety interlock system (dose rate alarm) described in §3.6, will serve as an independent warning system.

7.3 MathCAD worksheet results

The modelling discussed in §5.3 on page 58 also apply for the HEPRO facility, therefore only the results are presented in this section.

Figure 7.7 on page 96 presents the dose rates as a function of the radial distance from the source centreline position and the reliance of the dose attenuation factor on ordinary concrete shield wall of 175 cm in thickness.

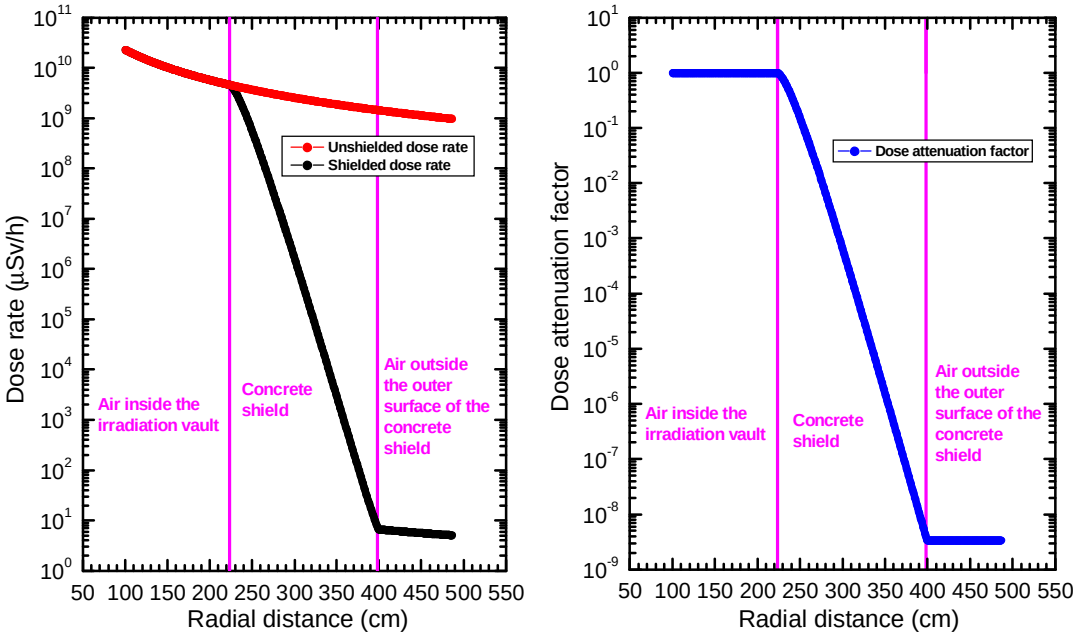

Figure 7.7: *Dose rates and dose attenuation factor for a 2 MCi ^{60}Co source that is shielded by 175 cm thick ordinary concrete.*

At 10 cm (point P") outside the outer surface of the concrete shield, the dose rate is 6.5 µSv/h. The red colour shown in Figure 7.7 illustrates what the dose rates would be without a shield, whilst the black line indicates the dependence of the dose rates on spatial position and the blue shows the reliance of the dose attenuation factor on shield thickness. The dose rates with shield in position is 3.3 , 10$^{\bullet 9}$ times lower than it would have been without the concrete shielding material. This indicates the degree of radiation attenuation by a 175 cm ordinary concrete and its adequacy in shielding a 2 MCi (74 PBq) ^{60}Co source.

7.4 Modelling with the code MCNPX

A similar procedure was employed to thoroughly model the HEPRO facility using the MCNPX computer code (Appendices E.2 and E.3), to confirm the results. The modelling using MCNPX has already been discussed in §5.4 and 6.3 on page 60 and 76. Figure 7.8 on page 97 presents a top and side view geometry of the HEPRO facility. The green colour indicates the concrete around the source, red represents the top and side view of the ^{60}Co source rack, whilst the blue colour depicts the air medium inside and outside the irradiation chamber.

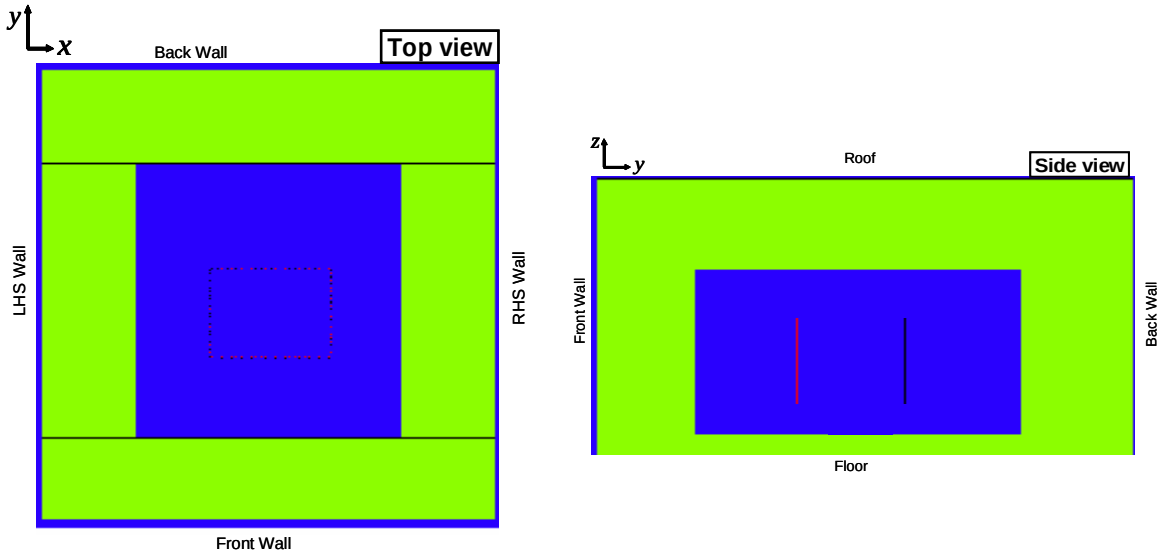

Figure 7.8: *Top and side view of the irradiation vault of the HEPRO facility showing the concrete shielding around the source.*

The ideal spherical geometry that was used with variance reduction method to reduce the computer time required for satisfactory results together with all statistical error satisfied is shown in Figure 7.9. The blue colour represents the air medium inside and outside the irradiation chamber, the red colour depicting the concrete shield and the solid lines (in black) indicates the variance reduction tool.

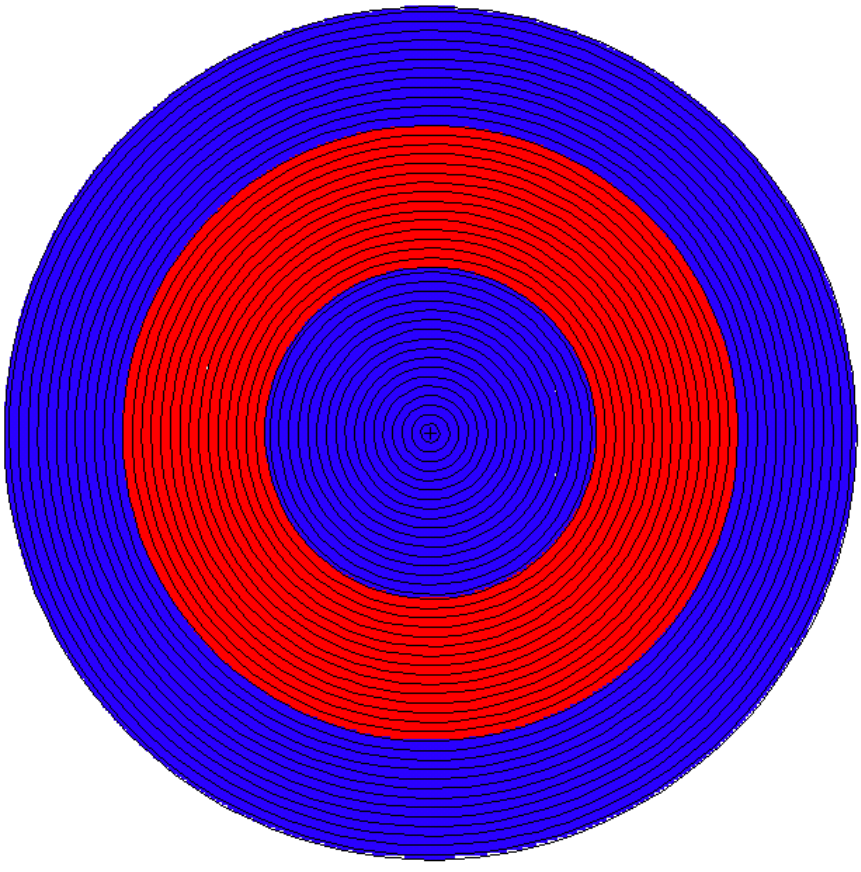

Figure 7.9: *A concrete shield of spherical geometry of the HEPRO facility.*

Of note is the point source location at the origin (0,0) with the shield starting at the 223.5 cm point and ending at the 398.5 cm point. These dimensions was chosen because the closest RHS wall to the ^{60}Co source is at 223.5 cm point.

7.4.1 MCNPX results

Spherical concrete shield geometry for external dose rate determinations

Figure 7.10 presents the dose rates attained at various radial distances from the source centreline along the line through point P" which is 10 cm outside the outer surface of the 175 cm thick spherical concrete shield, and directly opposite the exposed source.

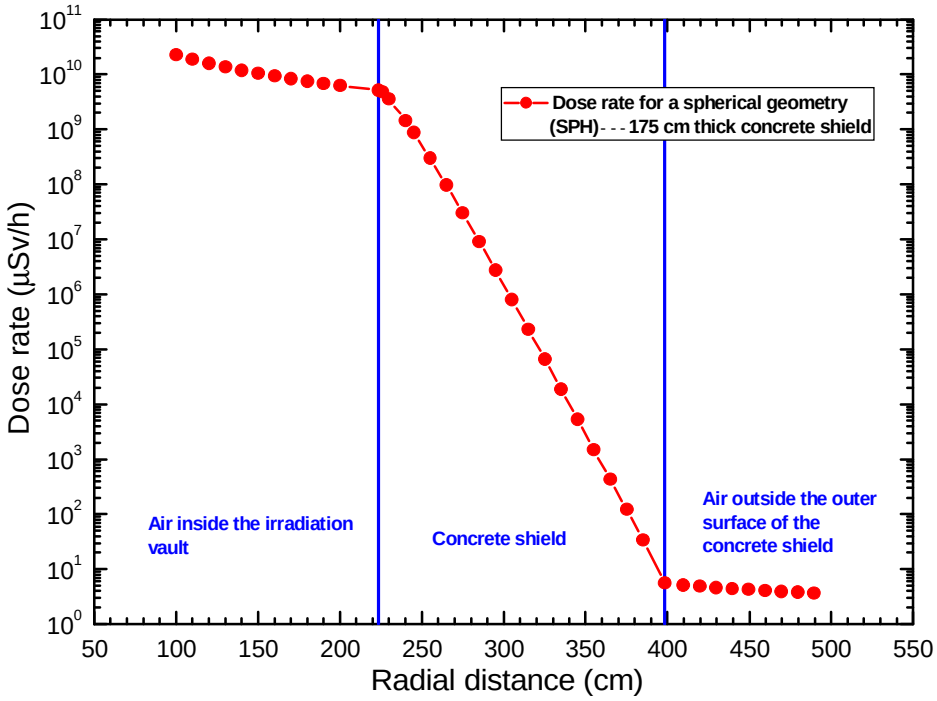

Figure 7.10: *Dose rates at different radial distances through a 175 cm thick spherical concrete shield.*

Again it is noted in Figure 7.10 that the dose rates rapidly decreases as the radiation streams across a 175 cm thick spherical concrete shield. The dose rate at about 10 cm outside the outer surface of the shield is 5.1 µSv/h.

Spatial variation of dose rates within and outside shielded facility

Figure 7.11 on page 99 shows how the spatial distribution of doses given in µSv/h changes from high to low values as the radiation streams across the concrete shield of the HEPRO irradiation facility. The facility is viewed from the top as in Figure 3.10 on page 43. The variation of dose rates are indicated in red, yellow, green and blue. The highest dose rates are depicted in red whereas the lowest in green and blue. As expected the highest dose rates are in the order of 10^{10} µSv/h.

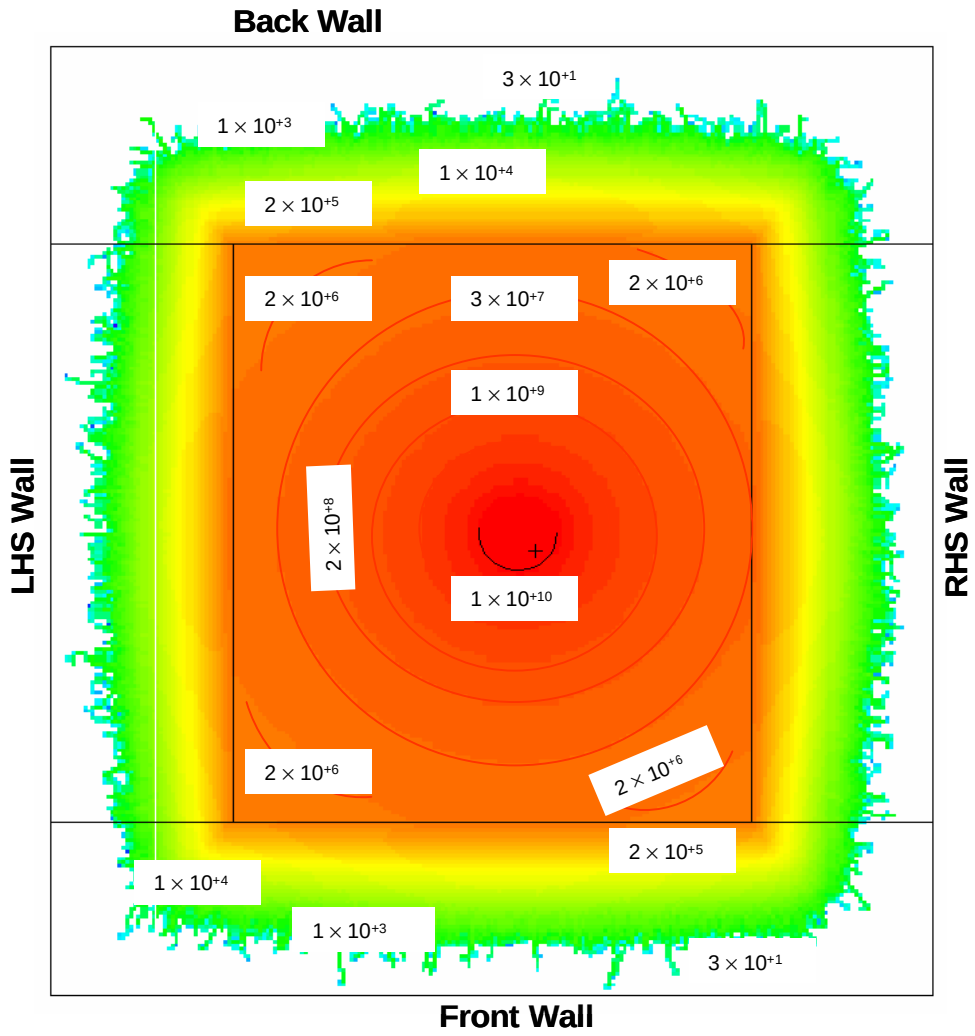

Figure 7.11: *The variation of spatial dose rate distributions within the concrete shielding that surrounds the ^{60}Co source, calculated with MCNPX.*

Of note in Figure 7.11 is that the radiation suffer multiple scattering and absorption as it streams through the concrete shield; especially within the back wall (200 cm thick concrete wall). The results support the conclusion that the concrete is largely effective for shielding a ^{60}Co source of 2 MCi (74 PBq) in activity.

7.5 Comparison of dose rate results

Spherical concrete shield geometry

Table 7.1 on page 100 gives dose rates at point P▪ calculated using MathCAD, QAD-CGGP and MCNPX computer codes simulation. As elaborated in §7.4, point P▪ is 10 cm outside the outer surface of the front wall and directly opposite and perpendicular the exposed ^{60}Co source (refer to Figure 3.10 on page 43). The comparison is shown graphically in Figure 7.12.

***Table 7.1** Comparison of the dose rate predictions at point P▪.*

Dose rate (µSv/h)		
MathCAD worksheet	QAD-CGGP	MCNPX
6.50	5.87	5.10

Figure 7.12 presents the calculated dose rate values using the three independent mentioned methods for the spherical geometry case.

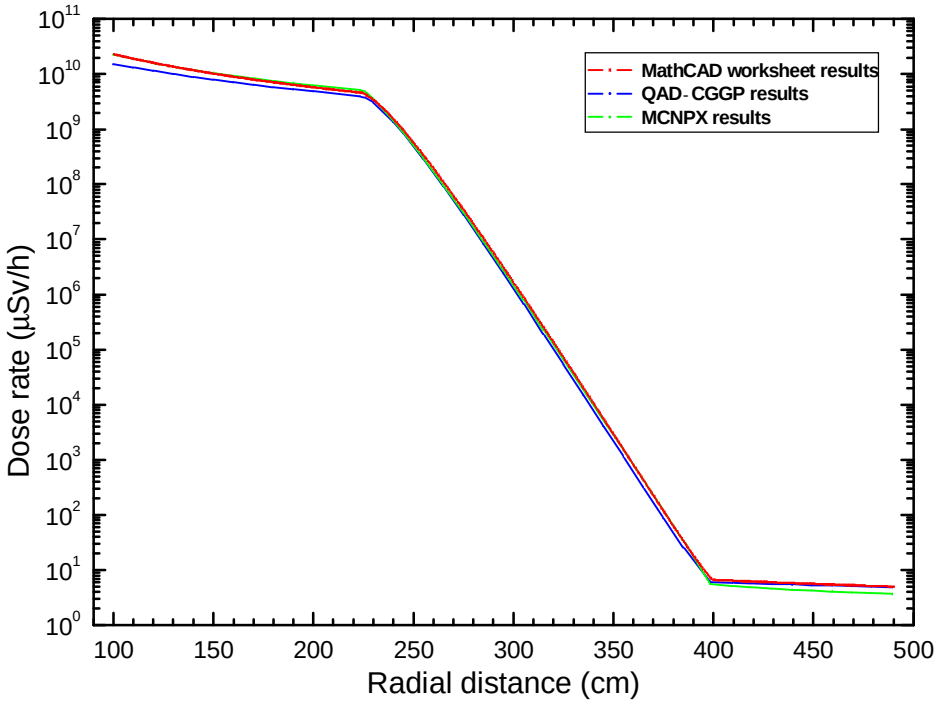

***Figure 7.12:** Dose rate profiles calculated using MathCAD worksheet, QAD-CGGP and MCNPX computer codes.*

As expected, the dose rates calculated using MathCAD are the highest. This was attributed to the assumptions made regarding the source being an isotropic point source and self-shielding within the source volume ignored. The MathCAD calculation for a dose rate at point P▪ agree with the QAD-CGGP value within 10%. The MathCAD relative error is 22% when compared to a value obtained using MCNPX. The QAD-CGGP code on the other hand over estimated the dose rate obtained by about 13% when compared to a value obtained using MCNPX. The slightly higher error of 13% is as a result of the deep penetration of radiation through a 175 cm thick concrete shield. Given the deep penetration of radiation through a 175 cm thick concrete shield, and a semi-analytical approach that the code QAD-CGGP uses, it can be concluded that the agreement can be considered satisfactory. As a result, the QAD-CGGP dose rate results presented in §7.2.1 can therefore be accepted as accurate.

7.6 Projected annual doses

The peak dose rates at 10 cm from the outside surface of the concrete shielding walls, directly opposite the source, and 50 cm above the outside outer surface of the concrete roof were used to calculate maximum realistic annual doses to radiation workers. The criteria for judging radiation shielding is presented in Appendix A.2. Assumptions pertaining to radiation workers:

- Maximum number of shifts per year of 360;
- Maximum daily stay time adjacent to the concrete wall, at peak dose rate position of 4 hours per shift;
- Maximum daily stay time inside the irradiation vault of 4 hours per shift;
- Maximum annual stay time on the roof being 24 hours per year.

Based on the assumptions, Table 7.2 presents a summary of the calculated dose rates and projected maximum realistic annual doses to radiation workers. It may be noted that the assumed realistic exposure time per year for the sides walls are slightly higher as compare to the assumptions made for the Citrusdal and Stellenbosch facility; this is because offices of radiation workers are closer to the irradiator chamber.

***Table 7.2** Maximum dose rates, annual occupancy time, and maximum realistic doses to radiation workers.*

Maximum realistic doses to radiation workers			
Wall or closest position	Peak dose rate (µSv/h)	Realistic exposure time (h/yr)	Maximum realistic annual dose (mSv/yr)
RHS	5.87	1440	8.45
LHS	4.79	1440	6.89
Front	4.47	1440	6.43
Back	0.18	1440	0.26
Roof	5.37	24	0.13
Water pool*	11.4	1440	16.41
Water pool**	9.4	1440	13.53

* Overhead source.
** 75 cm to the front of the source.

The maximum realistic doses for radiation-workers, as listed in Table 7.2, are below legal dose limits, and as well below the ICRP's recommended dose limits (e.g., ICRP publication 103, 2007; Appendix A.1).

The peak dose rates at 1000 cm away from the outside surface of the concrete shielding walls and 50 cm above the outer surface of the roof concrete were used to calculate the annual doses to members of the public. The following assumptions pertaining to non-radiation workers were adopted:

- Maximum number of shifts per year of 360;
- Maximum daily stay time adjacent to the concrete wall, at peak dose rate position of 5 hours per shift;
- Maximum annual stay time on the roof of 8 hours per year;
- Maximum annual stay time inside the irradiation vault being 8 hours per year.

Table 7.3 summarises calculated dose rates, occupancy levels and projected maximum realistic annual doses to members of the public (including non-radiation workers).

Table 7.3 *Maximum dose rates, with assumed annual occupancy times, and maximum realistic doses to members of the public.*

Maximum realistic doses to members of the public			
Wall or closest position	Peak dose rate (µSv/h)	Realistic exposure time (h/yr)	Maximum realistic annual dose (mSv/yr)
RHS	0.55	1800	0.99
LHS	0.54	1800	0.972
Front	0.53	1800	0.954
Back	0.02	1800	0.036
Roof	5.37	8	0.042
Water pool*	11.4	8	0.091
Water pool**	9.4	8	0.075

* Overhead of the source.
** 75 cm to the front of the source.

All the maximum realistic doses for non-radiation workers, shown in Table 7.3, are below legal dose limits and below the ICRP's recommended dose limits (e.g., ICRP publication 103, 2007; Appendix A.1). Some effective doses, however, exceed the recommended dose constraint of 0.3 mSv/yr by up to a factor of 3.3. From the values listed in Table 7.3, it can be concluded that the thicknesses of the present biological shielding places a limit on the housing of a source of not more than 2 MCi (74 PBq) in activity.

7.7 Dose distribution within the sample product undergoing irradiation

Modelling with the code MCNPX

A calculation with the code MCNPX was used to generate dose rates in a Cartesian mesh-tally, for instance, an 8 , 8, 12 , 12, 16 , 16 or 32 , 32 BC-grid, for a chosen cut through the vertical (D) dimension. The MDATA binary output file for mesh tally, generated by MCNPX, was converted to an ASCII file, using the GRIDCONV utility bundled with MCNPX. A Fortran-90 code (Chapman,1998) was written to read the ASCII version of the MDATA mesh-tally file. The code Fortran-90 employs an algorithm to calculate the dose-distribution for equal time irradiation of each of the four facets of the box and writes the calculated net dose distribution to an ASCII file that can easily be imported into plotting packages such as e.g., origin or sigma plot.

The systematic calculation method described above were done for a source-rack containing 4 , 25 œ 100 ^{60}Co pins which correspond to a total activity of about 1 MCi (3(PBq) as depicted in Figure 7.13. The yellow colour depicting ^{60}Co pins and blue for surrounding air medium. The C and B axis are shown with the D axis perpendicular to the page.

Figure 7.13: *A top-view geometry of the source-rack containing 4 , 25 œ 100 ^{60}Co pins.*

The active part of the source-rack was raised to an irradiation position above the water pool. The four boxes were stacked around a square source-rack about 50 cm away from the source centerline. Figure 7.14 on page 104 presents a top view geometry of four product boxes (in red colour) undergoing irradiation. Again, illustrated in blue colour is the surrounding air medium. The C and B axis are shown with the D axis perpendicular to the page.

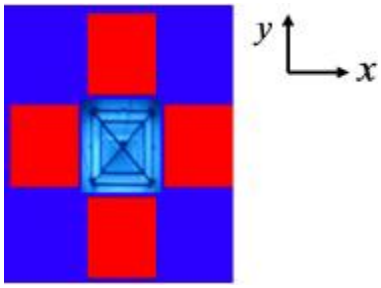

Figure 7.14: *A top-view geometry of four product boxes undergoing irradiation.*

For even dose distribution, each square box of sample product was turned three times so that each of the four side of the box faced the source rack once during an irradiation session.

Results and discussion

As explained in Chapter 5 (§5.7), the dose (process dose) needed to achieve a desired effect in the product is determined through radiation research, which involves determining the dose-effect relationship for the product. The amount of dose in a product box/container depend on the mass density and composition of the product to be irradiated, and as well as the time of exposure. Figure 7.15 shows the dose rate distribution in a sample product box in Gy/h, when irradiated from four sides with ^{60}Co source. Also shown is the intricate details of dose rate distribution in 2D (two dimension) that actual transpires the data in 3D (three dimension). The colour band depicts the dose received by the product in one hour of irradiation.

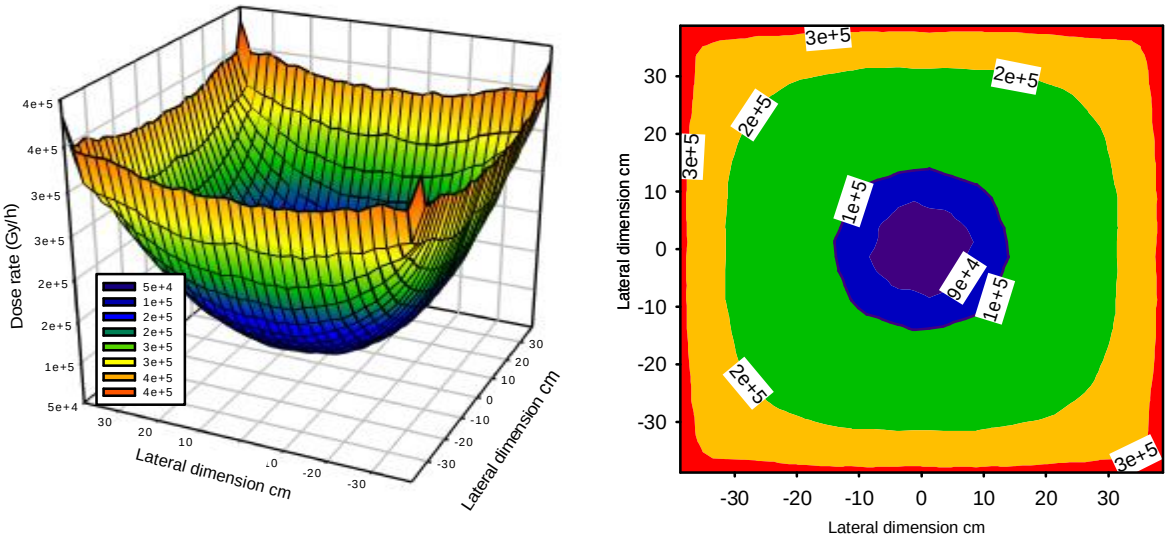

Figure 7.15: *The absorbed dose-distribution in a product box irradiated from four sides with ^{60}Co source.*

The simulation show that the absorbed dose is highest at the edges of the box, and even slightly higher at the four corners, nearest the source plaque. The absorbed dose is lowest at the centre of the sample product. This is an indication of absorption and scattering in the sample products contained in the box. This spatial dose gradient places a limit on the

size of product boxes that may be used. The higher the mass-density of the product, the higher the effective atomic number Z of the product, and the lower the products tolerance to non uniform dose the smaller the maximum box size will need to be. That is the effect will be more pronounced as the density increases.

7.8 Summary

Irradiation chamber

The satisfactory comparison between the point-kernel (QAD-CGGP and MathCAD worksheet) and the Monte Carlo (MCNPX) confirms that the HEPRO plant will still be radiological safe, when using a # MCi ((% PBq) ^{60}Co source, taken into account the location of the plant with respect to the personnel offices and the nearest members of the public (especial to the rear/back wall). The source strength of # MCi ((% PBq) is, however, the limiting source strength for the plant, and a further increase in source activity should not be allowed for the present shielding wall thicknesses of 175 cm.

Sample product undergoing irradiation

The results show the Monte Carlo, MCNPX code, to be an important tool for performing dose mapping of the HEPRO irradiator for each product to be irradiated. The results also reflect that a priori knowledge of dose distribution permits suitable irradiation plan, achieving good dose uniformity in the products, thus reducing preliminary experimental work.

Chapter 8
Summary and outlook

This study reports on the computational calculations results, and where possible measurements of radiation levels around the three irradiation facilities. Presented is an analysis needed for the design of the concrete shield for the Citrusdal facility, and as well shield verification calculations (radiological safety assessment) for the already constructed Stellenbosch and HEPRO irradiation facilities. Where appropriate modelling using of the code QAD-CGGP, the Monte Carlo MCNPX and MathCAD worksheet were used and the results compared. In addition, dose distribution using the MCNPX transport code was carried-out to determine the absorbed dose profile values in the irradiated insect containers of the Citrusdal facility, and sample product boxes of the HEPRO facility. For insects, the calculated dose values were compared to an average dose value. These are summarised separately below.

8.1 Citrusdal insect sterilization facility

Irradiation chamber

For this facility the profile of the calculated dose rates along the concrete shielding walls, the roof as well as the entrance/exit in critical points were considered. Most dose rates were below the legal dose limits and below the ICRP recommended annual dose limits for both radiation workers and non-radiation workers. It was also noticed that the dose rate profiles were below the generally recommended dose constraint value of 0.3 mSv/yr, and as well the average background dose value from natural occurring ionising radiation of approximate 2.5 mSv/yr. A slightly higher dose rates were noticed on top of the roof where maintenance work are hardly ever performed.

The dose rate at the nearest position ($P_{\#}$) to the source within the labyrinth was noted to be the highest. As the distance increases farther away from the ^{60}Co source along the labyrinth, the dose rates were observed to fall off very rapidly towards the entrance/exit door position.

Verification of the dose rate profiles calculated with the point-kernel integration code, the results obtained using a spherical concrete shield geometry were compared with MCNPX predictions. It was observed that the dose rates calculated with QAD-CGGP computer code are the lowest inside the irradiation vault to about where the concrete shielding wall ends (at 325 cm), except outside the concrete shield. The variation in dose rates can be attributed to the infinite medium buildup factor used in the QAD-CGGP calculation to account for the dose from scattered flux. The dose rate calculated with MathCAD worksheet at point P▪ differed by 13% from QAD-CGGP results. For QAD-CGGP and MCNPX the difference was 7%. Therefore, taking into consideration the semi-analytical approximation methodology of the point-kernel, the results show good agreement.

The satisfactory agreement between the three calculational methods used confirms that the Citrusdal facility with the shield thicknesses specified, appropriate radiation safety interlocks, radiation safety management system as well as a cautiously nurtured safety culture in the organisation in place, will operate safely.

Insects

The absorbed dose distributions within the insect containers were calculated with the model developed in MCNPX, for one hour of exposure. The variability of the calculated dose rates distribution inside the insect canisters were found to be within acceptable dose values for sterilising False Codling Moths when compared to measured dose rate values.

The conclusive agreement between the measured and calculated dose rate distribution values show the MCNPX code to be an effective method for performing dose mapping of the inside of insect housing containers for sterilization.

8.2 Stellenbosch insect sterilization facility

The shield verification calculations was performed using the model developed in MCNPX and QAD-CGGP computer codes, and where possible validated with measurements. The spatial distribution of dose rates around the shielding concrete walls, on top of the roof and various position along the multi-bend maze were considered. The maximum realistic annual dose were below the legal dose limits and also below the ICRP recommended annual dose limits for both radiation workers and non-radiation workers. Some of the dose rate values were however higher than the generally recommended dose constraint of 0.3 mSv/yr. The fact that the dose constraint of 0.3 mSv/yr is not considered as a legal dose limit per year but voluntary limit, and the average background dose to ionising radiation is approximate 2.5 mSv/yr, the results ought nevertheless be taken into consideration. The QAD-CGGP relative fractional error were within 31% when compared to measurements. The values obtained from measurements and MCNPX calculations were within 26%.

For the multi-bend maze the discrepancies increases with the distance. At point P% (at 436 cm) from the ^{60}Co source position, and P* (at 1200 cm farthest from the ^{60}Co source location) towards the entrance/exit door position within the labyrinth, the dose rate discrepancies between calculated and measured values of 14 to 52% were observed.

The comparison of the dose rate measurements with values predicted by QAD-CGGP and MCNPX calculations confirms that with suitable signposting on the RPP4 wall where there is cable penetration, and good radiation safety measurements in the organisation, the Stellenbosch insect sterilization facility will operate safely with the present shield thicknesses.

8.3 HEPRO irradiation facility

Irradiation chamber

The three aforementioned computational techniques were used to model the facility in order to verify the suitability of the existing shield for a source strength of 2 MCi. The exact geometry of the concrete shielding walls and the roof was calculated with the model developed in QAD-CGGP.

The actual geometry of the pool with the source submerged was also modelled to establish the shielding effectiveness of the water. The modelling details were similar except that an approximated source composition equivalent to that of water of density 1 g.cm$^{\bullet\$}$ was used. The results obtained from the model showed that in general the maximum annual realistic doses were below legal dose limits, and as well below the ICRP recommended dose limits. There were however some effective dose values which were higher than the recommended dose constraint of 0.3 mSv/yr by up to a factor of 3.3.

The spatial dose rate distributions were also calculated using the point-kernel integration code using a spherical concrete shield geometry. The results compared well with of the MCNPX predictions. As expected, the dose rates calculated using MathCAD gave the highest values. This was attributed to the assumptions made regarding the source being as an isotropic point source and self-shielding within the source volume was ignored. The MathCAD calculation for a dose rate at point P▪ agree with the QAD-CGGP value within 10%. The MathCAD relative error was 22% when compared to a value obtained using MCNPX. The QAD-CGGP code on the other hand over estimated the dose rate by about 13% when compared to the value obtained using MCNPX. The slightly higher error of 13% could be due to the radiation having to penetrate the 175 cm thick concrete shield.

The comparison of the dose rate profiles calculated with the computational model developed in the point-kernel (QAD-CGGP and MathCAD worksheet) and the Monte Carlo (MCNPX) confirms that the HEPRO plant will still be radiological safe, when using a # MCi ^{60}Co source, taken into account the location of the plant with respect to the personnel offices and the nearest members of the public. This was also further confirmed with the spatial distribution of dose rates measurements. The source strength of # MCi (**(%** PBq) is, however, the limiting source strength for the plant, and a further increase in source activity should not be allowed for the present shielding wall thicknesses of 175 cm.

Sample product undergoing irradiation

The absorbed dose distributions within the sample product boxes were calculated using a systematic computational calculation methodology, that is Fortran-90 utility code to read mesh-tally dose distributions calculated using the Monte Carlo code—MCNPX. It was noticed that the highest absorbed dose values were at the edges of the box and at the four corners. The lowest was apparent at the centre. These results reflects the degree of absorption and scattering from the sample products contained in the box. Such

satisfactory results serve as an indication that simulation using MCNPX can be used effectively to predict the dose distribution within sample product boxes in the irradiation chamber.

8.4 Concluding remarks on the use of point-kernel and Monte Carlo codes

The point-kernel (QAD-CGGP and the MathCAD worksheet) and the Monte Carlo (MCNPX) was used successfully for the design of the concrete shield for the Citrusdal facility, and as well shield verification calculations for the already constructed Stellenbosch and HEPRO irradiation facilities.

The codes proved to be well suited for the aforementioned study. The two codes complement each other—point-kernel calculations are very fast, but the code can not model radiation streaming through labyrinths and ducts. The code MCNPX uses far more computer time, but is able to model scattering and streaming because it simulates radiation transport rigorously whereas the point-kernel uses a semi-analytical, approximate methodology that is not able to account for radiation streaming through labyrinths, ducts and penetrations.

Appendix A: Quantification of shield worth

A.1 Dose limits and dose constraints

Latest ICRP dose limits

The latest dose limits for radiation workers, recommended by the ICRP publication 103 (2007), and incorporated into South African legislation, are given in Table A.1. From the perspective of radiation shielding design and evaluation of irradiation facilities, the most important of these dose limits for radiation workers is the annual effective dose limit value of 20 mSv.

Table A.1: *Latest ICRP recommended dose limits for occupational exposure to ionising radiation.*

Type of dose	**Dose limit**
Effective dose (excluding pregnant women)	20 mSv per year
Dose to the skin, hands and feet	500 mSv per year
Dose to lens of eye	150 mSv per year
Effective dose to pregnant women	1 mSv from diagnosis of pregnancy to its end
Radionuclide intake by pregnant woman	$\frac{1}{20}$ of regular limiting ALI* values, for duration of pregnancy

*ALI—annual limit on intake.

The latest public dose limits, i.e., for persons not registered as radiation workers, recommended by the ICRP, are given in Table A.2 on page 111. From the perspective of radiation shielding design and evaluation of irradiation facilities, the most important of these dose limit values for non radiation workers is the annual effective dose limit of 1 mSv.

Table A.2: *Latest ICRP recommended dose limits for exposure of the public to ionising radiation.*

Type of dose	Dose limit
Effective dose (excluding pregnant women)	1 mSv per year
Dose to the skin, hands and feet	50 mSv per year
Dose to lens of eye	15 mSv per year

Dose constraints for the exposure of radiation workers

The ICRP recommends that facilities adopt dose constraints considerations whereby dose values lying between 10% and 100% of the dose limit are recommended. A socially responsible and generally considered acceptable dose constraint values for the exposure of radiation workers, is about 50% of the dose limit, i.e., an effective dose of 10 mSv/yr.

Dose constraints for public exposure

The ICRP generally advises a dose constraint of 0.3 mSv/yr, i.e., 300 μSv/yr for non-radiation workers. The rationale for this is that members of the public could realistically be exposed to ionising radiation from three nuclear irradiation facilities.

A.2 Criteria for judging radiation shielding

Design-base dose; Dose budget

The International Commission on Radiological Protection (ICRP) recommended dose limits, usually find their way into national legislation. These recommendations are thoroughly revised every ~15 years. To comply with ICRP recommendations, facilities are in addition obliged to introduce the concept of dose constraints.

Based on dose constraints in force at a facility, calculated *derived dose constraints* are in addition introduced. In addition, jobs involving exposure must be subjected to management controls — principally safe operating procedures (SOPs) — to ensure that workers are not exposed above the dose constraints in force at a facility. It must be appreciated that the more effective shielding is, the longer allowed work times and the lower the necessity to rely on continuous human alertness, will be — effective shielding makes workplaces inherently safer.

Given (1) the maximum realistic source term, as well as (2) typical times that workers will spend performing specific jobs, shields can be designed and working procedures be developed that will maintain the total annual exposures of workers below a target dose constraint. This may be referred as the ***design-base dose constraint*** or ***dose budget*** for the task. The annual design-base dose constraint is a *realistic fraction of the annual dose constraint* applying to the worker, given that workers typically have a number of tasks in number of radiological areas.

Maximum tolerable dose rate

Shields must be designed with the design-base doses in mind. If the budgeted design-base effective dose is H_{eff}, and the worker must spend time t in a certain area, the constraint on the dose rate that can be tolerated, is $\frac{H_{eff}}{t}$. In other words, shielding must be designed to ensure that dose rates on the personnel-side of shields are lower than the value,

$$\text{Dose rate constraint for task } j = \frac{\text{Design-base dose constraint for task } j}{\text{Annual staytime for task } j}. \qquad \text{(A-1)}$$

Projected annual dose

Suppose that a worker has to work a maximum realistic annual staytime t_{yr} in a radiation area where the maximum realistic average dose rate will be $\dot{H}_{av}$. Then the projected annual dose that the worker will receive, will be,

$$\left(\begin{matrix}\text{Projected}\\ \text{annual dose}\end{matrix}\right) = \left(\begin{matrix}\text{Maximum realistic}\\ \text{dose rate}\end{matrix}\right) \cdot \left(\begin{matrix}\text{Maximum realistic}\\ \text{annual staytime}\end{matrix}\right) \qquad \text{(A-2)}$$

$$= \dot{H}_{av} \cdot t_{yr}$$

Dose attenuation factor

For a given application, a radiation shield has a dose attenuation factor (DAF), defined as

$$\text{DAF} = \frac{\text{Transmitted dose rate with shield in place}}{\text{Transmitted dose rate without shield in place}} \qquad \text{(A-3)}$$

If a shield has a DAF of 1/150, it means that a factor of 150 is gained in using the shield — the transmitted dose rate is lowered by a factor 150 by the shield, compared to what the dose rate would be at the same measuring point, in the absence of the radiation shield. It is more informative to express a dose attenuation factor (DAF) as a fraction $\frac{1}{150}$ than as a decimal number.

Appendix B: Observations, recommendations and contributions arising from the study

B.1 Contribution made to the industry

All three of the facilities under discussion, use high-activity sources, as such the unshielded dose rates are lethally high. The objective of the shield design and verification, i.e., radiological safety assessment performed for these facilities was to demonstrate that the plants are radiologically safe for operation using source activities at their licensed strength, namely: 20 kCi (740 TBq) for the Citrusdal facility, 10 kCi (0.37 PBq) for the Stellenbosch facility, and 2 MCi (2 , 37 PBq œ 74 PBq) for the HEPRO facility.

HEPRO management has been able to use preliminary results of the present investigation, to negotiate a new operating licence, that allowed them to operate the facility with a 2 MCi source. The Directorate of Radiation Control of the Department of Health, issued an upgraded license to HEPRO during an early phase of this project.

B.2 Observations and recommendations: HEPRO irradiation facility

B.2.1 Observations

In addition to the verification of the safety at HEPRO irradiation facility, observations and where possible measurements of spatial distribution of dose rates were conducted. A calibrated gamma-ray (ionising photon radiation) monitor, GRAETZ X5C, was employed for dose rate measurements along the walls, roof, inside irradiation vault, above water pool, pneumatic pipe penetrations, sliding plug-door, and ducts of the hoist-cable situated on the roof of the locked hut.

Walls and roof

Except at the hotspot shown in Figure B.1, measured dose rates were 0.3 µSv/h.

Cable penetration inside hut on roof

The dose rate values below 20 µSv/h were recorded.

Inside irradiation vault, above water pool, with the source at the bottom of the pool

Dose rates averaging around 0.4 µSv/h were measured.

Hotspot on the RHS wall

During the radiation survey an imperfection was noticed in the RHS shielding wall. It was located at 255 cm above floor level. Figure B.1 presents a contour plot of dose rates measured at the hotspot. The core of the hotspot is about 40 cm , 40 cm, and the entire hotspot dimension is approximately 70 cm wide by 100 cm high.

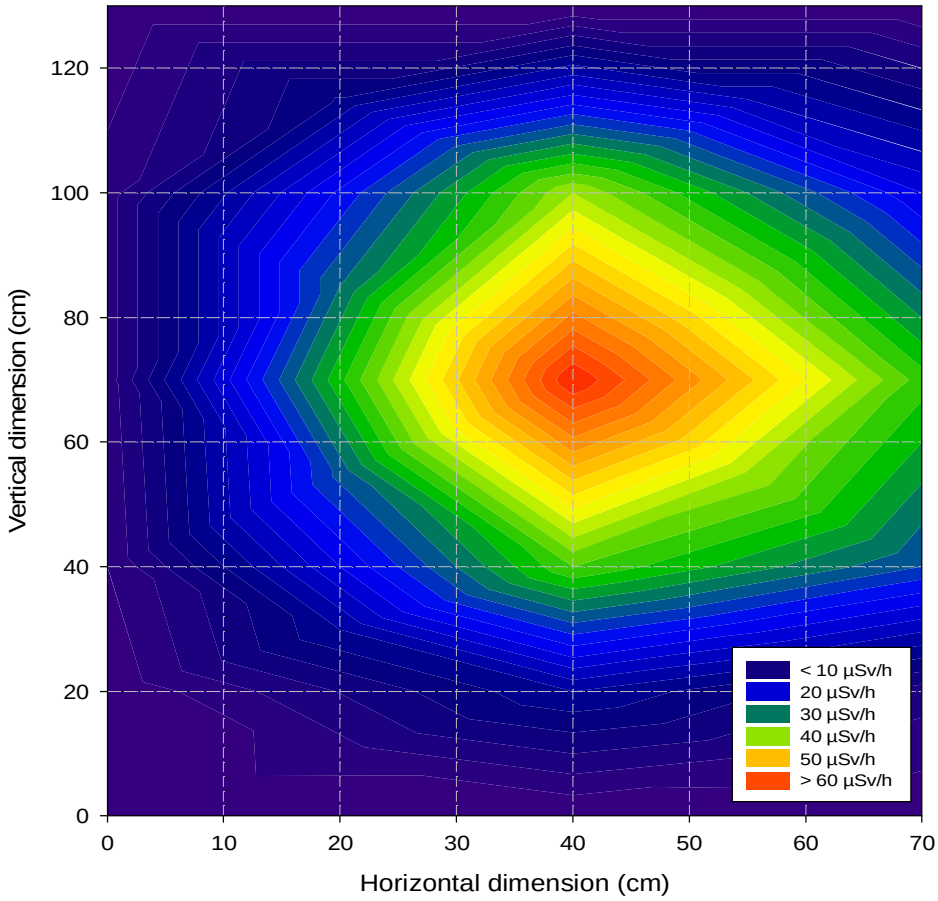

Figure B.1: *Dose rates measured at the significant hotspot on the RHS wall.*

At the centre of the hotspot (red colour in Figure B.1) values more than 60 µSv/h were measured.

Pneumatic pipe penetrations

A localised “shine-path” with unacceptably high dose rates was found at a site where pneumatic pipes penetrated through a service hole. This was reported to HEPRO management.

Sliding plug-door

Highly localised high dose rates, varying between 20 and 70 µSv/h (about 100 to 300 times above natural background levels) were measured at the RHS bottom of the sliding plug door. This was attributed to a relatively small "shine-path" at ground level. The entire area is about 40 cm below floor level.

Hoist cable duct on roof, inside locked hut

Peak dose rate of about 200 µSv/h was measured. The position of radiation beam "shining" through the small-diameter roof penetration feed through of the source-rack hoist-cable, was found to change when the ^{60}Co source was raised or lowered. The beam was however narrow and was directed vertically upwards.

Weakness

Other than the concrete casting error which resulted in a localised radiation "hotspot" no other weakness in radiation shielding was observed.

B.2.2 Recommendations: additional radiation safety engineering measures

B.2.2.1 Supplementary shielding: materials and thicknesses

Hotspot wall

An estimated combined void length of almost 60 cm of missing concrete covered the hotspot shown in Figure B.1.

The hotspot is about 3.5 m above ground level, and the "shine-path" of the radiation was found to be upward with an estimated angle of at least 20° with the horizontal.

At present, lead blankets with shielding effectiveness of 4 hung over the hotspot.

The following additional shielding to replace the lead blankets were recommended:

- A base layer of lead, 4 cm thick , 70 cm wide , 100 cm high, inside a steel frame, to cover the entire hotspot area.
- At the centre of the hotspot, an additional lead sheeting 4 cm thick , 50 cm wide , 80 cm high, also inside a sturdy steel frame, will have to be added on top of the base layer of Pb (to cover the "yellow/orange/red" core of the hotspot depicted in Figure B.1).

With additional shielding a considerably reduction in transmitted radiation levels onto adjacent areas and concrete walls, can be expected.

It was suggested that the added costs of the additional shielding specified should however be weighed against the extent of human occupancy. Bearing in mind that the volume of space affected by the radiation penetrating at the hotspot, is relatively small.

Penetration of pneumatic pipes

The "shine-path" was, subsequent to notification, blocked with lead-wool by HEPRO operational management. As human occupancy in this area is very low, and the shine-path is very narrow, collimated and at floor level, no additional measures was put forward.

Bottom of sliding plug-door

As the "shine-path" was highly localised, collimated and well below floor level, the area, on recommendation, was cordoned off and fitted with "no entry, high radiation levels" warning signs. This "shine-path" was further minimised by reducing the clearance between the sliding door and the surface beneath it. Sand was used for this purpose.

Hoist cable duct on roof

The door that provides roof entry is under access control, as is the door to the hut that surrounds the machinery that moves the source rack up or down. Because human occupation level very low, no further action resulting from the observations was recommended.

B.2.2.2 The radiation protection programme at HEPRO

The engineered radiation safety systems at HEPRO is based on the combination of (1) a radiation containment system, and (2) an access control system with interlocks and alarms. There is evidence of defence-in-depth. The present shielding walls are thick enough to accommodate a 2 MCi source. Management controls include following safe operating procedures. Evidence of a safety culture include staff attending radiation protection courses and the use of radiation safety experts.

Appendix C:
QAD-CGGP and MCNPX sample input files for the Citrusdal insect sterilization facility

A concise summary of the relevant QAD-CGGP and MCNPX input parameters are summarised below. A comprehensive description of QAD-CGGP version of QAD-P5A and MCNPX version 2.5.0 sample input files are described in the manual (RSICC CCC-493, 1989; RSICC CCC-730, 2005). This and the subsequent appendices presents the input files and the supplementary line by line explanation of the input data set that are pertinent to the three different facilities.

C.1 QAD-CGGP sample input data set

The QAD-CGGP input data set follows a specific standard sequence. Firstly, the problem in question is defined by the title using the Title card[8], then the control of data describing the physical problem. The control data includes the number of division increments along the axis which specify the division of source volume, total number of elements used in the problem, number of material compositions, number of gamma-ray energy groups, etc. Following next are the cards defining the source information, geometry information, buildup factors and elements, material identification, source energy and spectrum, response function; and last the detector position.

All input lines are limited to 72 columns. Alphabetic characters can be upper, lower or mixed case. Comments can only be written after column 72 which are not executed by the code. Given below is the QAD-CGGP sample input data set.

```
CITRUSDAL IRRADIATOR CHAMBER (RPP Geometric Bodies, dens=2.35g/cc)
15 15 15 13  3  1  2  0  0  3  1  0  0  0  0  0                        /Control Data For Gamma Source: Co-60
7.4E+14  0.0  0.0  0.0  0.0  0.0  0.0                                   /Source Information "Source Strength"

0.000E+00   1.000E-01   2.000E-01   3.000E-01   4.000E-01   5.000E-01
6.000E-01   7.000E-01   8.000E-01   9.000E-01   1.000E+00   1.100E+00
1.200E+00   1.300E+00   1.400E+00   1.500E+00                         /Coordinates of source volume
            division along the radius: R
```

[8]The term card(s) should be interpreted as a line of the input file.

```
0.000E+00   1.000E+00   2.000E+00   3.000E+00   4.000E+00   5.000E+00
6.000E+00   7.000E+00   8.000E+00   9.000E+00   1.000E+01   1.100E+01
1.200E+01   1.300E+01   1.400E+01   1.500E+01                          /Coordinates of source volume
        division along the height: Z
0.000E+00   4.189E-01   8.377E-01   1.257E+00   1.675E+00   2.094E+00
2.513E+00   2.932E+00   3.351E+00   3.770E+00   4.189E+00   4.608E+00
5.026E+00   5.445E+00   5.864E+00   6.283E+00                          /Coordinates of source volume
        division along the phi: Plane angle
    0    0          FACILITY GEOMETRY DESCRIPTION MODEL
  RPP    1  -99999.0  +99999.0  -99999.0  +99999.0  -99999.0  +99999.0        /ExVoid
  RPP    2  -99990.0  +99990.0  -99990.0  +99990.0  -99990.0  +99990.0        /InVoid
  RCC    3      +0.0      +0.0      +0.0      +0.0      +0.0     +15.0
               +1.5                                                         /Rod Containing Source
  RPP    4    -300.0    +680.0    +175.0    +325.0     -70.0    +150.0        /Rear Wall
  RPP    5    -300.0    +550.0    -325.0    -175.0     -70.0    +150.0        /Front Wall
  RPP    6    -300.0    -150.0    -175.0    +175.0     -70.0    +150.0        /Right Wall
  RPP    7    +150.0    +300.0    -075.0    +175.0     -70.0    +150.0        /RHS Labyrinth Wall
  RPP    8    +400.0    +550.0    -175.0    +075.0     -70.0    +150.0        /LHS Labyrinth Wall
  RPP    9    +650.0    +680.0    -325.0    +175.0     -70.0    +150.0        /Leftmost, Thin Wall
  RPP   10    -300.0    +400.0    -325.0    +325.0    +150.0    +270.0        /Roof CRT Slab 1
  RPP   11    +400.0    +680.0    -325.0    +325.0    +150.0    +210.0        /Roof CRT Slab 2
  END                                                                       /Termination of the body type
  Z01   20     +1     -2                                                    /Input zone and body numbers
  Z02   20     +2     -3     -4     -5     -6     -7     -8     -9    -10     /Input zone & body number
                 -11
  Z03   20     +3
  Z04   20     +4
  Z05   20     +5
  Z06   20     +6
  Z07   20     +7
  Z08   20     +8
  Z09   20     +9
  Z10   20    +10
  Z11   20    +11
  END                                                                   /Termination of zones and body numbers
  1     2   3   4    5    6    7    8    9    10    11                  /List of the zones used
  0  1000   2   1    1    1    1    1    1     1     1                  /Material number
99   1       6      7       8      11      12      13                  /Atomic numbers of all elements used in the problem
    14      16     19      20      26      82
```

```
CONC ABS
00.013  00.000  00.000  01.165  00.040  00.010  00.108
00.740  00.003  00.045  00.196  00.030  00.000                                  /1 Concrete Type NBS 04

00.000  00.000  00.000  00.000  00.000  00.000  00.000
00.000  00.000  00.000  00.000  08.000  00.000                                  /2 Steel PIN

00.000  00.000 1.03E-3 2.58E-4  00.000  00.000  00.000
00.000  00.000  00.000  00.000  00.000  00.000                                  /3 Air @ STD
   1.332     1.173                                                           /Two Energy Group: Co-60 Energies
   1.000     0.999                                                           /Yield"%" of The Energies
2.006E-8  1.816E-8                                                           /Gamma Flux-to-Dose Conversion Factor
   0.000     0.000                                                           /Gamma Flux-to-Heat Conversion Factor in Fe
=====================================================================
             /Dummy inserted symbol of no great importance
=====================================================================
+335.0   +30.0   -590.0      1   0  0  0                                     /Detectors positions
+335.0   +30.0   -580.0      1   0  0  0
+335.0   +30.0   -570.0      1   0  0  0
+335.0   +30.0   -560.0      1   0  0  0
+335.0   +30.0   -550.0      1   0  0  0
+335.0   +30.0   -500.0      1   0  0  0
+335.0   +30.0   -450.0      1   0  0  0
+335.0   +30.0   -400.0      1   0  0  0
+335.0   +30.0   -350.0      1   0  0  0
+335.0   +30.0   -300.0      1   0  0  0
+335.0   +30.0   -250.0      1   0  0  0
+335.0   +30.0   -200.0      1   0  0  0
+335.0   +30.0   -150.0      1   0  0  0
+335.0   +30.0   -100.0      1   0  0  0
+335.0   +30.0    -50.0      1   0  0  0
+335.0   +30.0    -40.0      1   0  0  0
+335.0   +30.0    -30.0      1   0  0  0
+335.0   +30.0    -20.0      1   0  0  0
+335.0   +30.0    -10.0      1   0  0  0
+335.0   +30.0    -09.0      1   0  0  0
+335.0   +30.0    -08.0      1   0  0  0
+335.0   +30.0    -07.0      1   0  0  0
+335.0   +30.0    -06.0      1   0  0  0
```

```
+335.0   +30.0    -05.0      1   0  0  0
+335.0   +30.0    -04.0      1   0  0  0
+335.0   +30.0    -03.0      1   0  0  0
+335.0   +30.0    -02.0      1   0  0  0
+335.0   +30.0    -01.0      1   0  0  0
+335.0   +30.0      0.0      1   0  0  0
+335.0   +30.0    +01.0      1   0  0  0
+335.0   +30.0    +02.0      1   0  0  0
+335.0   +30.0    +02.0      1   0  0  0
+335.0   +30.0    +03.0      1   0  0  0
+335.0   +30.0    +04.0      1   0  0  0
+335.0   +30.0    +05.0      1   0  0  0
+335.0   +30.0    +06.0      1   0  0  0
+335.0   +30.0    +07.0      1   0  0  0
+335.0   +30.0    +08.0      1   0  0  0
+335.0   +30.0    +09.0      1   0  0  0
+335.0   +30.0    +10.0      1   0  0  0
+335.0   +30.0    +40.0      1   0  0  0
+335.0   +30.0    +50.0      1   0  0  0
+335.0   +30.0   +100.0      1   0  0  0
+335.0   +30.0   +150.0      1   0  0  0
+335.0   +30.0   +200.0      1   0  0  0
+335.0   +30.0   +250.0      1   0  0  0
+335.0   +30.0   +300.0      1   0  0  0

   0.0     0.0      0.0     -1   0  0  0                              /Termination line
```

Explanation of input data set

```
CITRUSDAL IRRADIATOR CHAMBER (RPP Geometric Bodies, dens=2.35g/cc)
15 15 15 13  3  1  2  0  0  3  1  0  0  0  0  0         /Control Data For Gamma Source: Co-60
```

The first line is the problem title given as *"Citrusdal irradiator chamber (RPP Geometric Bodies, dens= 2.35 g/cc)"*. The fifteenth's are number of division increments along the axis of a right circular cylinder (RCC) which specify the division of source volume .Thirteen is the number of elements used in this problem. Three is the number of material composition. One is just dummy positive number. Two is the number of gamma-ray energy groups of the cobalt-60 source, i.e., **I▪ œ** 1.173 MeV and **I# œ** 1.332 MeV. The first zero is for indication

that the translation of the source is not employed and the second is for the geometry of the source, i.e., the right circular cylinder (RCC). Three is for indicating the most probable source region, i.e., in the geometry section the cobalt-60 source is contained in the RCC which is body number three, referred to as region three. One is for indication that the cosine-distributed source is used. The rest of the zeros are for indication that the photons calculation will be made, no effect for the first and second source point for which ray geometry printout is desired, no effect for the incremental steps size used to select additional points for ray geometry printout; and the last zero is for indicating that the will be no effect on number of additional calculational calculations to be made.

```
7.4E+14  0.0  0.0  0.0  0.0  0.0  0.0                    /Source Information "Source Strength"
```

7.4E+14 is the total source strength in decays per second of the cobalt-60. The rest of the zeros are for the constant for cosine source distribution function of a cylinder coordinates.

```
0.000E+00   1.000E-01   2.000E-01   3.000E-01   4.000E-01   5.000E-01
6.000E-01   7.000E-01   8.000E-01   9.000E-01   1.000E+00   1.100E+00
1.200E+00   1.300E+00   1.400E+00   1.500E+00                    /source volume division along the radius
0.000E+00   1.000E+00   2.000E+00   3.000E+00   4.000E+00   5.000E+00
6.000E+00   7.000E+00   8.000E+00   9.000E+00   1.000E+01   1.100E+01
1.200E+01   1.300E+01   1.400E+01   1.500E+01                    /Coordinates of source volume division along the height
0.000E+00   4.189E-01   8.377E-01   1.257E+00   1.675E+00   2.094E+00
2.513E+00   2.932E+00   3.351E+00   3.770E+00   4.189E+00   4.608E+00
5.026E+00   5.445E+00   5.864E+00   6.283E+00                    /Coordinates of source volume division along the azimuth
```

These are coordinates of the source volume divisions along the radial, **D** and **9** axis. The above input data set are free formart.

```
   0    0          FACILITY GEOMETRY DESCRIPTION MODEL
 RPP    1  -99999.0  +99999.0  -99999.0  +99999.0  -99999.0  +99999.0       /ExVoid
 RPP    2  -99990.0  +99990.0  -99990.0  +99990.0  -99990.0  +99990.0       /InVoid
 RCC    3     +0.0      +0.0      +0.0      +0.0      +0.0     +15.0
               +1.5                                                        /Rod Containing Source
 RPP    4    -300.0    +680.0    +175.0    +325.0    -70.0  +150.0          /Rear Wall
 RPP    5    -300.0    +550.0    -325.0    -175.0    -70.0  +150.0          /Front Wall
 RPP    6    -300.0    -150.0    -175.0    +175.0    -70.0  +150.0          /Right Wall
 RPP    7    +150.0    +300.0    -075.0    +175.0    -70.0  +150.0          /RHS Labyrinth Wall
 RPP    8    +400.0    +550.0    -175.0    +075.0    -70.0  +150.0          /LHS Labyrinth Wall
 RPP    9    +650.0    +680.0    -325.0    +175.0    -70.0  +150.0          /Leftmost, Thin Wall
 RPP   10    -300.0    +400.0    -325.0    +325.0  +150.0  +270.0          /Roof CRT Slab 1
```

```
RPP   11    +400.0    +680.0    -325.0    +325.0  +150.0  +210.0          /Roof CRT Slab 2
END                                                                       /Termination of the body type
```

This section is a combinatorial geometry which is a fixed format. The first line is the title of the geometry. Body 3 (RCC) is the stainless steel region containing the source. Defined as well is the geometric body type, body number assigned by the user and real data as thicknesses of the materials used to shield the cobalt-60 source.

```
Z01   20     +1     -2                                                    /Input zone and body numbers
Z02   20     +2     -3     -4     -5     -6     -7     -8     -9    -10    /Input zone & body number
                 -11
Z03   20     +3
Z04   20     +4
Z05   20     +5
Z06   20     +6
Z07   20     +7
Z08   20     +8
Z09   20     +9
Z10   20    +10
Z11   20    +11
END                                                                       /Termination of zones and body numbers
```

This part specify the alphanumeric name assigned to input zone by the user and the body number with the sign € or • as required for the zone description. *Note:* € œ *AND;* • œ *NOT.*

```
1     2   3   4    5    6    7    8    9    10    11                     /List of the zones used
```

These are regions number of each zone.

```
0  1000   2   1    1    1    1    1    1     1     1                     /Material number
```

The zero and a thousand is for external and internal void *"OUTSIDE WORLD-GRAVEYARD"*; the rest are medium (material) numbers in which the *ith* input zone is contained.

```
99   1       6       7       8       11      12      13                  /Atomic numbers of all elements used
    14      16      19      20      26      82
```

This is identification of buildup factors and elements.

```
CONC ABS
```

This is an indication that a buildup factor for concrete is used.

```
00.013  00.000  00.000  01.165  00.040  00.010  00.108
00.740  00.003  00.045  00.196  00.030  00.000                          /1 Concrete Type NBS 04
```

Partial density in g/cm$^{\$}$ of the concrete material used for shielding the cobalt-60 source. Partial density in g/cm$^{\$}$ of elements in corresponding order as listed above, i.e., one card for each material composition, with cards in the order of composition numbers.

```
00.000  00.000  00.000  00.000  00.000  00.000  00.000
00.000  00.000  00.000  00.000  08.000  00.000                             /2 Steel PIN
```

Partial density in g/cm$^{\$}$ of the stainless steel rod material containing the cobalt-60 source.

```
00.000  00.000 1.03E-3 2.58E-4  00.000  00.000  00.000
00.000  00.000  00.000  00.000  00.000  00.000                       /3 Air @ STD
```

Partial density in g/cm$^{\$}$ of the air medium inside the irradiation room.

```
   1.332     1.173                                                  /Two Energy Group: Co-60 Energies
```

Source energy: Mean gamma energy for each group (MeV) of the Cobalt-60 source.

```
   1.000     0.999                                                      /Yield"%" of The Energies
```

This is the gamma-ray of cobalt-60 source spectrum, i.e., the corresponding abundance for each energy listed above.

```
2.006E-8  1.816E-8                                          /Gamma Flux-to-Dose Conversion Factor
```

Response function: This is a the respectively gamma flux-to-dose conversion factor for each gamma-ray energy group listed above.

```
   0.000     0.000                                        /Gamma Flux-to-Heat Conversion Factor in Fe
```

Response function: This is a the respectively gamma flux-to-heat conversion factor in Fe for each gamma-ray group.

```
+335.0   +30.0   -590.0      1   0  0  0                          /Detectors positions
+335.0   +30.0   +250.0      1   0  0  0
+335.0   +30.0   +300.0      1   0  0  0
```

These are detectors coordinates. These detectors are placed with respect to the shielding wall and the position of the cobalt-6o source inside the irradiation room.

```
   0.0     0.0      0.0     -1   0  0  0                          /Termination line
```

This part is for terminating the execution of the program, i.e., the detectors cards are read until a negative one (• **"**) is encountered.

C.2 MCNPX sample input data set

The input data for MCNPX follows a specific syntax and structure. First the geometry is define by cell definitions followed by the surface that bound them. Following next is the data card cards, this includes: mode of operation, relative importance of each cell, and the source definition, material description, physics table, tallies, fluence-rate to dose-rate conversion factors. Lastly, the number of histories (or the computer time for calculation "*simulation*") and other output parameters are specified.

The input file is generally referred to as a deck consisting of four cards in the order as follows:

One Line Problem Title Card
Cell Cards
.....
.....
Blank Line Delimiter
Surface Cards
.....
.....
Black Line Delimiter
Data Cards
.....
.....

All input lines are limited to 80 columns. Alphabetic characters can be upper, lower or mixed case. Comment cards can be used anywhere in the input file by either placing a C in columns 1 to 5 followed by at least one blank and can be a total of 80 columns long, or can be appended to an existing input line by the dollar sign $ followed by a space and the comment to follow. Blank lines are used as delimiters and as an optional terminator. Data entries are separated by one or more blanks. Cell, surface, and data cards must all begin within the first five columns. MCNPX executes extensive input file checks for user errors, but is not foolproof. Given below is an example of a deck.

```
CITRUSDAL IRRADIATOR Vault (RPP Geometric Bodies)
c Cell Cards
01  0            +99                          imp:p=0  $ External World
02  1  -1.29e-3  -99 #3  #4  #5  #6  #7       &
```

```
                          #8 #9 #10 #11 #12   imp:p=1  $ AirBox at STP; Internal Void
03  3  -8.0       -3                         imp:p=1  $ Stainless Steel Rod with source
04  2  -2.35      -4                         imp:p=1  $ Rear CRT Wall
05  2  -2.35      -5                         imp:p=1  $ Front CRT Wall
06  2  -2.35      -6                         imp:p=1  $ LHS CRT Wall
07  2  -2.35      -7                         imp:p=1  $ L-Mid Labyr CRT Wall
08  2  -2.35      -8                         imp:p=1  $ R-Mid Labyr CRT Wall
09  2  -2.35      -9                         imp:p=1  $ RHS Thin CRT Wall
10  2  -2.35     -10                         imp:p=1  $ Thick LHS Roof Slab
11  2  -2.35     -11                         imp:p=1  $ Thinner RHS Roof Slab
12  2  -2.35     -12                         imp:p=1  $ Floor Slab
```

The above portion of the input file entails the Title Card containing information describing the problem *("CITRUSDAL IRRADIATOR RPP Geometric Bodies").* Following the Title Card is the Comment Card stating that all parameters to follow are within the cell card. These are the cell cards sequential written from one to twelve. However, the cell cards can only be understood with reference to the surface card section, which follows the cell card section. Cell 1 is void *"the external world"* with the importance (imp) of zero indicating that no particles (photons) are being tallied. Cell 2 contains material 1 with density 1.29E-3 g.cm$^{\bullet 3}$ (negative densities mean quantity is mass-density in unit g.cm$^{\bullet 3}$; positive densities mean unit is number of atoms per barn.cm). Cell 2 consists of the volume inside surface 99, but outside the rest of the surfaces. The importance (imp) of photons (p) inside cell 2, is 1. The $ sign signifies the beginning of an in-line comment; everything to the right of the $ sign, is only a comment. Cell 3 contains material 3 with density 8 g.cm$^{\bullet 3}$, is bounded by only one surface 3, and has an importance of 1. In most cases the comments given after a dollar sign indicates the materials used, e.g., $ Stainless steel rod with the source. Cell 4 to 12 contains material number 2, which has a density of 2.35 g.cm$^{\bullet 3}$. The importance (imp) of photons (p) inside cell 4 to 12, are 1.

By looking at the surface cards (page 127), it may now be easily understood that cell 3 is a right circular cylinder (RCC) stainless steel rod with the source. The RCC is 15 cm high with the radius of 1.5 cm positioned at the origin. Cell 4 is a rectangular parallelepiped shell (rear wall) consisting of ordinary concrete; it extends from 175 cm to 325 cm, i.e., the concrete thickness is 150 cm. Cell 99 is all space outside top-view of Figure 3.4. Particles that enter into this region of space, are not followed (tracked) any more by the Monte Carlo code.

In a Monte Carlo radiation transport calculation, it is important to model a few hundred cm of air outside any shield, because radiation can be backscattered by the air to the "detector" i.e. "receiver" positions. Backscattering media such as walls of rooms, must usually be included in the problem geometry. Always model the problem geometry as realistically as possible.

```
c Surface Cards
03  RCC      0.0     0.0      0.0     0.0     0.0    15.0  1.5     $ Rod with Source
04  RPP   -300.0  +680.0   +175.0  +325.0   -70.0  +150.0          $ Rear wall RPP4
05  RPP   -300.0  +550.0   -325.0  -175.0   -70.0  +150.0          $ Front Wall RPP5
06  RPP   -300.0  -150.0   -175.0  +175.0   -70.0  +150.0          $ Left Wall RPP6
07  RPP   +150.0  +300.0   -075.0  +175.0   -70.0  +150.0          $ LHS Labyrinth wall RPP7
08  RPP   +400.0  +550.0   -175.0  +075.0   -70.0  +150.0          $ RHS Labyrinth wall RPP8
09  RPP   +650.0  +680.0   -325.0  +175.0   -70.0  +150.0          $ Rightmost, thin wall RPP9
10  RPP   -300.0  +400.0   -325.0  +325.0  +150.0  +270.0          $ Roof CRT Slab – Thick part
11  RPP   +400.0  +680.0   -325.0  +325.0  +150.0  +210.0          $ Roof CRT Slab – Thin part
12  RPP   -600.0  +900.0   -500.0  +500.0  -370.0   -70.0          $ Floor Slab
99  RPP  -2000.0 +2000.0  -2000.0 +2000.0  -400.0 +4000.0          $ AirBox
```

The input data on the surface card describes the thicknesses of the materials used and their location with respect the radiation source. For example, surface 3 is a right circular cylinder confining the cobalt-60 source located at the centre. Surface 5 is a rectangular parallelepiped located at 175 cm with respect to the location of the source. This surface extend from 175 to 325 cm, as a result its thickness is 150 cm.

```
c Data Cards
c Mode: transport photons
mode p
```

The first two lines are comments shown by the first letter C concisely explains that is the beginning of the data card and the photons will be transported.

```
c source definition:
c ******************************
c source definition: CYLINDRICAL VOLUME ALONG Z-AXIS
sdef par=p  erg=d3                          &
     pos=0 0 0                              &
     axs=0 0 1 ext=d1  rad=d2  &
     cel=03
```

This part specify the characteristics of the radiation source. Line 3 is the comment indicating the structure of the source. The source particle is the photon. The source is a right circular cylinder extending on the **D** axis distributed as (d) number 1, denoted as d1 and the radius is

distributed as (d) number 2, denoted as d2 , located at position **B œ !ßC œ !ßD œ !**. The source energy, i.e., photon energy, is distributed as distribution (d) number 3, denoted as d3 . The source is bound by surface 3 in cell 3.

```
si1   0.0  15.0       $ Sampling of source point along the Z.min to Z.max Axial coordinate
si2   0.0   1.5       $ Sampling of source point along radial coordinate
```

The Source Information (SI) card number 1, i.e., the SI1 card, indicates that the circle lies in a plane perpendicular to AXS at the distance from POS which is sampled value of EXT, i.e., shown by d1 distribution. The SI card number 2, SI2 , is for position of the particles sampled uniformly on the circle whose radius is the sampled value of RAD, centered on the axis of the cylinder.

```
sp2  -21  1           $ Probability of sampling of source point in radial dimensionsi
sp3    0.999  1.000   $ Emission abundances
```

The Source Probability (SP) card SP2 states the probability of the source sampling distribution in the radial dimension d2 using built-in power law. The SP card SP3 states that, in source energy distribution d3 , the photon with energy **I" œ** 1.173 MeV is emitted with an emission yield **C" œ** 0.999 photons per radioactive transition, while the photon with energy **I# œ** 1.332 MeV is emitted with an emission yield of **C# œ** 1.000 photons per radioactive transition event.

```
c Material definitions
m1    7014  -0.79   8016  -0.21                                  $ Air at STP
```

This is material 1 among three materials used in the problem. Material 1 is air. The ZAID identity code of an isotope is **a**1000**^ € E**b. However, this is a photon transport problem and photon energies are very low, far below the threshold for nuclear reactions. At such low energies, photons will only interact according to the laws of quantum electrodynamics, and interaction cross-sections will for all practical purposes only depend on the atomic number **^** and not on the mass number, **E**. In other words, only the identity of the element is important; the specific isotope will not be important. Cross-sections will differ from element to element but not from isotope to isotope. Example: for interactions by low energy ionising photons, the cross-sections for ^{54}Fe, ^{56}Fe, ^{57}Fe and ^{58}Fe will be identical, for all practical purposes. Therefore the ZAID (**^-E**-Identity code) for an element will simply be 1000**^**, because only the atomic number **^** and not the mass number **E**, will be relevant to the radiation transport. (Note that in neutron problems, this is not the case, so that the full ZAID must

usually be specified for neutron problems. In neutron transport problems, a ZAID of e.g., 20000 indicates that the isotopic makeup of calcium is the natural abundance of Ca isotopes.)

The negative number following the ZAID, is the mass fraction of the material composed of that element. If the number was positive, it would have designated a number fraction and not a mass fraction.

Water, e.g., can be easily specified as

```
1000 +2 8000 +1
```

because its chemical formula is H_2O. Similarly, paraffin wax with representative chemical formula $C_{25}H_{52}$ can easily be specified as

```
1000  +52    6000  +25
```

Note: It is not necessary at all to use an explicit **+** sign as above, but it is a useful way of adding clarity to the input data set.

```
m2    1001  -0.013  8016  -1.165  11023  -0.040  12000  -0.010   &  $ Ordinary Concrete
     13027  -0.108 14000  -0.740 16000  -0.003  19000  -0.045   &  $ Ordinary Concrete
     20000  -0.196 26000  -0.030                                  $ Ordinary Concrete
m3    6000  -0.03   14000 -0.60   15000  -0.02   16000  -0.03    &  $ SS-316L
     24000 -17.50   25000 -1.70   26000 -64.52   28000 -13.00    &  $ SS-316L
     42000  -2.60                                                  $ SS-316L
c  Energy (MeV) and fluence-rate to dose-rate conversion factors: photons
c  Units: Convert fluence-rate to Sv/hr
#        de        df
       0.010    2.22E-10
       .....    ........
       15 .0    1.28E-07
       .....    ........
       10000.0  1.05e-6
```

This part also gives the other materials used in the input data set. Material 2 is an ordinary concrete and material 3 is the stainless steel with their corresponding material fractions. Following next are two commented lines describing the flux-to-dose conversion factors. The first column are the photon energies, and the second column are the conversion factors to convert the answer from fluence-rate to dose-rate in unit Sv/h.

The | # | indicates that the data is organised in columns. Note that this neat | # | option only works in some versions of MCNPX.

Important: Every ~15 years, the ICRP recommends new sets of radiation weighting factors and tissue weighting factors. New values for these weighting factors will have a small but definite effect on the values of the fluence-rate to dose-rate conversion factors, because these are calculated for expanded and aligned mono-energetic radiation fields incident upon anthropomorphic calculational phantoms, using Monte Carlo codes. Conclusion: The above conversion factors can not be used indefinitely. The scientific literature must be continually monitored for new conversion factors. Places to watch: new American Nuclear Society (ANS) standards, as well as ICRP publications. Also Radiation Protection and Dosimetry journal articles.

```
c ==== PRINT CONTROLS =====
PRINT 10 40 30 50 60 72 100 110 120 170 200 98
c === RUNTIME CONTROLS ======
tmesh
rmesh1:p dose 31 3 2 7.4e+14
    cora1  -400.0   78i  +400.0
    corb1  -900.0  128i  +400.0
    corc1   -70.0        +150.0
endmd
```

This part entail the print card and the mesh tally. The print card entries are optional and/or default tables printed on the output for analysis. The *tally* is the *result* calculated by the Monte Carlo code. The mesh tally, rmesh1, is a rectangular tally calculates the track length estimate of the particle flux, averaged over a mesh cell, in units of particles per area. cora1, corb1 and corc1 are subdivisions along the **B** axis, **C** axis and **D** axis, respectively.

```
c ===
ctme 3500
```

This is the computer execution time, i.e., the simulation will go on till the specified time of 3500 minutes.

C.3 MCNPX input data set for the SPH geometry case

```
CITRUSDAL IRRADIATOR ROOM SHIELD WALL DESIGN (Spherical case)
c Cell Cards
01  01  -1.29e-3    -1            $ Main Chamber Air Layer1
02  01  -1.29e-3    -2   +1       $ Main Chamber Air Layer2
03  01  -1.29e-3    -3   +2       $ Main Chamber Air Layer3
04  01  -1.29e-3    -4   +3       $ Main Chamber Air Layer4
05  01  -1.29e-3    -5   +4       $ Main Chamber Air Layer5
06  01  -1.29e-3    -6   +5       $ Main Chamber Air Layer6
07  01  -1.29e-3    -7   +6       $ Main Chamber Air Layer7
08  01  -1.29e-3    -8   +7       $ Main Chamber Air Layer8
09  01  -1.29e-3    -9   +8       $ Main Chamber Air Layer9
10  01  -1.29e-3   -10   +9       $ Main Chamber Air Layer10
11  01  -1.29e-3   -11  +10       $ Main Chamber Air Layer11
12  01  -1.29e-3   -12  +11       $ Main Chamber Air Layer6
13  01  -1.29e-3   -13  +12       $ Main Chamber Air Layer12
14  01  -1.29e-3   -14  +13       $ Main Chamber Air Layer13
15  01  -1.29e-3   -15  +14       $ Main Chamber Air Layer14
16  01  -1.29e-3   -16  +15       $ Main Chamber Air Layer15
17  01  -1.29e-3   -17  +16       $ Main Chamber Air Layer16
18  01  -1.29e-3   -18  +17       $ Main Chamber Air Layer17
19  02  -2.35      -19  +18       $ Concrete L1
20  02  -2.35      -20  +19       $ Concrete L2
21  02  -2.35      -21  +20       $ Concrete L3
22  02  -2.35      -22  +21       $ Concrete L4
23  02  -2.35      -23  +22       $ Concrete L5
24  02  -2.35      -24  +23       $ Concrete L6
25  02  -2.35      -25  +24       $ Concrete L7
26  02  -2.35      -26  +25       $ Concrete L8
27  02  -2.35      -27  +26       $ Concrete L9
28  02  -2.35      -28  +27       $ Concrete L10
29  02  -2.35      -29  +28       $ Concrete L11
30  02  -2.35      -30  +29       $ Concrete L12
31  02  -2.35      -31  +30       $ Concrete L13
32  02  -2.35      -32  +31       $ Concrete L14
```

```
33  02  -2.35      -33  +32        $ Concrete L15
34  01  -1.29e-3   -34  +33        $ Surrounding Air ThinShell
35  01  -1.29e-3   -35  +34        $ Surrounding Air Shell
36  01  -1.29e-3   -36  +35        $ Surrounding Air Shell
37  01  -1.29e-3   -37  +36        $ Surrounding Air Shell
38  01  -1.29e-3   -38  +37        $ Surrounding Air Shell
39  01  -1.29e-3   -39  +38        $ Surrounding Air Shell
40  01  -1.29e-3   -40  +39        $ Surrounding Air Shell
41  01  -1.29e-3   -41  +40        $ Surrounding Air Shell
42  01  -1.29e-3   -42  +41        $ Surrounding Air Shell
43  01  -1.29e-3   -43  +42        $ Surrounding Air Shell
44  01  -1.29e-3   -44  +43        $ Surrounding Air Shell
45  01  -1.29e-3   -45  +44        $ Surrounding Air Shell
46  01  -1.29e-3   -46  +45        $ Surrounding Air Shell
47  00                   +46        $ Surrounding Air Shell

c Surface Cards
01  SPH   0.0   0.0   0.0  +010.0    $ INNER AIR SHELL BOUND
02  SPH   0.0   0.0   0.0  +020.0    $ INNER AIR SHELL BOUND
03  SPH   0.0   0.0   0.0  +030.0    $ INNER AIR SHELL BOUND
04  SPH   0.0   0.0   0.0  +040.0    $ INNER AIR SHELL BOUND
05  SPH   0.0   0.0   0.0  +050.0    $ INNER AIR SHELL BOUND
06  SPH   0.0   0.0   0.0  +060.0    $ INNER AIR SHELL BOUND
07  SPH   0.0   0.0   0.0  +070.0    $ INNER AIR SHELL BOUND
08  SPH   0.0   0.0   0.0  +080.0    $ INNER AIR SHELL BOUND
09  SPH   0.0   0.0   0.0  +090.0    $ INNER AIR SHELL BOUND
10  SPH   0.0   0.0   0.0  +100.0    $ INNER AIR SHELL BOUND
11  SPH   0.0   0.0   0.0  +110.0    $ INNER AIR SHELL BOUND
12  SPH   0.0   0.0   0.0  +120.0    $ INNER AIR SHELL BOUND
13  SPH   0.0   0.0   0.0  +130.0    $ INNER AIR SHELL BOUND
14  SPH   0.0   0.0   0.0  +140.0    $ INNER AIR SHELL BOUND
15  SPH   0.0   0.0   0.0  +150.0    $ INNER AIR SHELL BOUND
16  SPH   0.0   0.0   0.0  +160.0    $ INNER AIR SHELL BOUND
17  SPH   0.0   0.0   0.0  +170.0    $ INNER AIR SHELL BOUND
18  SPH   0.0   0.0   0.0  +175.0    $ INNER AIR OD
19  SPH   0.0   0.0   0.0  +185.0    $ CRT LAYER 01 OD
20  SPH   0.0   0.0   0.0  +195.0    $ CRT LAYER 02 OD
21  SPH   0.0   0.0   0.0  +205.0    $ CRT LAYER 03 OD
22  SPH   0.0   0.0   0.0  +215.0    $ CRT LAYER 04 OD
```

```
23  SPH   0.0   0.0   0.0  +225.0    $ CRT LAYER 05 OD
24  SPH   0.0   0.0   0.0  +235.0    $ CRT LAYER 06 OD
25  SPH   0.0   0.0   0.0  +245.0    $ CRT LAYER 07 OD
26  SPH   0.0   0.0   0.0  +255.0    $ CRT LAYER 08 OD
27  SPH   0.0   0.0   0.0  +265.0    $ CRT LAYER 09 OD
28  SPH   0.0   0.0   0.0  +275.0    $ CRT LAYER 10 OD
29  SPH   0.0   0.0   0.0  +285.0    $ CRT LAYER 11 OD
30  SPH   0.0   0.0   0.0  +295.0    $ CRT LAYER 12 OD
31  SPH   0.0   0.0   0.0  +305.0    $ CRT LAYER 13 OD
32  SPH   0.0   0.0   0.0  +315.0    $ CRT LAYER 14 OD
33  SPH   0.0   0.0   0.0  +325.0    $ CRT LAYER 15 OD
34  SPH   0.0   0.0   0.0  +335.0    $ Thin AirShell just outside concrete OD
35  SPH   0.0   0.0   0.0  +345.0    $ Outer airshell partition boundary
36  SPH   0.0   0.0   0.0  +355.0    $ Outer airshell partition boundary
37  SPH   0.0   0.0   0.0  +365.0    $ Outer airshell partition boundary
38  SPH   0.0   0.0   0.0  +375.0    $ Outer airshell partition boundary
39  SPH   0.0   0.0   0.0  +385.0    $ Outer airshell partition boundary
40  SPH   0.0   0.0   0.0  +395.0    $ Outer airshell partition boundary
41  SPH   0.0   0.0   0.0  +405.0    $ Outer airshell partition boundary
42  SPH   0.0   0.0   0.0  +415.0    $ Outer airshell partition boundary
43  SPH   0.0   0.0   0.0  +425.0    $ Outer airshell partition boundary
44  SPH   0.0   0.0   0.0  +435.0    $ Outer airshell partition boundary
45  SPH   0.0   0.0   0.0  +445.0    $ Outer airshell partition boundary
46  SPH   0.0   0.0   0.0  +450.0    $ Outer airshell partition boundary

c Data Cards
c Mode: transport photons
mode p
c cell importance
imp:p 1 17r 2m 2m 2m 2m 2m 2m 2m 2m 2m 2m 2m 2m 2m 2m 2m 2m 2m 2m 9r 0
c source definition:
sdef par=p erg=d3 pos=0 0 0
si3 L  1.173  1.332
sp3    0.999  1.000
c
c Material definitions
m01   7014 -0.79    8016  -0.21                                                    $ Air at STP
m02   1001 -0.013   8016  -1.165   11023  -0.040   12000  -0.010  &   $ Ordinary Concrete
     13027 -0.108  14000  -0.740   16000  -0.003   19000  -0.045 &    $ Ordinary Concrete
```

```
     20000 -0.196  26000  -0.030                                                  $ Ordinary Concrete
c
c **** Physics Table *****
phys:p 100 0 0 -1  1
totnu
c
c **** Tallies *******
c
fc12 Tally: photon dose-rate
f12:p  1   2   3   4   5   6   7   8   9  10 11  12  13  14  15  16 17  18  &
19 20 21  22  23  24  25 26 27 28 29 30 31 32 33 34  35  36  37  38 39  40  &
41  42  43 44 45 46
fm12   7.4E14      $ 20 kCi Co-60
c  Energy (MeV) and fluence-rate to dose-rate conversion factors: photons
c  Units: Convert fluence-rate to Sv/hr
#      de12     df12
       0.010    2.22E-10
       0.012    3.35E-10
       0.013    4.70E-10
       0.016    6.14E-10
       0.018    7.58E-10
       0.021    8.91E-10
       0.024    1.01E-09
       0.028    1.11E-09
       0.032    1.19E-09
       0.037    1.26E-09
       0.043    1.32E-09
       0.050    1.39E-09
       0.058    1.45E-09
       0.067    1.54E-09
       0.078    1.64E-09
       0.090    1.78E-09
       0.104    1.96E-09
       0.120    2.19E-09
       0.139    2.50E-09
       0.161    2.93E-09
       0.186    3.43E-09
       0.216    4.01E-09
       0.250    4.67E-09
```

```
        0.289    5.42E-09
        0.335    6.27E-09
        0.387    7.22E-09
        0.448    8.28E-09
        0.519    9.46E-09
        0.601    1.08E-08
        0.695    1.22E-08
        0.805    1.38E-08
        0.931    1.56E-08
        1.078    1.75E-08
        1.248    1.96E-08
        1.445    2.19E-08
        1.672    2.43E-08
        1.935    2.71E-08
        2.24     3.00E-08
        2.593    3.33E-08
        3.002    3.69E-08
        3.474    4.08E-08
        4.022    4.52E-08
        4.655    5.01E-08
        5.388    5.56E-08
        6.237    6.19E-08
        7.219    6.90E-08
        8.356    7.72E-08
        9.672    8.68E-08
        11.196   9.80E-08
        12.959   1.11E-07
        15 .0    1.28E-07
        20.0     1.31E-07
        30.0     1.82E-07
        40.0     2.23E-07
        50.0     2.65E-07
        100.0    4.28E-07
        200.0    5.43E-07
        500.0    6.84E-07
        1000.0   7.70E-07
        10000.0  1.05E-06
c
fc24 Photon fluence-rate & spectrum tally
```

```
f24:p  6  7  22
e24    0.01  0.10  0.20  0.30  0.40  0.50  0.60  0.70  0.80  0.90    &
       1.00  1.10  1.15  1.20  1.25  1.30  1.35
fm24   7.4E14
c ==== PRINT CONTROLS =====
PRINT 10 40 50 60 72 100 110 120 170 200
c === RUNTIME CONTROLS ======
ctme 120
```

Line by line explanation

```
c source definition:
sdef par=p erg=d3 pos=0 0 0
si3 L  1.173  1.332
sp3    0.999  1.000
```

The source definition is: The source particle is the photon. The source is a point source located at position **B œ !ßC œ !ßD œ !**. The source energy, i.e., photon energy, is distributed as distribution (d) number 3, denoted as d3. The Source Information (SI) card number 3, i.e, the SI3 card, indicates that energy distribution d3 is a line distribution L, i.e., that there are discrete photon energies. There are 2 discrete line energies in distribution d3: **I" œ** 1.173 MeV and **I# œ** 1.332 MeV. The Source Probability card SP3 states that, in source energy distribution d3, the photon with energy **I" œ** 1.173 MeV is emitted with an emission yield **C" œ** 0.999 photons per radioactive transition, while the photon with energy **I# œ** 1.332 MeV is emitted with an emission yield of **C# œ** 1.000 photons per radioactive transition event.

```
fc12 Tally: photon dose-rate
f12:p  1   2   3   4   5   6   7   8   9  10 11  12  13  14  15  16 17  18  &
19 20 21  22  23  24  25 26 27 28 29 30 31 32 33 34  35  36  37  38 39  40  &
41  42  43 44 45 46
fm12   7.4E14      $ 20 kCi Co-60
```

The *tally* is the *result* calculated by the Monte Carlo code. An F2 tally is a surface fluence-rate (older term: “flux”) tally. The F2 tally card

f12:p 1 2 3.....46

instructs the code MCNPX to determine the fluence-rate, in unit $cm^{\bullet 2}.s^{\bullet 1}$, of photons ("p") that cross surfaces 1 to 46. Note that the last number in the tally name, f12, denotes the type of tally, i.e, number 2. An F4 tally is a cell volume averaged fluence-rate tally. An F6 tally is an energy deposition tally, and can be used to determine absorbed dose rate in e.g, the unit Gy/hr. The first number 1 in the tally designation f12 is simply a counter. Tally designations such as f12, f22, f32, f42, f52, etc, will all be F2 tally types, i.e., surface fluence-rate tallies in unit $cm^{\bullet 2}.s^{\bullet 1}$.

The fc12 card is the "tally comment card", i.e, it is simply the "name" of tally f12; this name will be printed in the output data set where the tally results are given for tally f12.

The fm12 card is the tally multiplication card for tally f12. In this simple problem, it simply specifies the source activity in unit Bq.

```
fc24 Photon fluence-rate & spectrum tally
f24:p  6  7  22
e24    0.01  0.10  0.20  0.30  0.40  0.50  0.60  0.70  0.80  0.90    &
       1.00  1.10  1.15  1.20  1.25  1.30  1.35
fm24   7.4E14
```

This part indicates an F4 tally which is a cell volume averaged fluence-rate tally and the energy tally E4. The energy tally is for subdividing the total flux into energy groups, for example, E1 to E2, E2 to E3, etc.

C.4 MCNPX input data set for verification: the actual concrete shield geometry of the Citrusdal facility

```
CITRUSDAL INSECT IRRADIATOR (Labyrinth Case)
c Cell Cards
01  0            +99                                                  imp:p=0  $ External World
02  1  -1.29e-3  -99 #3  #4  #5  #6  #7  #8  #9  #10 #11 #12   &
                     #20 #21 #22 #23 #24 #25 #26 #27 #28 #29 #30   imp:p=1  $ Internal Void
```

The above portion of the input file entails the Title Card containing information describing the problem *("CITRUSDAL IRRADIATOR RPP Geometric Bodies, particular for evaluating dose rates along the labyrinth ").* Following the Title Card is the Comment Card stating that all parameters to follow are within the cell card. Cell 1 is void *"the external world"* with the importance (imp) of zero indicating that no particles (photons) are being tallied.Cell 2 contains material 1 with density 1.29E-3 g.cm$^{\bullet 3}$. Cell 2 consists of the volume inside surface 99, but outside the rest of the surfaces. The importance (imp) of photons (p) inside cell 2, is 1.

```
03  3  -8.0       -3                                    imp:p=1  $ Stainless Steel Rod with source
04  2  -2.35      -4                                    imp:p=1  $ Rear CRT Wall
05  2  -2.35      -5                                    imp:p=1  $ Front CRT Wall
06  2  -2.35      -6                                    imp:p=1  $ RHS CRT Wall
07  2  -2.35      -7                                    imp:p=1  $ R-Mid Labyr CRT Wall
08  2  -2.35      -8                                    imp:p=1  $ L-Mid Labyr CRT Wall
09  2  -2.35      -9                                    imp:p=1  $ LHS Thin CRT Wall
10  2  -2.35     -10                                    imp:p=1  $ Thick RHS Roof Slab
11  2  -2.35     -11                                    imp:p=1  $ Thinner LHS Roof Slab
12  2  -2.35     -12                                    imp:p=1  $ Floor Slab
20  1  -1.29e-3  -20                                    imp:p=1  $ F4TallyBox in Labyrinth
21  1  -1.29e-3  -21                                    imp:p=1  $ F4TallyBox in Labyrinth
22  1  -1.29e-3  -22                                    imp:p=1  $ F4TallyBox in Labyrinth
23  1  -1.29e-3  -23                                    imp:p=1  $ F4TallyBox in Labyrinth
24  1  -1.29e-3  -24                                    imp:p=1  $ F4TallyBox in Labyrinth
25  1  -1.29e-3  -25                                    imp:p=1  $ F4TallyBox in Labyrinth
26  1  -1.29e-3  -26                                    imp:p=1  $ F4TallyBox in Labyrinth
27  1  -1.29e-3  -27                                    imp:p=1  $ F4TallyBox in Labyrinth
28  1  -1.29e-3  -28                                    imp:p=1  $ F4TallyBox in Labyrinth
```

```
29  1  -1.29e-3  -29                                    imp:p=1  $ F4TallyBox outside wall RPP5, opposite source
30  1  -1.29e-3  -30                                    imp:p=1  $ F4TallyBox outside wall RPP5,slightly opposite source
```

Cell 3 contains material 3 with density 8 g.cm$^{\bullet 3}$, is bounded by only one surface 3, and has an importance of 1. The material is Stainless steel rod with the source. Cell 4 to 12 contains material number 2, which has a density of 2.35 g.cm$^{\bullet 3}$. The importance (imp) of photons (p) inside cell 4 to 12, are 1. The $ sign signifies the beginning of an in-line comment; everything to the right of the $ sign, is only a comment.

Cell 20 to 28 are the cell tallies, F4, contains air, i.e., material number 1 for talling the flux along the labyrinth. Cell 29 and 30 are also, cell tallies, F4, tallies for the same purpose but placed outside wall RPP5, just opposite the source.

```
c Surface Cards
03  RCC     0.0     0.0     0.0     0.0     0.0    15.0  1.5          $ Rod with Source
04  RPP  -325.0  -175.0  -680.0  +300.0   -70.0  +150.0               $ Rear wall RPP4
05  RPP  +175.0  +325.0  -550.0  +300.0   -70.0  +150.0               $ Front Wall RPP5
06  RPP  -175.0  +175.0  +150.0  +300.0   -70.0  +150.0               $ Right Wall RPP6
07  RPP  -175.0  +075.0  -300.0  -150.0   -70.0  +150.0               $ RHS Labyrinth wall RPP7
08  RPP  -075.0  +175.0  -550.0  -400.0   -70.0  +150.0               $ LHS Labyrinth wall RPP8
09  RPP  -175.0  +325.0  -680.0  -650.0   -70.0  +150.0               $ Leftmost, thin wall RPP9
10  RPP  -325.0  +325.0  -400.0  +300.0  +150.0  +270.0               $ Roof CRT Slab – Thick part RHS
11  RPP  -325.0  +325.0  -680.0  -400.0  +150.0  +210.0               $ Roof CRT Slab – Thin part LHS
12  RPP  -500.0  +500.0  -900.0  +600.0  -370.0   -70.0               $ Floor Slab
20  RPP  +225.0  +325.0  -650.0  -550.0   -70.0  +150.0               $ F4TallyBox-Labyrinth
21  RPP   +75.0  +175.0  -650.0  -550.0   -70.0  +150.0               $ F4TallyBox-Labyrinth
22  RPP   -75.0   +25.0  -650.0  -550.0   -70.0  +150.0               $ F4TallyBox-Labyrinth
23  RPP  -175.0  -125.0  -650.0  -550.0   -70.0  +150.0               $ F4TallyBox-Labyrinth
24  RPP  -175.0   -75.0  -500.0  -400.0   -70.0  +150.0               $ F4TallyBox-Labyrinth
25  RPP  -175.0   -75.0  -350.0  -300.0   -70.0  +150.0               $ F4TallyBox-Labyrinth
26  RPP   -25.0   +75.0  -400.0  -300.0   -70.0  +150.0               $ F4TallyBox-Labyrinth
27  RPP  +125.0  +175.0  -400.0  -300.0   -70.0  +150.0               $ F4TallyBox-Labyrinth
28  RPP   +75.0  +175.0  -250.0  -150.0   -70.0  +150.0               $ F4TallyBox-Labyrinth
29  RPP  +325.0  +335.0   -10.0   +10.0   -30.0   +40.0               $ F4TallyBox-opposite RPP5
30  RPP  +325.0  +335.0   +20.0   +40.0   -30.0   +40.0               $ F4TallyBox-opposite RPP5
99  RPP -2000.0 +2000.0 -2000.0 +2000.0  -400.0 +4000.0               $ AirBox
```

```
c Data Cards
c Mode: transport photons
mode p
c source definition:
c ******************************
c source definition: CYLINDRICAL VOLUME ALONG Z-AXIS
sdef par=p  erg=d3                          &
     pos=0 0 0                              &
     axs=0 0 1 ext=d1  rad=d2               &
     cel=03
si1   0.0  15.0       $ Sampling of source point along Axial coordinate: start from Z.min to           Z.max
sp1  -21  1           $ Probability of sampling of source point in axial dimension: power law
si2   0.0   1.5       $ Sampling of source point along radial coordinate done from R.min to R.max
sp2  -21  1           $ Probability of sampling of source point in radial dimension: power law
```

Surfaces 3 to 12 are as previously explained including the source definition. Surfaces 20 to 30 are the dimensions of the tallies at the respectively dimensions. For example,

20 RPP +225.0 +325.0 -650.0 -550.0 -70.0 +150.0 $ F4TallyBox-Labyrinth

is placed at almost the door exit which is 100 cm along the **B** and **C** axis, and 220 cm along the **D** axis.

```
si3 L  1.173  1.332   $ Energies of gamma-photons emittted by radionuclide Co-60
sp3    0.999  1.000   $ Emission abundances with which the radionuclide Co-60 emits these gamma-photons
c
c Material definitions
m1    7014  -0.79   8016  -0.21                                    $ Air at STP
m2    1001  -0.013  8016  -1.165  11023  -0.040  12000  -0.010   &  $ Ordinary Concrete
     13027  -0.108 14000  -0.740 16000  -0.003  19000  -0.045   &  $ Ordinary Concrete
     20000  -0.196 26000  -0.030                                   $ Ordinary Concrete
m3    6000  -0.03   14000 -0.60   15000  -0.02   16000  -0.03    &  $ SS-316L
     24000 -17.50   25000 -1.70   26000 -64.52   28000 -13.00    &  $ SS-316L
     42000  -2.60                                                  $ SS-316L
c
c **** Tally *******
fc14 TALLY-BOX IN LABYRINTH; Photon dose-rate in Sv/hr.
f14:p 20 21 22 23 24 25 26 27 28
fm14 7.4e+14                                                       $ Transition rate in 20 kCi source; unit: Bq
```

This part gives the source information, probability distribution, materials used and the tallies. The tallies are numbered 1 of the type F4. In this case the tallies are placed along the maze for tallying the dose rates which are then platted using data analysis as a function of position.

```
c ============================
fc24 TALLY-BOX OUTSIDE RPP5, OPPOSITE SOURCE; Photon dose-rate in Sv/hr.
f24:p 29 30
fm24 7.4e+14                                                $ Transition rate in 20 kCi source; unit: Bq
```

The tallies are numbered 2 of the type F4. In this case the tallies are placed outside RPP5 wall, opposite the source for tallying the dose rates transverse the RPP5 wall.

```
c ============================
c  Energy (MeV) and fluence-rate to dose-rate conversion factors: photons
c  Units: Convert fluence-rate to Sv/hr
#        de        df
       0.010    2.22E-10
       .......  .......
       10000.0  1.05e-6
c ==== PRINT CONTROLS =====
PRINT 10 40 30 50 60 72 100 110 120 170 200 98
c === RUNTIME CONTROLS ======
ctme 3500
```

Appendix D:
QAD-CGGP and MCNPX sample input files for the Stellenbosch insect sterilization facility

D.1 QAD-CGGP sample input data set

```
STELLENBOSCH IRRADIATOR VAULT (RPP Geometric bodies, dens=2.635 g/cc)
15 15 15 13  4  1  2  0  0  3  1  0  0  0  0  0                          /Control Data For Gamma Source: Co-60
1.1951E+14  0.0  0.0  0.0  0.0  0.0  0.0                                  /Source Information "Source Strength"

   0.000E+00   7.000E-02   1.400E-01   2.100E-01   2.800E-01   3.500E-01
   4.200E-01   4.900E-01   5.600E-01   6.300E-01   7.000E-01   7.700E-01
   8.400E-01   9.100E-01   9.800E-01   1.050E+00

   0.000E+00   1.667E-01   3.333E-01   5.000E-01   6.667E-01   8.333E-01
   1.000E+00   1.167E+00   1.333E+00   1.500E+00   1.667E+00   1.833E+00
   2.000E+00   2.167E+00   2.333E+00   2.500E+00

   0.000E+00   4.189E-01   8.377E-01   1.257E+00   1.675E+00   2.094E+00
   2.513E+00   2.932E+00   3.351E+00   3.770E+00   4.189E+00   4.608E+00
   5.026E+00   5.445E+00   5.864E+00   6.283E+00
       0    0          FACILITY GEOMETRY DESCRIPTION MODEL
  RPP    1  -99999.0  +99999.0  -99999.0  +99999.0  -99999.0  +99999.0      /ExVoid
  RPP    2  -99990.0  +99990.0  -99990.0  +99990.0  -99990.0  +99990.0      /InVoid
  RCC    3      +0.0      +0.0      +0.0      +0.0      +0.0      +2.5
                +1.05                                                     /Rod Containing Source: Co-60
  RPP    4    -229.0    -122.0    -229.0    +335.0     -40.0    +189.0      /Passage outside the door Wall
  RPP    5    -358.0    -335.0    -229.0    +572.0     -40.0    +189.0      /Leftmost Wall
  RPP    6    -122.0    +122.0    -229.0    -122.0     -40.0    +189.0      /Front Wall
  RPP    7    +122.0    +229.0    -229.0    +122.0     -40.0    +189.0      /Right towards the front Wall
  RPP    8     335.0    +374.0    +191.0    +572.0     -40.0    +189.0      /Right towards the back Wall
```

```
  RPP    9    -335.0     +335.0    +549.0    +572.0     -40.0    +189.0        /Backmost Wall
  RPP   10    -229.0     +229.0    +335.0    +442.0     -40.0    +189.0        /Back No1 wall
  RPP   11     -05.0     +229.0    +122.0    +229.0     -40.0    +189.0        /Back No2 thick wall
  RPP   12    +229.0     +335.0    +191.0    +229.0     -40.0    +189.0        /Back No2 thin wall
  RPP   13    -358.0     +229.0    -229.0    +191.0    +189.0    +280.0        /Roof "front" wall
  RPP   14    -358.0     +373.0    +191.0    +572.0    +189.0    +280.0        /Roof "back" wall
  END                                                                         /Termination of the body type
  Z01   20     +1     -2                                                      /Input zone and body numbers
  Z02   20     +2     -3     -4     -5     -6     -7     -8     -9           /Input zone and body numbers
               -10    -11    -12    -13    -14                              /Input zone and body numbers
  Z03   20     +3                                                           /Input zone and body number
  Z04   20     +4                                                           /Input zone and body number
  Z05   20     +5                                                           /Input zone and body number
  Z06   20     +6                                                           /Input zone and body number
  Z07   20     +7                                                           /Input zone and body number
  Z08   20     +8                                                           /Input zone and body number
  Z09   20     +9                                                           /Input zone and body number
  Z10   20    +10                                                           /Input zone and body number
  Z11   20    +11                                                           /Input zone and body number
  Z12   20    +12                                                           /Input zone and body number
  Z13   20    +13                                                           /Input zone and body number
  Z14   20    +14                                                           /Input zone  and body number
  END                                                                         /Termination of zones and body numbers
  1     2   3   4    5    6    7    8    9    10    11    12    13    14      /Region number for each zone
  0  1000   2   4    4    4    4    4    4     4     4     4     4     4      /material identification
99   1       6      7       8      11      12      13
   14      16     19      20      26      82                                 /Atomic numbers of all elements used in the problem
CONC ABS
00.013  00.000  00.000  01.165  00.040  00.010  00.108
00.740  00.003  00.045  00.196  00.030  00.000                              /1 Concrete Type NBS 04

00.000  00.000  00.000  00.000  00.000  00.000  00.000
00.000  00.000  00.000  00.000  08.000  00.000                              /2 Steel PIN

00.000  00.000 1.03E-3 2.58E-4  00.000  00.000  00.000
00.000  00.000  00.000  00.000  00.000  00.000                              /3 Air @ STD

00.0081 00.0000  00.0000  00.8644 00.0074  00.0244 00.0614
00.0695 00.0000  00.0000  00.1849 01.4049  00.0000                         /4 High Dens Concrete
```

```
   1.332     1.173                                                    /Two Energy Group: Co-60 Energies
   1.000     0.999                                                    /Yield"%" of The Energies
2.006E-8  1.816E-8                                                    /Gamma Flux-to-Dose Conversion Factor
   0.000     0.000                                                    /Gamma Flux-to-Heat Conversion Factor in Fe
=======================================================================
=======================================================================  /Dummy inserted symbol of no great importance
=======================================================================
+239.0   +60.0  +191.0       1   0  0  0                              /Detector Points or Evaluation Points
+239.0   +60.0  +185.0       1   0  0  0
+239.0   +60.0  +180.0       1   0  0  0
+239.0   +60.0  +175.0       1   0  0  0
+239.0   +60.0  +170.0       1   0  0  0
+239.0   +60.0  +165.0       1   0  0  0
+239.0   +60.0  +160.0       1   0  0  0
+239.0   +60.0  +155.0       1   0  0  0
+239.0   +60.0  +150.0       1   0  0  0
+239.0   +60.0  +145.0       1   0  0  0
+239.0   +60.0  +140.0       1   0  0  0
+239.0   +60.0  +135.0       1   0  0  0
+239.0   +60.0  +130.0       1   0  0  0
+239.0   +60.0  +125.0       1   0  0  0
+239.0   +60.0  +120.0       1   0  0  0
+239.0   +60.0  +115.0       1   0  0  0
+239.0   +60.0  +110.0       1   0  0  0
+239.0   +60.0  +105.0       1   0  0  0
+239.0   +60.0  +100.0       1   0  0  0
+239.0   +60.0  +095.0       1   0  0  0
+239.0   +60.0  +090.0       1   0  0  0
+239.0   +60.0  +085.0       1   0  0  0
+239.0   +60.0  +080.0       1   0  0  0
+239.0   +60.0  +075.0       1   0  0  0
+239.0   +60.0  +070.0       1   0  0  0
+239.0   +60.0  +065.0       1   0  0  0
+239.0   +60.0  +060.0       1   0  0  0
+239.0   +60.0  +055.0       1   0  0  0
+239.0   +60.0  +050.0       1   0  0  0
+239.0   +60.0  +045.0       1   0  0  0
+239.0   +60.0  +040.0       1   0  0  0
+239.0   +60.0  +035.0       1   0  0  0
```

```
+239.0   +60.0  +030.0       1   0  0  0
+239.0   +60.0  +025.0       1   0  0  0
+239.0   +60.0  +020.0       1   0  0  0
+239.0   +60.0  +015.0       1   0  0  0
+239.0   +60.0  +010.0       1   0  0  0
+239.0   +60.0  +005.0       1   0  0  0
+239.0   +60.0  +000.0       1   0  0  0
+239.0   +60.0  -005.0       1   0  0  0
+239.0   +60.0  -010.0       1   0  0  0
+239.0   +60.0  -015.0       1   0  0  0
+239.0   +60.0  -020.0       1   0  0  0
+239.0   +60.0  -025.0       1   0  0  0
+239.0   +60.0  -030.0       1   0  0  0
+239.0   +60.0  -035.0       1   0  0  0
+239.0   +60.0  -040.0       1   0  0  0
+239.0   +60.0  -045.0       1   0  0  0
+239.0   +60.0  -050.0       1   0  0  0
+239.0   +60.0  -055.0       1   0  0  0
+239.0   +60.0  -065.0       1   0  0  0
+239.0   +60.0  -075.0       1   0  0  0
+239.0   +60.0  -085.0       1   0  0  0
+239.0   +60.0  -100.0       1   0  0  0
+239.0   +60.0  -120.0       1   0  0  0
+239.0   +60.0  -130.0       1   0  0  0
+239.0   +60.0  -140.0       1   0  0  0
+239.0   +60.0  -150.0       1   0  0  0
+239.0   +60.0  -160.0       1   0  0  0
+239.0   +60.0  -170.0       1   0  0  0
+239.0   +60.0  -190.0       1   0  0  0
+239.0   +60.0  -210.0       1   0  0  0
+239.0   +60.0  -220.0       1   0  0  0
+239.0   +60.0  -230.0       1   0  0  0
+239.0   +60.0  -240.0       1   0  0  0

     0.0       0.0      0.0      -1   0  0  0                                  /Termination Card
```

D.2 MCNPX input data set for verification: the actual concrete shield geometry of the Stellenbosch facility

```
STELLENBOSCH INSECT IRRADIATOR (RPP Geometric bodies)
c Cell Cards
01  0           +99                                                    imp:p=0  $ External World
02  1  -1.29e-3  -99 #3  #4  #5  #6  #7 #8 #9 #10 #11 #12 #13 #14 #15 imp:p=1  $ AirBox at STP; Internal Void
03  3  -8.0       -3                                                   imp:p=1  $ Stainless Steel Rod with source
04  4  -2.625     -4                                                   imp:p=1  $ Passage outside the door Wall
05  4  -2.625     -5                                                   imp:p=1  $ Leftmost Wall
06  4  -2.625     -6                                                   imp:p=1  $ Front Wall
07  4  -2.625     -7                                                   imp:p=1  $ Right towards the front Wall
08  4  -2.625     -8                                                   imp:p=1  $ Right towards the back Wall
09  4  -2.625     -9                                                   imp:p=1  $ Backmost Wall
10  4  -2.625     -10                                                  imp:p=1  $ Back No1 wall
11  4  -2.625     -11                                                  imp:p=1  $ Back No2 thick wall
12  4  -2.625     -12                                                  imp:p=1  $ Back No2 thin wall
13  4  -2.625     -13                                                  imp:p=1  $ Roof "front" wall
14  4  -2.625     -14                                                  imp:p=1  $ Roof "back" wall
15  4  -2.625     -15                                                  imp:p=1  $ Floor Slab

c Surface Cards
03  RCC    +0.0    +0.0    +0.0    +0.0     +0.0   +2.50  +1.05              $ Rod Containing Source
04  RPP  -229.0  -122.0  -229.0  +335.0    -40.0  +189.0                    $ Passage outside the door Wall
05  RPP  -358.0  -335.0  -229.0  +572.0    -40.0  +189.0                    $ Leftmost Wall
06  RPP  -122.0  +122.0  -229.0  -122.0    -40.0  +189.0                    $ Front Wall
07  RPP  +122.0  +229.0  -229.0  +122.0    -40.0  +189.0                    $ Left towards the front Wall
08  RPP  +335.0  +374.0  +191.0  +572.0    -40.0  +189.0                    $ Left towards the back Wall
09  RPP  -335.0  +335.0  +549.0  +572.0    -40.0  +189.0                    $ Backmost Wall
10  RPP  -229.0  +229.0  +335.0  +442.0    -40.0  +189.0                    $ Back No1 wall
11  RPP   -05.0  +229.0  +122.0  +229.0    -40.0  +189.0                    $ Back No2 thick wall
12  RPP  +229.0  +335.0  +191.0  +229.0    -40.0  +189.0                    $ Back No2 thin wall
13  RPP  -358.0  +229.0  -229.0  +191.0   +189.0  +280.0                    $ Roof "front" wall
14  RPP  -358.0  +373.0  +191.0  +572.0   +189.0  +280.0                    $ Roof "back" wall
15  RPP  -500.0  +500.0  -600.0  +600.0   -350.0   -40.0                     $ Floor Slab
```

```
99  RPP -2000.0 +2000.0 -2000.0 +2000.0   -400.0 +4000.0                    $ AirBox

c Data Cards
c Mode: transport photons
mode p
c source definition:
c ******************************
c source definition: CYLINDRICAL VOLUME ALONG Z-AXIS
sdef par=p  erg=d3                          &
     pos=0 0 0                              &
     axs=0 0 1  ext=d1  rad=d2              &
     cel=03
si1   0.0   2.5                                          $ Sampling of source point along Axial coordinate:
sp1  -21    1                                            $ Probability of sampling of source point in axial dimension
```

This part of the input data set is the cell parameters bounded by they respectively surfaces which defines the thicknesses of the concrete material and their location with respect to the position of the Cobalt-60 source. The density of the concrete is 2.625 g.cm^{-3}. The source is confined in an RCC with the axial along the **D** coordinate of 2.5 cm.

```
si2   0.0   1.05        $ Sampling of source point along radial coordinate
sp2  -21    1           $ Probability of sampling of source point in radial dimension
```

The sampling of the source along the radial **<** coordinates and the respectively probability of distribution.

```
si3 L  1.173  1.332   $ Energies of gamma-photons emittted by radionuclide Co-60
sp3    0.999  1.000   $ Emission abundances
c
c Material definitions
m1      7014  -0.79   8016  -0.21                                        $ Air at STP
c m2    1001  -0.013  8016  -1.165  11023  -0.040  12000  -0.010    &    $ Ordinary Concrete
       13027  -0.108 14000  -0.740  16000  -0.003  19000  -0.045    &    $ Ordinary Concrete
       20000  -0.196 26000  -0.030                                       $ Ordinary Concrete
m3      6000  -0.03   14000 -0.60   15000  -0.02   16000  -0.03     &    $ SS-316L
       24000 -17.50   25000 -1.70   26000 -64.52   28000 -13.00     &    $ SS-316L
       42000  -2.60                                                     $ SS-316L
m4     1001   -0.0081  8016  -0.8644 11023 -0.0074  12000 -0.0244   &
      13027   -0.0614  14000 -0.0695 20000 -0.1849  26000 -1.4049        $ High Dens Concrete
c ==============================
```

```
c  Energy (MeV) and fluence-rate to dose-rate conversion factors: photons
c  Units: Convert fluence-rate to Sv/hr
#        de        df
       0.010    2.22E-10
       ......   .......
       1000.0   7.70e-7
       10000.0  1.05e-6
c ==== PRINT CONTROLS =====
PRINT 10 40 30 50 60 72 100 110 120 170 200
c
tmesh
 rmesh1:p dose 31 3 2 1.1951e+14
  cora1  -400.0  198i  +400.0
  corb1  -300.0  298i  +600.0
  corc1   -30.0         +40.0
endmd
```

This part define source information, i.e., the two energy group of the Cobalt-60 source and the corresponding emission abundances. The materials used in the input data set, energy and fluence-rate to dose-rate conversion factors, the tables specified by the user which are printed as an output file, and the mesh tally.

```
c === RUNTIME CONTROLS ======
ctme 3500
```

D.3 MCNPX input data set: spherical approximation

```
STELLENBOSCH IRRADIATOR VAULT of DENSITY 2.625 g/cc (Spherical Case)
c Cell Cards
01  01  -1.29e-3   -1            $ Main Chamber Air Layer1
02  01  -1.29e-3   -2   +1       $ Main Chamber Air Layer2
03  01  -1.29e-3   -3   +2       $ Main Chamber Air Layer3
04  01  -1.29e-3   -4   +3       $ Main Chamber Air Layer4
05  01  -1.29e-3   -5   +4       $ Main Chamber Air Layer5
06  01  -1.29e-3   -6   +5       $ Main Chamber Air Layer6
07  01  -1.29e-3   -7   +6       $ Main Chamber Air Layer7
08  01  -1.29e-3   -8   +7       $ Main Chamber Air Layer8
09  01  -1.29e-3   -9   +8       $ Main Chamber Air Layer9
10  01  -1.29e-3   -10  +9       $ Main Chamber Air Layer10
11  01  -1.29e-3   -11  +10      $ Main Chamber Air Layer11
12  01  -1.29e-3   -12  +11      $ Main Chamber Air Layer12
13  01  -1.29e-3   -13  +12      $ Main Chamber Air Layer13
14  04  -2.625     -14  +13      $ Concrete L1
15  04  -2.625     -15  +14      $ Concrete L2
16  04  -2.625     -16  +15      $ Concrete L3
17  04  -2.625     -17  +16      $ Concrete L4
18  04  -2.625     -18  +17      $ Concrete L5
19  04  -2.625     -19  +18      $ Concrete L6
20  04  -2.625     -20  +19      $ Concrete L7
21  04  -2.625     -21  +20      $ Concrete L8
22  04  -2.625     -22  +21      $ Concrete L9
23  04  -2.625     -23  +22      $ Concrete L10
24  04  -2.625     -24  +23      $ Concrete L11
25  01  -1.29e-3   -25  +24      $ Surrounding Air Shell1
26  01  -1.29e-3   -26  +25      $ Surrounding Air Shell2
27  01  -1.29e-3   -27  +26      $ Surrounding Air Shell3
28  01  -1.29e-3   -28  +27      $ Surrounding Air Shell4
29  01  -1.29e-3   -29  +28      $ Surrounding Air Shell5
30  01  -1.29e-3   -30  +29      $ Surrounding Air Shell6
31  01  -1.29e-3   -31  +30      $ Surrounding Air Shell7
```

```
36  01  -1.29e-3   -36  +35       $ Surrounding Air Shell12
37  00                   +36       $ UmWelt
```

The first line is the Title of the problem. Defined as well are cells using a spherical geometric bodies (SPH). Cell 1 to 13 is the main chamber air indicated as material 1. The concrete begins at cell 14 which extends till cell 24, and then the air at the outwards surface.

```
c Surface Cards
01  SPH   0.0   0.0   0.0  +010.0              $ INNER AIR SHELL BOUND
02  SPH   0.0   0.0   0.0  +020.0              $ INNER AIR SHELL BOUND
03  SPH   0.0   0.0   0.0  +030.0              $ INNER AIR SHELL BOUND
04  SPH   0.0   0.0   0.0  +040.0              $ INNER AIR SHELL BOUND
05  SPH   0.0   0.0   0.0  +050.0              $ INNER AIR SHELL BOUND
06  SPH   0.0   0.0   0.0  +060.0              $ INNER AIR SHELL BOUND
07  SPH   0.0   0.0   0.0  +070.0              $ INNER AIR SHELL BOUND
08  SPH   0.0   0.0   0.0  +080.0              $ INNER AIR SHELL BOUND
09  SPH   0.0   0.0   0.0  +090.0              $ INNER AIR SHELL BOUND
10  SPH   0.0   0.0   0.0  +100.0              $ INNER AIR SHELL BOUND
11  SPH   0.0   0.0   0.0  +110.0              $ INNER AIR SHELL BOUND
12  SPH   0.0   0.0   0.0  +120.0              $ INNER AIR SHELL BOUND
13  SPH   0.0   0.0   0.0  +122.0              $ INNER AIR SHELL BOUND
14  SPH   0.0   0.0   0.0  +130.0              $ CRT LAYER 01 M_C
15  SPH   0.0   0.0   0.0  +140.0              $ CRT LAYER 02 M_C
16  SPH   0.0   0.0   0.0  +150.0              $ CRT LAYER 03 M_C
17  SPH   0.0   0.0   0.0  +160.0              $ CRT LAYER 04 M_C
18  SPH   0.0   0.0   0.0  +170.0              $ CRT LAYER 05 M_C
19  SPH   0.0   0.0   0.0  +180.0              $ CRT LAYER 06 M_C
20  SPH   0.0   0.0   0.0  +190.0              $ CRT LAYER 07 M_C
21  SPH   0.0   0.0   0.0  +200.0              $ CRT LAYER 08 M_C
22  SPH   0.0   0.0   0.0  +210.0              $ CRT LAYER 09 M_C
23  SPH   0.0   0.0   0.0  +220.0              $ CRT LAYER 10 M_C
24  SPH   0.0   0.0   0.0  +229.0              $ CRT LAYER 11 M_C
25  SPH   0.0   0.0   0.0  +239.0              $ Surrounding Air Shell1
26  SPH   0.0   0.0   0.0  +249.0              $ Surrounding Air Shell2
27  SPH   0.0   0.0   0.0  +259.0              $ Surrounding Air Shell3
28  SPH   0.0   0.0   0.0  +269.0              $ Surrounding Air Shell4
29  SPH   0.0   0.0   0.0  +279.0              $ Surrounding Air Shell5
30  SPH   0.0   0.0   0.0  +289.0              $ Surrounding Air Shell6
```

```
31  SPH   0.0   0.0   0.0  +299.0                    $ Surrounding Air Shell7
36  SPH   0.0   0.0   0.0  +400.0                    $ Start of Grveyard
```

Defined in this part are surfaces bounding the corresponding cells described in the cell card. The surfaces are spheres of the various radius serves as the thicknesses of the materials referred to in the material card. Surface 1 to 13 confines the main air in the irradiation room. The concrete material extends from surface 13 to 24.

```
c Data Cards
c Mode: transport photons
mode p
c source importance
imp:p 1 1 10r 2m 2m 2m 2m 2m 2m 2m 2m 2m 2m 2m 2m 7r 0
c source definition:
c ******************************
c source definition:
sdef par=p erg=d3 pos=0 0 0
si3 L  1.173  1.332
sp3    0.999  1.000
```

This is the data card section. Defined in the card is the mode of transport which is photon (mode p) and the source information as previously explained. Importance can either be defined in the cell card section (see previous input data set) or in the data card section. It incorporated the repeating and multiplication of the immediately preceding photon importance value for facilitating input card preparation.

```
c Material definitions
m1      7014  -0.79    8016  -0.21                                          $ Air at STP
c m2    1001  -0.013   8016  -1.165  11023  -0.040  12000  -0.010    &      $ Ordinary Concrete
       13027  -0.108  14000  -0.740  16000  -0.003  19000  -0.045    &      $ Ordinary Concrete
       20000  -0.196  26000  -0.030                                          $ Ordinary Concrete
m4     1001   -0.0081  8016  -0.8644 11023  -0.0074  12000 -0.0244   &
      13027   -0.0614  14000 -0.0695  20000 -0.1849  26000 -1.4049          $ High Dens concrete
c
c **** Tally *******
fc12 TALLY-BOX_SURFACE ESTIMATORS; Photon dose-rate in Sv/hr.
f12:p 1 2 3 4 5 6 7 8 9 10 11 12 13 14 15 16 17 18 19 20 21 22 23 24 25 26 27   &
28 29 30 31 32 33 34 35
fm12 1.1951E+14                                          $ Transition rate in 3.23 kCi source; unit: Bq
```

The materials, m1, m2, m4 and the F2 type tallies used in the problem are defined.

```
c ==============================
c  Energy (MeV) and fluence-rate to dose-rate conversion factors: photons
c  Units: Convert fluence-rate to Sv/hr
#         de         df
        0.010    2.22E-10
        ......   .......
        1000.0   7.70e-7
        10000.0  1.05e-6
c ==== PRINT CONTROLS =====
PRINT 10 40 30 50 60 72 100 110 120 170 200
c === RUNTIME CONTROLS ======
ctme 120
```

D.4 MCNPX input data set for the labyrinth case (actual geometry)

```
STELLENBOSCH INSECT IRRADIATOR (Labyrinth Case)
c Cell Cards
01  0            +99                                                    imp:p=0  $ External World
02  1  -1.29e-3  -99 #3  #4  #5  #6  #7 #8 #9 #10 #11 #12 #13 #14 #15 &
                     #22 #23 #24  #25 #26 #27 #28 #29 #30 #31           imp:p=1  $  Internal Void
```

The above portion of the input file entails the Title Card containing information describing the problem *("STELLENBOSCH INSECT IRRADIATOR—RPP Geometric Bodies, particular for evaluating dose rates along the labyrinth ").* Following the Title Card is the Comment Card stating that all parameters to follow are within the cell card section. Cell 1 is void *"the external world"* with the importance (imp) of zero indicating that no particles (photons) are being talied. Cell 2 contains material 1 which is air of the density 1.29E-3 g.cm$^{\bullet 3}$. Cell 2 consists of the volume inside surface 99, but outside the rest of the surfaces. The importance (imp) of photons inside cell 2, is 1.

```
03  3  -8.0        -3                          imp:p=1  $ Stainless Steel Rod with source
04  4  -2.625      -4                          imp:p=1  $ Passage outside the door Wall
05  4  -2.625      -5                          imp:p=1  $ Leftmost Wall
06  4  -2.625      -6                          imp:p=1  $ Front Wall
07  4  -2.625      -7                          imp:p=1  $ Right towards the front Wall
08  4  -2.625      -8                          imp:p=1  $ Right towards the back Wall
09  4  -2.625      -9                          imp:p=1  $ Backmost Wall
10  4  -2.625     -10                          imp:p=1  $ Back No1 wall
11  4  -2.625     -11                          imp:p=1  $ Back No2 thick wall
12  4  -2.625     -12                          imp:p=1  $ Back No2 thin wall
13  4  -2.625     -13                          imp:p=1  $ Roof "front" wall
14  4  -2.625     -14                          imp:p=1  $ Roof "back" wall
15  4  -2.625     -15                          imp:p=1  $ Floor Slab
22  1  -1.29e-3   -22                          imp:p=1  $ F4TallyBox in Labyrinth
23  1  -1.29e-3   -23                          imp:p=1  $ F4TallyBox in Labyrinth
24  1  -1.29e-3   -24                          imp:p=1  $ F4TallyBox in Labyrinth
25  1  -1.29e-3   -25                          imp:p=1  $ F4TallyBox in Labyrinth
26  1  -1.29e-3   -26                          imp:p=1  $ F4TallyBox in Labyrinth
27  1  -1.29e-3   -27                          imp:p=1  $ F4TallyBox in Labyrinth
28  1  -1.29e-3   -28                          imp:p=1  $ F4TallyBox in Labyrinth
```

```
29  1  -1.29e-3   -29                                  imp:p=1  $ F4TallyBox in Labyrinth
30  1  -1.29e-3   -30                                  imp:p=1  $ F4TallyBox in Labyrinth
31  1  -1.29e-3   -31                                  imp:p=1  $ F4TallyBox (RPP7)right opposite the source
```

These are cells with the corresponding materials number, densities, surfaces bounding them and the photon importance.

```
c Surface Cards
03  RCC    +0.0    +0.0    +0.0    +0.0     +0.0   +2.50  +1.05 $ Rod Containing Source
04  RPP  -229.0  -122.0  -229.0  +335.0    -40.0  +189.0        $ Passage outside the door Wall
05  RPP  -358.0  -335.0  -229.0  +572.0    -40.0  +189.0        $ Leftmost Wall
06  RPP  -122.0  +122.0  -229.0  -122.0    -40.0  +189.0        $ Front Wall
07  RPP  +122.0  +229.0  -229.0  +122.0    -40.0  +189.0        $ Left towards the front Wall
08  RPP  +335.0  +374.0  +191.0  +572.0    -40.0  +189.0        $ Left towards the back Wall
09  RPP  -335.0  +335.0  +549.0  +572.0    -40.0  +189.0        $ Backmost Wall
10  RPP  -229.0  +229.0  +335.0  +442.0    -40.0  +189.0        $ Back No1 wall
11  RPP   -05.0  +229.0  +122.0  +229.0    -40.0  +189.0        $ Back No2 thick wall
12  RPP  +229.0  +335.0  +191.0  +229.0    -40.0  +189.0        $ Back No2 thin wall
13  RPP  -358.0  +229.0  -229.0  +191.0   +189.0  +280.0        $ Roof "front" wall
14  RPP  -358.0  +373.0  +191.0  +572.0   +189.0  +280.0        $ Roof "back" wall
15  RPP  -500.0  +500.0  -600.0  +600.0   -350.0   -40.0        $ Floor Slab
22  RPP  -335.0  -229.0  +422.0  +522.0    -40.0  +189.0        $ F4TallyBox-Labyrinth
23  RPP  -179.0   -79.0  +442.0  +549.0    -40.0  +189.0        $ F4TallyBox-Labyrinth
24  RPP   -29.0   +71.0  +442.0  +549.0    -40.0  +189.0        $ F4TallyBox-Labyrinth
25  RPP  +121.0  +221.0  +442.0  +549.0    -40.0  +189.0        $ F4TallyBox-Labyrinth
26  RPP  +271.0  +331.0  +442.0  +549.0    -40.0  +189.0        $ F4TallyBox-Labyrinth
27  RPP  +229.0  +335.0  +292.0  +392.0    -40.0  +189.0        $ F4TallyBox-Labyrinth
28  RPP   +79.0  +179.0  +229.0  +335.0    -40.0  +189.0        $ F4TallyBox-Labyrinth
29  RPP   -71.0   +29.0  +229.0  +335.0    -40.0  +189.0        $ F4TallyBox-Labyrinth
30  RPP  -122.0   -05.0   +79.0  +179.0    -40.0  +189.0        $ F4TallyBox-Labyrinth
31  RPP  +229.0  +259.0   -30.0   +30.0    -40.0  +189.0        $ F4TallyBox-Labyrinth
99  RPP -2000.0 +2000.0 -2000.0 +2000.0   -400.0 +4000.0        $ AirBox
```

Surfaces bounding the cells defined in the cell card section with the correspondence concrete material thicknesses and their location with respect to the cobalt-60 source. These parameters (material thicknesses) are defined by the user.

```
c Data Cards
```

```
c Mode: transport photons
mode p
c source definition:
c ****************************
c source definition: CYLINDRICAL VOLUME ALONG Z-AXIS
sdef par=p  erg=d3                          &
     pos=0 0 0                              &
     axs=0 0 1  ext=d1  rad=d2              &
     cel=03
```

Defined in this data card is the source and the mode of transport to be photon.

```
si1   0.0   2.5         $ Sampling of source point along Axial coordinate
sp1  -21    1           $ Probability of sampling of source point in axial dimension: power
```

Source information and probability of distribution. This for along the axial **D** axis.

```
si2   0.0   1.05        $ Sampling of source point along radial coordinate done
sp2  -21    1           $ Probability of sampling of source point in radial dimension
Explanation:
```

Source information and probability of distribution. This for along the radial **<** coordinate.

```
si3 L  1.173  1.332   $ Energies of gamma-photons emittted by radionuclide Co-60
sp3    0.999  1.000   $ Emission abundances
c
c Material definitions
m1      7014  -0.79   8016  -0.21                                          $ Air at STP
c m2    1001  -0.013  8016  -1.165  11023  -0.040  12000  -0.010    &      $ Ordinary Concrete
       13027  -0.108 14000  -0.740  16000  -0.003  19000  -0.045    &      $ Ordinary Concrete
       20000  -0.196 26000  -0.030                                         $ Ordinary Concrete
m3      6000  -0.03   14000 -0.60   15000  -0.02   16000  -0.03     &      $ SS-316L
       24000  -17.50  25000 -1.70   26000  -64.52   28000 -13.00    &      $ SS-316L
       42000  -2.60                                                       $ SS-316L
m4     1001   -0.0081  8016  -0.8644 11023  -0.0074  12000 -0.0244  &
       13027  -0.0614  14000 -0.0695  20000 -0.1849  26000 -1.4049          $  High Dens concrete
c
c **** Tally *******
```

```
fc14 TALLY-BOX IN LABYRINTH; Photon dose-rate in Sv/hr.
f14:p 22 23 24 25 26 27 28 29 30 31
fm14 1.1951e+14                          $ Transition rate in 3.23 kCi source; unit: Bq
```

This part defines the energies of the gamma-photons emitted by the radionuclide cobalt-60 and the corresponding abundances. The materials and as well the type F4 tallies used are defined.

```
c ==============================
c  Energy (MeV) and fluence-rate to dose-rate conversion factors: photons
c  Units: Convert fluence-rate to Sv/hr
#        de        df
       0.010    2.22E-10
       ......   .......
       10000.0  1.05e-6
c ==== PRINT CONTROLS =====
PRINT 10 40 30 50 60 72 100 110 120 170 200
c
c === RUNTIME CONTROLS ======
ctme 3500
```

Appendix E:
QAD-CGGP and MCNPX sample input files for the HEPRO irradiation facility

E.1 QAD-CGGP sample input data set

```
HEPRO VAULT MODEL Reinf CONC dens=2.35g/cc "WALL"
100 100 100  13  3  1  2  0  0  3  1  0  0  0  0  0
```

The first line is the problem title given as (*HEPRO VAULT MODEL REINF CONC dens= 2.35 g/cc"WALL").* The hundreds are number of division increments along the axis of a right circular cylinder (RCC) which specify the division of source volume. Thirteen is the number of elements used in this problem. Three is the number of material composition. One is just dummy positive number. Two is the number of gamma-ray energy groups of the cobalt-60 source, i.e., μ_1 = 1.173 MeV and μ_2 = 1.332 MeV. The first zero is for indication that the translation of the source is not employed and the second is for the geometry of the source, i.e., the right circular cylinder (RCC). Three is for indicating the most probable source region, i.e., in the geometry section the cobalt-60 source is contained in the RCC which is body number three, referred to as region three. One is for indication that the cosine-distributed source is used. The rest of the zeros are for indication that the photons calculation will be made, no effect for the first and second source point for which ray geometry printout is desired, no effect for the incremental steps size used to select additional points for ray geometry printout; and the last zero is for indicating that the will be no effect on number of additional calculational calculations to be made.

```
7.4E+16  0.0  0.0  0.0  0.0  0.0  0.0
```

7.4E+16 is the total source strength in decays per second of the cobalt-60. The rest of the zeros are for the constant for cosine source distribution function of a cylinder coordinates.

```
0.000E+00   3.750E-01   7.500E-01   1.125E+00   1.500E+00   1.875E+00
2.250E+00   2.625E+00   3.000E+00   3.375E+00   3.750E+00   4.125E+00
4.500E+00   4.875E+00   5.250E+00   5.625E+00   6.000E+00   6.375E+00
6.750E+00   7.125E+00   7.500E+00   7.875E+00   8.250E+00   8.625E+00
9.000E+00   9.375E+00   9.750E+00   1.012E+01   1.050E+01   1.088E+01
1.125E+01   1.162E+01   1.200E+01   1.238E+01   1.275E+01   1.312E+01
1.350E+01   1.388E+01   1.425E+01   1.462E+01   1.500E+01   1.538E+01
1.575E+01   1.612E+01   1.650E+01   1.688E+01   1.725E+01   1.762E+01
1.800E+01   1.838E+01   1.875E+01   1.912E+01   1.950E+01   1.988E+01
2.025E+01   2.062E+01   2.100E+01   2.138E+01   2.175E+01   2.212E+01
2.250E+01   2.288E+01   2.325E+01   2.362E+01   2.400E+01   2.438E+01
2.475E+01   2.512E+01   2.550E+01   2.588E+01   2.625E+01   2.662E+01
2.700E+01   2.738E+01   2.775E+01   2.812E+01   2.850E+01   2.888E+01
2.925E+01   2.962E+01   3.000E+01   3.038E+01   3.075E+01   3.112E+01
3.150E+01   3.188E+01   3.225E+01   3.262E+01   3.300E+01   3.338E+01
3.375E+01   3.412E+01   3.450E+01   3.488E+01   3.525E+01   3.562E+01
3.600E+01   3.638E+01   3.675E+01   3.712E+01   3.750E+01
```

This indicate the coordinate of the source volume divisions along the radial axis.

```
0.000E+00   1.500E+00   3.000E+00   4.500E+00   6.000E+00   7.500E+00
9.000E+00   1.050E+01   1.200E+01   1.350E+01   1.500E+01   1.650E+01
1.800E+01   1.950E+01   2.100E+01   2.250E+01   2.400E+01   2.550E+01
2.700E+01   2.850E+01   3.000E+01   3.150E+01   3.300E+01   3.450E+01
3.600E+01   3.750E+01   3.900E+01   4.050E+01   4.200E+01   4.350E+01
4.500E+01   4.650E+01   4.800E+01   4.950E+01   5.100E+01   5.250E+01
5.400E+01   5.550E+01   5.700E+01   5.850E+01   6.000E+01   6.150E+01
6.300E+01   6.450E+01   6.600E+01   6.750E+01   6.900E+01   7.050E+01
7.200E+01   7.350E+01   7.500E+01   7.650E+01   7.800E+01   7.950E+01
8.100E+01   8.250E+01   8.400E+01   8.550E+01   8.700E+01   8.850E+01
9.000E+01   9.150E+01   9.300E+01   9.450E+01   9.600E+01   9.750E+01
9.900E+01   1.005E+02   1.020E+02   1.035E+02   1.050E+02   1.065E+02
1.080E+02   1.095E+02   1.110E+02   1.125E+02   1.140E+02   1.155E+02
1.170E+02   1.185E+02   1.200E+02   1.215E+02   1.230E+02   1.245E+02
1.260E+02   1.275E+02   1.290E+02   1.305E+02   1.320E+02   1.335E+02
1.350E+02   1.365E+02   1.380E+02   1.395E+02   1.410E+02   1.425E+02
1.440E+02   1.455E+02   1.470E+02   1.485E+02   1.500E+02
```

This is for coordinate of the source volume divisions along the axial **D** axis.

```
 0.000E+00   6.283E-02   1.257E-01   1.885E-01   2.513E-01   3.142E-01
 3.770E-01   4.398E-01   5.027E-01   5.655E-01   6.283E-01   6.912E-01
 7.540E-01   8.168E-01   8.796E-01   9.425E-01   1.005E+00   1.068E+00
 1.131E+00   1.194E+00   1.257E+00   1.319E+00   1.382E+00   1.445E+00
 1.508E+00   1.571E+00   1.634E+00   1.696E+00   1.759E+00   1.822E+00
 1.885E+00   1.948E+00   2.011E+00   2.073E+00   2.136E+00   2.199E+00
 2.262E+00   2.325E+00   2.388E+00   2.450E+00   2.513E+00   2.576E+00
 2.639E+00   2.702E+00   2.765E+00   2.827E+00   2.890E+00   2.953E+00
 3.016E+00   3.079E+00   3.142E+00   3.204E+00   3.267E+00   3.330E+00
 3.393E+00   3.456E+00   3.519E+00   3.581E+00   3.644E+00   3.707E+00
 3.770E+00   3.833E+00   3.896E+00   3.958E+00   4.021E+00   4.084E+00
 4.147E+00   4.210E+00   4.273E+00   4.335E+00   4.398E+00   4.461E+00
 4.524E+00   4.587E+00   4.650E+00   4.712E+00   4.775E+00   4.838E+00
 4.901E+00   4.964E+00   5.027E+00   5.089E+00   5.152E+00   5.215E+00
 5.278E+00   5.341E+00   5.404E+00   5.466E+00   5.529E+00   5.592E+00
 5.655E+00   5.718E+00   5.781E+00   5.843E+00   5.906E+00   5.969E+00
 6.032E+00   6.095E+00   6.158E+00   6.220E+00   6.283E+00
```

This is for coordinate of the source volume divisions along the angular **9** axis. The above input data set are free format.

```
     0    0          HEPRO MODEL                                          /No Gap before this line!
RPP    1  -99999.0  +99999.0  -99999.0  +99999.0  -99999.0  +99999.0      /ExVoid
RPP    2  -99990.0  +99990.0  -99990.0  +99990.0  -99990.0  +99990.0      /InVoid
RCC    3     +0.0     +0.0      +0.0      +0.0      +0.0    +150.0
           +37.5                                                          /Source
RPP    4    -449.5    -274.5    -468.0    +493.0       0.0    +312.0      /LHS Wall
RPP    5    -274.5    +224.5    +293.0    +493.0       0.0    +312.0      /BACK Wall
RPP    6    +224.5    +399.5    -468.0    +493.0       0.0    +312.0      /RHS Wall
RPP    7    -274.5    +224.5    -468.0    -293.0       0.0    +312.0      /FRONT Wall
RPP    8    -449.5    +399.5    -468.0    +493.0    +312.0    +487.0      /Roof
RPP    9    -274.5    +224.5    -293.0    +293.0    -610.0      +0.0      /Floor
END
```

This section is a combinatorial geometry which is a fixed format. The first line is the title of the geometry. Body 3 is the stainless steel region containing the source. Defined as well is the geometric body type, body number assigned by the user and real data as thicknesses of the materials used to shield the cobalt-60 source.

```
 Z01   20     +1     -2
 Z02   20     +2     -3     -4     -5     -6     -7     -8     -9
 Z03   20     +3
 Z04   20     +4
 Z05   20     +5
 Z06   20     +6
 Z07   20     +7
 Z08   20     +8
 Z09   20     +9
 END
```

This part specify the alphanumeric name assigned to input zone by the user and the body number with the sign € or • as required for the zone description. *Note:* € œ *AND;* • œ *NOT.*

```
 1     2   3   4    5    6    7    8    9
```

These are regions number of each zone.

```
 0  1000   3   1    1    1    1    1    1
```

The zero and a thousand is for external and internal void *"OUTSIDE WORLD—GRAVEYARD"*; the rest are medium (material) numbers in which the *ith* input zone is contained.

```
99   1       6       7       8      11      12      13
    14      16      19      20      26      82
```

This is identification of buildup factors and elements.

```
CONC ABS
```

This is an indication that a buildup factor for concrete is used.

```
00.013  00.000  00.000  01.165  00.040  00.010  00.108
00.740  00.003  00.045  00.196  00.030  00.000                          /1 Concrete Type NBS 04
```

Partial density in g/cm$ of the concrete material used for shielding the cobalt-60 source. Partial density in g/cm$ of elements in corresponding order as listed above, i.e., one card for each material composition, with cards in the order of composition numbers.

```
00.000  00.000  00.000  00.000  00.000  00.000  00.000
00.000  00.000  00.000  00.000  08.000  00.000                          /2 Steel PIN
```

Partial density in g/cm$ of the stainless steel rod material containing the cobalt-60 source

```
00.000  00.000 1.03E-3 2.58E-4  00.000  00.000  00.000
00.000  00.000  00.000  00.000  00.000  00.000                          /3 Air @ STD
```

Partial density in g/cm$ of the air medium inside the irradiation room.

```
   1.332     1.173
   1.000     0.999
2.006E-8  1.816E-8
   0.000     0.000
```

Defined is source energy: Mean gamma energy for each group (MeV) of the Cobalt-60 source. The gamma-ray of cobalt-60 source spectrum, i.e., the corresponding abundance for each energy listed above. Response function: This is the respectively gamma flux-to-dose conversion factor for each gamma-ray energy group listed above. This is the respectively gamma flux-to-heat conversion factor in Fe for each gamma-ray group.

```
============================================================
============================================================
-459.5   +100.0   -460.0      1   0  0  0
-459.5   +100.0   +380.0      1   0  0  0
-459.5   +100.0   +400.0      1   0  0  0
-459.5   +100.0   +420.0      1   0  0  0
-459.5   +100.0   +440.0      1   0  0  0
-459.5   +100.0   +460.0      1   0  0  0
```

```
-459.5   +100.0   +480.0      1   0  0  0
-459.5   +100.0   +500.0      1   0  0  0
```

These are detectors coordinates. These detectors are placed with respect to the shielding wall and the position of the cobalt-6o source inside the irradiation room.

```
  0.0      0.0      0.0     -1   0  0  0
```

This part is for terminating the execution of the program, i.e., the detectors cards are read until a negative one (• **"**) is encountered.

E.2 MCNPX sample input data set

```
HEPRO IRRADIATOR (RPP geometric Bodies)
c Cell Cards
01  0           +99                                 imp:p=0  $ External World
02  1  -1.29e-3  -99 #3 #4  #5  #6  #7 #10 #12  imp:p=1  $ AirBox at STP; Internal Void
03  1  -1.29e-3   -3                                imp:p=1  $ Source
04  2  -2.35      -4                                imp:p=1  $ LHS Wall
05  2  -2.35      -5                                imp:p=1  $ Back Wall
06  2  -2.35      -6                                imp:p=1  $ RHS Wall
07  2  -2.35      -7                                imp:p=1  $ Front Wall
10  2  -2.35     -10                                imp:p=1  $ Thick Roof Slab
12  2  -2.35     -12                                imp:p=1  $ Floor Slab
```

The above portion of the input file entails the Title Card containing information describing the problem *("HEPRO IRRADIATOR—RPP Geometric Bodies").* Following the Title Card is the Comment Card stating that all parameters to follow are within the cell card. Cell 1 is void *"the external world"* with the importance (imp) of zero indicating that no particles (photons) are being tallied. Cell 2 AND 3 contains material 1 with density 1.29E-3 g.cm$^{\bullet 3}$. Cell 2 consists of the volume inside surface 99, but outside the rest of the surfaces. The importance (imp) of photons (p) inside cell 2, is 1.

Cell 4 to 12 contains material number 2, which has a density of 2.35 g.cm$^{\bullet 3}$. The importance (imp) of photons (p) inside cell 4 to 12, are 1. The $ sign signifies the beginning of an in-line comment.

```
c Surface Cards
03  RCC     0.0     0.0     0.0     0.0     0.0  +150.0  37.5 $ Source
04  RPP  -449.0  -274.0  -293.0  +293.0   -01.0  +312.0       $ LHS wall RPP4
05  RPP  -449.0  +399.0  +293.0  +493.0   -01.0  +312.0       $ Back Wall RPP5
06  RPP  +224.0  +399.0  -293.0  +293.0   -01.0  +312.0       $ RHS Wall RPP6
07  RPP  -449.0  +399.0  -468.0  -293.0   -01.0  +312.0       $ Front wall RPP7
10  RPP  -449.0  +399.0  -468.0  +493.0  +312.0  +487.0       $ Roof CRT Slab
12  RPP  -449.0  +399.0  -468.0  +493.0  -610.0   -01.0       $ Floor Slab
99  RPP -9000.0 +9000.0 -9000.0 +9000.0  -800.0 +5000.0       $ AirBox
```

These are the surfaces confining the cells defined in the cell card section with the user defined thicknesses.

```
c Data Cards
c Mode: transport photons
mode p
c ******************************
c source definition: CYLINDRICAL VOLUME ALONG Z-AXIS
sdef par=p  erg=d3                          &
     pos=0 0 0                              &
     axs=0 0 1 ext=d1  rad=d2               &
     cel=03
```

Mode of transport and the source definition located at the origin.

```
si1   0.0  150.0       $ Sampling of source point along Axial coordinate:
```

Source information sampling along the axial **D** coordinates of the RCC material confining the source.

```
sp1  -21  1           $ Probability of sampling of source point in axial dimension:
```

Source probability; built-in power lower function distribution along the axial **D** axis.

```
si2   0.0   37.5       $ Sampling of source point along radial coordinate
```

Source information sampling along the radial **<** coordinates of the RCC material confining the source.

```
sp2  -21  1           $ Probability of sampling of source point in radial dimension
```

Source probability; built-in power lower function distribution along the radial **<** axis.

```
si3 L  1.173  1.332   $ Energies of gamma-photons emitted by radionuclide Co-60
sp3    0.999  1.000   $ Emission abundances
```

This part defines the energies of the gamma-photons emitted by the radionuclide cobalt-60 and the corresponding abundances.

```
c Material definitions
m1    7014  -0.79   8016  -0.21                                      $ Air at STP
m2    1001  -0.013  8016  -1.165  11023  -0.040  12000  -0.010   &  $ Ordinary Concrete
     13027  -0.108 14000  -0.740 16000  -0.003  19000  -0.045   &  $ Ordinary Concrete
     20000  -0.196 26000  -0.030                                    $ Ordinary Concrete
m3    6000  -0.03   14000 -0.60   15000  -0.02   16000  -0.03    &  $ SS-316L
     24000 -17.50   25000 -1.70   26000 -64.52   28000 -13.00    &  $ SS-316L
     42000  -2.60                                                  $ SS-316L
c  Energy (MeV) and fluence-rate to dose-rate conversion factors: photons
c  Units: Convert fluence-rate to Sv/hr
#        de        df
       0.010    2.22E-10
       ......   .......
       1000.0   7.70e-7
       10000.0  1.05e-6
c ==== PRINT CONTROLS =====
PRINT 10 40 30 50 60 72 100 110 120 170 200 98
c === RUNTIME CONTROLS ======
tmesh
rmesh1:p dose 31 3 2  7.4e+16
    cora1  -450.0   225i  +450.0
    corb1  -500.0   250i  +500.0
    corc1   -01.0         +312.0
endmd
```

The materials, energy and fluence-rate to dose-rate conversion factors, tables to be printed as part of the output and as well the type mesh tally used are defined.

```
c ===
ctme 4000
```

E.3 MCNPX input data set: spherical approximation

```
HEPRO IRRADIATOR ROOM SHIELD WALL DESIGN
c Cell Cards
01  01  -1.29e-3    -1           $ Main Chamber Air Layer1
02  01  -1.29e-3    -2   +1      $ Main Chamber Air Layer2
03  01  -1.29e-3    -3   +2      $ Main Chamber Air Layer3
04  01  -1.29e-3    -4   +3      $ Main Chamber Air Layer4
05  01  -1.29e-3    -5   +4      $ Main Chamber Air Layer5
06  01  -1.29e-3    -6   +5      $ Main Chamber Air Layer6
07  01  -1.29e-3    -7   +6      $ Main Chamber Air Layer7
08  01  -1.29e-3    -8   +7      $ Main Chamber Air Layer8
09  01  -1.29e-3    -9   +8      $ Main Chamber Air Layer9
10  01  -1.29e-3   -10   +9      $ Main Chamber Air Layer10
11  01  -1.29e-3   -11  +10      $ Main Chamber Air Layer11
12  01  -1.29e-3   -12  +11      $ Main Chamber Air Layer12
13  01  -1.29e-3   -13  +12      $ Main Chamber Air Layer13
14  01  -1.29e-3   -14  +13      $ Main Chamber Air Layer14
15  01  -1.29e-3   -15  +14      $ Main Chamber Air Layer15
16  01  -1.29e-3   -16  +15      $ Main Chamber Air Layer16
17  01  -1.29e-3   -17  +16      $ Main Chamber Air Layer17
18  01  -1.29e-3   -18  +17      $ Main Chamber Air Layer18
19  01  -1.29e-3   -19  +18      $ Main Chamber Air Layer19
20  01  -1.29e-3   -20  +19      $ Main Chamber Air Layer20
21  01  -1.29e-3   -21  +20      $ Main Chamber Air Layer21
```

The above portion of the input file entails the Title Card containing information describing the problem *("HEPRO IRRADIATOR ROOM SHIELD WALL DESIGN—SPH Geometric Bodies").* Following the Title Card is the Comment Card stating that all parameters to follow are within the cell card. Defined as well are cells using a spherical geometric bodies (SPH). Cell 1 to 21 is the air inside the irradiation vault indicated as material 1 of the density 1.29E-3 g.cm$^{\bullet 3}$.

```
22  02  -2.35      -22  +21      $ Concrete L1
23  02  -2.35      -23  +22      $ Concrete L2
24  02  -2.35      -24  +23      $ Concrete L3
25  02  -2.35      -25  +24      $ Concrete L4
```

```
26  02  -2.35      -26  +25       $ Concrete L5
27  02  -2.35      -27  +26       $ Concrete L6
28  02  -2.35      -28  +27       $ Concrete L7
29  02  -2.35      -29  +28       $ Concrete L8
30  02  -2.35      -30  +29       $ Concrete L9
31  02  -2.35      -31  +30       $ Concrete L10
32  02  -2.35      -32  +31       $ Concrete L11
33  02  -2.35      -33  +32       $ Concrete L12
34  02  -2.35      -34  +33       $ Concrete L13
35  02  -2.35      -35  +34       $ Concrete L14
36  02  -2.35      -36  +35       $ Concrete L15
37  02  -2.35      -37  +36       $ Concrete L16
38  02  -2.35      -38  +37       $ Concrete L17
39  02  -2.35      -39  +38       $ Concrete L18
40  02  -2.35      -40  +39       $ Concrete L19
```

These cells, 22 to 40, are layers of the concrete shielding the cobalt-60 source.

```
41  01  -1.29e-3   -41  +40       $ Main Chamber Air Layer1
42  01  -1.29e-3   -42  +41       $ Main Chamber Air Layer2
43  01  -1.29e-3   -43  +42       $ Main Chamber Air Layer3
44  01  -1.29e-3   -44  +43       $ Main Chamber Air Layer4
45  01  -1.29e-3   -45  +44       $ Main Chamber Air Layer5
46  01  -1.29e-3   -46  +45       $ Main Chamber Air Layer6
47  01  -1.29e-3   -47  +46       $ Main Chamber Air Layer7
48  01  -1.29e-3   -48  +47       $ Main Chamber Air Layer8
49  01  -1.29e-3   -49  +48       $ Main Chamber Air Layer9
50  01  -1.29e-3   -50  +49       $ Main Chamber Air Layer10
```

Cell 41 to 50 is again the air which extends to the outside of the concrete shield.

```
51  00                  +50            $ UmWelt
```

Cell 51 is a void "*general referred as outside world*"which no photons are tallied in this region.

```

c Surface Cards
01  SPH   0.0   0.0   0.0  +010.0    $ INNER AIR SHELL BOUND
```

```
02  SPH    0.0    0.0    0.0   +020.0    $ INNER AIR SHELL BOUND
03  SPH    0.0    0.0    0.0   +030.0    $ INNER AIR SHELL BOUND
04  SPH    0.0    0.0    0.0   +040.0    $ INNER AIR SHELL BOUND
05  SPH    0.0    0.0    0.0   +050.0    $ INNER AIR SHELL BOUND
06  SPH    0.0    0.0    0.0   +060.0    $ INNER AIR SHELL BOUND
07  SPH    0.0    0.0    0.0   +070.0    $ INNER AIR SHELL BOUND
08  SPH    0.0    0.0    0.0   +080.0    $ INNER AIR SHELL BOUND
09  SPH    0.0    0.0    0.0   +090.0    $ INNER AIR SHELL BOUND
10  SPH    0.0    0.0    0.0   +100.0    $ INNER AIR SHELL BOUND
11  SPH    0.0    0.0    0.0   +110.0    $ INNER AIR SHELL BOUND
12  SPH    0.0    0.0    0.0   +120.0    $ INNER AIR SHELL BOUND
13  SPH    0.0    0.0    0.0   +130.0    $ INNER AIR SHELL BOUND
14  SPH    0.0    0.0    0.0   +140.0    $ INNER AIR SHELL BOUND
15  SPH    0.0    0.0    0.0   +150.0    $ INNER AIR SHELL BOUND
16  SPH    0.0    0.0    0.0   +160.0    $ INNER AIR SHELL BOUND
17  SPH    0.0    0.0    0.0   +170.0    $ INNER AIR SHELL BOUND
18  SPH    0.0    0.0    0.0   +180.0    $ INNER AIR SHELL BOUND
19  SPH    0.0    0.0    0.0   +190.0    $ INNER AIR SHELL BOUND
20  SPH    0.0    0.0    0.0   +200.0    $ INNER AIR SHELL BOUND
21  SPH    0.0    0.0    0.0   +224.5    $ INNER AIR SHELL BOUND
```

These are surfaces bounding the cells with air inside the irradiation room.

```
22  SPH    0.0    0.0    0.0   +226.0    $ CRT LAYER 01 OD
23  SPH    0.0    0.0    0.0   +230.0    $ CRT LAYER 02 OD
24  SPH    0.0    0.0    0.0   +240.0    $ CRT LAYER 03 OD
25  SPH    0.0    0.0    0.0   +245.0    $ CRT LAYER 04 OD
26  SPH    0.0    0.0    0.0   +255.0    $ CRT LAYER 05 OD
27  SPH    0.0    0.0    0.0   +265.0    $ CRT LAYER 06 OD
28  SPH    0.0    0.0    0.0   +275.0    $ CRT LAYER 07 OD
29  SPH    0.0    0.0    0.0   +285.0    $ CRT LAYER 08 OD
30  SPH    0.0    0.0    0.0   +295.0    $ CRT LAYER 09 OD
31  SPH    0.0    0.0    0.0   +305.0    $ CRT LAYER 10 OD
32  SPH    0.0    0.0    0.0   +315.0    $ CRT LAYER 11 OD
33  SPH    0.0    0.0    0.0   +325.0    $ CRT LAYER 12 OD
34  SPH    0.0    0.0    0.0   +335.0    $ CRT LAYER 13 OD
35  SPH    0.0    0.0    0.0   +345.0    $ CRT LAYER 14 OD
36  SPH    0.0    0.0    0.0   +355.0    $ CRT LAYER 15 OD
37  SPH    0.0    0.0    0.0   +365.0    $ CRT LAYER 16 OD
```

```
38  SPH   0.0   0.0   0.0  +375.0    $ CRT LAYER 17 OD
39  SPH   0.0   0.0   0.0  +385.0    $ CRT LAYER 18 OD
40  SPH   0.0   0.0   0.0  +397.0    $ CRT LAYER 19 OD
```

These surfaces confine the cells with the concrete shielding material surrounding the irradiation source, cobalt-60.

```
41  SPH   0.0   0.0   0.0  +409.5    $ Outer airshell partition boundary
42  SPH   0.0   0.0   0.0  +419.5    $ Outer airshell partition boundary
43  SPH   0.0   0.0   0.0  +429.5    $ Outer airshell partition boundary
44  SPH   0.0   0.0   0.0  +439.5    $ Outer airshell partition boundary
45  SPH   0.0   0.0   0.0  +449.5    $ Outer airshell partition boundary
46  SPH   0.0   0.0   0.0  +459.5    $ Outer airshell partition boundary
47  SPH   0.0   0.0   0.0  +469.5    $ Outer airshell partition boundary
48  SPH   0.0   0.0   0.0  +479.5    $ Outer AirShell OD; start of UmWelt
49  SPH   0.0   0.0   0.0  +489.5    $ Outer AirShell OD; start of UmWelt
50  SPH   0.0   0.0   0.0  +600.0    $ Outer AirShell OD; start of UmWelt

c Data Cards
c Mode: transport photons
mode p
c cell importance
imp:p 1 17r 2m 2m 2m 2m 2m 2m 2m 2m 2m 2m 2m 2m 2m 2m 2m 2m 2m 2m 13r 0
c source definition:
sdef par=p erg=d3 pos=0 0 0
si3 L  1.173  1.332
sp3    0.999  1.000
c
c Material definitions
m01   7014 -0.79    8016  -0.21                                          $ Air at STP
m02   1001 -0.013   8016  -1.165   11023  -0.040   12000  -0.010  &     $ Ordinary Concrete
     13027 -0.108  14000  -0.740   16000  -0.003   19000  -0.045  &     $ Ordinary Concrete
     20000 -0.196  26000  -0.030                                         $ Ordinary Concrete
c
c **** Physics Table *****
phys:p 100 0 0 -1  1
totnu
c
c **** Tallies *******
c
```

```
fc12 Tally: photon dose-rate
f12:p  1   2   3   4   5   6   7   8   9  10 11  12  13  14  15  16 17  18  &
19 20 21  22  23  24  25 26 27 28 29 30 31 32 33 34  35  36  37  38 39  40  &
41  42  43 44 45 46 47 48 49
fm12   7.4E16      $ 2 MCi Co-60
c  Energy (MeV) and fluence-rate to dose-rate conversion factors: photons
c  Units: Convert fluence-rate to Sv/hr
#      de12     df12
       0.010    2.22E-10
       ......   ........
       1000.0   7.70E-07
       10000.0  1.05E-06
c
fc24 Photon fluence-rate & spectrum tally
f24:p  6  7  22
e24    0.01  0.10  0.20  0.30  0.40  0.50  0.60  0.70  0.80  0.90    &
       1.00  1.10  1.15  1.20  1.25  1.30  1.35
fm24   7.4E16
```

This part entails the surfaces that confine the cells of air on the outside of the concrete wall. It defines the mode of transport, the importance corresponding to each cell, the source cobalt-60; its energy and the abundances. The materials used, tallies, energy and fluence-rate to dose-rate conversion factors and as well as the physics using the physics card. The physics card (PHYS) is used to specify energy cutoffs and the physics treatments to be used for photons.

```
c ==== PRINT CONTROLS =====
PRINT 10 40 50 60 72 100 110 120 170 200
c === RUNTIME CONTROLS ======
ctme 120
```

Bibliography

ALPEN EL (ed.) 1990. *Radiation Biophysics.* Second edition. Academic Press.

AMERICAN NUCLEAR SOCIETY (ANS). 1991. *Neutron and gamma–ray fluence–to–dose factors.* Report ANSI/ANS–6.1.1–1991. La Grange Park, Illinois: American Nuclear Society. 19 p.

BARNES BN. 2006. Personal Communication, September 2006. Coordinator: Sterile Insect Release Programme, Plant Protection Division, ARC Infruiitec-Nietvoorbij, Stellenbosch, South Africa.

BASHTER II. 1997. *Calculation of radiation attenuation coefficients for shielding concrete.* Annals of Nuclear Energy, vol. **24**, No. 17 (**1997**) 1389 – 1401.

CEMBER H. (ed.) 1996. *Introduction to Health Physics. 3rd ed.* New York: McGraw–Hill.

CHAPMAN SJ. (ed.) 1998. *Introduction to Fortran 90/95. 1st ed.* New York: McGraw–Hill.

DE BEER GP. 1986. *[Informal, handwritten report on HEPRO shielding].* A formal report was possibly never published, or it has been lost. Calculations performed at Atomic Energy Corporation of SA Ltd.

ENTWISTLE B and ADRIAN HWW. 1986. *The Final Safety Report for the HEPRO (Pty) Ltd Western Cape Irradiation Facility.* Atomic Energy Corporation of SA Ltd.

FERRARI A, PELLICCIONI M and PILLON M. 1996. *Fluence to Effective Dose and Effective Dose Equivalent Conversion Coefficients for Photons from 50 keV to 10 GeV.* Journal of the Radiation Protection Dosimetry, vol. **67**, No. 4 **(1996)** 245– 251.

FERRARI A, PELLICCIONI M and PILLON M. 1997a. *Fluence to Effective Dose and Effective Dose Equivalent Conversion Coefficients for Electrons from 5 MeV to 10 GeV.* Journal of the Radiation Protection Dosimetry, vol. **62**, No. 2 **(1997)** 97– 104.

FERRARI A, PELLICCIONI M and PILLON M. 1997b. *Fluence to Effective Dose Conversion Coefficients for Protons from 5 MeV to 10 TeV.* Journal of the Radiation Protection Dosimetry, vol. **71**, No. 2 **(1997)** 85– 91.

FERRARI A, PELLICCIONI M and PILLON M. 1997c. *Fluence to Effective Dose Equivalent Conversion Coefficients for Neutrons up to 10 TeV.* Journal of the Radiation Protection Dosimetry, vol. **71**, No. 3 **(1997)** 165– 173.

HOFMEYR H. 2006. Personal Communication. Senior Research Entomologist: Sterile Insect Release Programme, Plant Protection Division, Citrusdal insect sterilization irradiator facility, SA.

IAEA. 1996. *International Basic Safety Standards for Protection Against Ionising Radiation and for the Safety of Radiation Sources. Safety Series No.* 115, IAEA, Vienna (1996).

IAEA. 1992. *Radiation Safety of Gamma and Electron Irradiation Facilities, Safety Series No.* 107, IAEA, Vienna (1992).

ICRP. 1983. *ICRP Publication 38—Radionuclide Transformations: Energy and Intensity of Emissions.* Annals of the ICRP (International Commission on Radiological Protection. Pergamon Press.

ICRP. 1990. *ICRP Publication 60— Recommendations of the International Commission on Radiological Protection.* Annals of the ICRP **21** (1-3). Pergamon Press, Oxford.

ICRP. 2007. *ICRP Publication 103— Recommendations of the International Commission on Radiological Protection.* Annals of the ICRP **37** (2-4).

KNOLL GF. (ed.) 1999. *Radiation Detection and Measurement, 3rd ed.* New York: John Wiley and Sons. 802 p. ISBN 0-471-07338-5.

KRANE, KS. 1987. *Introductory Nuclear Physics*. New York: John Wiley and Sons.

LEROY C and RANCOITA PG. (eds.) 2004. *Principles of radiation interaction in matter and detection, 2nd ed.* Hackensack, NJ : World Scientific.

MARMIER P. and SHELDON E. *Physics of nuclei and particles*. New York: Academic Press, 1969, Vol. I.

NATIONAL INSTITUTE of STANDARDS and TECHNOLOGY (NIST). March 1998. *XCOM: Photon Cross Sections Database.* [Online](Last Updated February 2009). Available at: http://physics.nist.gov/PhysRefData/Xcom/Text/XCOM.html [Accessed 06 May 2009].

OLIVEIRA C, SALGADO J and FERRO DE CARVALHO A. 2000. *Dose Rate Determinations in the Portuguese Gamma Irradiator Facility: Monte Carlo Simulations and Measurements.* Journal of the Radiation Physics and Chemistry, vol. **58 (2000)** 279–285.

OLIVEIRA C and SALGADO J. 2001. *Isodose distributions and dose uniformity in the Portuguese gamma irradiation facility calculated using the MCNP code.* Journal of the Radiation Physics and Chemistry, vol. **61 (2001)** 791 - 793.

OLIVEIRA C, FERREIRA LM, CONCALVES IF, and SALGADO J. 2002. *Monte Carlo Studies of the Irradiator Geometry of the Portuguese Gamma Irradiation Facility.* Journal of the Radiation Physics and Chemistry, vol. **65 (2002)** 293–295.

PRATT RH. 2004. *Tutorial on Fundamentals of Radiation Physics: Interactions of Photons with Matter.* Journal of the Radiation Physics and Chemistry, vol. **70 (2004)** 595– 603.

RAISALI G, HAJILOO N, HAMIDI S and ASLANI G. 2006. *Analysis of Neutron and Gamma-Ray Streaming Along the Maze of NRCAM Thallium Production Target Room.* Journal of the Applied Radiation and Isotopes, vol. **64 (2006)** 940 –947.

ROBINSON A, FRANZ G and FISHER K. 1999. *Genetic sexing strains in the medfly, Ceratitis capitata: Development, mass rearing and field application.* Trends Ent. **2 (1999)** 81– 104.

RSICC CODE PACKAGE CCC-493. 1989. *QAD-CGGP: A Combinatorial Geometry Version of QAD-P5A, A Point Kernel Code System for Neutron and Gamma-Ray Shielding Calculations Using the GP Buildup Factor.* Radiation Safety Information Computational Center, Oak Ridge National Laboratories, USA.

RSICC CODE PACKAGE CCC-730. 2005. *MCNPX: Monte Carlo N–Particle Transport Code System Including MCNPX Version 2.5.0 and Data Libraries MCNPXDATA.* Radiation Safety Information Computational Center, Oak Ridge National Laboratories, USA.

SARANGAPANI R, JOSE MT, MEENAKSHISUNDARAM V and SUBBAIAH, KV. 2006. *Measurement of Dose Rate Profile and Spectra Through a Cylindrical Duct vis-avis Monte Carlo Simulation Studies for Optimisation of Reactor Shield Design.* Annals of Nuclear Energy,vol. **33 (2006)** 385 –389.

SHULTIS, JK and FAW, RE. 1996. *Radiation Shielding.* Upper Saddle River, NJ: Prentice Hall. ISBN 0-13-125691-2.

TSAI WC, SHEU RD, and JIANG SH. 2005. *Evaluation of the Dose Rate Distribution for an Air-Type ^{60}Co Irradiation Facility*. Journal of the Radiation Protection Dosimetry, vol. **116 (2005)** 352 – 358.

TURNER, JE. 1995. *Atoms, radiation, and radiation protection,* 2nd ed. New York: John Wiley and Sons.

VAN ROOYEN, TJ. 2006. Personal Communication, October 2006. *Calculations with a MathCAD Worksheet, Using a Point-Kernel Method for Point Sources Surrounded by a Single-Material Shield in Spherical-Symmetrical Geometry*. Radiation and Reactor Theory Section, Necsa (South African Nuclear Energy Corporation), PO Box 582, Pretoria, 0001, South Africa.

Wrixon AD. 2008. *Review: New ICRP recommendations.* Journal of Radiological Protection. vol. **28 (2008)** 161 – 168.